Extracellular histones promote pulmonary fibrosis by multicellular interactions

Dissertation

zur Erlangung des Grades

„Doktor der Naturwissenschaften“

am Fachbereich Biologie
der Johannes Gutenberg-Universität in Mainz

Dennis Riehl

Matrikelnummer: 2645358

geb. am 16.03.1987 in Dieburg

Mainz, den 16.12.2016

Dekan:

External Supervisor:

Internal Supervisor:

Day of disputation: 4th April, 2017

Drafted at the Center for Thrombosis and Hemostasis (CTH), Mainz

For my beloved parents

Declaration

Herewith, I declare that I have written this PhD thesis independently. I have not used other than the declared sources or resources, and I have explicitly marked all material which has been quoted either literally or by content from the used sources. I have not submitted it at any other university worldwide.

_____

Dennis Riehl

Münster bei Dieburg, 16.12.2016

Table of Content

Summary

Pulmonary fibrosis is characterized by a dysregulated accumulation of extracellular matrix components. This chronic and irreversible disease has a poor prognosis because of limited treatment options. In the presented work, the cellular processes and cytokine networks initiated by extracellular histones during bleomycin-induced pulmonary fibrosis were studied in mice. As the cellular sources of extracellular histones, neutrophils and non-hematopoietic cells were identified by using chimeric H2B-eGFP reporter mice. In addition, citrullinated extracellular histones derived from neutrophil extracellular traps (NETs) were reduced after depletion of neutrophils in Ly6GCre/iDTR mice. This transient depletion of Ly6G+ neutrophils during the early phase of bleomycin-induced pulmonary fibrosis protected from extracellular matrix accumulation (collagen I,V) and the infiltration of pro-fibrotic Th17 cells into the lungs. Furthermore, blockade of extracellular histones (anti-histone H4 antibodies) protected from collagen I,V accumulation as well as epithelial/endothelial to mesenchymal transition. The blocked extracellular histones also led to reduced stress-induced gene expression levels in T regulatory cells. Histones activated platelets, followed by release of TGFβ1 during ex vivo studies. Lower concentrations of TGFβ1 and less collagen I,V accumulation were noted in PF4Cre/TGFβ1flox/flox mice. TGFβ1 inhibited IL-27 production in macrophages in a TGFbRI and TGFbRII dependent manner. The influence of TGFbRII on the release of IL-27 during bleomycin-induced pulmonary fibrosis was shown in LysMCre/TbRIIflox/flox mice. IL-27 apparently exerted anti-fibrotic activities, since IL-27RA-/- mice were more prone to fibrosis. The molecular inhibition mechanism of TGFβ1 was further analyzed by several in vitro studies: TGFβ1 engaged multiple downstream proteins such as p38 MAPK, Tristetraprolin and IL-10. A central signaling molecule of TGFβ1, Smad3, was shown to bind directly to the *il-27p28* and *ebi3* promoter regions. This work identifies extracellular histones as central key players during experimental pulmonary fibrosis. The extracellular histones appear to skew the reciprocal balance of IL-27 and TGFβ1 by triggering the release of platelet-derived TGFβ1. These data set extracellular histones in the focus of the search for future treatment options for pulmonary fibrosis.

I Introduction

1 Pathophysiology of Bleomycin-induced pulmonary fibrosis

1.1 Pulmonary fibrosis

Pulmonary fibrosis is a disease of the lung with dysregulated accumulation of extracellular matrix components between the alveoli and the blood vessels in the lung parenchyma (1). Symptoms are exertional dyspnea and cough (2). In the end, the pulmonary function is destroyed (3). Millions of people are affected by pulmonary fibrosis worldwide (4). For example, pulmonary fibrosis has a prevalence of 14 to 27.9 cases per 100,000 in the USA and 1.25 to 23.4 cases per 100,000 in Europe (5). Pulmonary fibrosis is a chronic and irreversible disease with unknown etiology (6), although several risk factors have been reported such as smoking (7), pollutants, viral infections (8) and ageing (9).

To date, the precise mechanisms driving the development and progression of pulmonary fibrosis are not known. Three processes are thought to play a role in the pathophysiology of pulmonary fibrosis: inflammation, oxidative stress and coagulation disturbances. These processes can result in a changed lung fibroblast phenotype, apoptosis of epithelial cells and production of extracellular matrix (10).

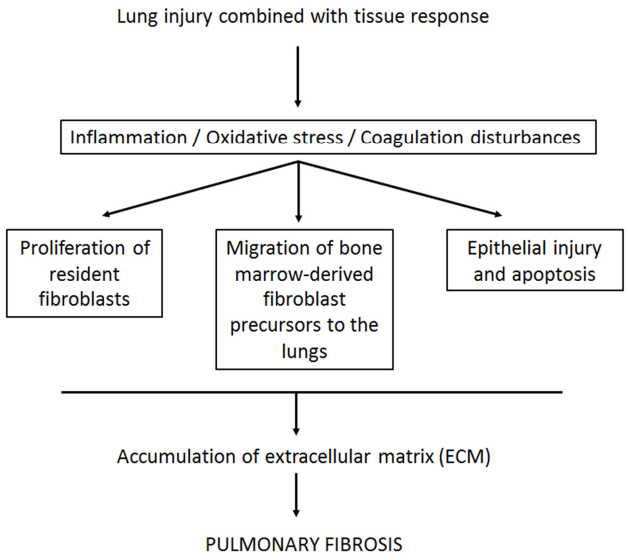

Fig. 1: Processes of pulmonary fibrosis development.
Schematic diagram of the three processes (inflammation, oxidative stress, and coagulation disturbances) which contribute to pulmonary fibrosis after lung injury. According to Lasithiotaki et al., 2011 (10).

Various immune cells infiltrate into the lung during pulmonary fibrosis and build a cytokine network, which orchestrates inflammation and fibrosis (11). For example, neutrophilia is a hallmark of pulmonary fibrosis (12) (13).

The Th1-cytokine, Interferon-γ (IFN-γ), prevents fibrosis by inhibiting fibroblast activation (14) and by activation of M1 macrophages which degrade extracellular matrix components (15). In contrast, the Th2-cytokines, Interleukin-4 (IL-4) and Interleukin-13 (IL-13), are activators of fibroblasts by increasing the expression of adhesion molecules and inflammatory cytokines (16) (17).

During bleomycin-induced injury, activation of the coagulation system is the first wound-healing response. Because of the cellular damage, platelets are activated by exposed collagen and by von-Willebrand factor (18). Activated platelets release different growth factors such as platelet-derived growth factor (PDGF) and transforming growth factor β 1 (TGFβ1). PDGF is a chemoattractant for fibroblasts (19) and TGFβ1 activates fibroblasts to generate extracellular matrix components (20). The origin of fibroblasts is unclear (21). Three theories try to explain the origin of fibroblasts: 1) resident lung fibroblasts get activated, 2) epithelial cells undergo epithelial-mesenchymal transition and 3) bone marrow–derived fibrocytes invade the lungs from bone marrow precursors.

During bleomycin-induced pulmonary fibrosis, the expression levels of TGFβ are increased two days after the injury (22). This correlates with the highest alveolar flooding after two days (23) and the finding that TGFβ increases the permeability of endothelial monolayers *in vitro* (24). On the other hand, TGFβ is produced in a latent form (Chap. I-4.2.1) and can be activated by the endothelial integrin $\alpha_v\beta_6$ in the lung (25).

1.2 Epithelial/Endothelial to mesenchymal transition in fibrosis

Epithelial-mesenchymal transition (EMT) is a process occuring in embryogenesis (26) and metastasis (27). During the process of EMT, epithelial cells lose their apical-basal cell polarity (26) and display reduced expression of cell-cell adhesion molecules, such as E-cadherins (epithelial marker) (28). In the end, the epithelial cells become mesenchymal stem cells which are multipotent stromal cells and can be

differentiate into myofibroblasts (29). The process of EMT depends on MAPK pathways and the activation of the transcription factor Snail (30), which can bind to the E-cadherin promoter and repress the activity (31). Other important transcription factors are: Slug (32) and Twist (33). Slug and Twist have been reported to repress the E-cadherin expression as well (34) (35). Other markers of EMT are: vimentin, α-smooth muscle actin (α-SMA) and the transcription factor Zeb2 (36).

Alveolar epithelial cells may undergo EMT under pro-fibrotic conditions and could be one source of the myofibroblasts during pulmonary fibrosis (37) (38). Blocking of the EMT process resulted in reduced pulmonary fibrosis in animal models (39). EMT can also be found in other organ fibrosis. Iwano et al., 2002 (40) showed in a model of kidney fibrosis, that only a small number of fibroblasts emigrated from the bone marrow. Large numbers of fibroblasts may arise from local EMT. Both populations of fibroblasts express collagen I. This was confirmed by Kim et al., 2006 (41) for pulmonary fibrosis. The authors identified primary alveolar epithelial cells as the source for fibroblast *in vivo*. The TGFβ pathway is a critical inducer of EMT during development and progression of fibrosis. In a model of renal fibrosis, mice lacking Smad3 ($Smad3^{-/-}$) were protected against fibrosis. *In vitro* experiments with primary renal tubular epithelial cells from $Smad3^{-/-}$ mice showed less TGFβ1-induced EMT (42).

An analogous process to the EMT is the Endothelial-mesenchymal transition (EndMT) (43). EndMT is, such as EMT, a pathological process and a common process during development (44). Markers for EndMT are: FSP-1, α-SMA and vimentin. CD31 (platelet endothelial cell adhesion molecule, PECAM-1) is expressed in an epithelial phenotype (36). Kalluri and colleagues (2003) (45) demonstrated for kidney fibrosis in mice that only 12% of the fibroblast derived from the bone marrow. About 30% of the fibroblasts were generated by EMT and about 35% by EndMT in the kidney. The remaining 23% are hypothesized to be generated by resident fibroblasts or mesenchymal cells. Hoyles et al., 2011 (46) showed a key role of resident pulmonary fibroblasts to develop pulmonary fibrosis as well. On the other hand, pericytes as stromal cells and two epithelial cell populations (Type I and Type II alveolar cells) were shown to be not the source of myofibroblasts during bleomycin-induced pulmonary fibrosis (47). Taken together, EMT is a potential source of

myofibroblasts during pulmonary fibrosis. The relevance of EMT is controversial and has to be further analysed (48) (49).

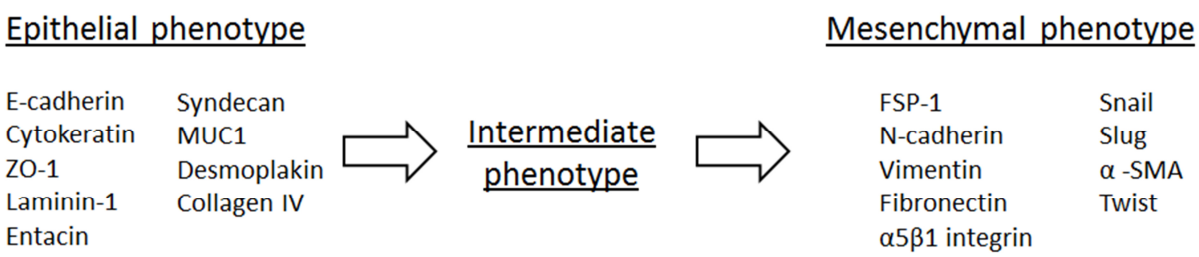

Fig. 2: Transition of epithelial cells to mesenchymal cells.
According to Kalluri and Weinberg, 2009 (36).

1.3 Bleomycin

Bleomycin is a mixture of different glycopeptide antibiotics which were first isolated from *Streptomyces verticillus* (50). So far, 16 natural agents have been reported. The skeletal structure of the bleomycins is the bleomycin acid. The structure of individual bleomycins represent amids of the bleomycin acid (51). In the present work, a mixture of the variants bleomycin A_2 and bleomycin B_2 are used. Bleomycins are used for cancer therapies against head and neck carcinomas and malignant lymphomas (52). However, there are several known side effects which are dose-dependent and include lung inflammation and progressive pulmonary fibrosis. Because of these side effects, bleomycins are widely used *in vivo* to study pulmonary fibrosis after intra-tracheal instillation (53) (54). Bleomycins bind metals such as Fe(II) and catalyze single-stranded or double-stranded DNA lesions, oxidative stress and the generation of free radicals (55) (56) (57). The epithelium is injured, followed by acute inflammation and a low level inflammation. These effects result in the development of fibrosis.

Bleomycins are non-permeable molecules which pass the plasma membrane by passive diffusion (58). Bleomycins are rather internalized a receptor-mediated endocytosis mechansim (52). A study with electropermeabilized cells identified 500 bleomycin molecules as sufficient to kill the cells. The cited study was performed with chinese hamster fibroblasts (DC-3F) and human epithelial cells from the submaxillary salivary gland (A253) (58).

2 The immune system

The immune system protects the host against invading pathogenic microorganisms such as bacteria, viruses, fungi, parasites. An integral part of immune defenses are specific immune cells originating from different organs all over the body, such as the thymus, the bone marrow, the lymph nodes and the lymphatic vessels or the spleen. These immune cells can be separated into the innate immune system and the adaptive immune system (59).

The innate immune system is evolutionarily conserved and recognizes foreign microorganisms by pattern recognition receptors (PRRs) which recognize structural conserved motifs known as pathogen-associated molecular patterns (PAMPs) (60). Immune cells belonging to the innate immune system are: macrophages, dendritic cells, natural killer cells, neutrophil granulocytes, basophil granulocytes and eosinophil granulocytes (61).

2.1 Macrophages

Macrophages recognize and phagocytose foreign microorganisms (62). For macrophages, several subsets with different functions are described. Here, only the classically activated macrophages (M1 macrophages) and the alternatively activated macrophages (M2 macrophages) are described in more detail. M1 macrophages are activated by PAMPs such as lipopolysaccharide (LPS) and mediators such as IFN-γ and they have been reported to express pro-inflammatory cytokines and inducible nitric-oxide synthase. M1 macrophages are fighting against bacteria, protozoa and viruses. Furthermore, M1 macrophages degrade ECM components in the context of wound healing or fibrosis (anti-fibrotic). M2 macrophages are activated by IL-4 and IL-13 and express arginase-1. The M2 macrophage subset is anti-inflammatory, regulates wound-healing and promote fibrosis by release of ECM components (63) (64).

2.2 Neutrophil Granulocytes and Neutrophil extracellular traps

Neutrophil Granulocytes (Neutrophils) are the most abundant cell population in the peripheral blood (50 – 70% of white blood cells) (65). They are constantly produced by the bone marrow and rapidly migrate to the site of injury or infection in a chemoattractant manner (65) (66) (67). As the first cells at the side of infection, neutrophils play an important role in the early immune response by phagocytosis and killing of extracellular bacteria and protozoa by reactive oxygen species (ROS) or

anti-bacterial peptides (68) (65). To mediate their biological function, neutrophils are packed by different granules with anti-bacterial peptides such as myeloperoxidase (MPO), α-defensins and bactericidal/permeability-increasing protein (BPI) (69).

2.2.1 Generation and architecture of Neutrophil extracellular traps

Another anti-bacterial mechanism of neutrophils are neutrophil extracellular traps (NETs). NETs are released by neutrophil granulocytes by a cell death process called "NETosis" (70). During this process, chromatin decondensation occurs, the inner and outer nuclear membranes detach from each other, the nuclear envelope loses its integrity and the nucleoplasm and the cytoplasm form a homogenous mass. In the end, the cell membrane ruptures and releases the interior of the cell into the extracellular space (71). NET formation is an active process which is ATP-dependent (72). The central process for chromatin decondensation is the hypercitrullination of histone H3 (H3-Cit) by peptidylarginine deiminase 4 (PAD4) (73) (74) (75) (76). The major constituents of NETs are DNA, and histones coated with antimicrobial proteins (72). NETs are web-such as structures of chromatin fibers with a diameter of approx. 17nm (72) (77) (78). A list of NET component is shown in Tab. 1.

Tab. 1: Components of Neutrophil extracellular traps.
According to Mesa and Vasquez, 2013 (79).

Nuclear components	DNA, Histones
Granular components	
Primary granules	Myeloperoxidase, cathepsin G, neutrophil elastase
Secondary granules	Lactoferrin, pentraxin 3
Tertiary granules	Gelatinase, peptidoglycan-binding protein
Cytoplasmatic components	Calprotectin, catalase

Many pathogens have been reported to induce NETs: *S. aureus* (71), *E. coli* (80), *C. albicans* (81) and HIV-1 (82). On the other hand, some microorganisms are able to degrade NETs by producing DNase as an immune evasion strategy (83).

NETs can be released in response to interactions of platelets with neutrophils. In detail, platelets can bind LPS via TLR4 and bind to neutrophils during sepsis. This leads to an activation of neutrophils and the release of NETs (84).

In summary, NETs are a part of the innate response against microorganisms. NETs prevent the spreading of microorganisms and concentrate antimicrobial agents in order to kill bacteria (72). On the other hand, the aggressive components of NETs induce damage of host cells. This can result in different diseases such as asthma (85), thrombosis (86) or acute lung injury (87). This tissue injury is mainly mediated by extracellular histones rather than DNA (88).

2.2.2 Extracellular Histones

Histones are alkaline proteins which are found in eukaryotic cell nuclei. They are important for the packaging of DNA into nucleosomes (89). Every nucleosome is formed by 145bp DNA and two of each following histone families: H1, H2A, H2B, H3 and H4 (90). Normally, the histones are located inside the cell nucleus but can be released by dying cells as damage-associated molecular pattern (DAMP) and are able to induce inflammation by ligation with TLR2 and TLR4 (91) (92). Once released, they are called extracellular histones. The stimulation of PRRs leads to the release of chemokines/cytokines - and in turn to the chemotaxis of immune cells by extracellular histones (93) (94). In addition, extracellular histones are important mediators of cell death (93). The histone H4 has the highest cytotoxicity of all histones (H4>H3>H2A>H2B>H1) (93) (94).

2.3 T cells and B cells

Effector cells of the adaptive immune system are T cells and B cells. The B cells develop directly from the hematopoietic stem cells of the bone marrow. The T cells migrate from the bone marrow to the thymus where they mature (59). B cells produce T cell-dependent or T cell-independent antibodies which belong to the humoral part of the adaptive immune system (95). The T cells are separated into several major subclasses: the $CD4^+$ T helper (Th) cells and the $CD8^+$ cytotoxic T cells. The cytotoxic T cells bind to MHCI-presented viral antigens via CD8 (96). They can directly induce apoptosis of the infected cell (97). $CD4^+$ T helper cells recognize MHCII-presented antigens (98). The antigen specific T helper cell answer is divided into two groups: Th1 and Th2 (99). Th1 cells secrete cytokines such as IFN-γ to support the cellular immune reaction. Th2 cells produce mainly IL-4, IL-5, IL-10 and IL-13. These cytokines inhibit the cellular immune reaction but support the humoral immune reaction (59).

2.3.1 T helper 17 cells

T helper 17 (Th17) cells, in analogy to Th1 and Th2 cells, are a subpopulation of $CD4^+$ helper T cells. To generate Th17 cells *in vitro*, TGFβ in combination with IL-6 and IL-21 is required. The differentiation of Th17 cells is orchestrated by several steps. First, IL-6 and TGFβ initiate IL-17 production (100) (101). In parallel IL-21 is produced as an autocrine factor (102). Finally, IL-23 acts to maintain the Th17 phenotype (103). The orphan nuclear receptor ROR gamma t (RORγt) is considered to be the master regulator transcription factor which directs the differentiation program of Th17 cells (104).

Cytokines produced by Th17 cells include IL-17A and IL-17F (105). IL-17A has been reported to play an important role in bleomycin-induced pulmonary fibrosis (106) (107). For example, IL-17A is involved in the recruitment of neutrophils by induction of CXC chemokines by bronchial epithelial cells (108) (109) (110) (111) (112). Neutrophils have a key role in the development of pulmonary fibrosis (113).

2.3.2 Regulatory T cells

Regulatory T cells (Tregs) are a subpopulation of $CD4^+$ T cells (114). There are two major subpopulations of Tregs: natural regulatory T cells (nTreg) and induced regulatory T cells (iTreg). The nTregs are generated in the thymus (115) and the iTregs are generated in the periphery by costimulation of the T cell-receptor and TGFβ (116). The master transcription factor Foxp3 is induced by TGFβ in $CD4^+CD25^+$ T cells. To induce $Foxp3^+$ Tregs, a stimulation of the T cell receptor, the IL-2 receptor and stimulation with TGFβ is required (117). If there is a costimulation with the cluster of differentiation 28 (CD28), the Foxp3 induction is prevented (117). CD28 is a costimulatory receptor (118) which is expressed on all T cells (119) and interacts with CD80 and CD86 on activated antigen presenting cells (120). The biological activity of Tregs is mediated by different cytokines, such as TGFβ (121), IL-10 (122) or IL-35 (123). With their different cytokines, Tregs play a very important role in controlling self-tolerance and autoimmunity (124). The functions of regulatory T cells during pulmonary fibrosis are not entirely clear at present. In fact, the beneficial or detrimental activities of Tregs appear to be context dependent, e.g. on the time point of pulmonary fibrosis (121).

Tab. 2: Specific cell markers for relevant immune cells in the present work.

Cell type	Markers	Citation
Neutrophil granulocytes	Ly6G/ Ly6C, CD11b	(125)
Macrophages, tissue	F4/80, CD11b	(126)
Macrophages, lung	F4/80, CD11c	(117)
Th1 T cells	CD3, CD4, IFN-γ	(127) (128)
Th17 T cells	CD3, CD4, IL-17	(129)
T regulatory T cells (Tregs)	CD3, CD4, Fopx3/ CD25	(130) (131)

2.4 Toll-like receptors

Toll-like receptors (TLRs) are conserved PRRs expressed on the cell surface or in intracellular compartments which recognize specific PAMPs leading to an effective immune response (132) (Tab. 3). Other families of PRRs include the cytosolic Rig-I (retinoic acid-inducible gene I), the NOD (nucleotide binding oligomerization domain) and the NOD-like receptors (NLR) (133).

Tab. 3: Ligands of the different Toll-like receptors.

According to Micera et al., 2016 (134).

TLR	Ligand
TLR1	Gram positive products, lipopeptides
TLR2	Gram positive products, LTA, PGN, fungi, hyaluronan, lipopeptides
TLR3	dsRNA, viruses mRNA
TLR4	Gram negative products, LPS, LAM, LTA, fungi, fibronectin, heparansulphate, hyaluronan
TLR5	Bacterial flagellin
TLR6	Gram positive products, lipopeptides, Mycoplasm
TLR7	ssRNA, mRNA, RNA/protein complex
TLR8	ssRNA
TLR9	Bacterial/viral dsDNA
TLR10	unknown
TLR11	Flagellin, profilin (135)
TLR12	Profilin (136)
TLR13	ribosomal subunit of bacterial RNA (23S rRNA) (137)

3 Platelets

Platelets are disc-shaped fragments of cytoplasm without nuclei, produced by megakaryocytes in the bone marrow (138) or directly in the lungs (139). Platelets as non-nucleated cell elements are the smallest structures of the blood (3.6 x 0.7µm). Their diameter is between 2-5µm (140). This leads to a surface area of approx. 8µm^2. In humans, the megakaryocytes produce around 35,000 – 40,000 platelets per day per µl blood (141). The major task of platelets is to prevent blood loss after vessel injury by the formation of plugs/thrombi as well as initiation of wound healing (142) (143) (144).

Platelets contain mRNA derived from their progenitors, the megakaryocytes. In the resting stage, the platelet-transcriptome is suppressed. Platelets can be activated through receptor-mediated recognition of thrombin, collagen, ADP and thromboxane A_2 (145). When platelets get activated, their protein synthesis is reactivated (146) and they secrete cytokines, such as IL-1β (147). Furthermore, the activation leads to a reorganization of the actin cytoskeleton and a rounding of the cell – the so called platelet “shape change” (148). The changed morphology increases the surface area by formation of lamellipodia to strengthen the contact to the vessel or other platelets.

Platelets contain an abundance of granules (149). Once activated, platelets secrete the content of their granules with more than 300 proteins (150). Typical proteins released by platelets are: hemostatic mediators, adhesion and signaling molecules, calcium (Ca^{2+}), ADP, ATP and serotonin (149). The α-granules are the most numerous of the platelets organelles and contain the growth factor TGFβ1 (151).

4 Cytokines

Cytokines are small proteins (approx. 25kDa) which are released by hematopoietic and non-hematopoietic cells (152) and mediate cell-cell-communication by binding to specific receptors (153) (154). The family of cytokines consists of interleukins (ILs), chemokines and interferons (IFNs) (152). Because of their short half-lives cytokines mediate immune responses in an autocrine or paracrine manner (152).

4.1 Interleukin-27

Interleukin-27 (IL-27) consists of the two subunits p28 and Epstein-Barr virus-induced gene 3 (EBI3). It is part of the Interleukin-12-family (155). Other members of this cytokine family are Interleukin-23 (IL-23), Interleukin-35 (IL-35) and Interleukin-12 (IL-12). IL-35 consists of p35 in combination with EBI3 (123). Because of this the p28 subunit can be used as the signature subunit of IL-27 (156). IL-27 is produced by antigen-presenting cells, such as macrophages and dendritic cells, under pro-inflammatory conditions (155).

4.1.1 Interleukin-27 production by macrophages

LPS as a cell-wall component of gram-negative bacteria is promoting pro-inflammatory conditions. After LPS recognition by TLR4 (157) two signaling pathways are initiated: the myeloid differentiation primary response gene 88 (MyD88)-dependent and the MyD88-independent pathway. This is possible by using the adaptor molecules TIR domain-containing adaptor protein (TIRAP) for the MyD88-dependent pathway and TRIF-related adaptor molecule (TRAM) for the MyD88-independent pathway (158) (159). The MyD88-dependent pathway is activated initially after TLR4 activation by TIRAP binding to the TLR4 receptor. This recruits MyD88 to the plasma membrane (160). After TLR4 activation the transcription factor nuclear factor 'kappa-light-chain-enhancer' of activated B-cells (NFκB) is activated (161) (162). The MAP kinase p38 is activated after LPS stimulation as well (163).

For the MyD88-independent pathway the TLR4-LPS complex is internalized and the molecules TRAM and TIR-domain-containing adapter-inducing interferon-β (TRIF) bind to the intracellular domain of TLR4 in the early endosomes (164) (165). Because of the requirement for prior internalization, this is a more delayed pathway. As a consequence of the TRIF pathway, the transcriptions factors Interferon regulatory transcription factor 3 (IRF3) and IRF7 are activated and translocate into the nucleus (159). The immediately starting MyD88-dependent pathway and the delayed starting MyD88-independent pathway result in a two-step activation of IL-27 after LPS stimulation (166).

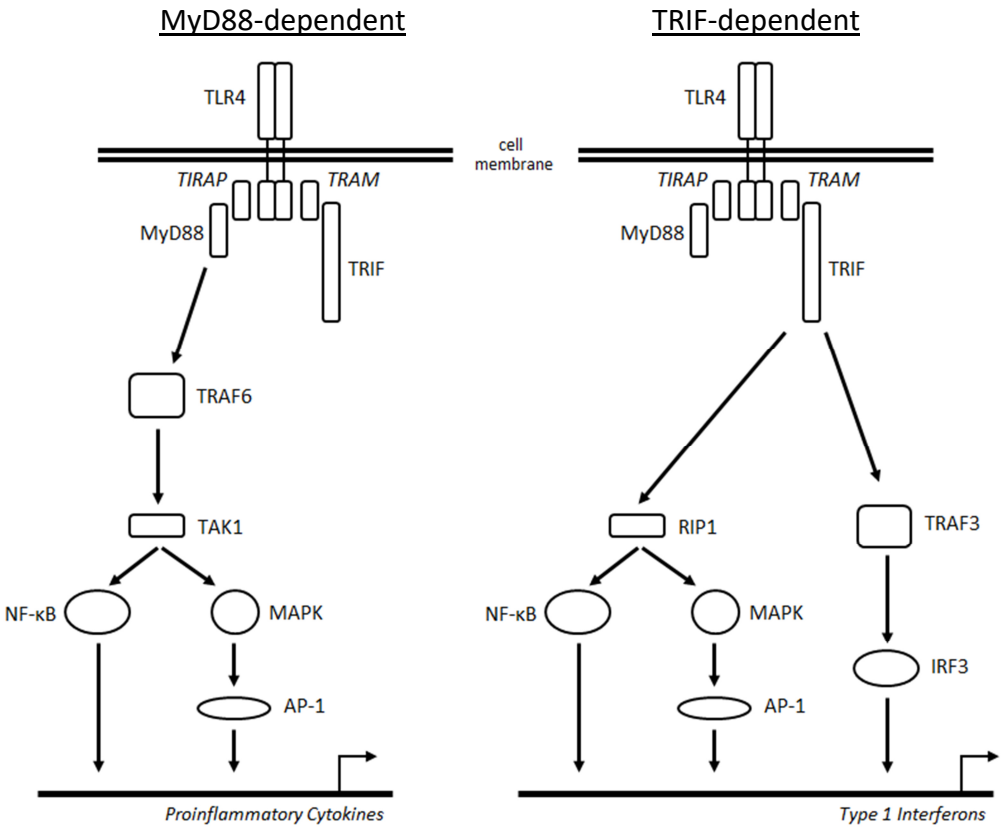

Fig. 3: Overview of MyD88-dependent and TRIF-dependent TLR4 signaling.
TLR = Toll-like receptor, TIRAP = TIR domain containing adaptor protein, TRAM = TRIF-related adaptor molecule, MyD88 = Myeloid differentiation primary response gene 88, TRIF = TIR-domain-containing adapter-inducing interferon-β, TRAF = TIR-domain-containing adapter-inducing interferon-β, TAK1 = Transforming-growth-factor-beta-activated kinase 1, RIP1 = receptor-interacting protein 1, NF-κB = Nuclear factor- κB, MAPK = Mitogen-activated protein kinase, AP-1 = Activator protein 1, IRF3 = Interferon regulatory factor 3. According to Lu et al., 2007 (167).

4.1.2 Biological functions of Interleukin-27

Interleukin-27 (IL-27) is a cytokine that modulates T cell functions. First, it was described as a T helper (Th) 1 promoting cytokine (155). Other pro-inflammatory effects are the clonal expansion of naïve $CD4^+$ T cells and the enhanced production of Interferon-γ (IFN-γ) by naïve T helper cells (155). The inhibition of forkhead box $P3^+$ ($Foxp3^+$) T regulatory cells (Tregs) has also been described (168). In addition, there are also anti-inflammatory roles known for Th1, Th2 and Th17 responses (169). Other anti-inflammatory effects are IL-27-induced production of IL-10 by T cells (169) and the inhibition of IL-2 production (170). IL-27 influences the biology of macrophages (171) and neutrophils (172) as well.

IL-27 is recognized by the heterodimeric IL-27 receptor (IL-27R). This receptor consists of two transmembrane proteins: WSX-1 and glycoprotein gp130 (155) (173). WSX-1 is a class I cytokine receptor with homology in sequence and structure to the β2 chain of the IL-12 receptor (174) (175). The subunit WSX-1 is also known as IL-27 receptor alpha (IL-27RA). For a functional IL-27 signal-transducing receptor both subunits (WSX-1 and gp130) are required (173). One subunit alone is not functional to mediate IL-27-induced signal transduction (173). Following activation the IL-27 receptor signals via phosphorylation of STAT1 and STAT3 pathways (176) (177).

4.2 Transforming growth factor β and signaling

4.2.1 Structure of Transforming growth factor β

Transforming growth factor β (TGFβ) was first described in 1981 due to its capability to stimulate the growth of healthy kidney fibroblast (178). Today, the TGFβ superfamily consists of nearly 30 proteins, such as TGFβ (1, 2, 3) (179) (180) (181), activins, inhibins, bone morphogenic proteins (BMPs) and growth/ differentiation factors (GDFs) (182). The present work is mainly focused on TGFβ1.

TGFβ is synthesized as a precursor protein and directed to the endoplasmatic reticulum. The precursor is made of a large N-terminal part, the latency-associated peptide (LAP) and a smaller C-terminal part, the biological active cytokine TGFβ (183) (184). Both parts, LAP and TGFβ, are disulfide-linked homodimers. The two homodimers are non-covalently linked to form the small latent complex (SLC) (185) (Fig. 4). In the lumen of the endoplasmatic reticulum, the endonuclease furin cleaves the latent TGFβ. After this cleavage, the small latent complex can be released. Before TGFβ can be secreted it has to bind to another protein, the latent TGFβ-binding protein (LTBP). This secreted complex is called large latent complex (LLC) (186).

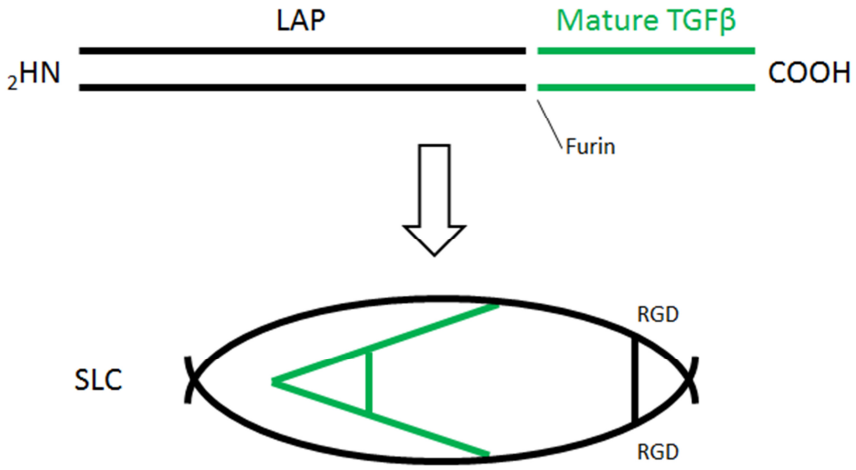

Fig. 4: Structure of the latent TGFβ.
TGFβ consists a large N-terminal part, the latency-associated peptide (LAP, shown in black), and a smaller C-terminal part, the biological active cytokine (shown in green). After furin cleavage, the two disulfide-linked homodimers of the N-terminal LAP and the C-terminal cytokine TGFβ1 are associated non-covalently. The furin cleavage site is indicated. SLC = Small latent complex. According to Travis et al., 2013 (187).

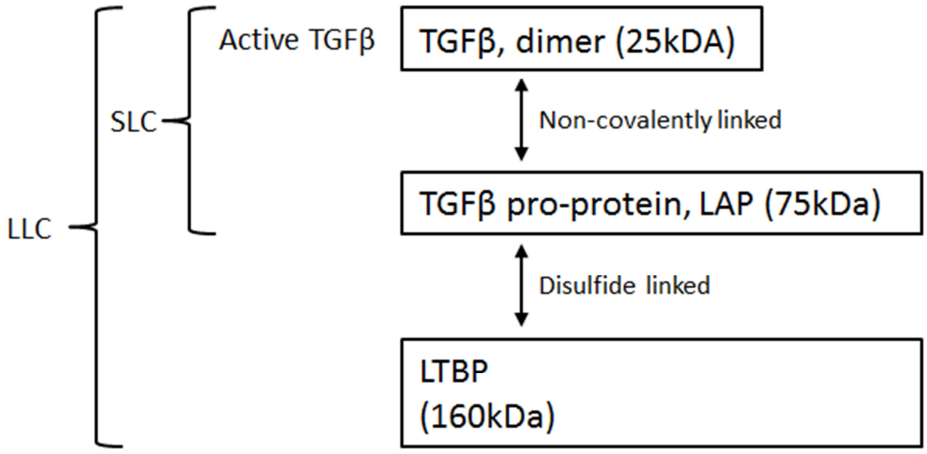

Fig. 5: Active TGFβ1 and the different latent complexes.
LAP = Latency-associated peptide, LLC = Large latent complex, LTBP = Latent TGFβ-binding protein, SLC = SLC = Small latent complex. Aaccording to Taylor et al., 2009 (188).

4.2.2 Activation of Transforming growth factor β

For activation, a RGD (Arg-Gly-Asp) motif in the pro-domain of TGFβ1 is important (189). This is supported by the fact that mice having a mutation in the RGD motif from RGD to RGE (Arg-Gly-Glu) display a similar phenotype as compared to TGFβ1-null mice (190). RGD motifs are mostly found in ligands of integrins and are important

for cell-cell-interactions (191). The RGD motif can be recognized by $\alpha_v\beta_6$ integrins (192). On the other hand, the $\alpha_v\beta_6$ integrin alone is not sufficient for the activation of TGFβ1 (189). A complete activation of TGFβ1 requires the presence of extracellular matrix components (ECM) with associated LTBP as well as the actin cytoskeleton (in addition to to $\alpha_v\beta_6$ integrin) (193) (25) (194). The hypothesis of activating TGFβ1 is that the integrin $\alpha_v\beta_6$ binds to the RGD motif and a traction is given between the ECM-LTBP-pro-domain-TGFβ1 complex and the integrin $\alpha_v\beta_6$. Because of this traction-mediated force, the conformation is changed and the active TGFβ1 can be released (193) (195).

4.2.3 Transforming growth factor β receptors and signaling

There are three known subclasses of TGFβ receptors: TGFβ-receptor I (TbRI), TGFβ-receptor II (TbRII) and TGFβ-receptor III (TbRIII), all three receptors are transmembrane proteins. The receptor TbRIII (also called β-glycan) has been reported to have a decoy function but enhances the access of bound TGFβ to TbRII (196) (197) (198).

In the absence of active TGFβ, the TbRI and TbRII are found as independent receptor pairs on the cell surface (199). For efficient signaling, the activated TGFβ binds to a homodimer of the TbRII. This binding recruits the homodimer of the TbRI to form a hetero-tetrameric complex (200) (201). The receptors TbRI and TbRII are serine/ threonine kinases. TbRII phosphorylates TbRI, which leads to a conformational change. Subsequently, TbRI phosphorylates the downstream signaling proteins such as the protein class *small mothers against decapentaplegic* (Smad) and MAP kinases such as p38 (202) (203).

4.2.4 Small mothers against decapentaplegic proteins (Smads)

Downstream of the activated TbRI the *small mothers against decapentaplegic* (Smad) proteins are the best studied effector molecules within the TGFβ signaling cascade (204) (205) (206). The Smad proteins have different members, which can be divided into three classes: receptor-regulated Smad proteins (R-Smad1-3, 5, 8), common mediator Smad (co-Smad4) and inhibitory Smads (I-Smad6 and 7) (202).

Smad proteins consist of two mother against decapentaplegic (MAD) homology domains: the N-terminal MH1 and the C-terminal MH2. The two domains interact with

each other to inactivate the Smad protein (207) (208) (205). The MH2 domain is important for the receptor binding and, if activated, the MH2 domain mediates the interaction with co-Smad4 and DNA binding proteins, such as transcription factors (209) (210) (211). Only the MH1 domain has DNA binding properties (212). Between these two domains a linker region can be found with several MAP kinase phosphorylation sites. The accumulation in the nucleus of the Smad proteins can be regulated by these phosphorylation sites (213).

The Smads bind to the activated TbRI and get phosphorylated by the TbRI at a C-terminal SS-X-S (Ser-Ser-X-Ser) motif (214) (215) (216). This phosphorylation in enabled by the *Smad anchor for receptor activation* (SARA) which mediates the membrane localization of Smad2 and Smad3 (217) (203). The phosphorylated R-Smads dissociate from the TbRI and form heterogenic complexes with co-Smad4 in the cytosol (218) (219). These heterogenic complexes translocate to the nucleus to regulate the transcription of different genes (205). For example, Smad3 binds the DNA sequence-motif CAGA (212). This short DNA sequence motif governs the need of additional DNA-binding proteins. The I-Smads can inhibit the TGFβ-signaling by binding to the TbRI and thus competitively interfering with the R-Smads. In addition, the I-Smads can disrupt the interaction of Smad3 and co-Smad4 in the cytosol (220) (221).

4.2.5 p38 Mitogen-activated protein kinases

The p38 mitogen-activated protein kinases (MAPK) were identified as a family of 38 kDa proteins (p38) that are rapidly phosphorylated after LPS stimulation (163). The p38 MAPK represents one of a plethora of different MAPK signal transduction pathways Chang and Karin, 2001 (222). Four isoforms have been reported for the p38 MAPK: p38α, p38β, p38γ and p38δ. The isoforms p38α and p38β are mainly important to mediate inflammatory stimuli as well as the activation of the innate immune system (223). The p38 MAPK as a *stress-activated protein kinase (SAPK)* (222) is mainly activated by UV radiation, pro-inflammatory stimuli (such as LPS) and hypoxia (224). Activated p38 MAPK regulates the production of IL-10 (225) (226) and is involved in Tristetraprolin regulation (225) (227).

4.3 Interleukin-10

Interleukin-10 (IL-10) is one of the most important anti-inflammatory cytokines (228). Bosmann et al., 2014 (229), identified IL-10 as a critical suppressive factor for IL-27p28 production in macrophages during sepsis. The immunosuppressive properties of IL-10 are mediated by the IL-10Rα/IL-10Rβ complex (230) (231). After IL-10 binding, the IL-10Rα associates with Jak1, IL-10Rβ and Tyk2. Phosphorylated Jak1 and Tyk2 interact with STAT3, the latter being essential for the regulation of IL-10-dependent genes (230) (232).

IL-10 is produced by different cell types, such as macrophages (233), B cells (234), mast cells (235) and Tregs (122). LPS- stimulated macrophages induce IL-10 expression in a p38 MAPK dependent manner as an autoregulatory feedback loop (236). For B cells, the production of IL-10 is important in modulating antigen presentation and mediating immunosuppression. The major IL-10 producing subset of B cells are the IL-10-producing regulatory B cells (B10 cells) (237). Mast cells have been reported to produce pro-inflammatory mediators during allergy or ultraviolet skin irritation. During this response, mast cells also produce IL-10 to limit leukocyte infiltration, inflammation and tissue damage (235). In addition, IL-10 is a critical mediator of Tregs to control inflammatory responses. On the other hand, myeloid and autocrine-derived IL-10 maintains Foxp3 expression in Tregs (238).

5 Heat Shock Proteins

The first report of heat-inducible proteins was published in 1962 by Ritossa et al. (239). Both, prokaryotes and eukaryotes are capable to express heat shock proteins (Hsps) after heat exposure (240) (241). The expression of Hsps is induced by common cellular stress as well. Under physiological conditions the Hsp70 is weakly expressed but is strongly induced by cellular stress, such as oxidative stress or cytotoxic substances (242).

In expansion to the traditional role of Hsps, these proteins may have unexpected functions during immune responses. Antigen presenting cells, such as dendritic cells (DCs), are presenting fragments of their intracellular proteins via MHC (Major Histocompatibility Complex) molecules to T cells (243). Thus, the dendritic cells also present fragments of Hsps. The circulating T cells recognize the presented Hsp

fragments as self-antigens and are not activated. If the DCs internalize foreign bacteria the Hsps of the bacteria are presented to T cells, which will become subsequently activated (244).

In Tregs, the Hsps have been reported to form complexes with Foxp3 to increase the stability of Foxp3. This may result in an increase of the inhibitory effects of Tregs (245) (246).

6 Tristetraprolin

Tristetraprolin (TTP) is a Cys-Cys-Cys-His (CCCH) zinc finger proteins (247). TTP was discovered as a protein induced by insulin in mouse NIH 3T3 HIR 3.5 cells with a molecular weight of 35kDa (248). TTP was described as a TNF-α and GM-CSF mRNA binding protein. TTP is degrading mRNA by targeting conserved AU-rich elements (AREs) in the 3'-untranslated region (3'-UTR) of the mRNA (248) (249). Binding of TTP leads to deadenylation and mRNA decay (248) (250). A direct relation of TTP and inflammation was found by using TTP knock out (KO) mice. Indeed, TTP KO mice develop a systemic inflammatory response syndrome, which may manifest as rheumatoid arthritis and systemic lupus erythematosus (251).

7 Aims of the present work

The present work sought to characterize cellular and molecular interactions which were regulated by extracellular histones during pulmonary fibrosis. The first aim was to characterize the role and the source of extracellular histones during bleomycin-induced pulmonary fibrosis. So far, extracellular histones were mainly studied in models of acute diseases. To analyze the source and the impact of extracellular histones derived by neutrophils, studies with inducible genetic depletion of $Ly6G^{+}$ neutrophils and studies with histone H2B-eGFP reporter chimeric mice were performed. How extracellular histones modulated the severity of pulmonary fibrosis was studied by blocking antibodies for histone H4. To figure out how NETs and extracellular histones modulated pulmonary fibrosis different mouse strains were used. The influence of platelet-derived TGFβ1 initiated by histones during pulmonary fibrosis was studied by using PF4Cre/$TGF\beta1^{flox/flox}$ mice. How TGFβ1 modulated the impact of macrophages on pulmonary fibrosis was investigated with the help of LysMCre/$TbRII^{flox/flox}$ mice. These experiments were used for macrophage-derived IL-27 during pulmonary fibrosis in dependence of TGFβ1 as well. The role of IL-27 was analyzed by $IL\text{-}27RA^{-/-}$ mice. In this context, novel data was uncovered on the role of T regulatory cells during pulmonary fibrosis.

The second aim was to identify mediators of the TGFβ1-mediated inhibition of IL-27p28 in macrophages. Therefore, blockade of p38 MAPK and IL-10 receptor was performed, or $IL\text{-}10^{-/-}$ mice were used. Promoter binding studies and lentiviral knock down of Smad3 were performed to characterize the influence of Smad3 during the TGFβ1-mediated inhibition of IL-27p28.

II Material and Methods

1 Material

1.1 Consumables

Tab. 4: Used consumables.

Material	Manufacturer
123count eBeads (counting beads)	eBioscience
Bassins (25ml), sterile, RNase/ DNase free	VWR
Bottletop Filter, 0.22µm, 45mm, CA membrane	Corning
Canula 18G, 20G, 21G, 23G, 26G, 30G	Becton Dickinson GmbH
Canula 19G	Braun B. Melsungen GmbH
Canula 20G, blunt end	Becton Dickinson GmbH
Chamber Slide™	Nunc
Cell counting chamber, Neubauer improved	Brand
Cell lifter, 180mm (sterile)	Fisher Scientific GmbH
Cell lifter, 300mm, moveable (sterile)	Biochrom AG
Cell strainer, 100µm (sterile)	Fisher Scientific GmbH
Cell strainer, 30µm (sterile)	Pluriselect
Cell culture Flask 182.5cm² (sterile)	VWR
Cell culture Flask 75cm² (sterile)	Greiner Bio-One GmbH
Cover slips	Menzel-Gläser
Cryo freezing container	Nalgene
Cryo tubes	Thermo Scientific
ELISA plates Nunc Plate Maxisorp	Sigma-Aldrich Aldrich
FACS tubes, 5ml	Sarstedt AG
Filter tips, 10µL (sterile), ART	Molecular BioProducts
Filter tips, 20µl, 200µl, 1000µl (sterile)	Starlab
Glass bottles, measuring cylinders	Schott Duran
Glass measuring beaker	VWR
MACS LS, MD, MS Column	Miltenyi
Mersilk, braided silk, 786G 6/0 G1 1x45cm	Johnson & Johnson MEDICAL
Microtest plates, PS, 96 well, V-bottom (sterile)	Corning BV

Material	Manufacturer
PCR-strips, 0.2ml and lid	Thermo Scientific
PCR-plates, 96 well	Bio-Rad
Perma-Hand ® Silk Suture, 6.0	Ethicon
Petri dish 100x15mm, PS	BD Falcon
Pipette tips 200µl, 300µl, 1000µl	Sarstedt AG
Plate, 96 well (black)	Thermo Scientific
PP-tubes, 15ml, 50ml (sterile)	Greiner Bio-One GmbH
Pre-Separation filter, 30µm	Miltenyi
Primaria cell culture dish, 30x10mm, PS (sterile)	BD Falcon
Reaction tube, 1.5ml	Kalensee, Herbert
Reaction tube, 1.5ml, safe-lock (PCR-clean)	Eppendorf
Reaction tube, 1.5ml, safe-lock, low protein binding	Eppendorf
Reaction tube, 2ml, safe-lock	Eppendorf
Serological Pipettes, 5ml, 10ml, 25ml, 50ml (sterile)	Geiner Bio-One GmbH
Spatula	Sarstedt AG
Steel beads, stainless, 7mm	Qiagen
Syringe "Hamilton", 100µl, Luer	Fisher Scientific GmbH
Syringe filters, CME, 0.22µm (sterile)	Carl Roth
Syringe, 10ml, 20ml, Luer	Becton Dickinson GmbH
Syringe, 1ml, Luer	Becton Dickinson GmbH
Syringe, 2ml, Luer	Braun B. Melsungen GmbH
TC-treated plates, 24 well (sterile)	CORNING BV
Three-way-stop adaptor (BD Connecta)	Becton Dickinson GmbH

1.2 Chemicals and reagents

Tab. 5: Used chemicals and reagents.

Chemical/Reagent	Manufacturer
10x PBS	Thermo Scientific
β-Mercaptoethanol, 50mM	Gibco
Acetic acid ($C_2H_4O_2$), 99.7%, 2N	Sigma-Aldrich
Agarose, LE	Biozym

Chemical/Reagent	Manufacturer
Albumin fraction V, >98%	Carl Roth
Bepanthen Eye and Nose Ointment	Bayer
BD Cytofix/Cytoperm	BD
BD Cytofix	BD
BD Perm/Wash (10x)	BD
BD Perm Buffer III	BD
BD Phosflow Perm Buffer	BD
Bovine serum albumin in DPBS, 35% (sterile)	Carl Roth
Calcium chloride dihydrate, ≥99 %, Ph.Eur.	Carl Roth
Carbonate-Bicarbonate Buffer	Sigma-Aldrich
Casein sodium salt	Sigma-Aldrich
Citrate (Sodiumcitrate), 3.13%	Eifelfango®
Desderman	Schülke & Mayr GmbH
Difco Thioglycollate Medium without dextrose	BD Biosciences
Dimethyl Sulphoxide (DMSO)	Sigma-Aldrich
Diphteria Toxin (*C. diphtheria*)	Millipore
Distilled water, Rnase and Dnase free	Gibco
DNA Ladder (100bp)	NEB
EDTA, 0.5M (sterile)	Promega
EGTA, ≥99%, p.a.	Carl Roth
Ethanol (C_2H_6O), 99.8% p.a.	Carl Roth
Flow Count Fluorospheres	BD Biosciences
Formaldehyde, 16%	Thermo Scientific
Formaldehyde, 37% (mol. biol. gr.)	AppliChem
Foxp3 Fix/Perm Buffer (4x)	BioLegend
Foxp3 Perm Buffer (10x)	BioLegend
GelRed (10,000x)	Biotium
Glucose, D(+)	Carl Roth
GolgiPlug, Brefeldin A (1000x)	BD Biosciences
GolgiStop, Monensin (1000x)	BD Biosciences
HEPES, 1M	Gibco
HEPES, 99.5%	Roth
Hydrochloric acid (HCl), 1M	AppliChem

Chemical/Reagent	Manufacturer
Isofluran (Forane), 100%	Abbott
Ketamin (50mg/ml)	hameln
Oligofectamin™ Reagent	Invitrogen
One comp eBeads	eBioscience
Penicillin-Streptomycin, liquid (10,000U penicillin, 10mg streptomycin per ml)	Invitrogen
pH-indicator strips, pH 0-14	Merck Millipore
Phenylmethylsulfonyl fluoride (PMSF)	AppliChem
Potassium chlorid (KCl), 99.5%	Sigma-Aldrich
ProLong® Gold + DAPI	Life Technologies
Propan-2-ol, 99.8%	Sigma-Aldrich
Rnase away	Molecular Bioproducts
Rompun (Xylazin), 2%	Bayer
Sodium azide (NaN_3)	Sigma-Aldrich
Sodium hydroxide (NaOH), 2N	Merck
Sodium hypochlorite (NaClO), 12%	Carl Roth
Sulfuric acid (H_2SO_4), 97%, 18M	AppliChem
TAE Buffer (50x)	Applichem
TE Buffer, pH 8.0	Ambion
Terralin liquid	Schülke & Mayr GmbH
TMB substrate	eBioscience
Tris hydrochlordide	AppliChem
Trypan Blue solution, 0.4%	Sigma-Aldrich
Tween® 20	Sigma-Aldrich

1.3 Kits

Tab. 6: Used kits.

Product	Manufacturer
Bio-Plex Pro™ cell signaling reagent kit	Bio-Rad
Bio-Plex Pro™ mouse cytokine group I	Bio-Rad
$CD4^+CD25^+$ Regulatory T Cell Isolation Kit, mouse	Miltenyi
cDNA Reverse Transcription Kit	Applied Biosystems

Product	Manufacturer
Cell Death Detection ELISA^{PLUS}	Roche
Collagen Assay, Collagen I,V (SIRCOL^{TM})	Biocolor
Endotoxin Quantification Kit (Pierce® LAL)	Thermo Scientific
InnuPREP RNA Mini Kit	Analytik Jena
iQ SYBR®Green Mastermix	Bio-Rad
Magna ChIP Kit	Millipore
Maxima Hot Start Green PCR Master Mix (2x)	Thermo Fisher
Mouse IL-10 ELISA	R&D Systems
Mouse Albumin ELISA	Biomol
Mouse IL-27p28/IL-30 ELISA	R&D Systems
Mouse IL-35 ELISA	BioLegend
Mouse TGFβ1 ELISA	R&D Systems
RNeasy Mini Kit	Qiagen

1.4 Media and buffers

Tab. 7: Used media and buffers.

Medium/ Buffer	Constitution/ Manufacturer
Albumin coating Buffer	0.05M Carbonate-Bicarbonate (pH 9.6)
BMDM-Medium	50% RPMI 1640, 30% L-cell supernatant, 20% FCS, 1% P/S
ELISA Wash Buffer	PBS, 1% Tween20
FACS-Buffer	PBS, 1% FCS, 0.09% NaN_3
Fetal bovine serum, different Lots (tested)	Sigma-Aldrich/Biozym
Freeze-Medium	50% cell specific medium, 40% FCS, 10% DMSO
HBSS (1x), w/o $CaCl_2$, w/o $MgCl_2$	Gibco
L929 cell-Medium	RPMI 1640, 10% FCS, 1% P/S
Macrophage-Medium	RPMI 1640, 0.1% BSA, 1% P/S
MACS-Buffer	PBS, 0.5% BSA, 2mM EDTA
PBS (1x), w/o $CaCl_2$, w/o $MgCl_2$	Gibco
PBS (1x), $CaCl_2$, $MgCl_2$	Gibco
RAW-Medium	RPMI 1640, 10% FCS, 1% P/S

Medium/ Buffer	Constitution/ Manufacturer
Reagent Diluent	PBS, 1% BSA
RPMI 1640, [+] L-Glutamin, [+] 25mM HEPES	Gibco
T cell-Medium	RPMI 1640, 10% FCS, 1% P/S
TGFβ-Blocking Buffer	PBS, 5% Tween20
TGFβ-Reagent Diluent	PBS, 1.4% BSA, 0.05% Tween20
Trypsin-EDTA, 0.25%	Gibco
Tyrode's buffer	137mM NaCl, 2mM KCl, 12mM $NaHCO_3$, 0.3mM NaH_2PO_4 x $2H_2O$, 5.5mM Glucose, 5mM HEPES, 0.35% BSA

1.5 Agonists and Antagonists

Tab. 8: Used Agonists and antagonists with typical used amounts/concentrations.

Agonist/Antagonist	Amount/Concentration	Manufacturer
5' ppp-dsRNA	200ng	InvivoGen
Actinomycin D	4µM	Sigma-Aldrich
BIRB 796	50nM	Calbiochem
Bleomycin (A_2 + B_2), Bleomedac®	0.02-0.03mU	Medac GmbH
Histones (for cell culture, endotoxin n.d.)	10µg/ml	Roche
Histones (for Aggregometry)	50µg/ml	Sigma-Aldrich Aldrich
LPS (E.coli 0111:B4)	100ng/ml	Sigma-Aldrich Aldrich
LTA	10µg/ml	InvivoGen
PH-797804	10nM	Selleckchem
Poly(I:C)	1µg/ml	InvivoGen
Puromycin	5µM	Sigma-Aldrich
recombinant human TGFβ1	10ng/ml	PeproTech
recombinant murine IFN-γ	10ng/ml	PeproTech
recombinant murine IL-10	10ng/ml	PeproTech
recombinant murine IL-2	20ng/ml	PeproTech

Agonist/Antagonist	Amount/Concentration	Manufacturer
SB203580	10µM	Jena Bioscience
SB431542	1-20µM	Tocris
Thrombin (Endotoxin: <1.0 EU per 1µg)	100ng/ml	R&D Systems
Zymosan	10µg/ml	InvivoGen

1.6 Antibodies

1.6.1 Flow cytometry antibodies

Tab. 9: Used antibodies for flow cytometry.

Description	Isotype	Clone	Manufacturer
anti-mouse Smad3 (rabbit)	Rabbit IgG	E.980.9	Thermo Sc.
APC Isotype Ctrl	Rat IgG2a,κ	RTK2758	BioLegend
APC anti-mouse CD4	Rat IgG2a,κ	RM4-5	BioLegend
APC anti-mouse F4/80	Rat IgG2a,κ	BM8	BioLegend
APC anti-mouse Ly6G	Rat IgG2a,κ	1A8	BioLegend
APC rat IgG2a κ Isotype Control		eBR2a	eBioscience
APC anti-mouse/rat IL-17A	Rat IgG2a,κ	eBio17B7	eBioscience
eFluor660 anti-Foxp3	Mouse IgG1,κ	150D/E4	eBioscience
FITC Isotype Control	Rat IgG2a,κ	eBR2a	eBioscience
FITC CD4	Rat IgG2a,κ	RM4-5	eBioscience
FITC mouse IgG2b Isotype Control			Abcam
Pacific Blue Isotype Ctrl	Hamster IgG	HTK888	BioLegend
Pacific Blue anti-mouse CD3ε	Hamster IgG	145-2C11	BioLegend
Pacific Blue Isotype Ctrl	Rat IgG2a,κ	RTK4530	BioLegend
Pacific Blue anti-mouse/human CD11b	Rat IgG2b,κ	M1/70	BioLegend
Pacific Blue anti-CD4	Rat IgG2b k	RM4-5	BioLegend
PE F(ab')2 donkey anti-rabbit IgG		polyclonal	eBioscience
PE Isotype Ctrl	Rat IgG2a,κ	RTK2758	BioLegend
PE Isotype Ctrl	Rat IgG2a,κ	eBR2a	eBioscience
PE anti-mouse IL-27p28	Mouse IgG2a,κ	MM-27-7B1	eBioscience
PE Isotype Ctrl	Mouse IgG1,κ	MOPC-21	BioLegend

Description	Isotype	Clone	Manufacturer
PE anti-mouse/rat/human Foxp3	Mouse IgG1,κ	150D	BioLegend
PE anti-mouse pSmad2 (pS465/pS467)/ pSmad3 (pS423/pS425)	Mouse IgG1,κ	O72-670	BD
V450 Isotype Control	rat IgG1,κ	R3-34	BD
V450 rat anti-mouse IFN-γ	Rat IgG1,κ	XMG1.2	BD
TruStain fcX (anti-mouse CD16/32)	Rat IgG2a,λ	93	BioLegend

1.6.2 Chromatin Immunoprecipitation antibodies

Tab. 10: Antibodies used for Chromatin Immunoprecipitation.

Description	Isotype	Clone	Manufacturer
anti-mouse Smad3	rabbit IgG	polyclonal	Abcam
anti-histone H3	rabbit IgG	D2B12	Cell Signaling
normal rabbit IgG		#2729	Cell Signaling

1.6.3 Stimulation-, inhibition- and ELISA-antibodies

Tab. 11: Antibodies used for stimulation, inhibition and ELISA.

Description	Isotype	Clone/ Lot	Source
anti-histone H3 (citrulline R2 + R8 + R17)	IgG, polyclonal	ab5103	abcam
anti-histone H4, MHIS1952	IgG2		Charles Esmon
mIgG2aK1753			Charles Esmon
anti-IL10R	rat IgG1	1B1.3a	Markus Radsak
rat IgG1			Markus Radsak
anti-mouse CD3ε, LEAF™	A. Ham. IgG	145-2C11	BioLegend
anti-mouse CD28, LEAF™	S. Ham. IgG	37.51	BioLegend

1.7 Primers

Murine sequence-specific oligonucleotides (primers) were synthesized by Invitrogen™.

Tab. 12: Used Primers for qPCR.

Target gene	Sequence (5‘-3‘)
collagenI, V_fo	CCAGAGTGGAACAGCGATTAC
collagenI, V_re	GCAGGCGAGATGGCTTATTT
ebi3_fo	GGCTGAGCGAATCATCAA
ebi3_re	GAGAGAGAAGATGTCCGGGAA
ebi3_prom_fo	CAGGTTCCCTGTGTGAGTCC
ebi3_prom_re	GCTCTGTGGCTCTGTTCCTT
gapdh_fo	TACCCCCAATGTGTCCGTCGTG
gapdh_re	CCTTCAGTGGGCCCTCAGATGC
il-10_fo	AGACACCTTGGTCTTGGAGC
il-10_re	TTTGAATTCCCTGGGTGAGA
il-17a_fo	GGTCAACCTCAAAGTCTTTAACTC
il-17a_re	TTAAAAATGCAAGTAAGTTTGCTG
il-27p28_fo	GGCCATGAGGCTGGATCTC
il-27p28_re	AACATTTGAATCCTGCAGCCA
il-27p28_prom_fo	CCCTCTGGGAAGGGAAATTA
il-27p28_prom_re	CCTCTGTGTGCAGCCATCT
smad3_fo	GGATGGTCGGCTGCAGGTGTCC
smad3_re	TGTTGAAGGCAAACTCACAGAGC
ttp_fo	TTATGTTCCAAAGTCCTCCGA
ttp_re	CCATGGATCTCTCTGCCATC

1.8 Sequences of shRNA and MISSION® pLKO.1-puro vector map

Tab. 13: Sequences of the different used shRNAs.

Cell line	Sequence (5'-3')
Smad3/shRNA1	CCGG**CCCATGTTTCTGCATGGATTT**CTCGAG **AAATCCATGCAGAAACATGGG**TTTTTG
Smad3/shRNA2	CCGG**GCACACAATAACTTGGACCTA**CTCGAG **TAGGTCCAAGTTATTGTGTGC**TTTTTG
Smad3/shRNA3	CCGG**CCTTACCACTATCAGAGAGTA**CTCGAG **TACTCTCTGATAGTGGTAAGG**TTTTTG
Smad3/shRNA4	CCGG**CTGTCCAATGTCAACCGGAAT**CTCGAG **ATTCCGGTTGACATTGGACAG**TTTTTG
Smad3/shRNA5	CCGG**CATCCGTATGAGCTTCGTCAA**CTCGAG **TTGACGAAGCTCATACGGATG**TTTTTG
nonMammalian/shRNA	CCGG**CAACAAGATGAAGAGCACCAA**CTCAG **TTGGTGCTCTTCATCTTGTTG**TTTTTG

The sense and antisense area of the shRNA is shown in bolt. The loop sequence is underlined.

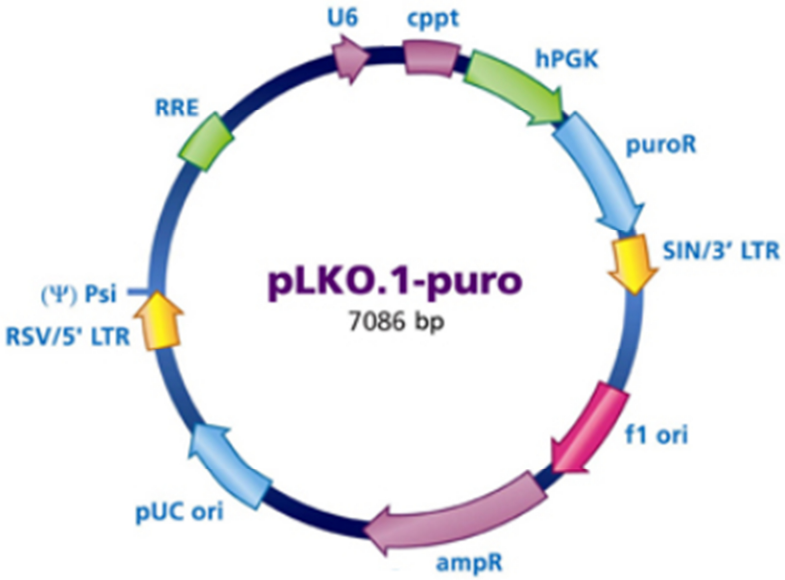

Fig. 6: MISSION® pLKO.1-puro vector map.
The specific shRNA is inserted at the indicated position (red line). The total size varies with the different shRNA. Source: http://www.sigmaaldrich.com/life-science/functional-genomics-and-rnai/shrna/library-information/vector-map.html (last visited on December, 12th 2016).

Tab. 14: Abbreviations used within the vector map.

Name	Description
U6	U6 Promoter
cppt	Central polypurine tract
hPGK	Human phosphoglycerate kinase eukaryotic promoter
puroR	Puromycin resistance gene for mammalian selection
SIN/3' LTR	3’ self-inactivating long terminal repeat
f1 ori	f1 origin of replication
ampR	Ampicillin resistance gene for bacterial selection
pUC ori	pUC origin of replication
5’ LTR	5’ long terminal repeat
Psi (ψ)	RNA packaging signal
RRE	Rev response element

1.9 Cell lines

Tab. 15: Commercial cell lines in this work.

Organism of all used cell lines was *Mus musculus*.

Cell line	Cell type	ATCC® number
RAW264.7	macrophage; Abelson murine leukemia virus transformed	ATCC® TIB-71™
L929	fibroblast	ATCC® CRL-2648™
MH-S	macrophage (alveolar)	ATCC® CRL-2019™

Tab. 16: Generated cell lines in this work.

Cell lines were generated as described in Chap. II-2.3.1.

Cell line	Clone	Product number
RAW264.7-Smad3/shRNA1	TRCN0000089023	SHCLNV
RAW264.7-Smad3/shRNA2	TRCN0000089024	SHCLNV
RAW264.7-nonMammalian/shRNA		SHC002V

1.9 Mice

C57BL/6J

C57BL/6J mice were purchased from The Jackson Laboratory, initially. For the experiments the mice were bred in house or ordered directly from Harlan or Janvier.

IL-27RA$^{-/-}$

IL-27RA$^{-/-}$ (B6N.129P2-Il27ratm1Mak/J, C57BL/6NJ background, (252) mice were obtained from The Jackson Laboratory, backcrossed for one generation to C57BL/6J and bred at the TARC Facility, Johannes Gutenberg University, Mainz. C57BL/6J mice were used as control mice.

PF4Cre/TGFb1$^{flox/flox}$

Pf4cre$^{+/-}$ (C57BL/6-Tg(Pf4-cre)Q3Rsko/J, #008535, C57BL/6J background) mice and TGFβ1$^{flox/flox}$ (Tgfb1tm2.1Doe/J, # 010721, 129S6/SvEvTac background) mice were purchased from The Jackson Laboratory (253) (254). These Cre-lox mice were crossed initially for two generations to obtain the mouse strain PF4Cre/TGFβ1$^{flox/flox}$ and littermates were used as control animals.

LysMcre/TbRII$^{flox/flox}$

The strain LysMcre/TbRII$^{flox/flox}$ was kindly provided by Prof. Dr. S. Eming, University of Cologne with permission of Dr. J. Roes, University College London, United Kingdom for breeding at the TARC Facility, Johannes Gutenberg University, Mainz (255). Originally, LysMcre$^{+/-}$ mice (Lyz2tm1(cre)Ifo, C57BL/6J background) had been crossed with TbRII$^{flox/flox}$ mice (Tgfbr2tm1Roes, C57BL/6J background) mice to obtain the LysMcre/TbRII$^{flox/flox}$ genotype. Littermates were used as control animals.

B6.IL-10$^{-/-}$

B6.IL-10$^{-/-}$ (B6.129P2- Il10^{tm1Cgn}, C57BL/6J background) mice were kindly provided by Prof. Dr. M. Radsak, University Medical Center, Mainz (256). C57BL/6J mice were used as control animals.

IL-17DKO

The IL-17-double-KO mice (IL17af$^{-/-}$, C57BL/6J background) were kindly provided by Prof. Dr. A. Waismann, University Medical Center, Mainz with permission of Prof. Dr. I. Prinz, Hannover Medical School (257). C57BL/6J mice were used as control animals.

H2BeGFP

H2BeGFP (B6.Cg-Tg(HIST1H2BB/EGFP)1Pa/J, C57BL/6J background) mice were purchased from The Jackson Laboratory and were bred at the TARC Facility, Johannes Gutenberg University, Mainz with C57BL/6J mice to generate heterozygous mice (258). C57BL/6J mice were used as control animals.

Ly6GCre/H2BeGFP

Ly6GCre-tdTomato mice (C57BL/6J background) were provided by Prof. Dr. A. Waismann, University Medical Center, Mainz with permission of Prof. Dr. M. Gunzer, University Duisburg-Essen and crossed at the TARC Facility, Johannes Gutenberg University, Mainz with H2BeGFP mice (B6.Cg-Tg(HIST1H2BB/EGFP)1Pa/J, C57BL/6J background) (258) (259). Littermates were used as control animals.

Ly6GCre/iDTR

Ly6GCre/iDTR (C57BL/6J background) mice were provided by Prof. Dr. A. Waismann, University Medical Center, Mainz with permission of Prof. Dr. M. Gunzer, University Duisburg-Essen (259) (260). As controls we used littermates which were also provided by Prof. Dr. A. Waismann.

$TTP^{-/-}$

$TTP^{-/-}$ (TTP(-/-), C57BL/6J background) mice were provided by Prof. Dr. H. Kleinert from the University Medical Center, Mainz. As controls littermates ($TTP^{+/+}$) were used which were also provided by Prof. Dr. H. Kleinert (251).

$PAD4^{-/-}$

$PAD4^{-/-}$ (B6(Cg)-Padi4tm1.2Kmow J) mice were provided by Prof. Dr. W. Ruf from the University Medical Center, Mainz (261). C57BL/6J mice were used as control animals.

All mice were housed under specific pathogen-free conditions with normalized temperature and humidity and dry food pellets and water *ad libitum* in a 12h light/dark cycle at the TARC animal facility of the Johannes Gutenberg University, Mainz. The housing and the handling of the mice was in accordance with FELASA and GV-SOLAS. All animal experiments were performed in compliance with the German animal protection law (TierSchG BGBI. I S. 1206, 1313; 18.05.2006/ BGBl. I S. 2178; 03.12.2015) under the permit number 23 177-07/ G12-1-038.

1.10 Instruments

Tab. 17: Used instruments.

Description	Manufacturer
Animal Irradiator, Type OB 58-BA	Buchler
Aggregometer, APACT 4S PLUS	DiaSys Greiner
Bioanalyzer	Agilent
Bio-Plex 200 System	Bio-Rad
Bio-Plex Pro II Wash Station	Bio-Rad
Brightfield camera, SC30/CMOS	Olympus
Canto II flow cytometer	BD
Cell culture incubators	Memmert/ Binder
Cell Separation Magnet	BD
Centrifuge, 5417 C/R	Eppendorf
Centrifuge, Allegra X-15R	Beckman Coulter
Centrifuge, Rotanta/RP	Hettich
Fluorescence Mircroscope	Carl Zeiss
Fluoroskan Ascent FL	Thermo
Gel Doc EZ Imager	Bio-Rad
Hematology Diagnostics, KX-21N	Sysmex
Lightmicroscope, inverted IX73	Olympus
MACS stand	Miltenyi
Magnetic Mixer, MTS 2/4	IKA®
Mastercycler ProS	Eppendorf
Nano Drop 2000c	Thermo Scientific
Nutating Mixer	VWR
Octo-MACS	Miltenyi
Opsys MR	Dynex Technologies
Orbital Shaker	VWR
pH-meter, HI2211 pH/ORP Meter	HANNA instruments
Pipettes, Accurpette	VWR
Pipettes	Gilson
Power Supply, Power Pac™ HC	Bio-Rad
Quattro-MACS	Miltenyi

Description	Manufacturer
Qubit Fluorometer	Thermo Scientific
RCT classic IKAMAG®	VWR
Rotater Mixer Multi-1	Star Lab
Scale, AY612	Sartorius
Scale, CPA1003P	Sartorius
Sonicator, Q700	Qsonica
Thermal cycler C1000	Bio-Rad
Thermomixer comfort	Eppendorf
Tissue Lyser II	Qiagen
Vortex Genie 2	Scientific Industries
Waterbath	Julabo
Workbench, HERA safe	Thermo Scientific

1.11 Software

Tab. 18: Used software.

Description	Software
Aggregometry analysis	APACT 4S PLUS, v1.21c
Bio-Plex analysis	Bio-Plex Manager 6.1
ELISA analysis	Revelation G3.2
Flow cytometry analysis	FlowJo 10.0.00003
Fluorometer analysis	Ascent Software 2.6
GraphPad Prism 6	GraphPad Software Inc
Microscopy, brightfield	cellSens Dimension 1.13
qPCR analysis	CFX Manager 3.1
Fluorescence confocal microscope analysis	ZENLight 2009

2 Methods

2.1 *In vitro* and *ex vivo* models

All *in vitro* and *ex vivo* experiments were performed as independent biological replicates for a minimum of three times each typically performed in duplicate wells (technical replicates).

2.1.1 Bone marrow derived macrophages

Bone marrow derived macrophages (BMDMs) were obtained from the isolated bone marrow of the femurs and tibias of mice. Briefly, the femurs and tibias were removed and freed from the soft tissue. After separating femur and tibia from each other, the bones were placed into ice-cold PBS without Ca^{2+} and Mg^{2+}.

The following steps were made under sterile working conditions. First, the isolated bones were rinsed in Terralin and afterwards rinsed in PBS without Ca^{2+} and Mg^{2+}. After cutting both ends of each bone with a bone cutter, the bone marrow was flushed out and filtered with ice-cold PBS without Ca^{2+} and Mg^{2+} through a 100µm mesh into a 50ml tube. After centrifugation for 5min at 300g (4°C) the supernatants were discarded and the cells were resuspended in pre-warmed L929 cell conditioned BMDM-Medium. For differentiation, the cells were seeded in 10ml BMDM-Medium in 10cm petri dishes and incubated for 7 days at 37°C, 5% CO_2. On day 4, the medium was refreshed with 10ml fresh pre-warmed L929 cell conditioned BMDM-Medium. After 7 days, the supernatants were discarded and the plates were washed with pre-warmed PBS without Ca^{2+} and Mg^{2+}. In the next step, the cells were detached from the plates by using a cell scraper in pre-warmed PBS (without Ca^{2+} and Mg^{2+}, 0.5mM EDTA) and were collected in a 50ml tube. After centrifugation (300g for 5min, RT), the cells were resuspended in pre-warmed Macrophage-Medium. For the experiments the BMDM were seeded in pre-warmed Macrophage-Medium. The purity of cell preparations was confirmed by flow cytometry (≥95% $F4/80^+CD11b^+$ macrophages).

2.1.2 Polarized macrophages

BMDM were generated as described in Chap. II-2.1.1. $5x10^5$ cells were seeded (day 0) and the medium was changed (day 1) with incubation at 37°C, 5% CO_2. On day 1, 10ng/ml IFNγ was added for 6h (classically activated macrophages, M1). After 6h, the medium was changed again and the M1 polarized macrophages were stimulated

for the experiment. On day 1, 10ng/ml IL-4 was added over night to obtain alternatively activated macrophages (M2) (262).

2.1.3 Peritoneal elicited macrophages

Peritoneal elicited macrophages (PEM) were generated by intraperitoneal (i.p.) injection of 1.5ml thioglycollate 2.4% (w/v) 4 days prior to the experiment. At the day of the experiment the PEM were collected by flushing the peritoneal cavity with 10ml HBBS. After centrifugation for 5min at 300g rpm (4°C), the pellet was resuspended in pre-warmed Macrophage-Medium and $5x10^5$/well/ml cells were incubated at 37°C, 5% CO_2. The purity of cell preparations was confirmed by flow cytometry (≥85-90% $F4/80^+CD11b^+$ macrophages).

2.1.4 Peritoneal elicited neutrophils

Peritoneal elicited neutrophils (PENs) were generated by i.p. injection of 1ml casein (9% w/v in PBS without Ca^{2+} and Mg^{2+}). After 20h another i.p. injection of 1ml of casein was performed and 3h later mice were sacrificed and PENs were isolated. To isolate the cells, the peritoneal cavity was flushed with 10ml PBS (without Ca^{2+} and Mg^{2+}). The cell suspension was transferred and filtered through a 30µm mesh and centrifuged at 300g for 5min (4°C). The cell pellet was resuspended in pre-warmed Macrophage-Medium and seeded for the experiment. The purity of cell preparations was confirmed by flow cytometry (≥95% $Ly6G^+CD11b^+$ neutrophils).

2.1.5 Primary alveolar Macrophages

Primary alveolar macrophages (AM) were collected by bronchoalveolar lavage (BALF). Briefly, a 20G needle (blunt end) was inserted into the trachea. The 20G needle was attached to a three-way-stop-adapter and a 10ml syringe. To collect the primary alveolar macrophages, the lungs were flushed with 1ml PBS + 0.5mM EDTA 10 times. To collect the cell suspension, the three-way-stop-adapter was used to transfer the cell suspension in a second syringe. The BALF was centrifuged for 5min at 300g (4°C). The cell pellet was resuspended, counted and seeded in 24-well plates in pre-warmed Macrophage-Medium (229) (263) (264).

2.1.6 Platelet isolation (washed platelets)

The mice were anesthetized with ketamine and xylazine (100mg/kg body weight in PBS) by i.p. injection. The blood was carefully drawn by intracardial blood collection in using a 16G needle and syringe with 170 µl citrate as anticoagulant. The blood

was transferred to FACS-tubes and 2µl EGTA was added per 1ml blood. Prewarmed Tyrode's Buffer (pH 6.5, 37°C) was used to adjust the sample volume to 2ml. After centrifugation for 10min at 100g at RT (without break), the platelet rich plasma (PRP) was collected and transferred into new FACS-tubes. The volume was adjusted to 4 ml with prewarmed Tyrode's Buffer (pH 6.5, 37°C) and the platelets were incubated for 5min at 37°C. Next, the platelet suspensions were centrifuged for 10min at 300g at RT (with break) and the supernatants were discarded. The pellets were resuspended in 500–1000µl prewarmed Tyrode's Buffer (pH 7.4, 37°C) and the platelets were counted with the help of a Hematology Diagnostics System (KX-21N, Sysmex). Finally, the platelets were adjusted to a concentration of $2x10^8$ platelets/ml with prewarmed Tyrode's Buffer (pH 7.4, 37°C) and 1mM $CaCl_2$ was added to regain platelet function.

2.1.7 Platelet Aggregometry (Born)

The light transmission aggregometry (first described by Born) is a method to measure the aggregation of platelets *ex vivo*. A light beam is passing the platelet suspension and the light transmission is measured. The detectable light transmission increases with the degree of platelet aggregation.

As samples, 200µl of a platelet suspension ($2x10^8$ platelets/ml) was transferred into a cuvette and platelet agonists (e.g. thrombin, histones) were added by pipetting followed by measurements for 10min at 37°C (APACT 4S PLUS, DiaSys Greiner).

2.1.8 Confocal Fluorescence Microscopy of NETs

To study the generation of NETs, PENs (Chap. II-2.1.4) of the mouse strain Ly6GCre/H2BeGFP were isolated and seeded at 100,000 cells per 300µl pre-warmed Macrophage-Medium in a Chamber Slide. After 15min incubation at 37°C, 5% CO_2, the cells were stimulated for the individual experiments and incubated for 4h at 37°C, 5% CO_2. At the end of the experiments, a final concentration of 2% formaldehyde was added to the medium followed by incubation for 20min in the dark at RT. Next, the supernatants were removed and the cells were carefully washed 2x with 200µl PBS without Ca^{2+} and Mg^{2+}. Afterwards, the chamber cases were removed and the fixed cells were mounted in ProLong® Gold in the dark for a minimum of 24h. The fluorescence was detected by confocal fluorescence microscopy (Zeiss LSM 710-NLO) at the core facility of the University Medical Center, Mainz with the help of Dr. D. Strand.

2.1.9 Bone marrow transplantation

To transplant bone marrow, the mice were irradiated with γ-rays. In this work, cesium (^{137}Cs) was used as the γ-ray source. The mice were received fractionated irradiation 2x with 6.5Gy separated by 3h. This irradiation protocol has been evaluated for effective depletion of alveolar macrophages (265). Subsequently, recipient mice were transfused with 5x10^6 cells of bone marrow in 200µl 0.9% NaCl by tail vein injection. Here, freshly isolated or thawed bone marrow from donor mice was used for transplantation.

For the next 5 weeks, mice were provided with acidified water (pH 3) ad libitum to reduce the side effects of irradiation. After 5 weeks a sufficient engraftment of donor bone marrow was confirmed by flow cytometry or by qPCR analysis (Chap. II-2.5.4) for the specific donor genotype.

2.1.10 Naïve regulatory T cells

Naïve Tregs were isolated from spleens of untreated mice. The spleen was isolated and smashed by using a 100µm mesh and the plunger of a 2ml syringe. The mesh was rinsed with ice-cold MACS-Buffer. The cell suspension was filtered with a 30µm mesh. Afterwards, the cell suspension was centrifuged at 300g for 10min (4°C). To purify the Tregs in the cell suspension the next steps were done as described in Chap. II-2.3.2 ($CD4^+CD25^+$ Regulatory T Cell Isolation Kit, Miltenyi). After the purification, the cells were counted and seeded in T cell-Medium until further use.

2.2 Cell culture and cell culture methods

2.2.1 L929 cell conditioned Medium

L929 cells were cultivated in T175 flasks at 37°C, 5% CO_2 until 80%-90% confluency was reached. The cells were passaged 1:10 twice weekly by washing with prewarmed PBS without Ca^{2+} and Mg^{2+} follwed by treatment with 2ml prewarmed 0.25% Trypsin-EDTA. To obtain the L929 cell conditioned medium, the cells were grown for five days after passaging, the medium collected, sterile filtered (0.22 µm) and stored at -80°C.

2.2.2 RAW264.7 macrophages

RAW264.7 macrophages were cultivated in RAW-Medium in T175 flasks at 37°C, 5% CO_2. Two times per week the cells were splitted 1:10. The cells were washed with 10ml pre-warmed PBS without Ca^{2+} and Mg^{2+}. Next, 2ml pre-warmed PBS (without

Ca^{2+} and Mg^{2+}, 0.5mM EDTA) was added and the cells were detached from the flask by using a cell scraper. The RAW264.7 macrophage cell line was used for a maximum of 15 passages.

2.2.3 Counting of cells

Suspensions of cells were counted using a cell counting chamber (Neubauer improved). 10µl of the cell suspensions were added to 40µl Trypan Blue solution and 10µl of this mixture was added to the cell counting chamber. The cells in the 4 corner squares were counted and total cell concentrations were calculated by applying the following formula:

$$\frac{cell\ count}{4} \text{ x 5 (dilution factor) x volume cell suspension (ml) x 10,000} = \frac{cells}{ml}$$

2.2.4 Freezing of cells

Cells were cultured in a T175 flask to a confluency of 80-90% (logarithmic growth phase and most suitable for freezing). The medium was removed and the cells were washed with pre-warmed PBS without Ca^{2+} and Mg^{2+}. Then, the cells were detached with a cell scraper in 2ml PBS (without Ca^{2+} and Mg^{2+}, 0.5mM EDTA) followed by a centrifugation step at 300g for 5 min (4°C). The pellet was resuspended in ice-cold freezing medium and 1ml was aliquoted into pre-cooled cryo-tubes. The cryo-tubes were placed in a pre-cooled cryo freezing container which ensures a cooling rate of 1°C per minute and transferred to a -80°C freezer. After 24h at -80°C, the cells were transferred into liquid nitrogen.

2.2.5 Thawing of cells

To thaw cells, one aliquot was thawed at RT until the frozen cells were moveable. The content of the tube was given directly into 25ml of the cell type-specific pre-warmed medium (37°C) followed by a centrifugation step at 300g for 5min. Next, the pellet was resuspended in 12ml fresh cell type-specific pre-warmed medium. This step is important to remove toxic DMSO. The cell suspension was transferred to a T75 flask and was incubated at 37°C. If necessary, it is possible to add selective antibiotics 24h after thawing.

2.2.6 Cell stimulation and in vitro sample collection

After seeding in 24-/48-/96-well plates, the cells were allowed to rest for 2h at 37°C, 5% CO_2. To start the experiment, most stimulators or inhibitors were added as 100x stock solution. Other volumes/concentrations of reagents are indicated in the individual experiments.

To detect cell-derived proteins, the supernatants were collected at indicated time points. After centrifugation at 650g for 5min (4°C) the cell-free supernatants were transferred to new 1.5ml reaction tubes which were stored at -80°C.

For RNA isolation the supernatants of the cells were stored as previously described and the cells were lysed as described in Chap. II-2.5.1.

2.3 Cell biological methods

2.3.1 Lentiviral knock-down of RAW264.7 macrophages

To generate a lentiviral knock-down in macrophages, $5x10^4$ RAW264.7 cells were seeded on day 0 in 1ml RAW-Medium in a 24-well plate. After 2h, the cells were transduced in 300µl medium using the lentivirus with a MOI 20. On day 2, the medium was changed and on day 4 the cells were scraped off the surface using pre-warmed PBS (without Ca^{2+} and Mg^{2+}, 0.5mM EDTA). The cells were transferred into a T25 flask and the medium was supplemented with 5µg/ml puromycinfor 2 weeks for selection of transduced cell clones Puromycin treatment was repeated every other passage.

2.3.2 Magnetic Activated Cell Sorting (MACS)

Magnetic Activated Cell Sorting (MACS) was used to purify $CD25^+$ Tregs from bronchoalveolar lavage fluid, spleen or mediastinal lymph nodes. The lymph nodes were isolated and smashed by using a 100µm mesh and the plunger of a 2ml syringe. The $CD4^+CD25^+$ Regulatory T Cell Isolation Kit was used according to the manufacturer's protocol. A pre-separation filter (30µm) was used for every column.

2.3.3 Multiplex analysis (Bio-Plex Pro™)

Multiplex analyses for cytokines were performed with the Bio-Plex Pro™ mouse cytokine group I (Bio-Rad). The analysis of the p38 MAPK was performed with the Bio-Plex Pro™ cell signaling reagent kit (Bio-Rad). Both analyses were used according to the manufacturer's protocol as described before (266).

2.3.4 Markers of endothelial-mesenchymal transition

The detection of endothelial-mesenchymal transition (EndMT) markers CD31 (PECAM-1) and α-smooth muscle actin (SMA) in provided lung sections was done in the laboratory of Prof. Dr. K. Schäfer at the University Medical Center, Mainz. The pictures were acquired by confocal microscopy by Dr. Nina Xia, University Medical Center, Mainz.

2.4 Protein biochemistry

2.4.1 Enzyme-linked immunosorbent assay (ELISA)

The samples (e.g. cell culture supernatants, EDTA-plasma or BALF) were diluted with the specific reagent diluent of the manufacturer's protocol to fit in the standard curve. 96-well plates were coated with the capture antibody overnight at RT. Next day, the wells were washed 3-5 times with 300µl ELISA Wash Buffer and blocked with 100µl Reagent Diluent for 1h at RT. Next, the wells were washed 3-5 times using 300µl ELISA Wash Buffer. Then, 100µl of the diluted samples and the standards were added and incubated for 1-2h in the dark at RT. After washing 3-5 times with 300µl ELISA Wash Buffer, the detection antibody was added and incubated for 1-2h in the dark at RT. The wells were washed 3-5 times using 300µl ELISA Wash Buffer and streptavidin labeled HRP conjugate was added to the wells for 20min in the dark at RT. After washing 3-5 times with 300µl ELISA Wash Buffer, 100µl TMB substrate per well was added and incubated for 10-30min in the dark at RT. The reaction was stopped by using 50µl ELISA Stop Solution (2N H_2SO_4) per well. Finally, the plate was analyzed with a spectrophotometer at 450nm (reference 550nm) within 30 min.

To quantitate TGFβ1, the TGFβ1 was activated by acidification prior to the ELISA. The samples were diluted with the TGFβ-Reagent Diluent and were acidified with 20µl 1N HCl per 100µl diluted sample. Incubation was performed for 10min at RT. Afterwards, the samples were neutralized with 22µl 1.2N NaOH + 0.5M HEPES per 100µl diluted sample. For establishing the acidification protocol, indicator paper was used to confirm a ~pH 7.4 after neutralization. The activation step is necessary to release the latent TGFβ1 which can be detected by the TGFβ1 ELISA.

2.4.2 Histone measurement

For measurements of total histones, the Cell Death Detection ELISA^{PLUS} from Roche was used. This assay detects the core histones H2A, H2B, H3 and H4 as well as linker histone H1, but not H5. To measure histones derived from neutrophil extracellular traps, this assay was modified. The capture antibody (α-H3, citrulline R2 + R8 + R17, #ab5103) was coated with 4µg/ml in Albumin Coating Buffer at RT for 1h. After washing 3 times with 300µl ELISA Wash Buffer, the plate was blocked with 300µl Reagent Diluent for 30min at RT. In the following steps, the protocol of the Cell Death Detection ELISA^{PLUS} was performed as recommended without using the anti-histone-biotin antibody. This antibody was removed to get specific binding of the H3-Cit). If the ELISA was done with the ABTS substrate delivered by the kit, the plate was analyzed at 405nm. In case of using TMB substrate the plate was analyzed at 450nm.

2.4.3 Flow cytometry analysis

For flow cytometry analysis a BD Canto II flow cytometer (BD Biosciences) was used for data acquisition. Typically, >30.000 events were acquired. In case of lymph node-derived samples, fewer event numbers (approx. 15.000) were acquired. For all staining conditions the matched fluorochrome-labeled isotype control antibodies were used. The FlowJo 10.0 software was used for data analysis.

Macrophages were stained for CD11b, F4/80 and IL-27p28. For this staining panel the cells had to be fixed and permeabilized prior to the intracellular staining procedure.

Macrophages were stimulated and incubated at 37°C, 5% CO_2 for 20h. Monensin (1:1000, golgi inhibitor) was added 2h after the stimulation. After incubation, the cells were washed with PBS without Ca^{2+} and Mg^{2+} and detached in PBS (without Ca^{2+} and Mg^{2+}, 0.5mM EDTA) by using a cell scraper. After centrifugation at 300g for 5min (4°C), the cell pellet was resuspended in 96-well plates (V-bottom) with 100µl per well Fixation/Permeabilization solution (BD). The plate was incubated on ice in the dark for 20min. The cells were spun at 300g for 5min (4°C) and washed with 200µl Perm Wash Buffer (BD) two times. The pellet was resuspended in 100µl Perm Wash Buffer (BD) including 2µl TruStain® to block unspecific antibody binding. After 15min in the dark at RT, the staining antibodies were added in the recommended concentrations. The staining was performed in the dark at RT for 30min. The cells

were centrifuged again at 500g for 5min (4°C) and washed twice with 200µl Perm Wash Buffer (BD). In the end, the pellet was resuspended in 200µl FACS-Buffer, stored at 4°C. The cells were analyzed within the next 72h. To calculate the total numbers of cells, 20µl counting beads were added immediately before the flow cytometry acquisition. In case of pSmad3/2 staining, the described protocol was modified by using BD Perm Buffer III instead of Perm Wash Buffer (BD).

For Treg staining (CD4, Foxp3), a recommended protocol including buffers was used from BioLegend. Cells for Treg staining were collected from BALF or mediastinal lymph nodes.

Th17 (CD4, IL-17A) and Th1 (CD4, IFN-γ) cells were analyzed in the BALF and in mediastinal lymph nodes. The lymph nodes were isolated and smashed by using a 100µm mesh and the plunger of a 2ml syringe. The collected cells were seeded in 24-well plates at 37°C, 5% CO_2 for 2h. Each sample was split to one well with α-CD3/α-CD28 stimulation and one well without antibody stimulation. The antibodies were previously coated overnight in PBS with Ca^{2+} and Mg^{2+} at 4°C and helped to induce the production of IL-17A and IFN-γ. (Wells without α-CD3/α-CD28 served as negative controls to set the regions during flow cytometry data analysis.) Brefeldin A (1:1000) was added to the medium and incubated at 37°C, 5% CO_2 for two additional hours. The cells were collected and transferred to a 96-well plate. All steps were performed on ice. The pellet was resuspended in 100µl FACS-Buffer including 2µl TruStain® to block unspecific antibody binding. After 15min in the dark, the cells were stained with α-CD4 in FACS-Buffer for 10min followed by centrifugation at 300g for 5min (4°C) and washing twice with 200µl FACS-Buffer. The cell pellet was resuspended in 100µl Perm Wash Buffer (BD) and incubated in the dark for 10min on ice. The antibodies (IL-17A and IFN-γ) were added in the recommended concentrations and incubated in the dark for 20min on ice. Afterwards, the cells were centrifuged at 300g for 5min (4°C) and washed twice with 200µl Perm Wash Buffer (BD). Fixation was performed with 2% Formaldehyde in the dark for 20min. After centrifugation at 300g for 5min (4°C), the cells were resuspended in 200µl FACS-Buffer and stored at 4°C until flow cytometry analysis.

For analysis of surface proteins, the regions were adjusted by using the specific isotype antibodies. For intracellular stained proteins, a *Fluorescence Minus One*

control was used. For Th17/Th1 staining, the samples without antibody treatment were used as negative unstained controls and for adjusting the regions.

2.4.4 Fluorometry

Fluorometry was used to detect the histone release in samples obtained from *in vivo* experiments. Histone reporter mice ($H2BeGFP^{+/-}$) were treated with bleomycin to induce pulmonary fibrosis (Chap. II-2.6.1). After two days, 500µl BALF was collected (Chap. II-2.6.2). After centrifugation with 300g for 5min (4°C), the cell-free supernatant was transferred to 96-well plates to analyze the fluorescent signal of GFP in the samples. An excitation of 485nm and an emission of 538nm were set. A FITC-labeled antibody was used as a positive working control.

2.4.5 Collagen Assay

To measure the total amount of collagen I, V in lungs, the SIRCOL collagen assay was used as described in the manufacturer's protocol. The collagen standard was prepared in 0.5M acetic acid.

2.5 Molecular biological methods

2.5.1 Isolation of RNA

Cells from *in vitro* experiments ($5x10^5$ cells) were lysed by using 350µl RLT Buffer (Qiagen). For the isolation, the RNeasy Mini Kit (Qiagen) was used as described in the manufacturer's protocol.

In case of RNA isolation from lungs, 30mg of the lung tissue was used. 600µl of RLT lysis Buffer + 1% β-mercaptoethanol and two steel beads were added. The lung tissue was lysed with the Qiagen Tissue Lyser II for 5min, 30Hz. The lysate was centrifuged at 20,000g for 5min (4°C). The supernatant was used for RNA isolation.

RNA isolation of Tregs after MACS purification was performed with the innuPREP RNA Mini kit (Analytik Jena) as described in the manufacturer's protocol.

At the end of the isolation protocol, the RNA was eluted in RNase-free deionized water. Usually, the concentration of RNA was measured with the NanoDrop 2000c. For advanced molecular biology approaches such as RNA-Seq (Next Generation Sequencing), the RNA concentration was quantified by a Qubit Fluorometer (Thermo Scientific) and the quality of the RNA (RNA integrity number >9.0) was confirmed by a Bioanalyzer (Agilent).

2.5.2 Photometric concentration measurement of nucleic acids

The concentration of nucleic acids was measured photometrically by the Nanodrop 2000c system (Thermo Scientific) with a wavelength of 260nm against the solvent. At 260nm, the purin base and the pyrimidin base absorb the light. With the help of the quotient of the absorption at 260nm and 280nm it is possible to check if the sample is contaminated with proteins (the amino acid tryptophan absorbs light at 280nm).

2.5.3 Reverse Transcription (cDNA synthesis)

All RNA samples from one experiment were adjusted to the same RNA amount. Normally, an RNA amount between 100ng-1µg was used in 10µl RNase-free distilled water. The Reverse Transcription was performed with the High-Capacity cDNA Reverse Transcription Kit (Applied Biosystems) in a 20µl reaction volume. Volumes needed for one reaction are shown in Tab. 19.

Tab. 19: Components of the Reverse Transcription Mastermix (per reaction).

Volume	Component
2µl	10x RT Buffer
0.8µl	25x dNTP Mix (100mM)
2µl	10x RT Random Primers
1µl	MultiScribe® Reverse Transcriptase
1µl	RNase Inhibitor
3.2µl	Nuclease-free H_2O

Of this Mastermix, 10µl were added to the adjusted RNA samples to yield 20µl. The cDNA synthesis was realized with the following program:

Tab. 20: PCR program for cDNA generation.

	Step 1	**Step 2**	**Step 3**	**Step 4**
Temperature	25°C	37°C	85°C	4°C
Time	10min	120min	5min	∞

∞ Infinitely

After cDNA synthesis, 80µl Nuclease-free distilled water was added to each sample to adjust the cDNA concentration for quantitative PCR analysis.

2.5.4 Quantitative Polymerase Chain Reaction

Quantitative Polymerase Chain Reaction (qPCR) was employed to quantify the expression intensity of a gene of interest in comparison to a housekeeping gene (e.g. *gapdh*).

Tab. 21: qPCR Mastermix (per reaction).

Volume	Component
10µl	iQ SYBR®Green Mastermix
4µl	Nuclease-free H_2O
2µl	Forward Primer (5µM)
2µl	Reverse Primer (5µM)

20µl per reaction

For each sample 2µl cDNA (1-2ng cDNA) were added to 18µl qPCR Mastermix.

The following qPCR protocol was used:

Tab. 22: qPCR program.

Step	Temperature	Time
1	95°C	3min
2	95°C	15sec
3	60°C	1min
4	72°C	10sec (Plate read)
5	-	Repeat step 2-4 for 40 times
6	Melt curve: 75°C to 95°C, increment 0.2°C for 10sec (Plate read)	

The results were analyzed by using the 2-ddCT method using *gapdh* as housekeeping gene. The expression levels were normalized to the unstimulated control (*in vitro*), the sham group or the wild type group (*in vitro*/*in vivo*).

2.5.5 Transcriptome Analysis with Next-Generation Sequencing

The next generation sequencing HiSeq 2000 system (Illumina-Solexa) was used for whole transcriptome sequencing (RNA-Seq, NGS). This system is working with a glass slide (flow cell) of eight lanes. Each lane contains millions of oligonucleotide anchors where denaturized, labeled DNA fragments can bind to via previously ligated DNA adapters. Each anchor is a primer for amplification. A new DNA strand is synthesized which is covalently attached to the anchor on the flow cell. In the next step, the DNA is denaturized and the original DNA strand is washed away. The new synthesized DNA strand can bind to a new anchor to build a bridge. This process is called bridge-amplification. The new bound anchors can again function as primers and by reversible amplification; clusters are built (267). These DNA-containing clusters are the basis of the sequencing which is a sequencing-by-synthesis method (268). The following sequencing is based on a fluorescence labeled chain termination reaction, which is reversible.

For RNA-Seq, the Tregs were purified out of mediastinal lymph nodes as described in Chap. II-2.3.2 and the RNA was isolated by the innuPREP RNA Mini kit (Analytik Jena) (Chap. II-2.5.1). The quality check (RNA integrity number >9.0), as well as the library preparation and the sequencing was performed at the Genomics Core Facility (Institute of Molecular Biology gGmbH, Mainz) by Dr. C. Han. For cDNA generation the SMARTer Ultra Low Input RNA Kit for Sequencing - v3 (Clonetech) was used. The library preparation was performed by the Nextera XT DNA Library Preparation Kit (Illumina). The sequencing was performed as single read, 68bp at an Illumina HiSeq. The sequencing depth was between 13-17 mio. reads. The data analysis was performed by F. Marini at the Institute of Medical Biostatistics, Epidemiology and Informatics (IMBEI, Mainz). The mapping to the reference genome (ENSEMBL Mus_Musculus.GRCm38) was performed by STAR aligner (version 2.4.0b). To perform the differential expression levels at the gene level, the Bioconductor DESeq2 package (version 1.6.3) was used. The total analysis was implemented in R version 3.1.2.

2.5.6 Polymerase Chain Reaction

With the help of a Polymerase Chain Reaction (PCR), a specific part of the DNA can be amplified. PCR was used to genotype several transgenic mouse strains. The protocols for the specific genotyping were established in accordance with protocols provided by The Jackson Laboratory. For PCR, the Maxima Hot Start Green PCR Mastermix (Thermo Fisher Scientifific) was used as described in the manufacturer's protocol.

2.5.7 Agarose Gel Electrophoresis

Fragments of DNA or RNA were separated by size with the help of agarose gel electrophoresis. Gels between 0.8 - 2.5% (w/v) agarose were made. The agarose was cooked in 1x TAE Buffer until the agarose dissolved. Afterwards, 2µl GelRed per 100ml were added. This solution was poured into a gel chamber containing a pocket strip and allowed to polymerize at RT. The gel was transferred into the electrophoresis chamber and was coated with 1x TAE Buffer. The different samples were placed into the pockets. The marker (100bp ladder, NEB) was used with a volume of 3µl. For separation of the different fragments, a voltage between 60V and 120V was used. The added GelRed intercalates into the DNA double helix and can be visualized by UV-light excitation.

2.5.8 Transfection

BMDMs were stimulated *in vitro* with the Rig-I agonist 5'ppp-dsRNA by transfection using Oligofectamine™. The 24-well plate format was used as described in the manufacturer's protocol.

2.5.9 Chromatin Immunoprecipitation

For Chromatin Immunoprecipitation (ChIP), the Magna ChIP kit was used as described in the manufacturer's protocol. The fixation of the cells was changed to 1% formaldehyde for 8min at RT. DNA was sonicated to a length of 500bp – 700bp at 4°C (4x10 cycles, 50% amplitude, 30sec pulse, 30sec rest) with a sonicator Q700. The following antibodies were used: anti-Smad3 (abcam), anti-Histone H3 (cell signaling, clone D2B12), normal rabbit IgG (cell signaling). All antibodies were used in a concentration of 1.5µg/µl.

2.6 *In vivo* models

2.6.1 Bleomycin-induced pulmonary fibrosis

For bleomycin-induced pulmonary fibrosis, 8-10 week old mice were anesthetized by i.p. injection of ketamine and xylazine (100mg/kg body weight) in PBS. The mouse was suspended on its back on a ~60° inclined board with a rubber band running under the upper incisors (269) (Fig. 7). The cervical skin was disinfected with Desderman® and a small medial incision (1cm) was made in the area of the trachea. After blunt preparation of the trachea, 40µl bleomycin in 0.9% NaCl were given very slowly (~ 1µl/sec) into the trachea. The aspiration rate of the mouse was observed during the injection to ensure proper bleomycin spreading in the lungs. For all pulmonary fibrosis experiments a bleomycin dose of 1U/kg BW i.t. was given, unless specified otherwise in the text or figure legends. After aspiration of the whole bleomycin solution, the skin incision was closed with 6.0 surgical sutures.

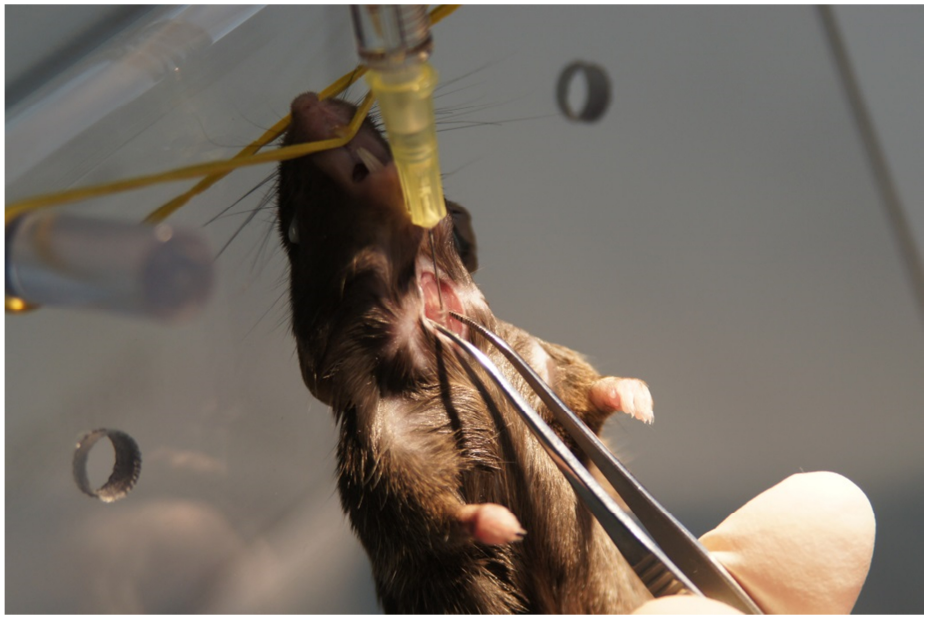

Fig. 7: Surgical aspiration procedure (intra-tracheal injection) in the mouse model of bleomycin-induced pulmonary fibrosis.

2.6.2 Sample collection, *in vivo*

At the end of bleomycin-induced pulmonary fibrosis experiments, several types of specimens were collected: BALF (bronchoalveolar lavage fluid), the left lung lobes for SIRCOL collagen assay, the right lung lobes for RNA isolation, the mediastinal lymph nodes, EDTA-plasma and lungs for histology.

The BALF was obtained by flushing the lungs with 1ml (2x 1ml in case of cell staining) cold PBS (without Ca^{2+} and Mg^{2+}). The collected BALF was centrifuged at 650g for 5min (4°C). In maximum, 1ml of the supernatant was frozen at -80°C to measure different mediators. The cell pellet could be used for different staining procedures.

To collect the lungs for collagen assay or RNA isolation, the chest was opened and the lung lobes were transferred to a 2ml reaction tube. The lung lobes were frozen in liquid nitrogen, immediately and stored at -80°C until further analysis.

The mediastinal lymph nodes were taken from the right side of the proximal aorta. The isolated lymph nodes were smashed by using a 100µm mesh and a plunger of a 2ml syringe. The nylon mesh was flushed with sterile PBS (without Ca^{2+} and Mg^{2+}) and centrifuged at 300g for 10min (4°C). The pelleted cells were used for downstream analysis such as flow cytometry or magnetic purification (MACS, Miltenyi).

EDTA-plasma was collected by retro-bulbar puncture.10µl EDTA (0.5M) was added to the collected blood. The blood was centrifuged at 300g for 10min (4°C), no break. The upper phase (plasma) was collected and stored at -80°C until further analysis.

Lungs for histology were filled with 500µl formalin (4% formaldehyde in PBS) and the trachea was closed by surgical ligation. The whole heart-lung-package was isolated, fully covered with formalin and embedded in paraffin. Paraffin sections were prepared by the histology core facility (University Medical Center, Mainz). The paraffin sections were stained according to established protocols: Masson's Trichrome (Goldner) and Hematoxylin and eosin staining (H&E stain). With the Masson's trichrome (Goldner) staining the collagen in the lung was colorized in green. Pictures were generated with an OLYMPUS IX73 inverted microscope and SC30/CMOS Color camera.

2.6.3 Diphtheria toxin depletion of cells (DTX model)

Neutrophils were depleted in the mouse strain Ly6GCreiDTR with the help of diphtheria toxin (DTX). The mouse strain Ly6GCreiDTR expresses the DTX-receptor under control of the Ly6G promotor. The mice were injected with 25ng/g bodyweight (high dose) DTX i.p. for three consecutive days.

2.7 Statistical analysis

Cell culture experiments, representative results of three independent experiments each in performed in duplicate wells are shown, unless indicated otherwise in the figure legends. For statistical analysis Student's t test was performed for calculation between two independent groups. Tukey post hoc test with one-way ANOVA was performed for calculation for more than two groups. Analysis was performed using GraphPad Prism 6. Data were expressed as ± standard error of the mean (SEM). Significance was considered at value differences with $p < 0.5$ and was indicated by asterisks: *$p < 0.05$, **$p < 0.01$, ***$p < 0.005$ and ****$p < 0.001$.

III Results

1 Time course of bleomycin-induced pulmonary fibrosis

To establish a model of bleomycin-induced pulmonary fibrosis, dose response and time course studies were performed. In initial experiments, the dose of bleomycin was titrated to obtain less than 10% mortality rates (data not shown).

The pathobiology of bleomycin-induced pulmonary fibrosis was studied over time (four-week kinetic). Bleomycin-induced pulmonary fibrosis was induced as described in Chap. II-2.6.1. 1U/kg bodyweight (BW) bleomycin was instilled intratracheally (i.t.). Samples were collected every week for a period of four weeks. Samples of the 0 week time point were collected immediately before bleomycin instillation on day 0. Sham-surgery samples were collected after four weeks. The sham-group was treated with 40µl 0.9% NaCl i.t.. The sample collection was performed as described in Chap. II-2.6.2.

A hallmark of pulmonary fibrosis is the increased deposition of extracellular matrix components such as collagen in lungs. During the kinetic of bleomycin-induced pulmonary fibrosis the collagen I,V amount was analyzed to assess the severity of the pulmonary fibrosis. One week after bleomycin instillation, the amounts of collagen I,V in lungs was similar to the amount before bleomycin instillation (Fig. 8.1). Between one week and four weeks after bleomycin administration, the collagen I,V amount increased constantly to almost 3-foldin bleomycin treated mice in comparison to the baseline time point (0 week). After four weeks, the collagen I,V amount in the sham-group was increased by approx. 74% as compared to the group of mice at week 0. The collagen I,V amount was analyzed by collagen assay (Chap. II-2.4.5).

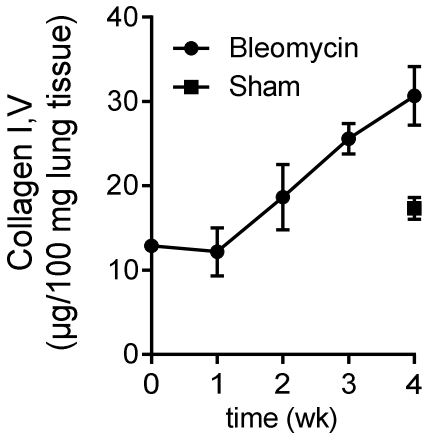

Fig. 8.1: Time course studies of collagen I,V amount during pulmonary fibrosis.
1U/kg BW bleomycin in 40µl 0.9% NaCl was instilled i.t.; Sham = 40µl 0.9% NaCl i.t.. Collagen I,V amount was normalized to 100mg whole lung tissue, collagen assay. All values are presented as the mean ± SEM. n = five male mice/time point.

Macrophages have been described to play a key role during pulmonary fibrosis (270). The number of F4/80$^+$ macrophages in the Bronchoalveolar lavage fluid (BALF) of bleomycin treated mice (stained as described in Chap. II-2.4.3) increased strongly after one week, reached the maximum after two weeks and decreased after three weeks. The sham-group did not show a relevant increase of F4/80$^+$ macrophages after four weeks (Fig. 8.2). The F4/80$^+$ macrophages were analyzed by flow cytometry and counted with the help of counting beads. The region for the positive cell population was adjusted by using the appropriate isotype control antibodies.

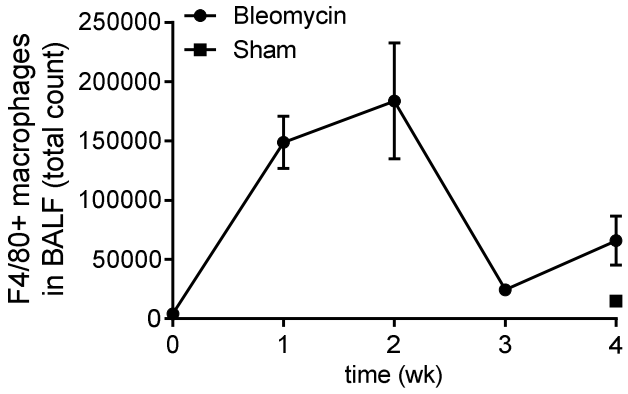

Fig. 8.2: Time course of F4/80$^+$ macrophages in BALF during pulmonary fibrosis.
1U/kg BW bleomycin in 40µl 0.9% NaCl was instilled i.t.; Sham = 40µl 0.9% NaCl i.t.. Flow cytometry analyses were performed. All values are presented as the mean ± SEM. n = five male mice/group.

Macrophages produce IL-27 under pro-inflammatory conditions. The IL-27p28 concentrations (analyzed by ELISA, Chap. II-2.4.1) in the BALF increased one week after bleomycin administration and reached a maximum two weeks after treatment (Fig. 8.3A).

TGFβ1 as a central cytokine during pulmonary fibrosis was also analyzed by ELISA (Chap. II-2.4.1) during the four-week kinetic. TGFβ1 in the BALF was already detectable in naïve mice (time point 0) and increased in the next two weeks (Fig. 8.3B). After two weeks, the TGFβ1 concentration reached the maximum. In the last two weeks of the kinetic, the TGFβ1 amount in the BALF maintained on an intermediate level between the highest amount after two weeks and the sham-group. Taken together, the increase of IL-27p28 concentrations preceded the TGFβ1 concentrations. When the TGFβ1 concentrations reached its maximum, the IL-27p28 concentration started to decrease.

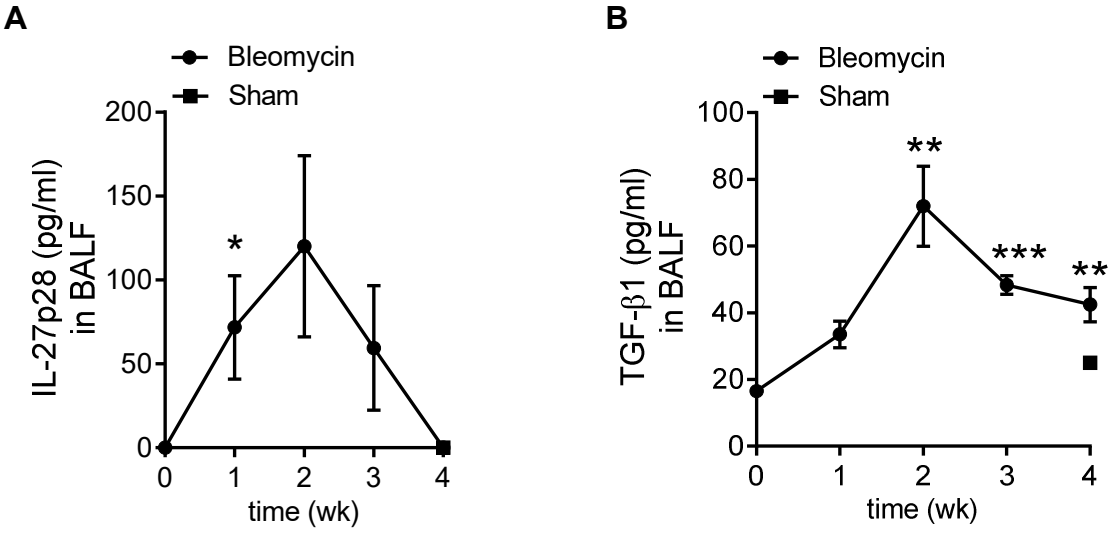

Fig. 8.3: Time course of IL-27p28 and TGFβ1 in the BALF during pulmonary fibrosis.
(A) Concentrations of IL-27p28 in the BALF, ELISA. (B) Concentrations of TGFβ1 in the BALF, ELISA. 1U/kg BW bleomycin in 40µl 0.9% NaCl was instilled i.t.; Sham = 40µl 0.9% NaCl i.t.. All values are presented as the mean ± SEM. *p<0.05, **p<0.01 and ***p<0.005 vs. sham, one-way ANOVA. n = five male mice/group.

Several T cell populations play different roles during pulmonary fibrosis. First, the infiltrating $CD4^+$ T cells were stained in the BALF and in the mediastinal lymph nodes as described in Chap. II-2.4.3, analyzed by flow cytometry and counted with the help of counting beads. The $CD4^+$ T cells were gated by using isotype control antibodies.

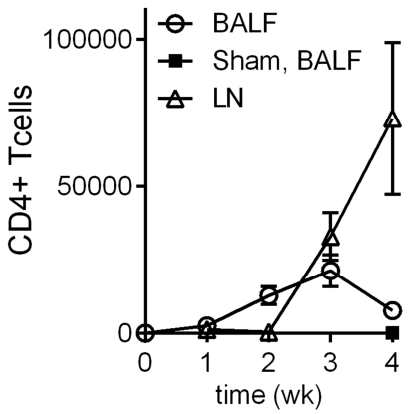

Fig. 8.4: Time course of $CD4^+$ T cells in the BALF and in the mediastinal lymph nodes during pulmonary fibrosis.
1U/kg BW bleomycin in 40µl 0.9% NaCl was instilled i.t.; Sham = 40µl 0.9% NaCl i.t.. $CD4^+$ T cells were analyzed by flow cytometry. No $CD4^+$ T cells were detectable in the BALF and mediastinal lymph nodes of the sham-group. All values are presented as the mean ± SEM. LN = mediastinal lymph nodes. n = five male mice/group.

Peripheral $CD4^+$ T cells started to infiltrate the lungs one week after bleomycin administration (Fig. 8.4) and reached the highest cell count after three weeks. After four weeks, $CD4^+$ T cell numbers significantly decreased in comparison to the three weeks' time point in the BALF. The $CD4^+$ T cells in the mediastinal lymph nodes were not detectable until two weeks after bleomycin administration (Fig. 8.4). The $CD4^+$ T cells strongly increased in the mediastinal lymph nodes between two and four weeks.

In the mediastinal lymph nodes of the sham-group no $CD4^+$ T cells could be isolated after four weeks (data not shown).

The $CD4^+$ T cell subpopulations of $CD4^+IL\text{-}17A^+$ cells (Th17) (Fig. 8.5A) and $CD4^+IFN\text{-}\gamma^+$ cells (Th1) (Fig. 8.5B) in the BALF and in the mediastinal lymph nodes were stained, analyzed by flow cytometry and counted with the help of counting beads. The regions for the positive cell populations were defined by using a sample without α-CD3/α-CD28 stimulation for every biological sample.

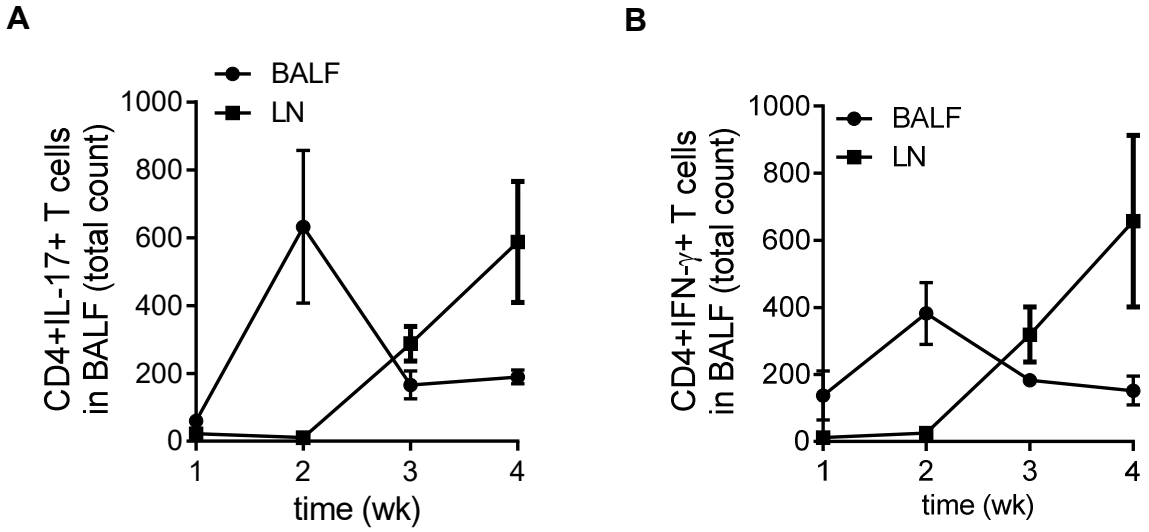

Fig. 8.5: Time course of $CD4^+IL\text{-}17A^+$ cells (Th17) and $CD4^+IFN\text{-}\gamma^+$ cells (Th1) in the BALF and in the mediastinal lymph nodes during pulmonary fibrosis.
(A) Kinetic of Th17 cells in the BALF and in the mediastinal lymph nodes, flow cytometry analysis. (B) Kinetic of Th1 cells in the BALF and in the mediastinal lymph nodes, flow cytometry analysis. 1U/kg BW bleomycin in 40µl 0.9% NaCl was instilled i.t.; Sham = 40µl 0.9% NaCl i.t.; LN = mediastinal lymph node. All values are presented as the mean ± SEM. n = five male mice/group.

Both cell types reached their maximum in the BALF after two weeks and started to decrease after three weeks. Both cell types were not detectable in the mediastinal lymph nodes until two weeks and started to increase between two and four weeks. Before bleomycin instillation and in the sham-group neither Th17 cells nor Th1 cells were detectable in the BALF (data not shown). In mediastinal lymph nodes of the sham-group no sufficient number of cells could be isolated.

In summary, these data indicated an immune response with elevated macrophage, increased IL-27p28 concentrations in BALF and increased Th17 and Th1 cell in the BALF and the mediastinal lymph nodes. The model of bleomycin-induced pulmonary

fibrosis showed increased TGFβ1 concentrations in BALF and collagen I,V in lungs. The time points of 2-4 weeks were used for subsequent experiments.

2 Neutrophils drive bleomycin-induced pulmonary fibrosis

To examine cell type-specific roles in bleomycin-induced pulmonary fibrosis neutrophils were depleted in mice using the Diphtheria toxin (DTX) mouse model (Chap. II-2.6.3). Here, the inducible Diphtheria toxin receptor (iDTR) is under control Ly6G control. Both groups Ly6GCre/iDTR (neutrophil depletion strain) and iDTR (control strain) were injected i.p. with DTX (25ng/g bodyweight) on two consecutive days before (day -2 and day -1) and on the day of the induction of fibrosis (day 0). On day 0, the depletion efficiency of the $Ly6G^+CD11b^+$ neutrophils was analyzed in blood by flow cytometry. The regions for the positive cell populations were set by using isotype antibodies. After three days of depletion with DTX, the strain Ly6GCre/iDTR showed a reduction of neutrophils of about half of the control strain in the blood (18.7% vs. 9.59%) (Fig. 9.1). Blood was collected as described in Chap. II-2.6.2 at the indicated time points. On day 0, the blood was collected before the bleomycin-instillation. Three male mice per group were analyzed to determine neutrophil numbers or depletion efficiency.

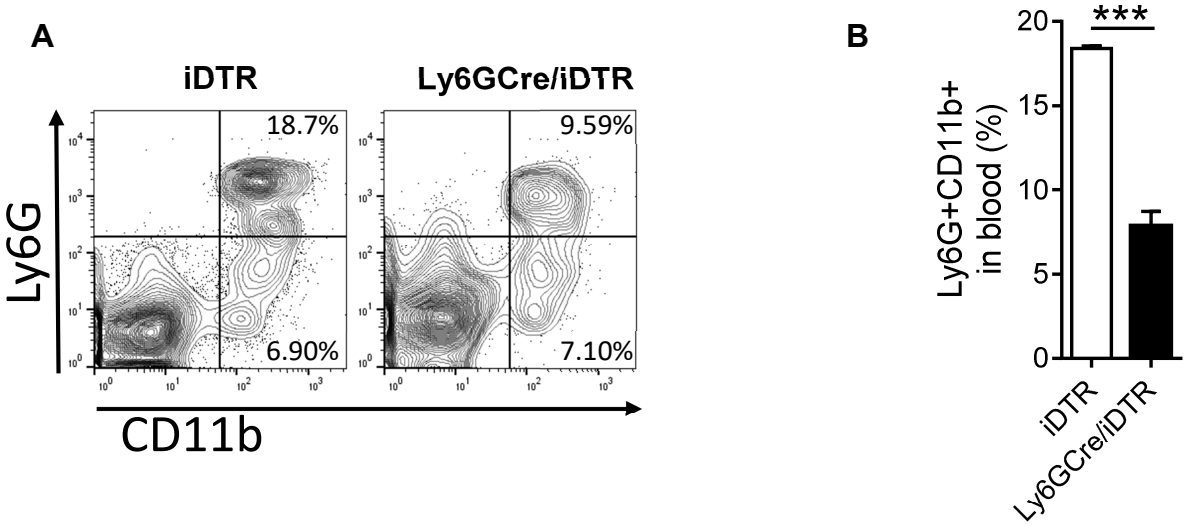

Fig. 9.1: Depletion of $Ly6G^+CD11b^+$ neutrophils in the blood.
(A) Representative contour plot of Ly6G/CD11b in the blood on day 0, flow cytometry analysis. (B) Bar graph of the flow cytometry analyses. The values are presented as the mean ± SEM. ***p<0.005 vs. iDTR, Student's t test. Diphtheria toxin (DTX) was given i.p. for three days (day -2, -1, 0), 25ng/g bodyweight. n = six male mice/group.

After two weeks of bleomycin-induced pulmonary fibrosis (1U/kg BW bleomycin i.t.), the neutrophil numbers in the BALF were not significantly different in both strains (Fig. 9.2). This indicated that discontinuation of DT injections resulted in a recovery of neutrophil numbers after two weeks. This experiment was stopped after two weeks because several mice in the Ly6GCre/iDTR group had a Body Condition Scoring (271) of 2 or below and were sacrificed for ethical concerns. This may have been due to additive toxic effects of combined Bleomycin and diphteria toxin. The transient depletion of $Ly6G^+$ neutrophils resulted in a dramatic decrease of $CD4^+$ T cell numbers and Th17 cells (Fig. 9.2) in BALF. The $F4/80^+CD11b^+$ macrophages did not show any differences, when the neutrophil depleted group and the non-depleted control group were compared (Fig. 9.2).

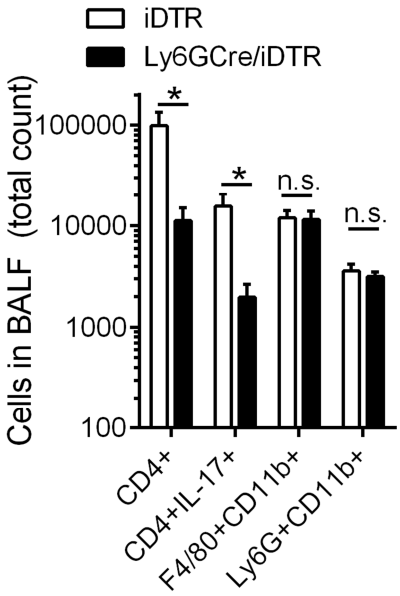

Fig. 9.2: Cell types in BALF during bleomycin-induced pulmonary fibrosis in $Ly6G^+CD11b^+$ depleted mice.
Diphtheria toxin (DTX) was given i.p. from day -2 to day 0, 25ng/g bodyweight. 1U/kg BW bleomycin in 40µl 0.9% NaCl was instilled i.t. on day 0. Sample collection after two weeks followed by flow cytometry analyses. All values are presented as the mean ± SEM. *p<0.05 vs. iDTR, Student's t test. n.s. = not significant, n = six male mice/group. Flow cytometry analyses were performed.

To study the influence of neutrophil depletion on pulmonary fibrosis, collagen was analyzed in the lungs. After i.t. administration of bleomycin, the neutrophil-depleted group (Ly6GCre/iDTR) showed less green-cyan collagen staining in the lungs as compared to the non-depleted control group (iDTR) (Fig. 9.3). Lungs were removed and histology sections were prepared (Masson's trichrome staining, Goldner) as described in Chap. II-2.6.2. The *collagen I,V* mRNA expression (Chap. II-2.5.1 - II-2.5.4) in whole lung tissue was approx. three times higher in the control group (iDTR) as compared to the neutrophil-depleted group (Ly6GCre/iDTR) (Fig. 9.4A). This was also reflected in the amount of collagen I,V in lung tissue. Again, the neutrophil-depleted group showed significantly less collagen I,V in comparison to the non-depleted control group (Fig. 9.4B).

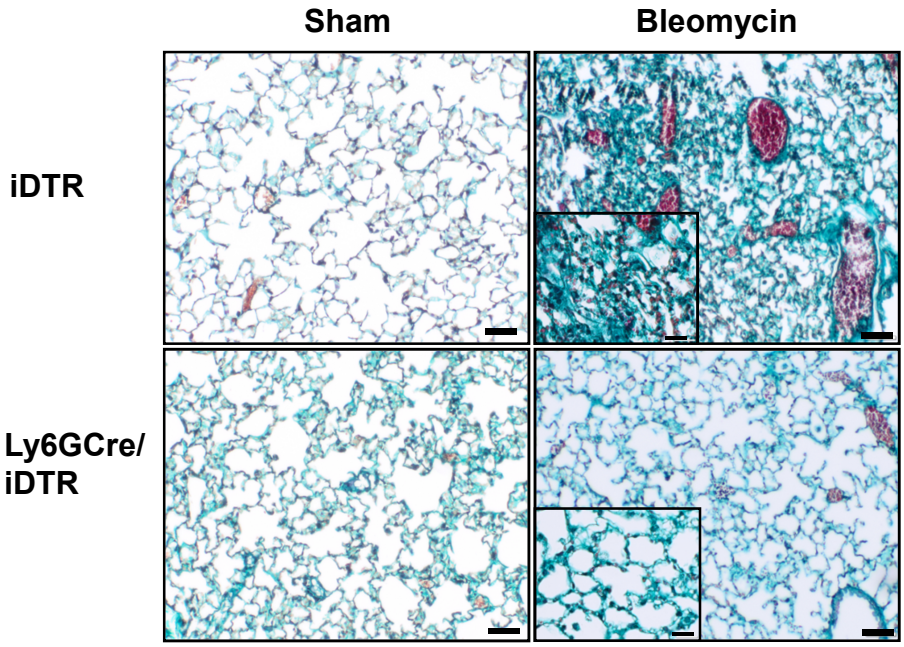

Fig. 9.3: Histology of neutrophil depleted lung sections during pulmonary fibrosis.
Diphtheria toxin (DTX) was given i.p. from day -2 to day 0, 25ng/g bodyweight. 1U/kg BW bleomycin in 40µl 0.9% NaCl was instilled i.t. on day 0 for two weeks. Representative lung areas are shown for all groups of Ly6GCre/iDTR and iDTR mice. Masson's trichrome staining (Goldner): collagen = green-cyan, nuclear chromatin = brownish-black, cytoplasm = bright red, erythrocytes = dark red, muscle = red. Magnification: 10x. Scale bar: 50µm (large picture); 20µm (small picture).

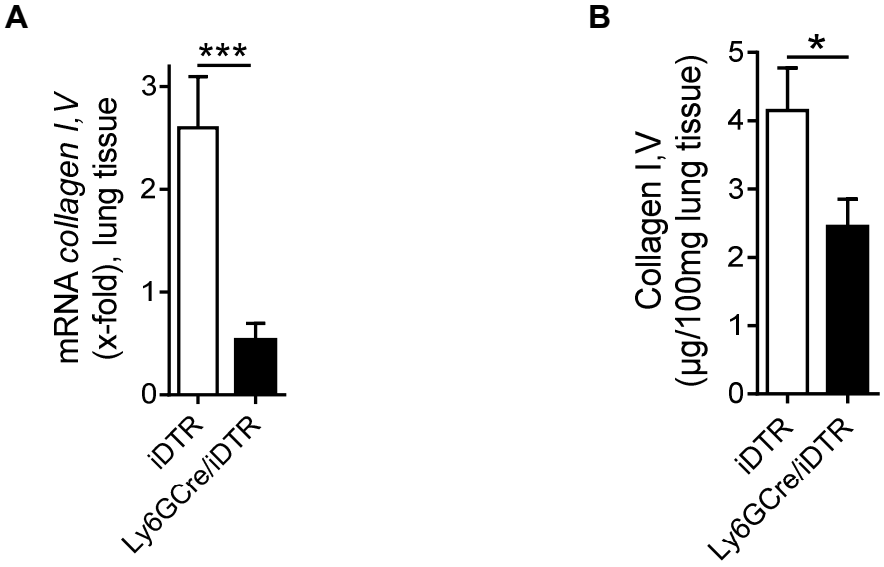

Fig. 9.4: Expression of *collagen I,V* mRNA and total collagen I,V in whole lung tissue during pulmonary fibrosis with neutrophil depletion.
(A) *Collagen I,V* mRNA expression in whole lung tissue, qPCR analysis. Expression was normalized to *gapdh* mRNA expression. (B) Total Collagen I,V amount in lung tissue, collagen assay. Collagen I,V amount was normalized to 100mg lung tissue. Diphtheria toxin (DTX) was given i.p. from day -2 to day 0, 25ng/g bodyweight. 1U/kg BW bleomycin in 40µl 0.9% NaCl was instilled i.t. on day 0 for two weeks. All values are presented as the mean ± SEM. *p<0.05 and ***p<0.005 vs. iDTR, Student's t test, n = six male mice/group.

There were strong differences for the cytokines TGFβ1 and IL-27p28 between the two groups. The cytokines TGFβ1 and IL-27p28 were detected by ELISA. The neutrophil-depleted group contained significantly less TGFβ1 in BALF and significantly more IL-27p28 (Fig. 9.5) in BALF in comparison to the non-depleted control group. IL-12p70 and IL-35 were analyzed because these cytokines are also members of the IL-12 family. IL-35 was detected by ELISA. The cytokine IL-12p70 was detected by Bio-Plex (Chap. II-2.3.3). In contrary to IL-27p28, other IL-12 family cytokines showed no significant differences in the BALF after two weeks of bleomycin-induced pulmonary fibrosis (Fig. 9.5).

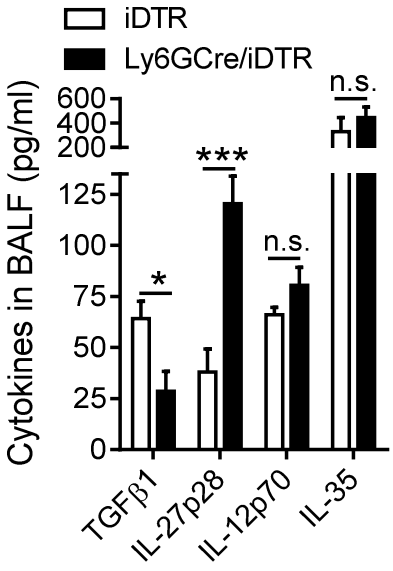

Fig. 9.5: Cytokines in BALF in bleomycin-induced pulmonary fibrosis after neutrophil depletion.
Diphtheria toxin (DTX) was given i.p. from day -2 to day 0, 25ng/g bodyweight. 1U/kg BW bleomycin in 40µl, 0.9% NaCl was instilled i.t. on day 0 for two weeks. Cytokines were quantified by ELISA (TGF-β1, IL-27p28) or by Bio-Plex (IL-12p70, IL-35). All values are presented as the mean ± SEM. *$p<0.05$ and ***$p<0.005$ vs. iDTR, Student's t test. n.s. = not significant. n = six male mice/group.

Epithelial cells undergo a process called epithelial-mesenchymal-transition (EMT) during pulmonary fibrosis. The expression levels of the EMT markers Slug and Snail were analyzed in whole lung tissue by qPCR analysis to investigate the influence of neutrophils on EMT. The expression levels EMT markers Slug and Snail were decreased by half in the neutrophil-depleted group in comparison to the non-depleted group (Fig. 9.6).

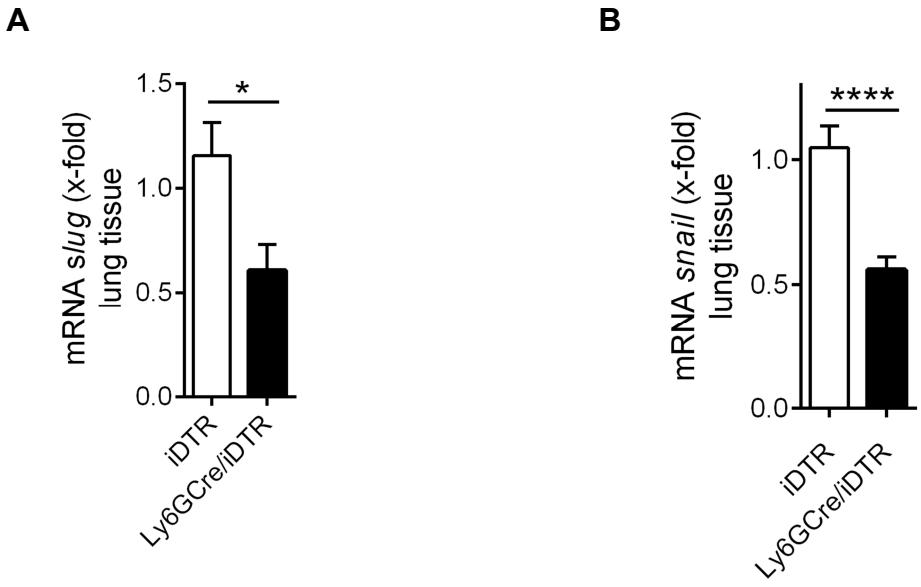

Fig. 9.6: Expression of *slug* mRNA and *snail* mRNA in whole lung tissue during pulmonary fibrosis with neutrophil depletion.
(A) *Slug* mRNA expression in whole lung tissue, qPCR analysis. (B) *Snail* mRNA expression in whole lung tissue, qPCR analysis. Expressions were normalized to *gapdh* mRNA expression. Diphtheria toxin (DTX) was given i.p. from day -2 to day 0, 25ng/g bodyweight. 1U/kg BW bleomycin in 40µl 0.9% NaCl was instilled i.t. on day 0 for two weeks. All values are presented as the mean ± SEM. *p<0.05 and ****p<0.001 vs. iDTR, Student's t test. n = six male mice/group.

3 Histones as key players during bleomycin-induced pulmonary fibrosis

3.1 Release of histones during bleomycin-induced pulmonary fibrosis

Bleomycin is cytotoxic and induces necrosis (272) (52). During this process histones are released by cells. Histone concentrations were analyzed after induction of bleomycin-induced pulmonary fibrosis by ELISA. The mice were treated with 1U/kg BW bleomycin i.t. on day 0. The sham-groups were treated with 40µl 0.9% NaCl i.t.. On day 0, 1, 2 and 3 the BALF was collected as described. The BALF of the sham-groups were collected after three days.

Histone concentrations were significantly increased in the BALF two days after bleomycin administration (Fig. 10.1A). Three days after the bleomycin administration, the histone concentration decreased to the levels of day 1. These findings were confirmed by using a histone-reporter mouse strain (H2BeGFP$^{+/-}$). Here, the mice were treated with 1U/kg BW bleomycin i.t. and 0.9% NaCl (sham) on day 0. After two days, the cell-free BALF was collected followed by analysis of green fluorescence (Chap. II-2.4.4). A FITC labeled antibody was used as a functional control. Two days after bleomycin administration, in the BALF of the H2BeGFP$^{+/-}$ group, a strong eGFP signal was detectable in comparison to the C57BL/6J (WT) group (Fig. 10.1B). The sham mice did not show any eGFP fluorescence in the BALF of both groups after two days.

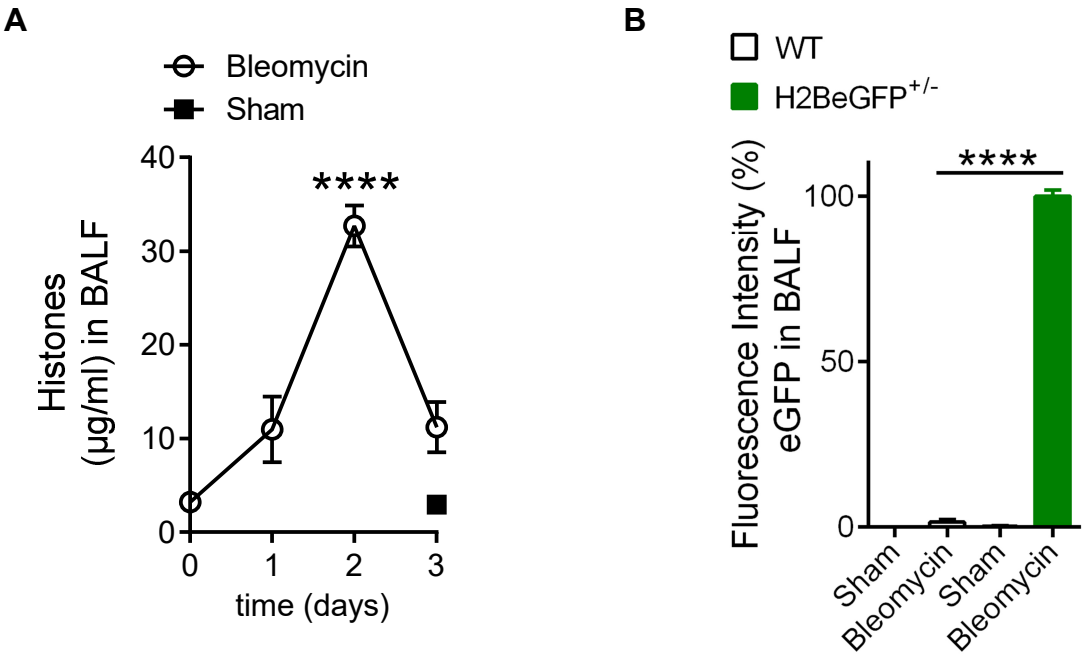

Fig. 10.1: Histone release in BALF.
(A) Time course of histone release in BALF, ELISA. n = six male mice for each time point. All values are presented as the mean ± SEM. ****p<0.001 vs. sham, one-way ANOVA. (B) Fluorescence intensity of H2BeGFP in BALF, fluorometry analysis. Fluorescence intensity of H2BeGFP$^{+/-}$ was set at 100%. Sample collection on day 2. n(bleomycin) = six male mice/group, n(sham) = three male mice/group. Excitation: 485nm, Emission: 538nm. The values are presented as the mean ± SEM. ****p<0.001 vs. WT, Student's t test.
1U/kg BW bleomycin in 40µl 0.9% NaCl was instilled i.t.; Sham = 40µl 0.9% NaCl i.t.; WT = wild type (C57BL/6J).

To investigate the cellular sources of the released histones, a bone marrow transplantation experiment as described in Chap. II-2.1.9 was performed. H2BeGFP$^{-/-}$ and H2BeGFP$^{+/-}$ bone marrow was transplanted into C57BL/6J or H2BeGFP$^{+/-}$ mice. After five weeks, the bone marrow was isolated (Chap. II-2.1.1) and the engraftment efficacy of the H2BeGFP$^{+/-}$ cells were analyzed by flow cytometry. The regions were adjusted by using isotype control antibodies. The vast majority of the Ly6G^{+}CD11b^{+} neutrophils in the bone marrow were eGFP positive (Fig. 10.2).

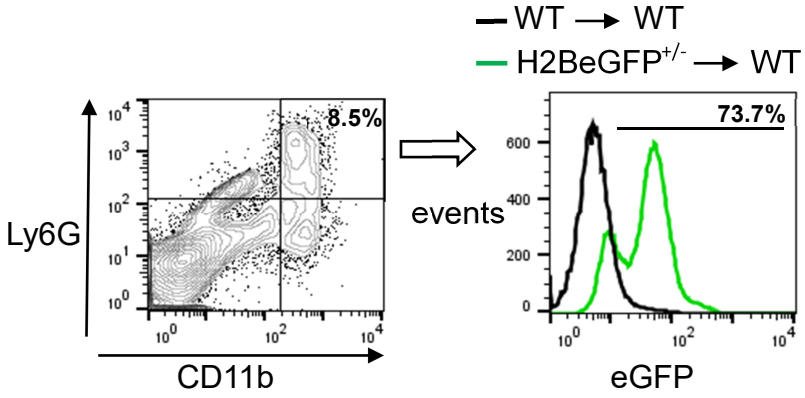

Fig. 10.2: Efficacy of H2BeGFP bone marrow transplantation.
Isolated bone marrow from C57BL/6J (WT) or H2BeGFP$^{+/-}$ donor mice was injected i.v. in irradiated (2x6.5Gy) C57BL/6J (WT) recipient mice. After five weeks, the bone marrow cells of the chimeric mice were gated on Ly6G^{+}CD11b^{+} neutrophils by flow cytometry analyses and the eGFP fluorescence was quantified. Three male mice/group were analyzed and representative plots are shown.

After five weeks of bone marrow engraftment, 1U/kg BW bleomycin and 40µl 0.9% NaCl for the sham-group was instilled intratracheally. Two days after bleomycin administration, cell-free BALF was collected and analyzed by fluorometry (Fig. 10.3). No eGFP-fluorescence was detectable in the BALF of the H2BeGFP$^{-/-}$→C57BL/6J

negative control group. The highest amount of eGFP-fluorescence was analyzed in the BALF of the H2BeGFP$^{+/-}$→H2BeGFP$^{+/-}$ group. The H2BeGFP$^{+/-}$→C57BL/6J group (only myeloid cells are eGFP positive) showed about 50% of the fluorescence intensity (FI) in the BALF as compared to the H2BeGFP$^{+/-}$→H2BeGFP$^{+/-}$ group of mice. The eGFP fluorescence was not detectable in BALF of sham-treated mice (negative controls). A FITC labeled antibody was used as a functional control.

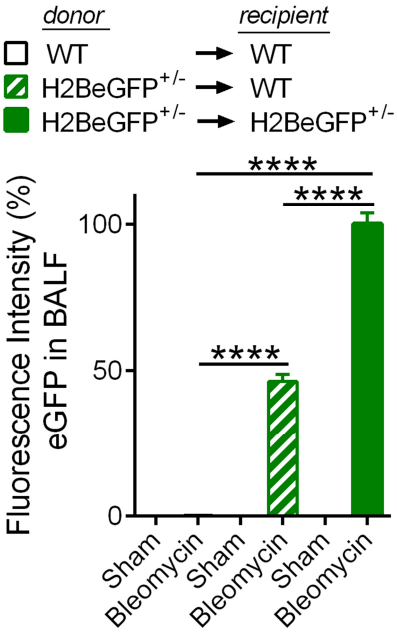

Fig. 10.3: Fluorescence intensity of H2BeGFP in BALF after bleomycin instillation in bone marrow transplanted mice.
1U/kg BW bleomycin in 40µl 0.9% NaCl was instilled i.t.; Sham = 40µl 0.9% NaCl i.t.. Sample collection on day 2. H2BeGFP was quantified by fluorometry. Fluorescence intensity of H2BeGFP$^{+/-}$ → H2BeGFP$^{+/-}$ was set at 100%. Excitation: 485nm, Emission: 538nm. All values are presented as the mean ± SEM. ****p<0.001 vs. WT → WT or H2BeGFP$^{+/-}$ → WT. WT = wild type (C57BL/6J). n(bleomycin) ≥ six male mice/group, n(sham) = two male male /group.

The alveolar/capillary lung barrier is damaged after bleomycin instillation because of the dying cells and ensuing inflammation. A damaged alveolar/capillary lung barrier leads to an increase of serum albumin in the BALF (also known as albumin leakage). The albumin amount of the different BALF samples was quantified by ELISA. The severity of the bleomycin-mediated injury to the alveolar/capillary lung barrier was comparable in the three groups (Fig. 10.4).

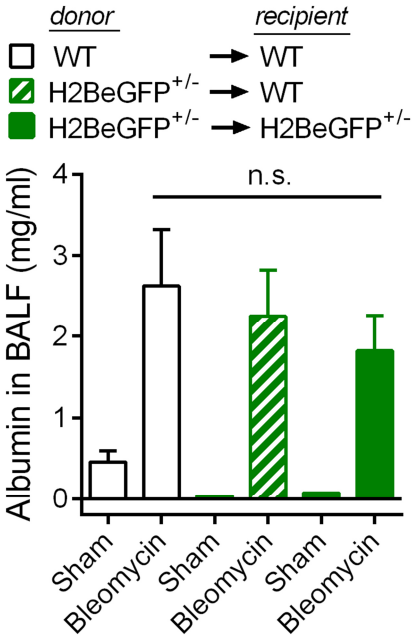

Fig. 10.4: Albumin concentration in BALF after bleomycin instillation in bone marrow transplanted mice.
1U/kg BW bleomycin in 40µl 0.9% NaCl was instilled i.t.; Sham = 40µl 0.9% NaCl i.t.; WT = wild type (C57BL/6J). Sample collection on day 2 before albumin quantification by ELISA. All values are presented as the mean ± SEM. n.s. = not significant. Samples were used from the same experiment as shown in Fig. 3.3.

To study the release of histones to the extracellular compartment, citrullinated histones H3 (H3-Cit) were analyzed by ELISA in the same samples as in Fig. 3.1A. Two days after bleomycin administration (1U/kg BW, i.t.), the amount of H3-Cit in the BALF significantly increased and reached the highest levels (Fig. 10.5A). On day 3, there was still significantly more H3-Cit in the bleomycin treated group in comparison to the sham-group.

Citrullinated H3 was also analyzed in the BALF of neutrophil-depleted mice (Ly6GCre/iDTR) in comparison to non-depleted control mice (iDTR) after two days of bleomycin administration. Before the surgery, neutrophils were depleted for three days with DTX (25ng/g bodyweight). The H3-Cit significantly decreased in neutrophil depleted mice in comparison to the non-depleted iDTR control mice (Fig. 10.5B).

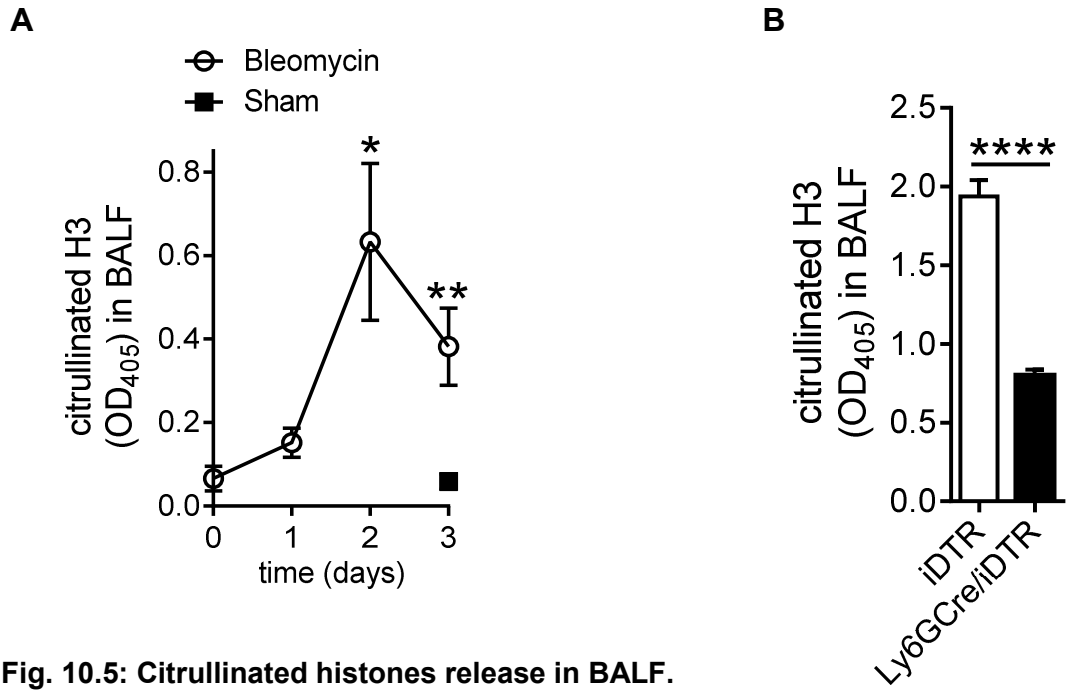

Fig. 10.5: Citrullinated histones release in BALF.
(A) Time course of citrullinated histones in BALF, ELISA. All values are presented as the mean ± SEM. *p<0.05 and **p<0.01 vs. sham, One-way ANOVA. (B) Citrullinated histones in BALF after neutrophil-depletion, ELISA. Diphtheria toxin (DTX) was given i.p. with 25ng/g BW from day -2 to day 0. Sample collection on day 2. n ≥ six male mice/group. The values are presented as the mean ± SEM. ****p<0.001 vs. iDTR, Student's t test.
1U/kg BW bleomycin in 40µl 0.9% NaCl was instilled i.t. on day 0; Sham = 40µl 0.9% NaCl i.t..

The citrullination of histones is mediated by the peptidylarginine deiminase 4 (PAD4) (Chap. I-2.2.1). In PAD4 knock out (PAD4$^{-/-}$) mice the citrullinated histones were significantly reduced (Fig. 10.6). BALF were collected 2 days following bleomycin administration.

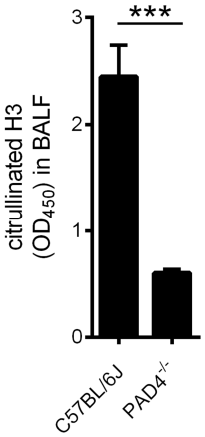

Fig. 10.6: Citrullinated histones in BALF of PAD4$^{-/-}$ mice after bleomycin instillation.
1U/kg BW bleomycin in 40µl 0.9% NaCl was instilled i.t.; Sham = 40µl 0.9% NaCl i.t.. Sample collection on day 2 before quantification of citrullinated H3 by ELISA. The values are presented as the mean ± SEM. ***p<0.005 vs. C57BL/6J, Student's t test. n ≥ six male mice/group.

Depletion of neutrophils had a strong influence on the severity of pulmonary fibrosis and H3-Cit is released by neutrophils in the forms of NETs. In the next experiments, the influence of IL-27 on H3-Cit produced by neutrophils was studied. Peritoneal elicited neutrophils (PENs) were generated as described in Chap. II-2.1.4, $5x10^5$ cells were seeded in 300µl Medium and incubated with the indicated stimuli for 4h (37°C, 5% CO_2). LPS was added with 100ng/ml, recombinant murine IL-27 (rmIL-27) was added with 200ng/ml and cell-free BALF (24h) was added with 10µl per sample. The BALF (24h) was collected from a separate experiment where C57BL/6J mice had received 1U/kg BW bleomycin i.t.. After 24h the cell-free BALF was collected. LPS showed the highest release of H3-Cit by PENs after 4h. The BALF (24h) contained nearly the same amounts of H3-Cit as compared to LPS (positive control). When rmIL-27 was added in addition to the BALF (24h), the amount of H3-Cit was significantly reduced. Recombinant murine IL-27 alone did not influence the release of H3-Cit (Fig. 10.7A). Taken together, IL-27 affected the release of H3-Cit in PENs *in vitro*. The activity of BALF is most likely related to endogenous inflammatory mediators (e.g. cytokines) released in response to bleomycin. Bleomycin itself has a short biological half-life of 2 hours. Hence, the activated BALF (24h) was presumably free of bleomycin.

In addition, the inhibition release of H3-Cit release by IL-27 was studied *in vivo*. C57BL/6J mice and IL-27-deficient receptor α knock out mice (IL-27RA$^{-/-}$) mice received 1U/kg BW bleomycin i.t. for two days before cell-free BALF was collected. In addition, the Ly6G$^+$CD11b$^+$ neutrophils in BALF were counted by flow cytometry analyses with the help of counting beads. The regions for the positive cell populations were adjusted by using isotype antibodies. The amount of H3-Cit was normalized to 1,000 neutrophils in the BALF. If the IL-27 signaling was genetically disrupted (IL-27RA$^{-/-}$), the amount of H3-Cit in the BALF significantly increased in comparison to the control group (C57BL/6J) (Fig. 10.7B).

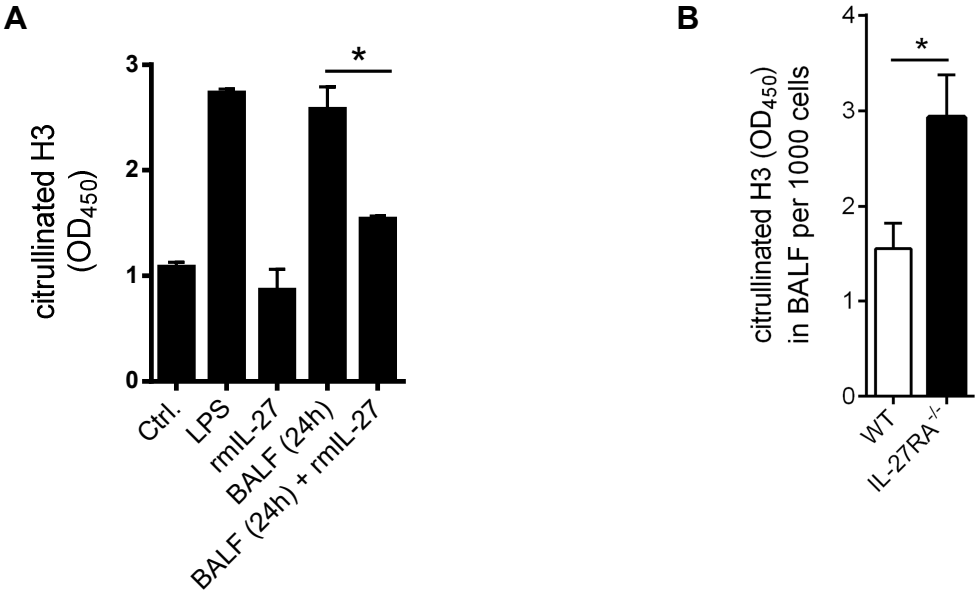

Fig. 10.7: Release of Citrullinated H3 in dependence of IL-27 and IL-27RA.
(A) Citrullinated H3 released by peritoneal elicited neutrophils, ELISA. C57BL/6J peritoneal elicited neutrophils stimulated at 37°C, 5% CO_2 for 4h. Ctrl. = control, unstimulated; LPS (100ng/ml); rmIL-27 = recombinant murine IL-27 (200ng/ml); BALF (24h) indicates transferred cell-free BALF of C57BL/6J mice treated with 1U/kg BW bleomycin i.t. in 0.9% NaCl for 24h (10µl). All values are presented as the mean ± SEM. *p<0.05 vs. BALF (24h), Student's t test.
(B) Citrullinated H3 in BALF of IL-27RA$^{-/-}$ and C57BL/6J mice, ELISA. 1U/kg BW bleomycin in 40µl 0.9% NaCl was instilled i.t.; normalized to 1,000 cells in BALF. Sample collection on day 2. n ≥ eight male mice/group. WT = wild type (C57BL/6J). The values are presented as the mean ± SEM. *p<0.05 vs. WT, Student's t test.

Next, NET formation was studied with the help of laser scanning confocal fluorescence microscopy. PENs were obtained from Ly6GCre/H2BeGFP reporter mice. In the Ly6GCre strain, the fluorophore tandem dimer Tomato (tdTomato) is expressed under the control of the neutrophil marker Ly6G. This results in red fluorescence of neutrophils. In addition, histones were conjugated to eGFP. $1x10^5$ cells/sample/300µl were seeded and allowed to rest for 2h. The neutrophils were stimulated with 100ng/ml LPS, 200ng/ml rmIL-27, 10µl BALF (24h) or with BALF (24h) + rmIL-27 for 4h.

In Fig. 10.8, representative NETs are shown. LPS (positive control) resulted in strong NET formation. Recombinant murine IL-27 alone did not show NET formation capacity and the BALF (24h) did show NET formation, comparable to the LPS stimulated samples. If rmIL-27 was added to the BALF (24h), the NET formation was significantly reduced. These data confirmed the H3-Cit ELISA (Fig. 10.7A). Confocal

fluorescence microscopy was done by Dr. Dennis Strand (Laser Scanning Mircroscopy Core Facility, University Medical Center Mainz).

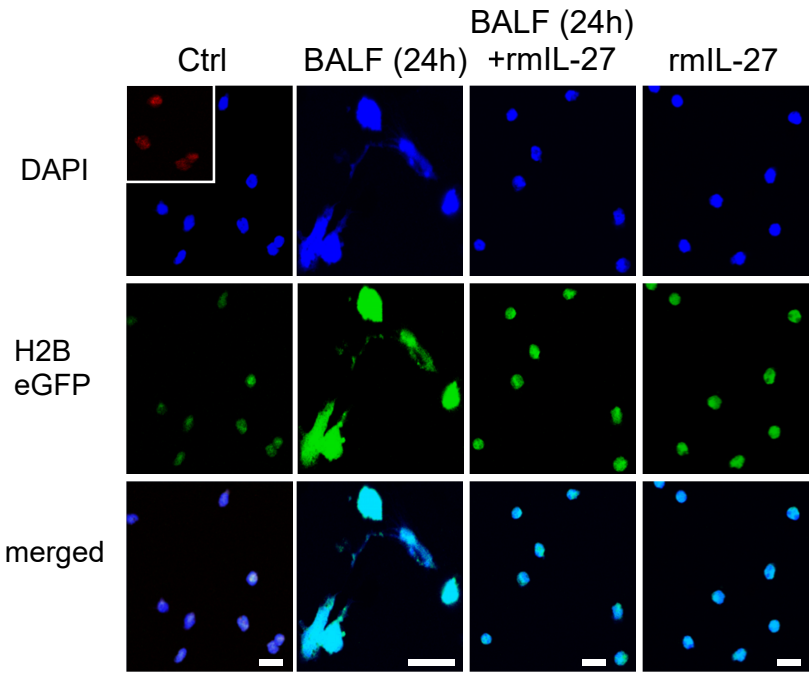

Fig. 10.8: NET formation in confocal fluorescence microscopy.
Representative images of Ly6GCre/H2BeGFP peritoneal elicited neutrophils stimulated at 37°C, 5% CO_2 for 4h. Ctrl. = unstimulated; LPS (100ng/ml); rmIL-27 = recombinant murine IL-27 (200ng/ml); BALF (24h) = BALF of C57BL/6J mice treated with 1U/kg BW bleomycin i.t. in 0.9% NaCl for 24h (10µl). Three male mice were used.
Top row: single channel fluorescence of DAPI (DNA staining), middle row: eGFP (Histone reporter). Small picture: tdTomato (under Ly6G expression control). For the merge pictures only DAPI and eGFP were detected. Scale bar: 20µm. DAPI: Excitation: 485nm, Emission: 538nm; tdTomato: Excitation: 554nm, Emission: 581nm; eGFP: Excitation: 358nm, Emission: 461nm. Magnification: 63x oil immersion, different zoom factors can be appreciated by scale bars.

3.2 The severity of bleomycin-induced pulmonary fibrosis in dependence of extracellular histones

As shown in Fig. 10.5, citrullinated histones are released by neutrophils after bleomycin administration. To study the role of extracellular histones in bleomycin-induced pulmonary fibrosis, histone H4 was blocked by monoclonal antibodies. Histone H4 was used as blocking target due to the highest cytotoxicity of the histone subclasses H1, H2, H3 and H4 (93) (94). The blocking antibody (anti-H4, MHIS1952) and a matched isotype control antibody (mIgG2a) were injected intravenously to male C57BL/6J mice in 250µl 0.9% NaCl on day 0. Antibodies were given in a dose of

10mg/kg body weight. Mice received 1U/kg BW bleomycin i.t. on the same day (day 0). In Fig. 10.9, representative lung images of bleomycin treated mice are depicted. After administration of bleomycin, the mice with neutralization of extracellular histones displayed reduced green collagen staining in the lung as compared to the control group.

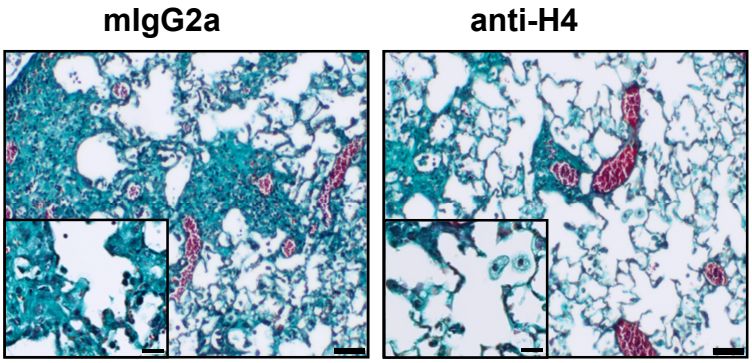

Fig. 10.9: Histology of lung sections after histone blocked pulmonary fibrosis.
Representative lung sections from bleomycin-induced pulmonary fibrosis of the two groups with either blocked histones (anti-H4) or control antibody (mIgG2a) are shown after two weeks. Antibodies were injected i.v. on day 0 with 10mg/kg body weight. Masson's trichrome staining (Goldner): collagen = green-cyan, nuclear chromatin = brownish-black, cytoplasm = bright red, erythrocytes = dark red, muscle = red. Magnification: 10x. Scale bar: 50µm (large picture); 20µm (small picture). 1U/kg BW bleomycin in 40µl 0.9% NaCl was instilled i.t..

These results were confirmed by collagen assay after four weeks. In Fig. 10.10A, the histone blocked group had significantly less collagen I,V as compared to the control group. The expression levels of *collagen I,V* mRNA in whole lung tissue confirmed the results of the collagen assay. The histone blocked group expressed less *collagen I,V* mRNA in lungs as was observed for the control group (Fig. 10.10B). The collagen I,V amount and the expression of *collagen I,V* mRNA in lung tissue was studied after four weeks (1U/kg BW bleomycin i.t.). Antibodies were injected intravenously with 10mg/kg bodyweight on day 0.

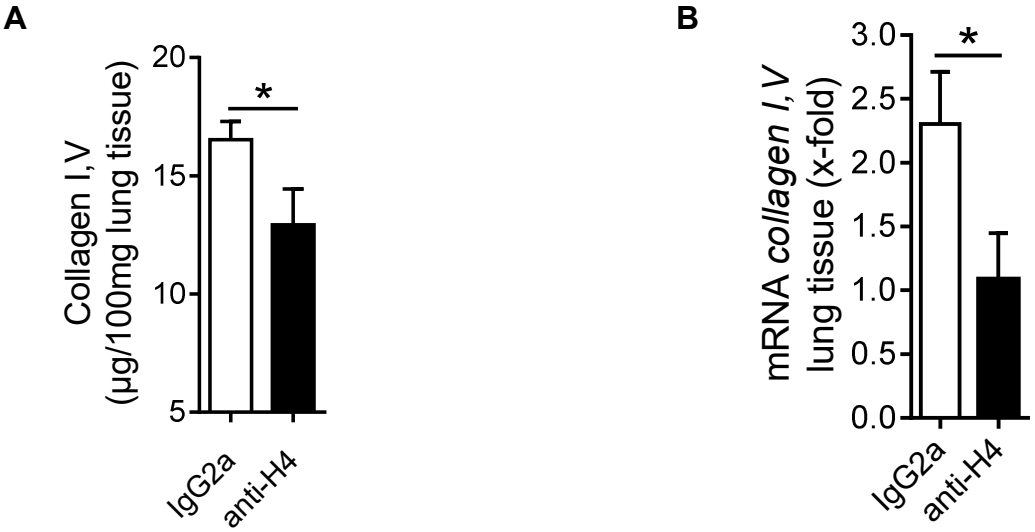

Fig. 10.10: Collagen I,V and *collagen I,V* mRNA expression in the lungs after histone blocked pulmonary fibrosis.
(A) Collagen I,V in the lungs 4 weeks after histone blockade, collagen assay. The values are presented as the mean ± SEM. *p<0.05 vs. mIgG2a, Student's t test. Collagen I,V amount was normalized to 100mg lung tissue. (B) Expression of collagen I,V mRNA in whole lung tissue 4 weeks after histone blockade, qPCR. 1U/kg BW bleomycin in 40µl 0.9% NaCl was instilled i.t.. Antibodies (10mg/kg body weight i.v.) were injected on day 0. The values are presented as the mean ± SEM. *p<0.05 vs. mIgG2a, Student's t test. (A+B), n = seven male mice/group.

The IL-27p28 levels in the BALF were analyzed after two weeks of bleomycin-induced pulmonary fibrosis (1U/kg BW bleomycin i.t.). The BALF of the anti-H4 treated group showed significantly higher IL-27p28 concentrations as compared to the control group (Fig. 10.11A). No significant difference in IL-27p28 in the BALF was detectable between the two groups after four weeks (data not shown). The concentrations of TGFβ1 were reduced by about 50%, when extracellular histones were neutralized during bleomycin-induced pulmonary fibrosis (Fig. 10.11B).

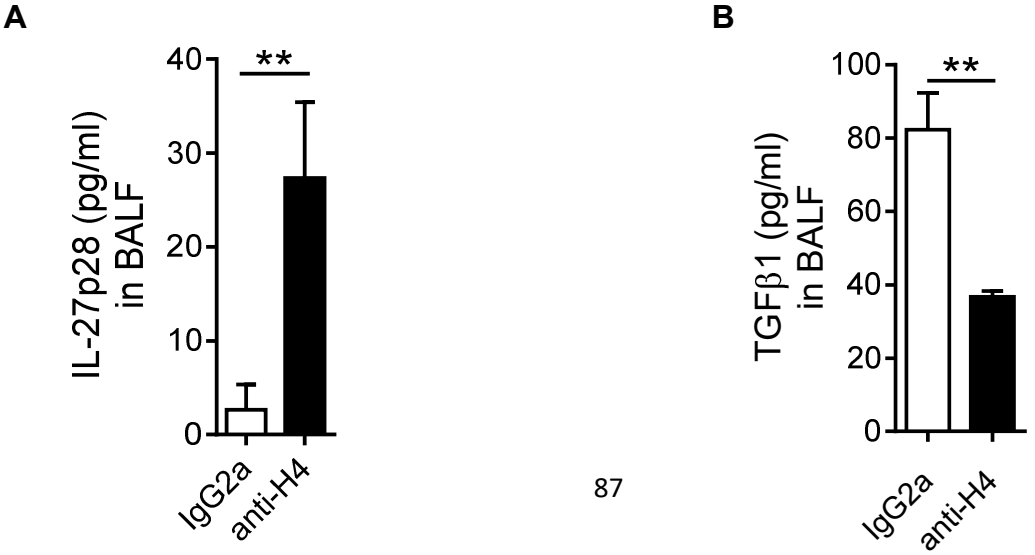

Fig. 10.11: Cytokine levels in the BALF after histone blocked pulmonary fibrosis.
(A) IL-27p28 levels in the BALF after histone blockade, ELISA. (B) TGFβ1 levels in the BALF after histone blockade, ELISA. n ≥ seven male mice/group.
1U/kg BW bleomycin in 40µl 0.9% NaCl was instilled i.t.. Both antibodies were given by 10mg/kg body weight i.v. on day 0. The duration of the experiment was 2 weeks (IL-27p28) or 4 weeks (TGFβ1). All values are presented as the mean ± SEM. **p<0.01 vs. mIgG2a, Student's t test.

Myofibroblasts are major producers of ECM components during fibrosis. Replenishment of the pool of myofibroblast may occur by differentiation of endothelial cells and epithelial cells in the process of epithelial/endothelial-to-mesenchymal transition (EMT/EndMT). The expression levels of the EMT specific transcription markers Slug, Snail and Zeb2 were detected in whole lung tissue after administration of 1U/kg BW bleomycin i.t., after four weeks. In addition, the expression levels of the markers for EMT and for EndMT were analyzed in the same samples: Fibroblast-specific protein 1 (FSP-1), Vimentin and alpha smooth muscle Actin (α-SMA). In the whole lung tissue of the histone blocked group, the three EMT markers Slug, Snail and Zeb2 were expressed about 50% less as compared to the control group (Fig. 10.12A). Likewise, the markers for EMT/EndMT, FSP-1, Vimentin and α-SMA were reduced by around 50% in the anti-H4 treated group in comparison to the isotype control group (Fig. 10.12B). In summary, EMT and EndMT markers were reduced by blockade of histone H4.

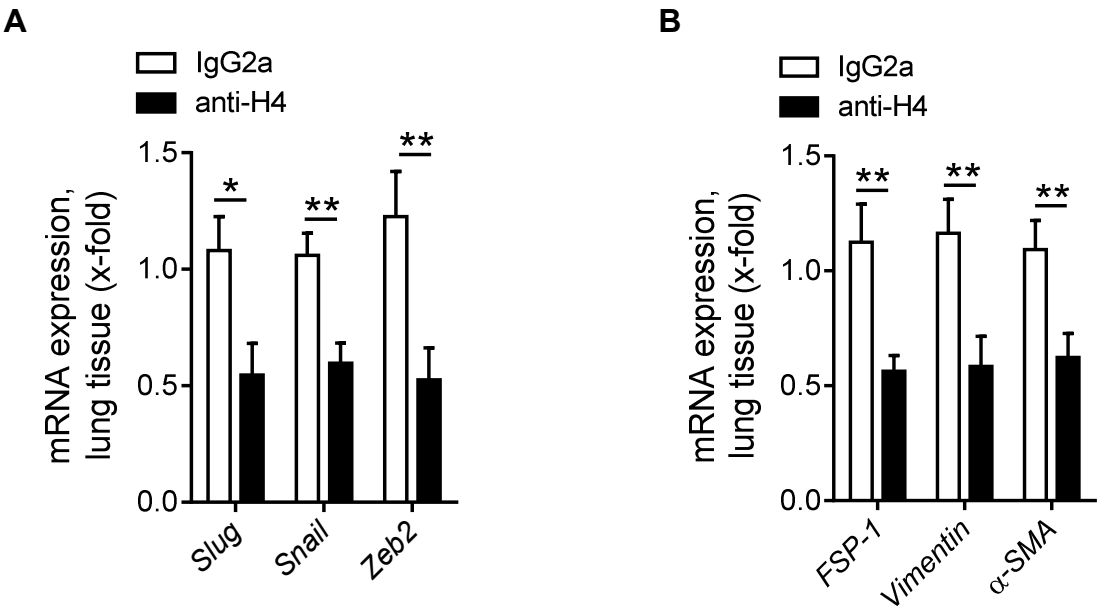

Fig. 10.12: Expression of EMT-specific transcription factors and EndMT-markers after histone blocked pulmonary fibrosis.
(A) Expression of EMT-specific transcription factors Slug, Snail and Zeb2 in whole lung tissue, qPCR. (B) Expression of EMT- and EndMT-markers FSP-1, Vimentin, α-SMA in whole lung tissue, qPCR. 1U/kg BW bleomycin in 40µl 0.9% NaCl was instilled i.t.. Both antibodies were given in a concentration of 10mg/kg bodyweight i.v. on day 0 and lungs were collected after four weeks. Expressions were normalized to *gapdh* mRNA expression. FSP-1: Fibroblast-specific protein 1, α-SMA: alpha smooth muscle actin. All values are presented as the mean ± SEM. *p<0.05 and **p<0.01 vs. mIgG2a, Student's t test. n ≥ seven male mice/group .

The EndMT was also studied by immunofluorescent histologies (Chap. II-2.3.4). The lung sections and the staining for EndMT-markers CD31 (endothelial cell marker) and α-SMA were performed by AG Schäfer, University Medical Center Mainz. The confocal fluorescence microscopy was done with the help of Dr. Nina Xia (Department of Pharmacology, University Medical Center Mainz). In the control group, typical EndMT changes could be observed. α-SMA (green) production was increased whereas the CD31 (red) molecules were reduced. On the other hand, the typical EndMT changes were much less pronounced in the histone blocked group (Fig. 10.13).

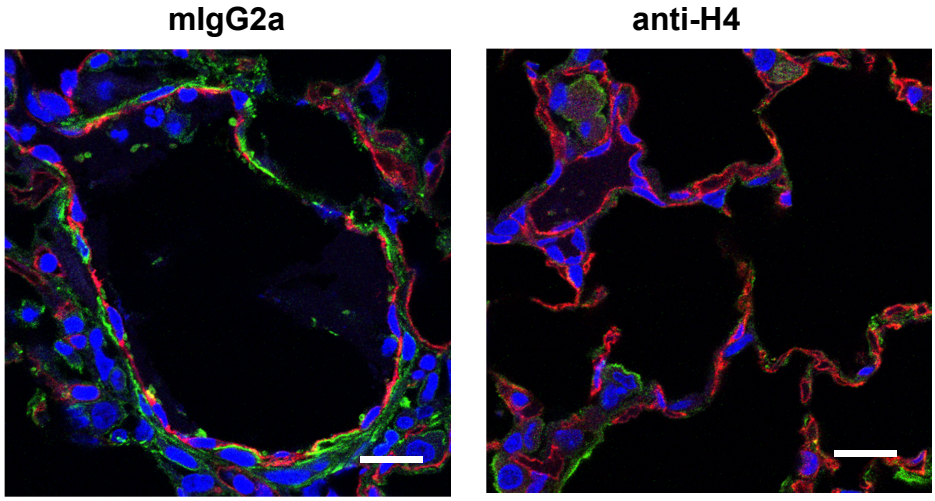

Fig. 10.13: Confocal fluorescence microscopy of EndMT in lung sections after histone blocked pulmonary fibrosis.
Endothelial cell marker CD31 (red) and EndMT marker α-SMA (green) are shown. DAPI is shown in blue. 1U/kg BW bleomycin in 40µl 0.9% NaCl was instilled i.t.. Neutralizing anti-H4 antibodies and isotype control antibodies were given by 10mg/kg bodyweight i.v. on day 0. Magnification: 63x, oil immersion, scale bar = 20µm. α-SMA: alpha smooth muscle Actin. Representative lung areas are shown.

To date, the role of $CD4^+Foxp3^+$ T regulatory cells (Tregs) is not completely understood during pulmonary fibrosis. To study the effects of extracellular histones on Tregs two groups of male mice received antibodies (anti-H4 and mIgG2a isotype) with 10mg/kg bodyweight i.v. and 1U/kg BW bleomycin i.t. on day 0. After two weeks, the mediastinal lymph nodes were collected, lymphocytes isolated and stained for CD4 and Foxp3. The numbers of Tregs were analyzed by flow cytometry with the help of counting beads. To define the positive cell population an isotype antibody for CD4 was used. For Foxp3, fluorescence *minus one* control was performed. The blockade of histones affected the total numbers of Tregs in the mediastinal lymph nodes after two weeks of bleomycin administration. The mediastinal lymph nodes of the histone blocked group contained reduced frequencies of $CD4^+Foxp3^+$ Tregs as compared to the control group (Fig. 10.14A).

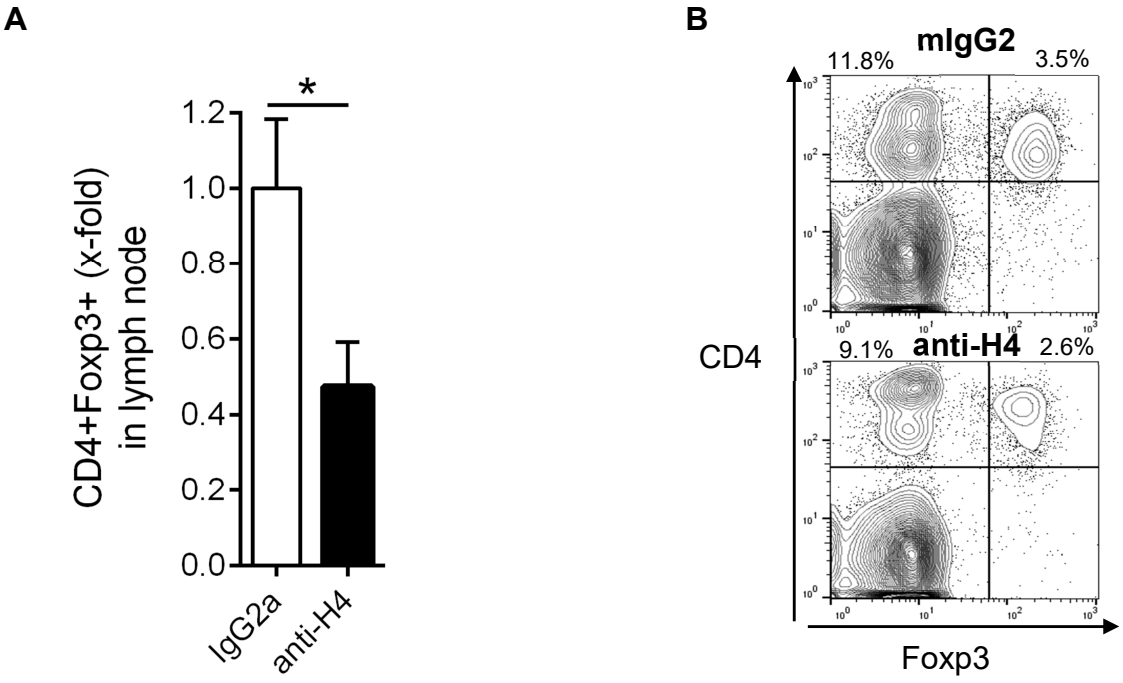

Fig. 10.14: $CD4^+Foxp3^+$ Tregs in mediastinal lymph nodes after histone blocked pulmonary fibrosis.

(A) Percentage of total number of $CD4^+Foxp3^+$ Tregs in mediastinal lymph nodes. The values are presented as the mean ± SEM. *p<0.05 vs. mIgG2a, Student's t test. (B) Flow cytometry analyses of $CD4^+Foxp3^+$ Tregs in mediastinal lymph nodes.

1U/kg BW bleomycin in 40µl 0.9% NaCl was instilled i.t.. Both antibodies were given in a dose of 10mg/kg bodyweight i.v. on day 0 and samples were collected after two weeks. n ≥ 13 male mice/group.

Taken together, these data indicate that extracellular histones (released by NETs) exert pro-fibrotic effects. The extracellular histones influenced cytokine levels in BALF as well as the $CD4^{+}Foxp3^{+}$ Treg numbers in mediastinal lymph nodes.

4 Histones regulate a subset of stress-induced genes in Tregs

T regulatory cells are differentially regulated during bleomycin-induced pulmonary fibrosis and their role appears to be context dependent (121). To have a closer look at intracellular processes and gene expression of Tregs in dependence of extracellular histones, a RNA-Sequencing approach was performed.

C57BL/6J mice were treated with 1U/kg BW bleomycin i.t.. An anti-H4 antibody (clone MHIS1952) and an isotype control antibody (mIgG2a) were given intravenously with 10mg/kg BW on day 0. On day 28, the mediastinal lymph nodes were collected and the $CD4^+CD25^+$ Tregs of the different groups were isolated by MACS (Chap. II-2.3.2). The flow cytometry analyses showed a purity of 94.6% (mIgG2a) and 94.4% (anti-H4) $CD4^+CD25^+$ Tregs (Fig. 11.1A). The isotype antibody for CD4 was used to identify the negative cell population.

To confirm the co-localization of the MACS-isolated $CD25^+$ cells with $CD4^+Foxp3^+$ Tregs splenocytes from male C57BL/6J mice were stained for CD4, CD25 and Foxp3. Isotype antibodies were used to gate the positive populations for $CD4^+$ and $CD25^+$ cells. For the Foxp3 positive region, fluorescence minus one control was performed. Fig. 11.1B shows the co-localization of $CD4^+CD25^+$ and $CD4^+Foxp3^+$ Tregs. The cells were previously gated for $CD4^+$ cells.

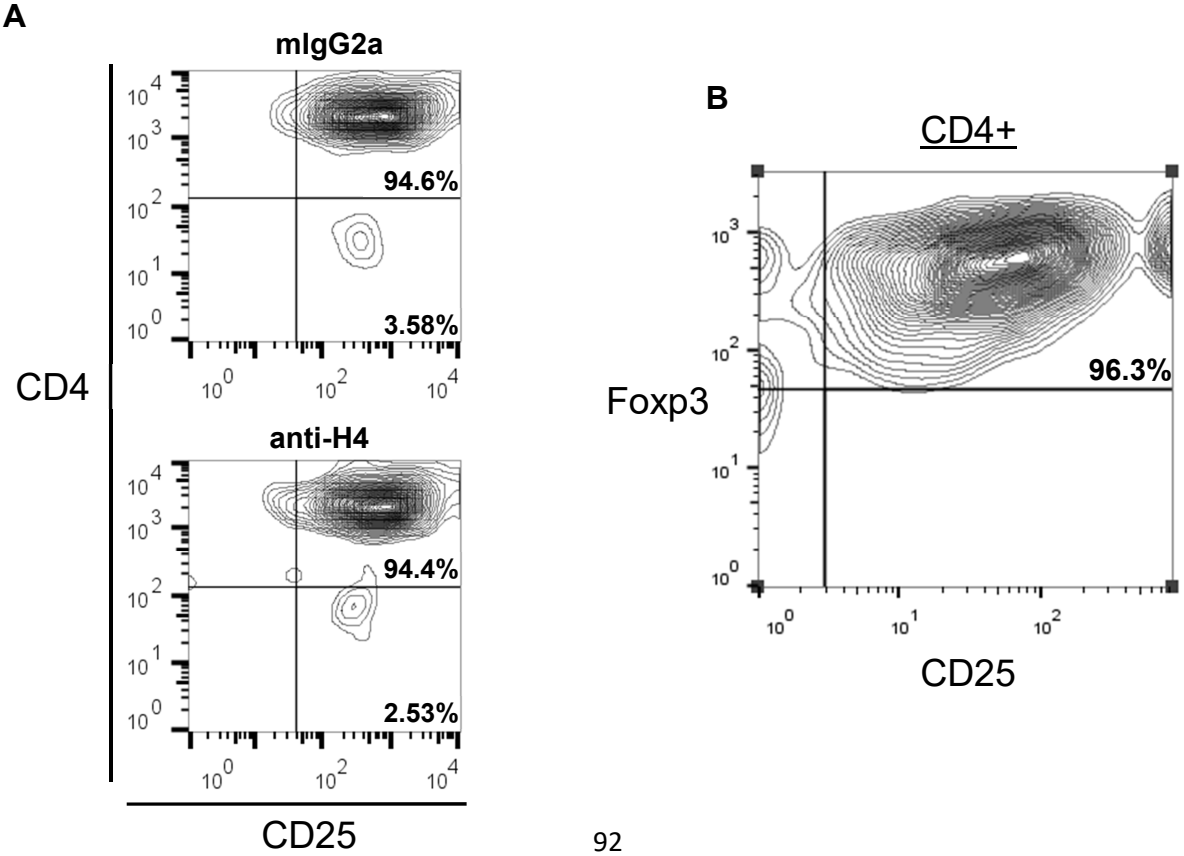

Fig. 11.1: Purity and characterization of $CD4^+CD25^+$ Tregs.
(A) Purity of $CD4^+CD25^+$ Tregs after MACS, flow cytometry analysis. $CD4^+CD25^+$ Tregs were purified by MACS from mediastinal lymph nodes of C57BL/6J mice after bleomycin-induced pulmonary fibrosis (1U/kg BW bleomycin in 40µl 0.9% NaCl i.t., four weeks). Representative contour plots are shown, n ≥ 6 male mice/group. (B) $CD4^+CD25^+$ Tregs and $CD4^+Foxp3^+$ Tregs were an identical population, flow cytometry analysis. Representative contour plot is shown. $CD4^+CD25^+$ naïve Tregs were purified by MACS from spleens of three single untreated C57BL/6J mice. In addition, the cells were stained for Foxp3. Contour plot is pre-gated for $CD4^+$ cells.

The total RNA of the $CD4^+CD25^+$ Tregs (Chap. II-2.3.2) of the mediastinal lymph nodes was isolated (Chap. II-2.5.1) and used for RNA-Sequencing (Chap. II-2.5.5: Next Generation Sequencing, Institute of Molecular Biology Mainz; Dr. Han). The mRNA expression levels of the stress-induced genes *hspa1a*, *hspa1b*, *dnajb1*, *stip1*, *hsph1* were significantly reduced after histone blockade (anti-H4) treatment in comparison to the isotype control (mIgG2a) treatment (Fig. 11.2). The bioinformatics analysis was done by Federico Marini (Institute of Medical Biostatistics, Epidemiology and Informatics, Mainz) with the program R (version 3.1.2).

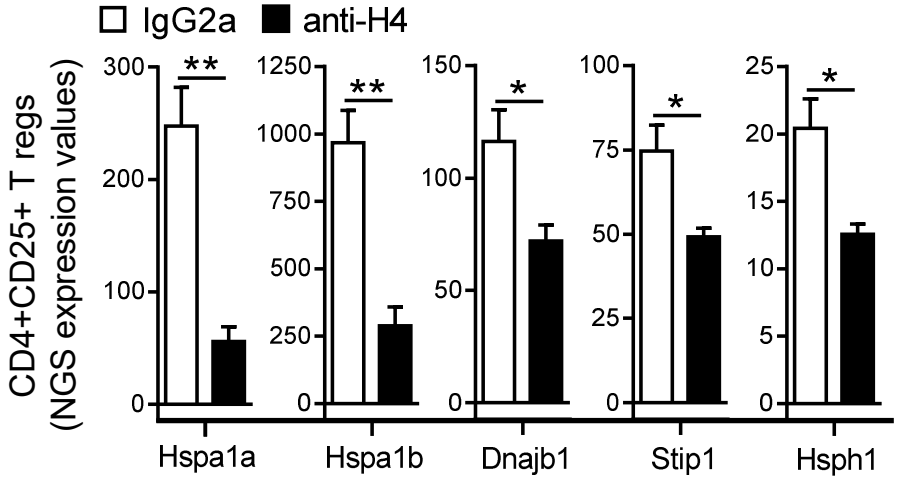

Fig. 11.2: RNA-Sequencing expression values of differentially expressed genes in $CD4^+CD25^+$ Tregs after histone blocked pulmonary fibrosis.
$CD4^+CD25^+$ Tregs were purified by MACS from mediastinal lymph nodes of C57BL/6J mice after bleomycin-induced pulmonary fibrosis (1U/kg BW bleomycin in 40µl 0.9% NaCl i.t., four weeks). The antibodies mIgG2a and anti-H4 were given i.v. (10mg/kg bodyweight) on day 0. mIgG2a = isotype control antibody, anti-H4 = histone blocking antibody, NGS = Next Generation Sequencing. Samples of 2-3 mice/group were pooled and low-input RNA-Sequencing of the Treg-RNA was done by Dr. Han, IMB Mainz. All values are presented as the mean ± SEM. *p<0.05 and **p<0.01 vs. mIgG2a, Student's t test. Anti-H4: 6 male mice; mIgG2a: 8 male mice.

Tab. 23: Differentially expressed genes in Tregs after anti-H4 treatment.

P-value <0.05 (Student's t test) is shown.

Gene	p-value
Hsph1*	0.000248
Cpt1a	0.001185
Hspa1a*	0.001616
Trerf1	0.001616
Dnajb1*	0.001918
Jun	0.007270
Dusp1	0.007270
Stip1	0.008353
Rnf214	0.017914
Lclat1	0.024419
Hspa1b*	0.041055

* Heat shock proteins

The expression levels of different stress-induced genes in Tregs were affected by histone blockade (anti-H4) during bleomycin-induced pulmonary fibrosis. Next, an *in vitro* experiment with naïve Tregs was performed to investigate, if extracellular histones could directly induce the expression of stress-induced genes. In addition, the influence of IL-27 on the expression of stress-induced genes in Tregs was studied. Naïve Tregs ($CD4^+CD25^+$) were isolated by MACS from spleens of male C57BL6/J mice. $4x10^4$ cells/sample/200µl (96 well scale) were seeded and allowed to rest overnight in rmIL-2 (100ng/ml) containing Treg Medium. The cells were stimulated with different reagents: histones (1µg/ml), rmIL-27 (200ng/ml) and histones + rmIL-27 for 8h.

After 8h, the *hspa1b* mRNA expression was found to be 3-fold higher in comparison to unstimulated controls (Ctrl) (Fig. 11.3). Recombinant mouse IL-27 alone did not significantly affect the *hspa1b* mRNA expression levels in comparison to unstimulated control cells. Recombinant mouse IL-27 in combination with purified histones, significantly reduced the *hspa1b* mRNA expression. As a positive control, α-CD3 (3µg/ml) and α-CD28 (2.5µg/ml) antibodies were added to the cell culture medium at the 0h time point. The positive control resulted in a significant higher *hspa1b* mRNA expression as expected. The expression levels of stress-induced

genes, such as the heat shock proteins (Hsp), were induced in Tregs by histones and were negatively regulated by recombinant murine IL-27 (rmIL-27) (Fig. 11.3). In parallel, splenocytes of three male C57BL/6J mice and three male IL-27RA$^{-/-}$ mice were isolated as described in Chap. II-2.1.10, without magnetic purification. A number of 1x10^6 splenocytes were stained for CD3, CD4 and IL-27RA. Isotype control antibodies were used to define the positive populations. The splenocytes of IL-27RA$^{-/-}$ mice were used as negative controls. The CD3$^+$CD4$^+$ T cells from the spleen of C57BL/6J mice were present in a frequency of 93.7% double positive CD4$^+$IL-27RA$^+$ T cells. The splenocytes of IL-27RA$^{-/-}$ mice did not show a relevant IL-27RA staining (0.44% CD4$^+$IL-27RA$^+$) (Fig. 11.4), thereby confirming both the specificity of the IL-27RA staining antibody and the expected phenotype of the IL-27RA$^{-/-}$ mice.

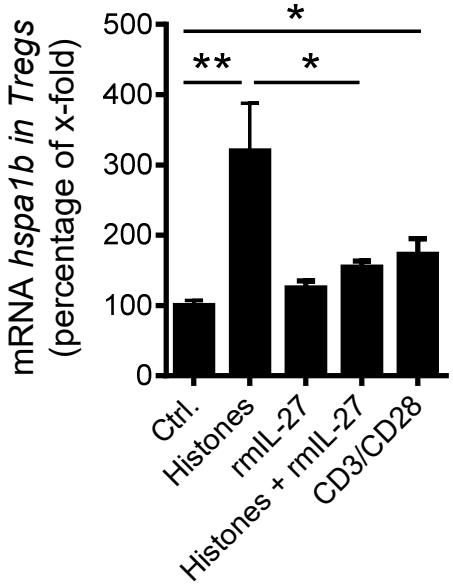

Fig. 11.3: Expression of *hspa1b* mRNA in naïve Tregs.
Cultures of 4x10^4 naïve Tregs (from spleen, C57BL/6J) were stimulated with purified histones (1µg/ml), rmIL-27 (200ng/ml) or histones + rmIL-27 at 37°C, 5% CO_2 for 8h. *hspa1b* mRNA expression values were quantified by qPCR. Expression levels were normalized to *gapdh* mRNA expression. CD3/CD28 (= positive control) was given with 3µg/ml α-CD3 and 2.5µg/ml α-CD28 to the medium. rmIL-27 = recombinant murine IL-27, Ctrl = unstimulated. All values are presented as the mean ± SEM. *p<0.05 and **p<0.01 vs. Ctrl or Histones, one-way ANOVA.

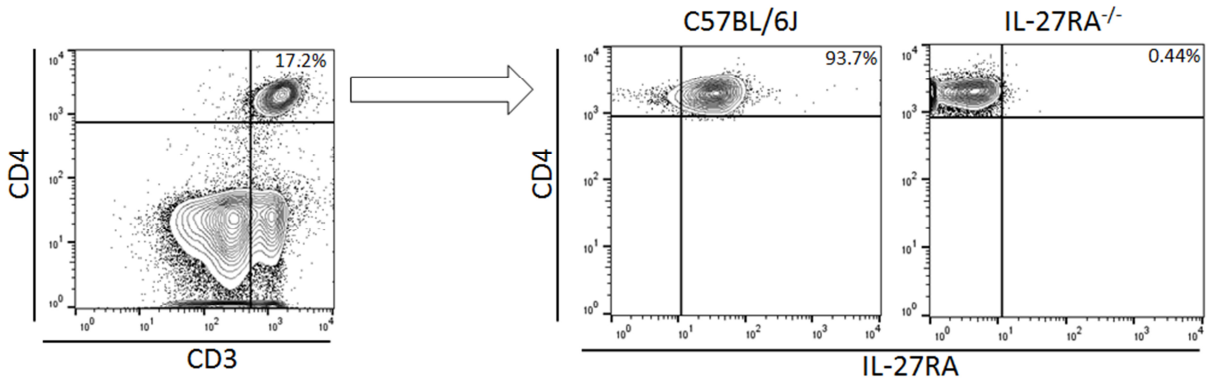

Fig. 11.4: Expression of IL-27RA on $CD3^+CD4^+$ T cells.
A number of $1x10^6$ splenocytes from male C57BL/6J and IL-$27RA^{-/-}$ (negative control) mice were stained and previously gated for $CD3^+CD4^+$ double positive T cells. Representative flow cytometry contour plots for each strain are shown.

The gene expression in Tregs was modulated by histones and IL-27. To study if this changed gene expression affected the plasticity of the Tregs, an adoptive transfer experiment was performed. First, male wild type mice (C57BL/6J) were used in the model of bleomycin-induced pulmonary fibrosis. An anti-H4 antibody (MHIS1952, five mice) and an isotype control antibody (mIgG2a, eight mice) were given intravenously with 10mg/kg BW and 1U/kg BW bleomycin was instilled i.t. on day 0. After two weeks, the mediastinal lymph nodes were collected and the $CD4^+CD25^+$ Tregs were isolated by MACS. The pooled purified Tregs of individual groups were given intravenously to recipient mice ($3x10^5$ Tregs i.v. in 200µl 0.9% NaCl). Bleomycin-induced pulmonary fibrosis was performed for the recipient groups with a reduced bleomycin dose of 0.3U/kg BW bleomycin i.t. on the same day. The bleomycin dose for the second experiment was reduced to avoid that the effects mediated by the transplanted Tregs were not disguised by exuberant disease severity. The duration of the second experiment (after adoptive Treg cell transfer) was four weeks.

The mice receiving Tregs of anti-H4 antibody treated mice displayed less collagen I,V amount in the lungs (Fig. 11.5A). Accordingly, reduced levels of *collagen I,V* mRNA expression was detectable in the whole lung tissues of mice which received Tregs of anti-H4 treated mice as compared to the control group (Fig. 11.5B).

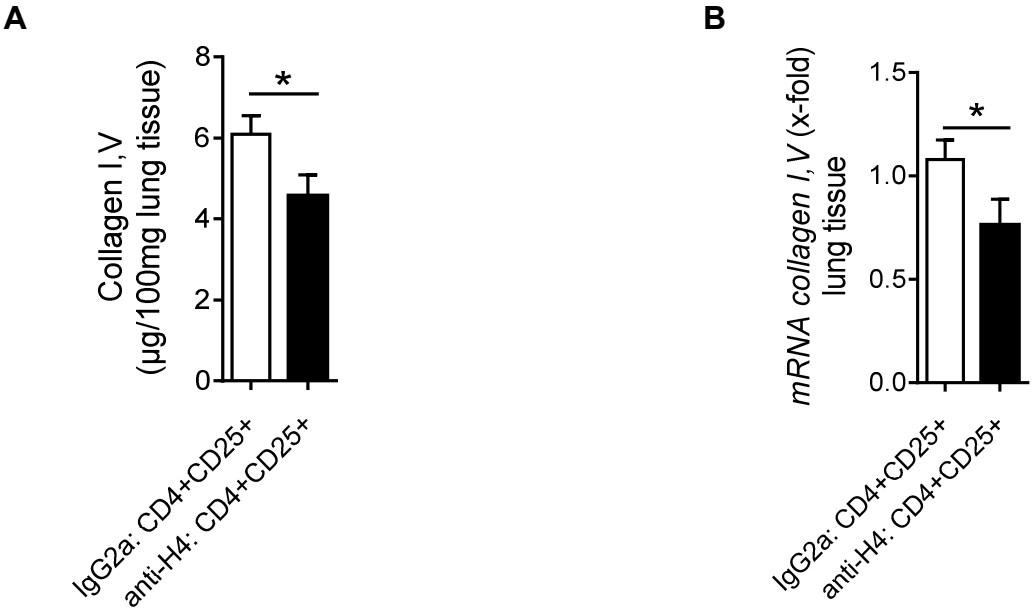

Fig. 11.5: Collagen I,V and *collagen I,V* mRNA in lungs after adoptive transfer of CD4$^+$CD25$^+$ Tregs during pulmonary fibrosis.

(A) Total collagen I,V amount in whole lung tissue after adoptive transfer of Tregs, collagen assay. The values are presented as the mean ± SEM. *p<0.05 vs. mIgG2a: CD4+CD25+, Student's t test.

(B) *Collagen I,V* mRNA expression in whole lung tissue after adoptive transfer of Tregs, qPCR. Expression was normalized to *gapdh* mRNA expression. The values are presented as the mean ± SEM. *p<0.05 vs. mIgG2a: CD4+CD25+, Student's t test.

C57BL/6J mice were treated with mIgG2a or with anti-H4 i.v. (10mg/kg bodyweight) and used for bleomycin-induced pulmonary fibrosis (1U/kg BW bleomycin in 40µl 0.9% NaCl, i.t.) for two weeks. Purified CD4$^+$CD25$^+$ Tregs (purified by MACS) of these mice were transferred i.v. to recipient C57BL/6J mice. The recipient mice received 0.3U/kg BW bleomycin in 40µl 0.9% NaCl, i.t.) for four weeks. anti-H4: five male mice; mIgG2a: eight male mice.

In addition, the transferred Tregs appeared to influence other T cell subsets in the mediastinal lymph nodes (Fig. 11.6). The frequencies of all analysed T cell subsets (CD4$^+$, CD4$^+$IFN-γ$^+$, CD4$^+$IL-17A$^+$, CD4$^+$Foxp3$^+$) were significantly increased in the group which received the Tregs of anti-H4 treated mice.

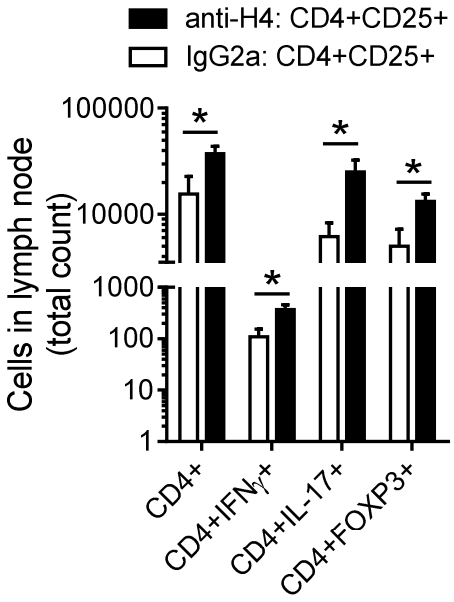

Fig. 11.6: T cell subsets in mediastinal lymph nodes after adoptive transfer of Tregs during pulmonary fibrosis.
C57BL/6J mice were treated with mIgG2a or with anti-H4 i.v. (10mg/kg bodyweight) and used for bleomycin-induced pulmonary fibrosis (1U/kg BW bleomycin in 40µl 0.9% NaCl, i.t.) for two weeks. Purified $CD4^+CD25^+$ Tregs (purified by MACS) of these mice were transferred i.v. to recipient C57BL/6J mice. The recipient mice received 0.3U/kg BW bleomycin in 40µl 0.9% NaCl, i.t.) for four weeks. mIgG2a = isotype control antibody, anti-H4 = histone H4 blocking antibody. $CD4^+IFN\gamma^+$ = Th1, $CD4^+IL\text{-}17A^+$ = Th17, $CD4^+Foxp3^+$ = Tregs. All values are presented as the mean ± SEM. *$p<0.05$ vs. mIgG2a: $CD4^+CD25^+$, Student's t test. anti-H4: five male mice; mIgG2a: eight male mice. Flow cytometry analyses were performed.

In summary, these results suggested a direct effect of extracellular histones on Tregs. Furthermore, the modulated gene expression levels affected the plasticity of the Tregs and other T cell subsets.

5 IL-27 and IL-17 as counter players during bleomycin-induced pulmonary fibrosis

IL-27 is present in BALF during bleomycin-induced pulmonary fibrosis and it has been reported to alleviate severity of fibrosis. IL-27RA$^{-/-}$ mice were used to characterize the role of IL-27 signaling in bleomycin-induced pulmonary fibrosis. After four weeks of 1U/kg BW bleomycin i.t., IL-27RA$^{-/-}$ mice showed an increased green-cyan collagen staining pattern (Masson's Trichrome, Goldner) in histology as compared to the C57BL/6J (WT) control mice (Fig. 12.1).

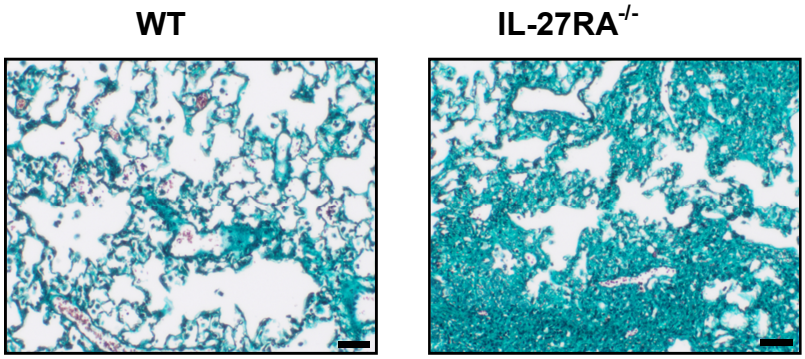

Fig. 12.1: Lung histology of IL-27RA$^{-/-}$ mice and wild type control mice during pulmonary fibrosis.
1U/kg BW bleomycin in 40µl 0.9% NaCl was instilled i.t. and lung sections were prepared after four weeks. Representative lung areas are shown. Masson's trichrome staining (Goldner): collagen = green-cyan, nuclear chromatin = brownish black, cytoplasm = bright red, erythrocytes = dark red, muscle = red. Magnification: 10x. Scale bar: 50µm. WT = wild type (C57BL/6J).

There was an ~3-fold higher amount of collagen I,V in IL-27RA$^{-/-}$ lungs in comparison to the C57BL/6J (WT) lungs as well (Fig. 12.2A). These observations were supported by alterations in the expression levels of *collagen I,V* mRNA in whole lung tissue (Fig. 12.2B). The *collagen I,V* mRNA was ~3-fold higher expressed in IL-27RA$^{-/-}$ whole lung tissue as compared to C57BL/6J whole lung tissue.

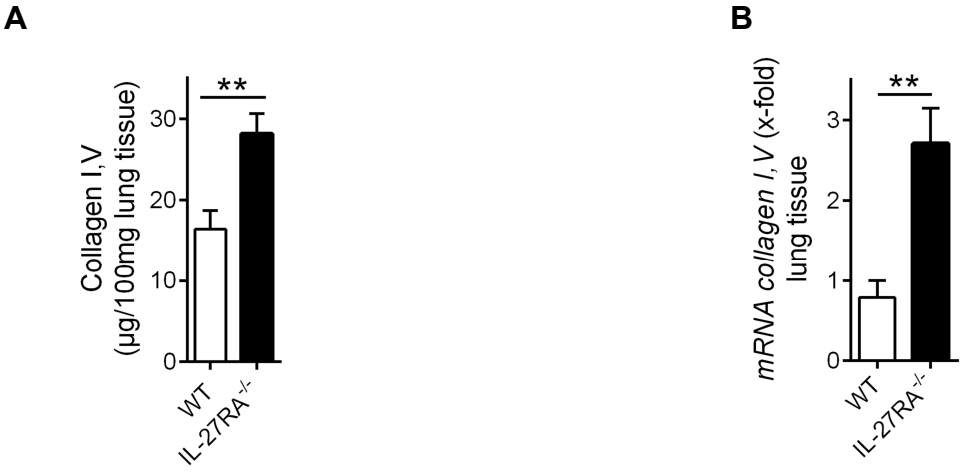

Fig. 12.2: Collagen I,V and *collagen I,V* mRNA in lungs in dependency of IL-27RA signaling during pulmonary fibrosis.
(A) Total collagen I,V amount in the whole lung tissue, collagen assay. Collagen I,V amount was normalized to 100mg lung tissue. (B) Expression of *collagen I,V* mRNA in whole lung tissue, qPCR. Expression was normalized to *gapdh* mRNA expression.
The values are presented as the mean ± SEM. **p<0.01 vs. WT, Student's t test. 1U/kg BW bleomycin in 40µl 0.9% NaCl was instilled i.t. and samples collected after four weeks. WT = C57BL/6J. n ≥ six male mice/group.

The numbers of different T cell subsets were affected in the BALF of IL-27RA$^{-/-}$ mice during bleomycin-induced pulmonary fibrosis. The T cell subsets were analyzed by flow cytometry analyses of the BALF after four weeks. The CD4^{+}IFN-γ^{+} T cell population (Th1) in the BALF of C57BL/6J mice was doubled in comparison to the IL-27RA$^{-/-}$ mice (Fig. 12.3). On the other hand, the CD4^{+}IL-17A^{+} T cell population (Th17) was doubled in IL-27RA$^{-/-}$ mice (Fig. 5.3). The genetic deficiency of IL-27RA also had significant effects on the CD4^{+}Foxp3^{+} Treg cell population. A 3-fold reduction in the frequency of Tregs was observed in IL-27RA$^{-/-}$ BALF as compared to C57BL/6J wild type BALF (Fig. 12.3).

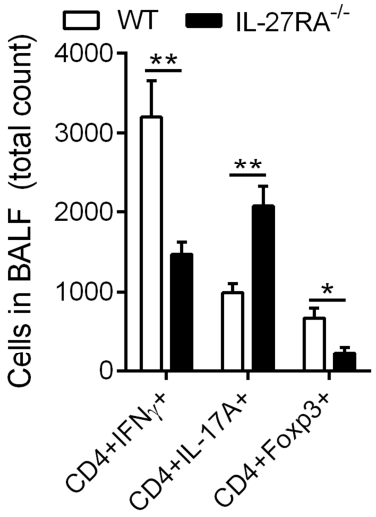

Fig. 12.3: Peripheral lung T cell subsets after bleomycin-induced pulmonary fibrosis in IL-27RA$^{-/-}$ mice.
T cell subsets in BALF during bleomycin-induced pulmonary fibrosis of WT mice and IL-27RA$^{-/-}$ mice were analyzed after four weeks by flow cytometry. 1U/kg BW bleomycin in 40µl 0.9% NaCl was instilled i.t.. WT = wild type (C57BL6/J). All values are presented as the mean ± SEM. **p<0.01 vs. WT, Student's t test. n ≥ six male mice/group.

IL-17A has been reported as a pro-fibrotic cytokine and Th17 cells were negatively regulated by IL-27RA signaling during bleomycin-induced pulmonary fibrosis. To further study the role of IL-17 family members during pulmonary fibrosis, double knock out mice for IL-17A and IL-17F (IL-17DKO) were used in bleomycin-induced pulmonary fibrosis. The collagen amount was analyzed after four weeks. The lungs of IL-17DKO mice had approx. 20% less collagen I,V as compared to the lungs of C57BL/6J wild type mice (Fig 12.4).

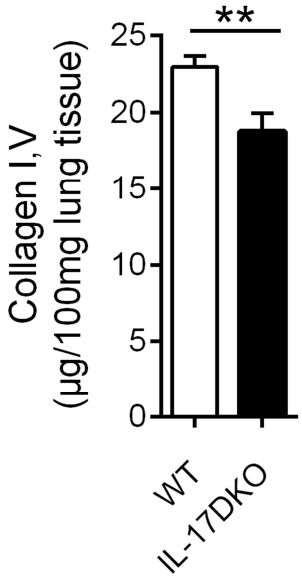

Fig. 12.4: Collagen I,V amount in the whole lung tissue in IL-17DKO mice after bleomycin-induced pulmonary fibrosis.
Collagen I,V amount of whole lung tissue was analysed by collagen assay after four weeks. 1U/kg BW bleomycin in 40µ 0.9% NaCl was instilled i.t.. Collagen I,V amount was normalized to 100mg lung tissue. WT = wild type (C57BL/6J). The values are presented as the mean ± SEM. **p<0.01 vs. WT, Student's t test. n ≥ eight male mice/group.

To summarize the data, missing IL-27RA signaling influenced the abundancy of different T cell subtypes in BALF. Especially the balances of Th1 cells and Th17 cells were disturbed.

6 Platelets drive bleomycin-induced pulmonary fibrosis

6.1 Platelets as a source of TGFβ1

Murine washed platelets were isolated from pooled blood of four male C57BL/6J mice. To document the platelet activation, 200µl of $2x10^8$ platelets/ml were observed by Born aggregometry for 10min at 37°C (Chap. II-2.1.7). The washed platelets were stimulated with endotoxin-free thrombin (100ng/ml), purified histones (50µg/ml) or PBS buffer as negative control. Thrombin resulted in an aggregation of approx. 90%, histones resulted in an aggregation of approx. 35% at the 10 min time point. Thrombin-activated platelets released 3.5-fold more TGFβ1 as compared to histone stimulation. The histone stimulation also resulted in a significant release of TGFβ1 in comparison to the PBS control (Fig. 13.1).

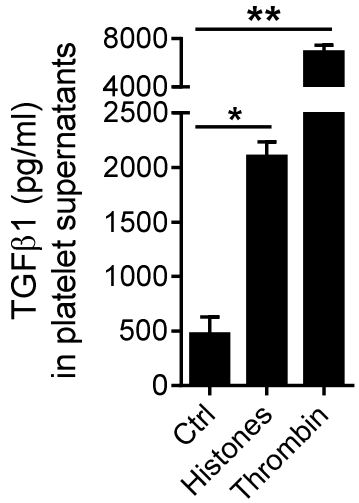

Fig. 13.1: TGFβ1 released by activated platelets.
Murine washed platelets were stimulated by PBS (Ctrl), purified histones (50µg/ml) or thrombin (100ng/ml) for 10min at 37°C (Born Aggregometry). TGFβ1 was detected in cell-free supernatants by ELISA. All values are presented as the mean ± SEM. *p<0.05 and **p<0.01 vs. Ctrl, one-way ANOVA.

Platelets derived from mice with platelet-specific genetic deletion of TGFβ1 (PF4Cre/TGFβ1$^{fl/fl}$) released significantly less TGFβ1 after thrombin (100ng/ml) stimulation for 10 min (evaluated by Born aggregometry followed by ELISA) in comparison to littermate control platelets (TGFβ1$^{fl/fl}$) (Fig. 13.2A).

In the next step, these findings were transferred to the model of bleomycin-induced pulmonary. Mice with TGFβ1-deficient platelets (PF4Cre/TGFβ1$^{fl/fl}$) and littermate mice with littermate control platelets (TGFβ1$^{fl/fl}$) were subjected to bleomycin-induced pulmonary fibrosis. Plasma was collected after four weeks. The plasma of mice with TGFβ1-deficient platelets contained significantly less TGFβ1 as compared to the plasma of mice with littermate control platelets (Fig. 13.2B).

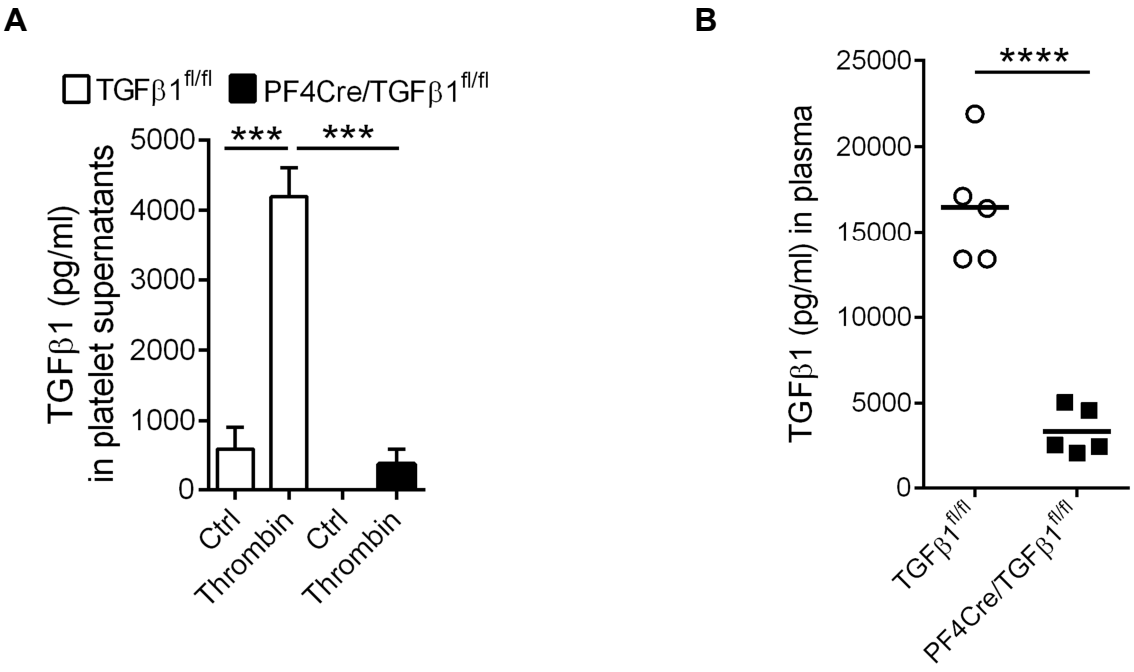

Fig. 13.2: Curtailed TGFβ1 release by TGFβ1-deficient platelets.
(A) TGFβ1-deficient platelets released less TGFβ1 after stimulation, ELISA. Murine washed platelets of the strains TGFβ1$^{fl/fl}$ and PF4Cre/TGFβ1$^{fl/fl}$ were stimulated with thrombin (100ng/ml) or PBS (Ctrl) for 10min at 37°C. All values are presented as the mean ± SEM. ***p<0.005 vs. Ctrl (TGFβ1$^{fl/fl}$) or Thrombin (TGFβ1$^{fl/fl}$), one-way ANOVA. (B) Concentrations of TGFβ1 in plasma four weeks after bleomycin i.t., ELISA. n = five male mice/group. The values are presented as the mean ± SEM. ****p<0.001 vs. TGFβ1$^{fl/fl}$, Student's t test.

In Fig. 13.3, the various aggregation curves of thrombin-activated (100ng/ml thrombin) platelets of the three mouse strains C57BL/6J, TGFβ1$^{fl/fl}$ and PF4Cre/TGFβ1$^{fl/fl}$ are depicted. Aggregation assays were performed using 200µl of 2x10^{8} platelets/ml at 37°C for 10min. The aggregation was not affected by the deficiency of TGFβ1 (PF4Cre/TGFβ1$^{fl/fl}$). The negative control stimulus (PBS) did not induce platelet aggregation in samples of any strain.

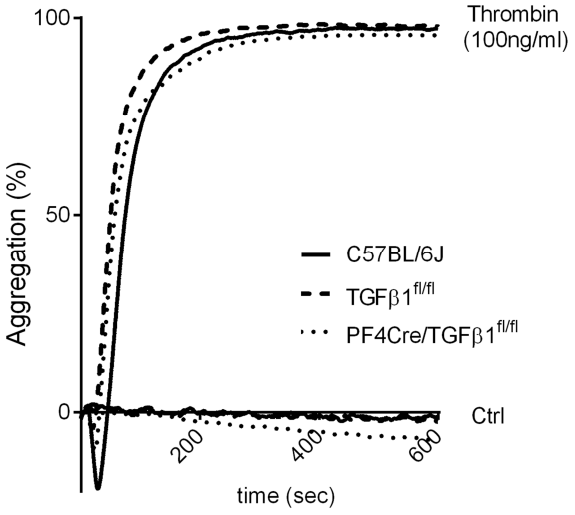

Fig. 13.3: Aggregation of washed platelets.
Murine washed platelets of the strains C57BL/6J, TGFβ1$^{fl/fl}$ and PF4Cre/TGFβ1$^{fl/fl}$ were activated with thrombin (100ng/ml) or PBS (Ctrl) for 10min at 37°C (Born aggregometry). The blood of four male mice per strain were pooled.

Purified histones were shown to induce the release of TGFβ1 by washed platelets *ex vivo* (Fig. 13.1). To further expand these findings by *in vivo* experiments, littermate control mice (TGFβ1$^{fl/fl}$) and mice with TGFβ1-deficient platelets (PF4Cre/TGFβ1$^{fl/fl}$) were treated with 100µg histones in 40µl 0.9% NaCl i.t. for 8h. The sham-groups were treated with 40µl 0.9% NaCl i.t. for 8h. The concentrations of TGFβ1 in BALF was significantly reduced in mice with TGFβ1-deficient platelets (PF4Cre/TGFβ1$^{fl/fl}$) in comparison to littermate control mice (TGFβ1$^{fl/fl}$) (Fig. 13.4). In summary, purified histones induced TGFβ1 release by platelets in the lungs.

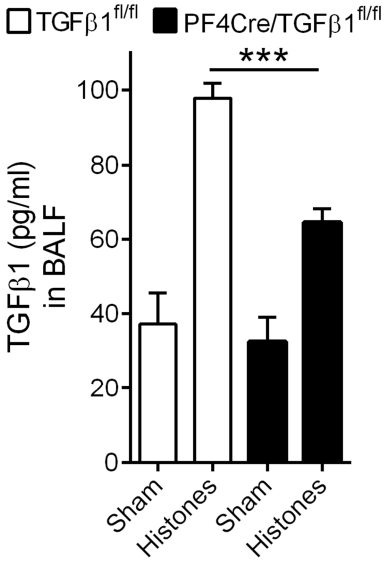

Fig. 13.4: TGFβ1 release in BALF induced by *in vivo* challenge with purified histones.
100µg histones in 40µl 0.9% NaCl were instilled i.t.; Sham = 40µl 0.9 NaCl i.t.. The duration of the experiment was 8h. Analysis by ELISA. All values are presented as the mean ± SEM. ***p<0.005 vs. Histones (TGFβ1$^{fl/fl}$), Student's t test. n = 6 male mice per histone-treated group, n(sham) = two male mice/group.

On the other hand, histones have been demonstrated to be an agonist for the TLR2 receptor for mediating pro-inflammatory conditions (91) (92). IL-27 is produced under pro-inflammatory conditions.

6.2 Bleomycin-induced pulmonary fibrosis in platelet specific TGFβ1 deficient mice

TGFβ is a major key player during pulmonary fibrosis (Chap. I-1.1) and platelets contain high amounts of TGFβ1 (Fig. 13.1). To investigate the specific role of platelet-derived TGFβ1 during bleomycin-induced pulmonary fibrosis a mouse strain with TGFβ1-deficient platelets (PF4Cre/TGFβ1$^{fl/fl}$) was used.

Mice with TGFβ1-deficient platelets (PF4Cre/TGFβ1$^{fl/fl}$) and littermate control mice (TGFβ1$^{fl/fl}$) were used for bleomycin-induced pulmonary fibrosis. In Fig. 13.5, the histologic slides of representative lung areas of both groups are shown after four weeks of bleomycin-induced pulmonary fibrosis. The group with TGFβ1-deficient platelets (PF4Cre/TGFβ1$^{fl/fl}$) showed less green-cyan collagen staining in lungs as compared to the TGFβ1$^{fl/fl}$ mice. Lungs from TGFβ1$^{fl/fl}$ mice displayed signs of alveolar simplification.

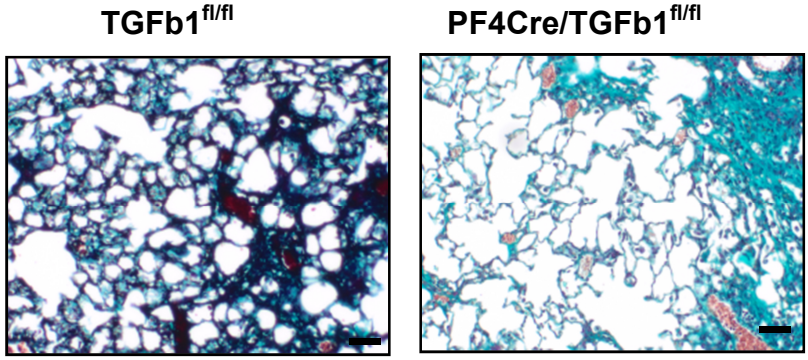

Fig. 13.5: Histology of lung sections of platelet specific TGFβ1-deficient mice during pulmonary fibrosis.
1U/kg BW bleomycin in 40µl 0.9% NaCl was instilled i.t. for four weeks. Representative lung areas of the two groups are shown. Masson's trichrome staining (Goldner): collagen = green-cyan, nuclear chromatin = brownish black, cytoplasm = bright red, erythrocytes = dark red, muscle = red. Magnification: 10x. Scale bar: 50µm.

The histologic observations were confirmed by reduced expression levels of *collagen I,V* mRNA in the whole lung tissue of the TGFβ1-deficient platelets group (PF4Cre/TGFβ1$^{fl/fl}$) after four weeks of bleomycin administration (Fig. 13.6A). There was also less collagen I,V in lung tissue from mice with TGFβ1-deficient platelets (PF4Cre/TGFβ1$^{fl/fl}$) after four weeks (Fig. 13.6B).

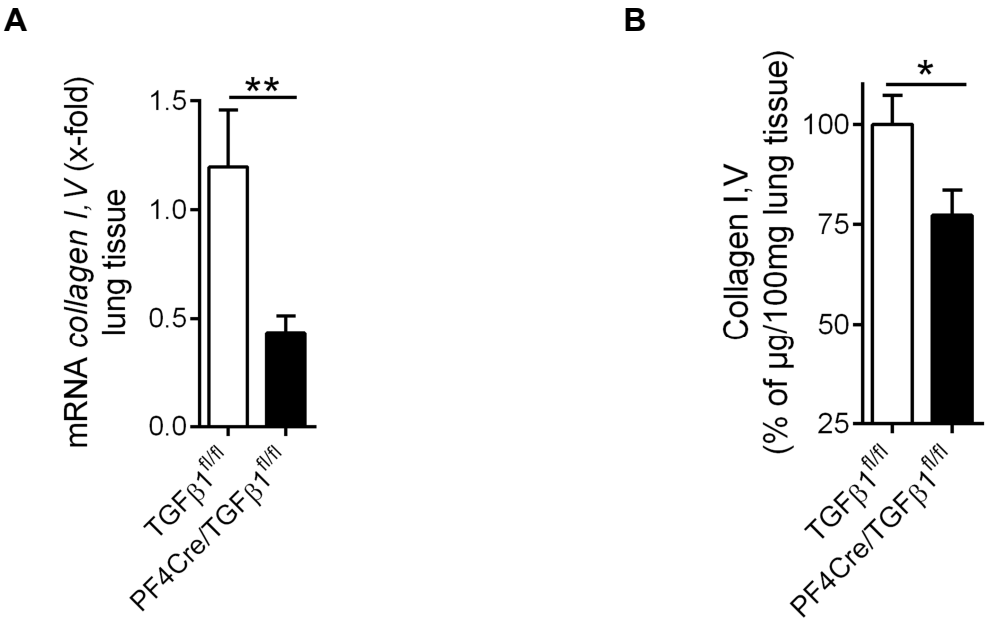

Fig. 13.6: Collagen I,V in dependency of platelet-specific genetic deletion of TGFβ1 during pulmonary fibrosis.
(A) Expression of *collagen I,V* mRNA in whole lung tissue of TGFβ1-deficient platelet containing mice, qPCR. The values are presented as the mean ± SEM. **p<0.01 vs. TGFβ1$^{fl/fl}$, Student's t test. (B) Total Collagen I,V amount in whole lung tissue of TGFβ1-deficient platelet containing mice, collagen assay. The values are presented as the mean ± SEM. *p<0.05 vs. TGFβ1$^{fl/fl}$, Student's t test.
1U/kg BW bleomycin in 40µl 0.9% NaCl was instilled i.t. for four weeks. The duration of the experiment was four weeks. n ≥ 7 male mice/group.

After four weeks of bleomycin administration, the IL-27p28 levels in the BALF of mice with TGFβ1-deficient platelets (PF4Cre/TGFβ1$^{fl/fl}$) were significantly elevated in comparison to littermate control mice (TGFβ1$^{fl/fl}$) (Fig. 13.7). These observations suggest a role of platelet-derived TGFβ1 during bleomycin-induced pulmonary fibrosis. This is in contrast to earlier concepts that myeloid cells are the predominant cellular source of TGFβ1 during pulmonary fibrosis (270). Notably, the release of TGFβ1 by myeloid cells was not altered in the PF4Cre/TGFβ1$^{fl/fl}$ strain (data not shown).

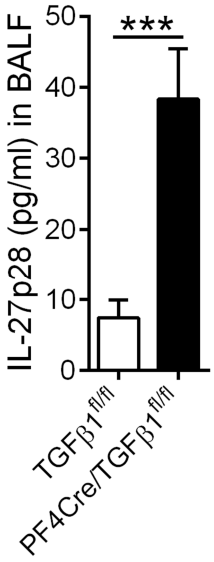

Fig. 13.7: IL-27p28 release in BALF of TGFβ1-deficient platelet containing mice in pulmonary fibrosis.
1U/kg BW bleomycin in 40µl 0.9% NaCl was instilled i.t. for four weeks. IL-27p28 was analyzed by ELISA. The values are presented as the mean ± SEM. ***p<0.005 vs. $TGF\beta1^{fl/fl}$, Student's t test. n ≥ seven male mice/group.

In summary, these data indicated a platelet-dependent TGFβ1 release during bleomycin-induced pulmonary fibrosis. The released TGFβ1 inhibited the anti-fibrotic IL-27p28 in BALF and resulted in more severe pulmonary fibrosis.

7 Inhibition of IL-27p28 by TGFβ1 in Macrophages

IL-27 is produced by antigen presenting cells such as macrophages. To evaluate the production of IL-27 in macrophages during lung disease, bleomycin-induced pulmonary fibrosis was performed. After two weeks, BALF cells were collected and flow cytometry staining was performed (without golgi inhibitor monensin). The isotype antibodies were used for defining regions and positive cell populations. In Fig. 14.1, a representative sample is shown. Nearly all $F4/80^+CD11b^+$ macrophages were also $F4/80^+IL\text{-}27p28^+$ cells. Hence, during bleomycin-induced pulmonary fibrosis $F4/80^+CD11b^+$ macrophages were a source of IL-27p28.

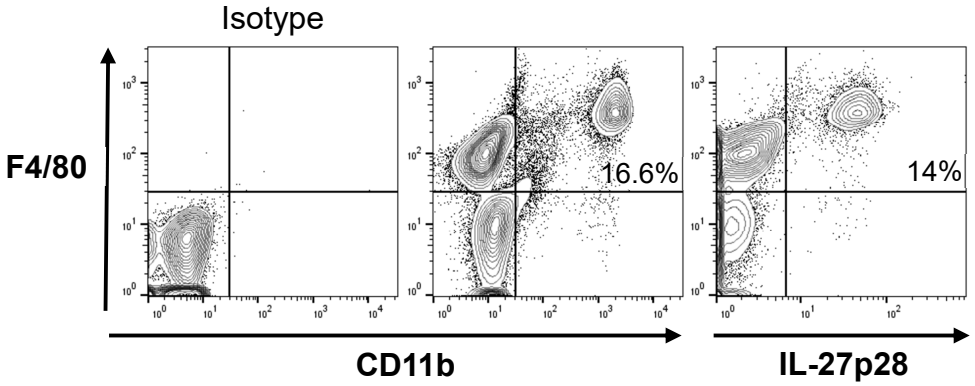

Fig. 14.1: $F4/80^+CD11b^+$ macrophages were the source of IL-27p28 during pulmonary fibrosis.
Five male mice (C57BL/6J) were instilled with 1U/kg BW bleomycin in 40µl 0.9% NaCl i.t. for two weeks. Representative flow cytometry plots are shown.

As shown in Fig. 14.1, the cellular source of IL-27p28 during pulmonary fibrosis were macrophages. In previous experiments, the concentrations of IL-27p28 in BALF appeared to be inversely correlated with the levels of TGFβ1 in BALF to later time points (Fig. 8.3). This suggested an inhibition of IL-27p28 by TGFβ1.

Next, different cells of the monocytic-macrophage lineage were studied. BMDMs (C57BL/6J, Chap. II-2.1.1), RAW264.7, MH-S (Chap. II-2.2.2) and peritoneal elicited macrophages (PEMs, C57BL/6J, Chap. II-2.1.3) were seeded in a density of $5x10^5$ cells/sample/ml. Alveolar macrophages (AM, Chap. II-2.1.5) were seeded with $2x10^5$ cells per 200µl Macrophage-Medium. After seeding, all cell types were incubated without further treatment for 2h. Thereafter, all cell types were stimulated with LPS (100ng/ml) alone or in combination with TGFβ1 (10ng/ml) for 24h.

TGFβ1 was a consistent and reliable suppressor of IL-27p28 release in all studied mononuclear phagocytic cells. The strongest inhibition appeared to occur in AM. The LPS-mediated IL-27p28 production was moderately less inhibited by TGFβ1 in BMDMs and RAW264.7 cells (Fig. 14.2).

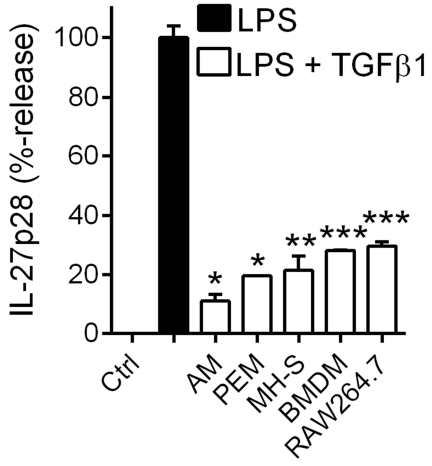

Fig. 14.2: Inhibition of LPS-mediated IL-27p28 by TGFβ1 in different cell types.
Different cell types were stimulated with 100ng/ml LPS or LPS + 10ng/ml TGFβ1 at 37°C, 5% CO_2 for 24h. The supernatant was analyzed for IL-27p28 by ELISA (LPS-mediated IL-27p28 release of every cell type was set to 100%). $5x10^5$ cells/sample/ml (AM = $2x10^5$ cells/sample/ml). AM = Alveolar macrophages, PEM = Peritoneal elicited macrophages (C57BL/6J), MH-S = alveolar macrophage cell line, BMDM = Bone marrow derived macrophages (C57BL/6J), RAW264.7 = Macrophage cell line, Ctrl = unstimulated sample of every cell type. All values are presented as the mean ± SEM. *p<0.05, **p<0.01 and ***p<0.005 vs. LPS, Student's t test.

Dose-response curves were performed to characterize the potency of TGFβ1-mediated inhibition. For the following experiments BMDMs were used because BMDMs a cell population that was abundantly available to us with a high degree of purity. BMDMs from C57BL/6J mice were seeded with $5x10^5$ cells/sample/ml and allowed to rest for 2h before incubation with LPS and TGFβ1. TGFβ1 in a range from 10ng/ml to 500pg/ml was a consistent inhibitor of IL-27p28 secretion in LPS-stimulated BMDMs after 24h. At lower concentrations, the inhibitory potency of TGFβ1 started to become dose-dependent. The IC_{50} of TGFβ1 was <100pg/ml. These experiments showed a dose dependency of the TGFβ1-mediated inhibition of IL-27p28 in BMDMs (Fig. 14.3).

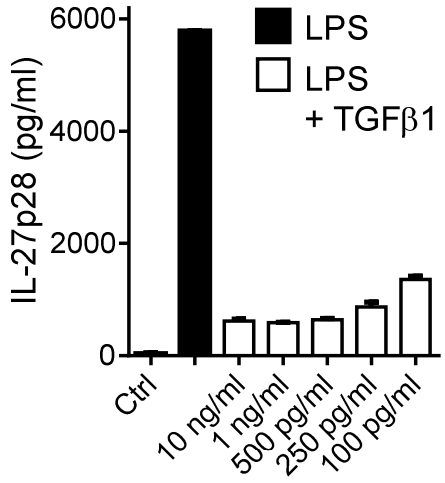

Fig. 14.3: Dose-response curve of TGFβ1-mediated inhibition of IL-27p28 after LPS treatment.
C57BL/6J BMDMs ($5x10^5$ cells/sample/ml) were stimulated with 100ng/ml LPS or LPS + TGFβ1 (indicated concentrations) at 37°C, 5% CO_2 for 24h before quantification of IL-27p28 by ELISA. Ctrl = unstimulated cells. All values are presented as the mean ± SEM.

In Fig. 13.7, it was shown that mice with TGFβ1-deficient platelets (PF4Cre/TGFb1$^{fl/fl}$) displayed higher IL-27p28 levels in the BALF during pulmonary fibrosis. To test the hypothesis that these observations were attributable to a direct inhibitory effect of platelet-derived TGFβ1, platelet supernatants of stimulated washed platelets were used in an *in vitro* transfer experiment. The stimulation of washed platelets (200µl of $2x10^8$ platelets/ml) was performed with 100ng/ml thrombin at 37°C for 10min. After the thrombin activation, cell-free supernatants were collected (Chap. II-2.2.6) and acid-activated (Chap. II-2.4.1). The different platelet supernatants were added with a volume corresponding to $5x10^5$ platelets to cultures of BMDMs from C57BL/6J mice. Next, the BMDMs were stimulated with 100ng/ml LPS. The supernatants of TGFβ1-deficient platelets (TGFb1$^{fl/fl}$PF4Cre) failed to inhibit the IL-27p28 production of LPS-activated BMDMs as compared to littermate control platelets (TGFb1$^{fl/fl}$) (Fig. 14.4). This suggested that TGFβ1 was a platelet-derived mediator of IL-27p28 inhibition in macrophages.

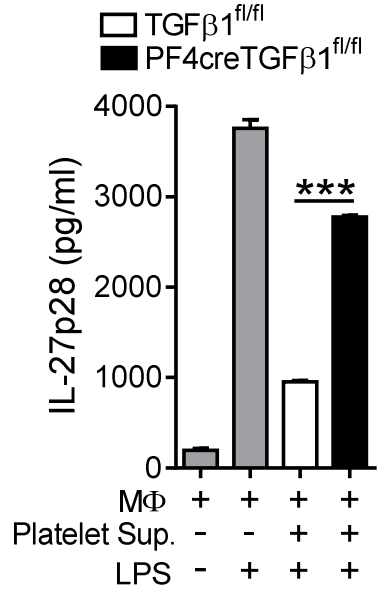

Fig. 14.4: Inhibition of LPS-induced IL-27p28 by platelet supernatants *in vitro.*
Treatment of $5x10^5$ C57BL/6J BMDMs with LPS (100ng/ml) or LPS + platelet releasates (volume corresponding to $5x10^5$ platelets/ml) at 37°C, 5% CO_2 for 24h. Platelets were previously activated with 100ng/ml thrombin at 37°C for 10min. Platelet supernatants were acid-activated. IL-27p28 was analyzed in the supernatant by ELISA. MΦ = Macrophages. All values are presented as the mean ± SEM. ***p<0.005 vs. $TGFβ1^{fl/fl}$, Student's t test.

Notably, resting (unstimulated) BMDMs secreted TGFβ1 in low amounts (Fig. 14.5). BMDMs (C57BL/6J) were generated, seeded with $5x10^5$ cells/sample/ml and allowed to rest for 2h without further treatment. The supernatants were collected after 24h. The unstimulated BMDMs secreted TGFβ1 in a range of 142pg/ml ±15.6pg/ml.

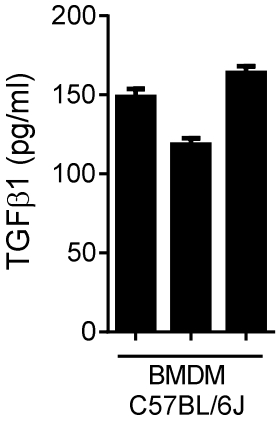

Fig. 14.5: Secreted TGFβ1 of untreated BMDMs.
Unstimulated BMDMs (C57BL/6J) were incubated at 37°C, 5% CO_2 for 24h. TGFβ1 was analyzed by ELISA. $5x10^5$ cells/sample/ml were seeded. All values are presented as the mean ± SEM.

Next, mRNA expression analysis was performed to gather information on transcriptional inhibition of IL-27p28 by TGFβ1. In these experiments, the second subunit of IL-27, EBI3, was also studied. (EBI3 was not studied on the protein level due to the absence of commercially available ELISA kits).

BMDMs (C57BL/6J) were generated, seeded with $5x10^5$ cells/sample/ml and could rest overnight without further treatment. The BMDMs were stimulated with 100ng/ml LPS or with LPS + 10ng/ml TGFβ1 for the indicated time points (0h, 3h, 6h, 9h, 24h).

Stimulation of BMDMs with LPS strongly induced the expression of *il-27p28* mRNA already after 3h. The maximum expression level of *il-27p28* mRNA was reached after 9h. Stimulation of BMDMs with LPS + TGFβ1 resulted in a reduced expression in comparison to LPS-stimulation alone. Here, the maximum was reached after 6h and started to decline between 6-9h and reached the same levels as the unstimulated controls after 24h.

The increase in expression of *ebi3* mRNA following LPS-activation was somewhat delayed (3h: 18-fold, 6h: 27-fold) in comparison to the *il-27p28* mRNA expression (3h: 30-fold, 6h: 48-fold). Around 6-9h, the *ebi3* mRNA expression levels increased very strongly. The *ebi3* mRNA expression surged after 9h with 94-fold (*il-27p28* mRNA, 9h: 53-fold) as compared to baselines and maintained on a high level until 24h. The expression of *ebi3* mRNA after LPS + TGFβ1 stimulation showed no significant increase during all time points studied.

The LPS-induced expression of the *il-27p28* mRNA (Fig. 14.6A) and the *ebi3* mRNA (Fig. 14.6B) were both inhibited by TGFβ1 in BMDMs. This suggested a transcriptional inhibition of both subunits, *il-27p28* and *ebi3*, by TGFβ1.

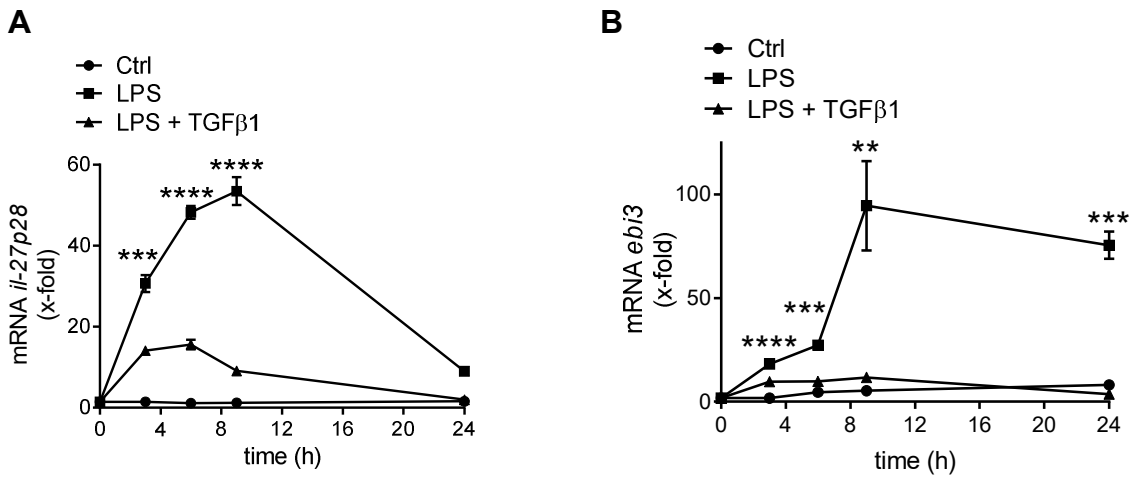

Fig. 14.6: Kinetic of the mRNA for IL-27 subunits in BMDMs.
(A) Kinetic of *il-27p28* mRNA expression in BMDMs, qPCR. All values are presented as the mean ± SEM. ***p<0.005 and ****p<0.001 vs. LPS, one-way ANOVA. (B) Kinetic of *ebi3* mRNA expression in BMDMs, qPCR. All values are presented as the mean ± SEM. **p<0.01, ***p<0.005 and ****p<0.001 vs. LPS, one-way ANOVA.
$5x10^5$ C57BL/6J BMDMs were stimulated with 100ng/ml LPS or LPS + 10ng/ml TGFβ1 at 37°C, 5% CO_2 for 3h, 6h, 9h and 24h. The 0h samples were collected at the time of stimulation. Ctrl = unstimulated cells. The expression of *gapdh* was used for normalization of gene expression.

The TGFβ1-mediated inhibition of IL-27p28 in LPS stimulated BMDMs in qPCR studies was already seen after 3h (Fig. 14.6A). To study the time dependent TGFβ1-mediated IL-27p28 inhibition BMDMs (C57BL/6J) were generated, seeded with $5x10^5$ cells/sample/ml and could rest overnight without further treatment. On the protein level (IL-27p28 ELISA), the TGFβ1-mediated inhibition was observed in BMDMs after 6h (Fig. 14.7). At later time points (6h, 10h, 24h), significantly less IL-27p28 was secreted if the BMDMs were stimulated by LPS + TGFβ1 in comparison to LPS stimulation. The gap of the released IL-27p28 between the two groups was overt over time. Between 10h and 24h, the LPS-mediated IL-27p28 release was still increasing. The difference between LPS (100ng/ml) stimulated BMDMs and LPS + TGFβ1 (10ng/ml) stimulated BMDMs increased over time.

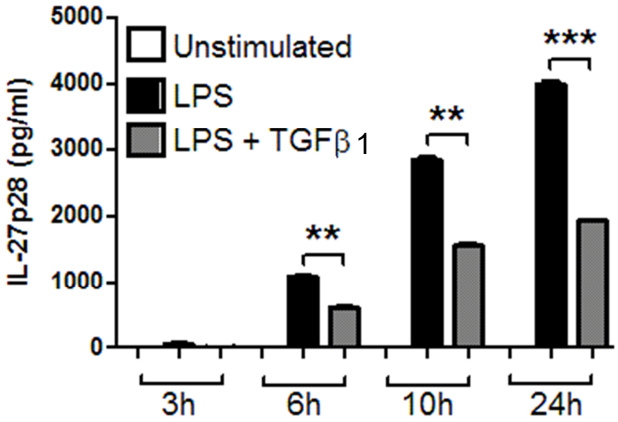

Fig. 14.7: Kinetic of IL-27p28 secretion in BMDMs.
$5x10^5$ C57BL/6J BMDMs were stimulated with 100ng/ml LPS or LPS + 10ng/ml TGFβ1 at 37°C, 5% CO_2 for 3h, 6h, 10h and 24h before quantification of IL-27p28 by ELISA. All values are presented as the mean ± SEM. ***p<0.005 and ****p<0.001 vs. LPS, one-way ANOVA.

In Fig. 14.1, macrophages are shown as the source of IL-27p28 *in vivo* during pulmonary fibrosis. Flow cytometry analyses were used to demonstrate the direct TGFβ1-mediated inhibition of IL-27p28 in macrophages *in vitro*. $1x10^6$ C57BL/6J BMDMs were stimulated with 100ng/ml LPS or with LPS + 10ng/ml TGFβ1 for 12h (golgi transport inhibitor monensin was added at +2h). After 12h, the cells were stained for the surface proteins F4/80 (marker for macrophages) and CD11b (marker for macrophages and neutrophils) and for intracellular IL-27p28. To define the positive cell populations for F4/80, CD11b and IL-27p28, the matching isotype antibodies were used (data not shown).

In flow cytometry analyses, 45.6% of the $F4/80^+$ cells were positively stained for IL-27p28 after LPS treatment. With TGFβ1 treatment, this staining was reduced to 10.9% $F4/80^+IL\text{-}27p28^+$ double positive cells. Unstimulated cells contained 4.7%

F4/80$^+$IL-27p28$^+$ cells (Fig. 14.8). Hence, F4/80$^+$CD11b$^+$ double positive macrophages were the source of IL-27p28 *in vitro* and a target of TGFβ1.

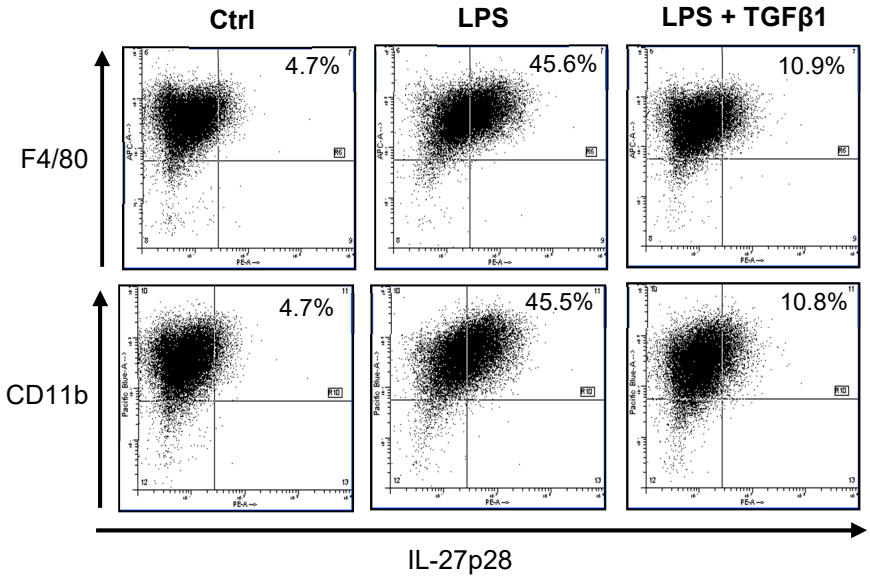

Fig. 14.8: IL-27p28 was produced by F4/80$^+$CD11b$^+$ macrophages *in vitro*.
C57BL/6J BMDMs were stimulated with 100ng/ml LPS or LPS + 10ng/ml TGFβ1 at 37°C, 5% CO_2 for 12h before analyzed by flow cytometry. Monensin (golgi transport inhibitor) was added 2h after stimulation. 1x10^6 BMDMs were seeded. Ctrl = unstimulated cells.

During pulmonary fibrosis classically activated (M1) and alternatively activated (M2) macrophages participate (273) Therefore, the inhibition potency of TGFβ1 was studied in polarized macrophages. Polarized macrophages (C57BL/6J) were generated as described in Chap. II-2.1.2. M1 polarized macrophages secreted approx. 64% more IL-27p28 as compared to the M2 polarized macrophages. The TGFβ1-mediated inhibition of the IL-27p28 release is comparable in both macrophage subpopulations (M1: approx. 48% reduction, M2: approx. 40% reduction) (Fig. 14.9). Classically activated (M1) and alternatively activated (M2) macrophages produced different amounts of IL-27p28.

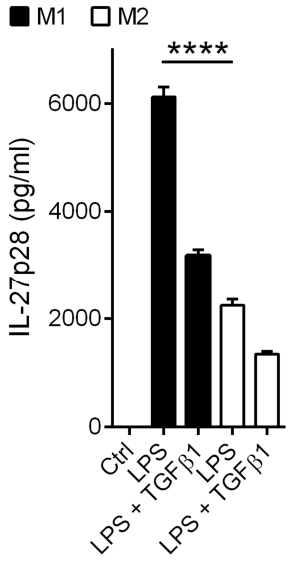

Fig. 14.9: Polarized macrophages released different amounts of IL-27p28.
Quantification of IL-27p28 by ELISA in cell culture supernatants of $5x10^5$ polarized C57BL/6J macrophages, which were stimulated with 100ng/ml LPS or with LPS + 10ng/mml TGβ1 at 37°C, 5% CO_2 for 24h. M1 = classically activated macrophages (10ng/ml IFNγ for 6h); M2 = alternatively activated macrophages (10ng/ml IL-4 overnight). Ctrl = unstimulated cells of both subpopulations. All values are presented as the mean ± SEM. ****p<0.001 vs. LPS (M1), Student's t test.

So far, in the presented work only LPS was used as a stimulus for IL-27p28 production by macrophages. Next, other agonists were also studied and the TGFβ1 inhibition potency of these agonists.

In Figure 14.10, the IL-27p28 production mediated by several agonists in dependence of TGFβ1 (10ng/ml) after 24h is shown. All agonists were directly added to the cell culture medium, except the Rig-I agonist, 5'ppp-dsRNA, which was transfected as described in Chap. II-2.5.8. The IL-27p28 production of the TLR2 agonists, Zymosan (10µg/ml; 94.4% inhibited), and LTA (10µg/ml; 93% inhibited) were most influenced by TGFβ1. The IL-27p28 response of IFN-γ (10ng/ml) was reduced by 85.4%. The inhibition of the IL-27p28 response after LPS (100ng/ml), an agonist for TLR4 (71.7% inhibited), was comparable to the inhibition of Poly(I:C) (1µg/ml, 68.3% inhibited, TLR3 agonist). On the other hand, the IL-27p28 production of the Rig-I agonist, 5'ppp-dsRNA (200ng), was less inhibited (39.2% inhibition). In summary, TGFβ1 consistently inhibited the IL-27p28 release of several stimuli in BMDMs.

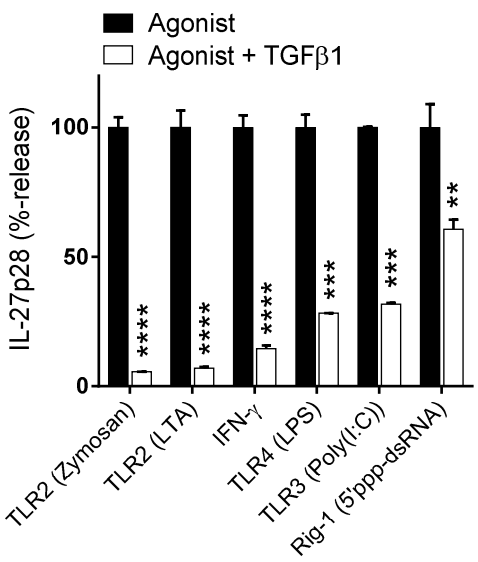

Fig. 14.10: TGFβ1 inhibited the IL-27p28 release induced by several stimuli in macrophages.
Relative release of IL-27p28 (ELISA) in $5x10^5$ C57BL/6J BMDMs that were stimulated with the indicated agonists alone or agonist + 10ng/ml TGFβ1 at 37°C, 5% CO_2 for 24h. Zymosan (10µg/ml), LTA (10µg/ml), IFN-γ (10ng/ml), LPS (100ng/ml and Poly(I:C) (1µg/ml) were added directly to the cell culture medium. 5'ppp-dsRNA (200ng) was transfected. The IL-27p28 release of the single agonist was set to 100%. All values are presented as the mean ± SEM. **p<0.01, ***p<0.005 and ****p<0.001 vs. Agonist, Student's t test.

Several independent signaling pathways are involved in mediating gene expression of IL-27p28 (Chap. I-4.1.1). The most important signaling adaptor molecules of TLRs are MyD88 and TRIF. Knock out mice for these proteins were used to identify the major inhibitory pathway of TGFβ1. $5x10^5$ BMDMs of C57BL/6J, MyD88$^{-/-}$ and TRIF$^{-/-}$ mice were treated with 100ng/ml LPS or LPS + 10ng/ml TGFβ1 for 24h. The BMDMs were allowed to rest for 2h without further treatment. In C57BL/6J BMDMs, the IL-27p28 release was reduced by TGFβ1 by 60%. In MyD88$^{-/-}$ BMDMs, TGFβ1 inhibited the IL-27p28 release by 85% in comparison to LPS treatment. The strongest inhibition of IL-27p28 by TGFβ1 was seen in TRIF$^{-/-}$ BMDMs. Here, the IL-27p28 release was inhibited by 95% (Fig. 14.11).

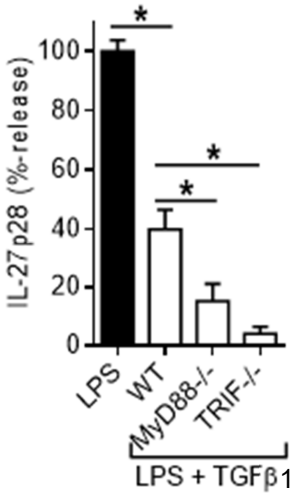

Fig. 14.11: TGFβ1-mediated inhibition of the IL-27p28 release after LPS in dependence of MyD88 and TRIF in macrophages.
$5x10^5$ BMDMs (WT = C57BL/6J, MyD88$^{-/-}$, TRIF$^{-/-}$) were stimulated with 100ng/ml LPS or LPS + 10ng/ml TGFβ1 at 37°C, 5% CO_2 for 24h before quantification of IL-27p28 by ELISA. The IL-27p28 release after LPS stimulation was set to 100% for each genotype. All values are presented as the mean ± SEM. *p<0.05 vs. LPS or WT (LPS + TGFβ1), one-way ANOVA.

TGFβ1 engages three distinct receptor units (Chap. I-4.2.3), although the TGFβ Receptor III does not have any direct signaling properties. In a first step, the influence of the TGFβ Receptor I (TbRI) on the TGFβ1-mediated inhibition of IL-27p28 in macrophages was studied (Fig. 14.12A). BMDMs were stimulated with 100ng/ml LPS or LPS + 10ng/ml TGFβ1 for 24h. The TbRI was inhibited by SB431542 (a small molecule antagonist, which inhibits the TbRI signaling by binding to the ATP binding domain) in different concentrations (1-20μM). The TGFβ1-mediated inhibition of IL-27p28 after LPS recovered by treatment with SB431542. This effect was dose dependent. With a SB431542 concentration of 20μM, TGFβ1 failed to inhibit the IL-27p28 release after LPS treatment in BMDMs. The highest concentration (20μM) of SB431542 alone had no effect on the IL-27p28 production by the BMDMs (data not shown).

Next, myeloid-specific TGFβ Receptor II (TbRII) KO mice (LysMCre/TbRII$^{fl/fl}$) and littermate controls (TbRII$^{fl/fl}$) were used to characterize the role of TbRII in TGFβ1-mediated inhibition of IL-27p28 in LPS-activated BMDMs (Fig. 14.12B). The BMDMs were stimulated with 100ng/ml LPS or with LPS + 10ng/ml TGFβ1 for 24h. The myeloid-specific TbRII KO BMDMs (LysMCre/TbRII$^{fl/fl}$) had a significant abolishment of the TGFβ1-mediated inhibition of IL-27p28 production by LPS-treated BMDMs in comparison to littermate control BMDMs (TbRII$^{fl/fl}$). Hence, the TGFβ1-mediated inhibition of IL-27p28 in BMDMs was TbRI as well as TbRII dependent.

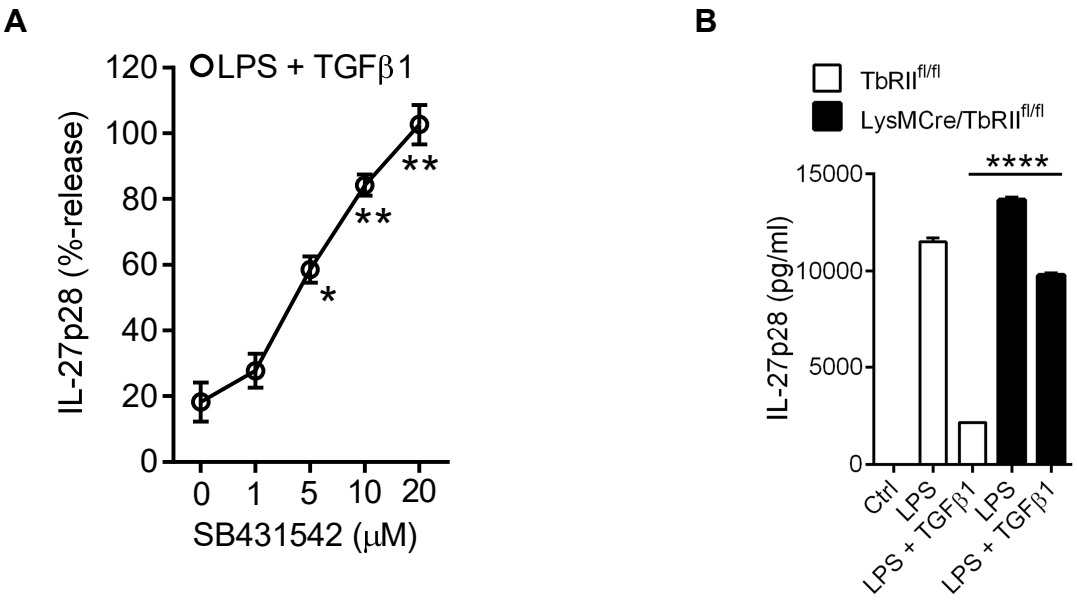

Fig. 14.12: TGFβ1-mediated inhibition of IL-27p28 in BMDMs in dependence of TbRI and TbRII.
(A) TbRI-inhibition by SB431542 influenced the TGFβ1-mediated inhibition of IL-27p28, ELISA. The inhibitor SB431542 was added with 1µM, 5µM, 10µM, 20µM. All values are presented as the mean ± SEM. *p<0.05 and **p<0.01 vs. 0µM SB431542, one-way ANOVA. The results of LPS stimulated samples were used as 100% to calculate relative values. (B) Myeloid-specific TbRII KO were resistant to the TGFβ1-mediated inhibition of IL-27p28, ELISA. All values are presented as the mean ± SEM. ****p<0.001 vs. LPS + TGFβ1 ($TbRII^{fl/fl}$), Student's t test.
$5x10^5$ BMDMs (C57BL/6J) were stimulated with 100ng/ml LPS or LPS + 10ng/ml TGFβ1 for 24h (37°C, 5% CO_2).

In the present work several inhibitors (e.g. SB431542) were dissolved in DMSO. To exclude an impact by DMSO on the IL-27p28 production in macrophages BMDMs were treated with DMSO. The BMDMs were stimulated with 100ng/ml LPS or with LPS + DMSO (1:1000) for 24h. DMSO did not influence the LPS induced production of IL-27p28 in macrophages (Fig. 14.13).

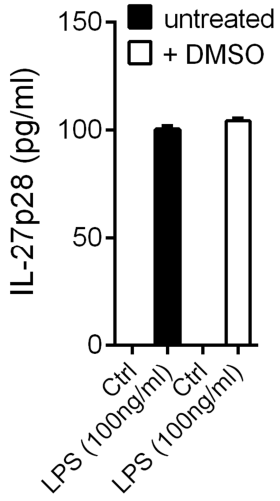

Fig. 14.13: Control for the effects of DMSO on BMDMs.
$5x10^5$ BMDMs (C57BL/6J) were unstimulated (Ctrl) or stimulated with 100ng/ml LPS at 37°C, 5% CO_2 for 24h. Quantification of IL-27p28 was performed by ELISA. DMSO (1:1000) was either added or not added (untreated). All values are presented as the mean ± SEM.

Flow cytometry analyses confirmed the results of Fig. 14.12B. The BMDMs were stimulated with 100ng/ml LPS or with LPS + 10ng/ml TGFβ1 for 20h (golgi inhibitor monensin was added at +2h). Littermate control BMDMs ($TbRII^{fl/fl}$) and the myeloid-specific TbRII KO BMDMs ($LysMCre/TbRII^{fl/fl}$) were gated for $F4/80^+CD11b^+$ double positive macrophages.

$F4/80^+CD11b^+$ double positive macrophages contained 11.2% $F4/80^+IL\text{-}27p28^+$ double-positive macrophages in the LPS treated control BMDMs. This IL-27p28 positive population was reduced by TGFβ1 to 0.54%. The $F4/80^+IL\text{-}27p28^+$ double positive population in LPS treated myeloid-specific TbRII KO ($LysMCre/TbRII^{fl/fl}$)

macrophages contained 16.1% double-positive macrophages. With TGFβ1, the F4/80$^+$IL-27p28$^+$ double positive population was reduced by only to 12.1% double-positive macrophages. Figure 14.14 shows the flow cytometry results and Fig. 14.15 shows the data of the same experiments in a bar graph.

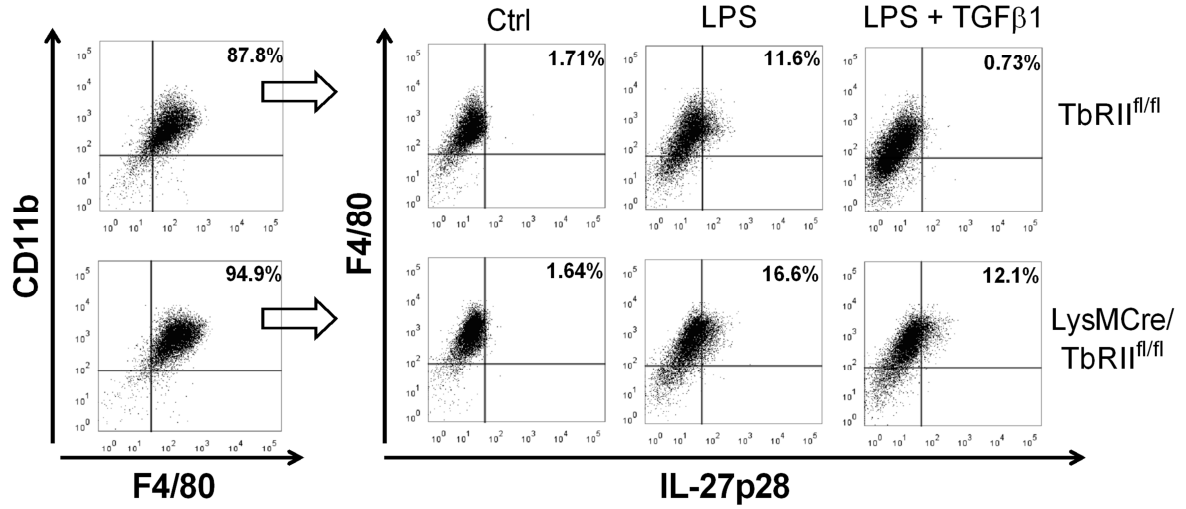

Fig. 14.14: TGFβ1-mediated inhibition of IL-27p28 was influenced by TbRII in F4/80$^+$CD11b$^+$ double positive macrophages.
1x10^6 BMDMs were stimulated with 100ng/ml LPS or LPS + 10ng/ml TGFβ1 at 37°C, 5% CO_2 for 20h before flow cytometry analyses. Monensin was added 2h after stimulation. Ctrl = unstimulated cells.

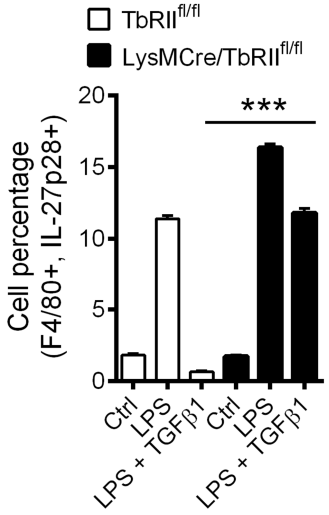

Fig. 14.15: TGFβ1-mediated inhibition of IL-27p28 production in LPS-treated TbRII KO BMDMs.
1x10^6 BMDMs were stimulated with 100ng/ml LPS or LPS + 10ng/ml TGFβ1 at 37°C, 5% CO_2 for 20h. Monensin was added 2h after stimulation. Analysis was done as shown in Fig. 7L by flow cytometry. Ctrl = unstimulated cells. All values are presented as the mean ± SEM. ***p<0.005 vs. LPS + TGFβ1 (TbRII$^{fl/fl}$), Student's t test.

In summary, these data indicated a TGFβ1-mediated inhibition of IL-27p28 in LPS-stimulated macrophages. Furthermore, TGFβ1 inhibited the IL-27p28 production after different stimuli in BMDMs. The TbRI as well as the TbRII were both critical involved in the TGFβ1-mediated inhibition of IL-27p28 in BMDMs.

8 TGFβ1 signaling by TbRII influenced bleomycin-induced pulmonary fibrosis

IL-27p28 was produced by macrophages *in vivo* during pulmonary fibrosis (Fig. 14.1). To investigate TGFβ1-mediated effects on IL-27 production during bleomycin-induced pulmonary fibrosis, myeloid-specific TbRII KO mice (LysMCre/TbRII$^{fl/fl}$) and littermate control mice (TbRII$^{fl/fl}$) were used. After four weeks, the lungs of all mice were prepared for histology and stained for collagen (Masson's trichrome staining, Goldner). The lungs of myeloid-specific TbRII KO mice (LysMCre/TbRII$^{fl/fl}$) showed substantially less green-cyan collagen staining in histology as compared to the littermate control mice (TbRII$^{fl/fl}$). Representative lung areas are shown in Fig. 15.1.

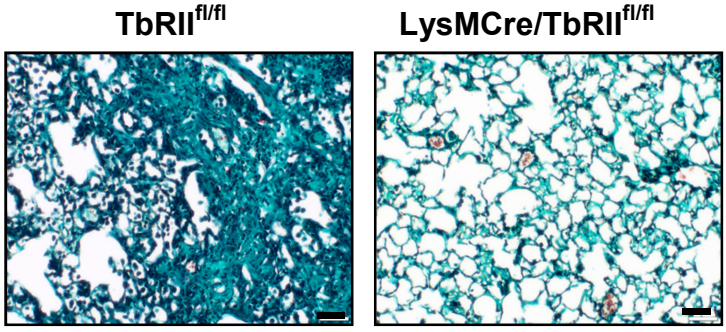

Fig. 15.1: Lung histology of myeloid-specific TbRII KO mice and littermate control mice.
1U/kg BW bleomycin in 40µl 0.9% NaCl was instilled i.t. for four weeks; Sham = 40µl 0.9% NaCl i.t.. Representative lung areas are shown. Masson's trichrome staining (Goldner): collagen = green-cyan, nuclear chromatin = brownish black, cytoplasm = bright red, erythrocytes = dark red, muscle = red. Magnification: 10x. Scale bar: 50µm.

Furthermore, the collagen amount in the lung homogenates and cytokine levels in BALF were studied in additional independent experiments. After four weeks of bleomycin-induced pulmonary fibrosis, myeloid-specific TbRII KO mice (LysMCre/TbRII$^{fl/fl}$) had accumulated significantly less collagen I,V in lungs as compared to the littermate control mice (TbRII$^{fl/fl}$) (Fig. 15.2A). Genetic deletion of TbRII in macrophages (LysMCre/TbRII$^{fl/fl}$) resulted in 2-fold higher concentrations of IL-27p28 in BALF as compared to littermate control mice (TbRII$^{fl/fl}$) (Fig. 15.2B). IL-27p28 was analyzed by ELISA in cell-free BALF.

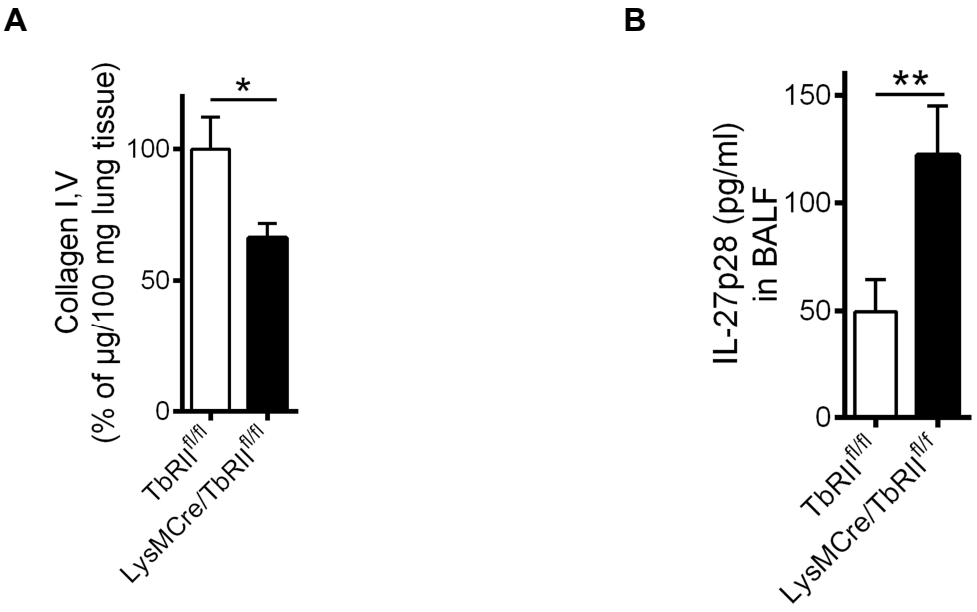

Fig. 15.2: Collagen I,V amount in the lung and IL-27p28 levels in the BALF of myeloid-specific TbRII KO mice.

(A) Total Collagen I,V amount in the lungs, collagen assay. The values are presented as the mean ± SEM. *p<0.05 vs. TbRII$^{fl/fl}$, Student's t test. (B) IL-27p28 amount in BALF, ELISA. The values are presented as the mean ± SEM. **p<0.01 vs. TbRII$^{fl/fl}$, Student's t test.
1U/kg BW bleomycin in 40µl 0.9% NaCl was instilled i.t. for four weeks. n ≥ 7 male mice/group.

These data demonstrated that genetic disruption of TGFβ signaling was associated with higher release of anti-fibrotic IL-27p28. IL-27p28 was produced by macrophages.

9 Smad3 mediates the inhibitory effects of TGFβ1 in macrophages

9.1 Confirmation of Smad3 knock down in lentiviral transduced RAW264.7 macrophages

Before starting with the knock down of the *smad3* gene in RAW264.7 macrophages, a suitable Puromycin concentration was determined. This was important, because Puromycin is an antibiotic against pro- and eukaryotic cells (inhibits the peptidyl-transferase on ribosomes). $5x10^5$ RAW264.7 macrophages per 1ml RAW-Medium were seeded and allowed to rest for 2h without further treatment. Puromycin was added in the indicated concentrations (5µg/ml, 10µg/ml and 100µg/ml). No Puromycin was added to the control (Ctrl) samples. The RAW264.7 macrophages were incubated for 24h and 48h. The cells were scraped off and counted by using trypan blue (Chap. II-2.2.3). The percentages of dead cells were calculated (Fig. 16.1). For lentiviral knock down of Smad3 in RAW264.7 macrophages, 5µg/ml Puromycin was used as this was a concentration of low toxicity.

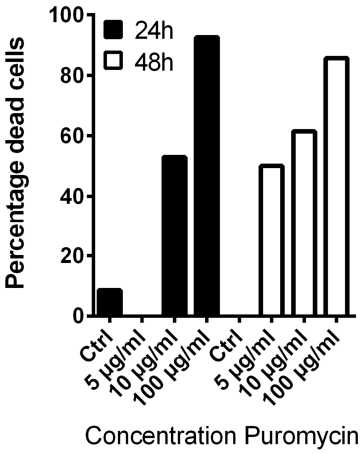

Fig. 16.1: Survival rate of RAW264.7 macrophages after different Puromycin concentrations.
Puromycin was added with 5µg/ml, 10µg/ml and 100µg/ml to $5x10^5$ RAW264.7 macrophages for 24h and 48h (37°C, 5% CO_2). Dead cells were identified by trypan blue staining. Ctrl = untreated cells.

Lentiviral knock down of the *smad3* gene in RAW264.7 was done as described in Chap. II-2.3.1. To confirm the knock down of the *smad3* gene, $5x10^5$ cells/sample/ml were seeded and incubated for 24h. After 24h, the expression levels of the *smad3* gene were analyzed by qPCR. Of five tested shRNA clones the clones shRNA1 and shRNA2 displayed the highest knock down efficiency of *smad3* gene expression. Accordingly, the clones shRNA1 and shRNA2 were used for all further studies. In fact, the clone shRNA2 showed the most efficient knock down. The Ctrl shRNA had no overt effects on the *smad3* expression levels (Fig. 16.2A).

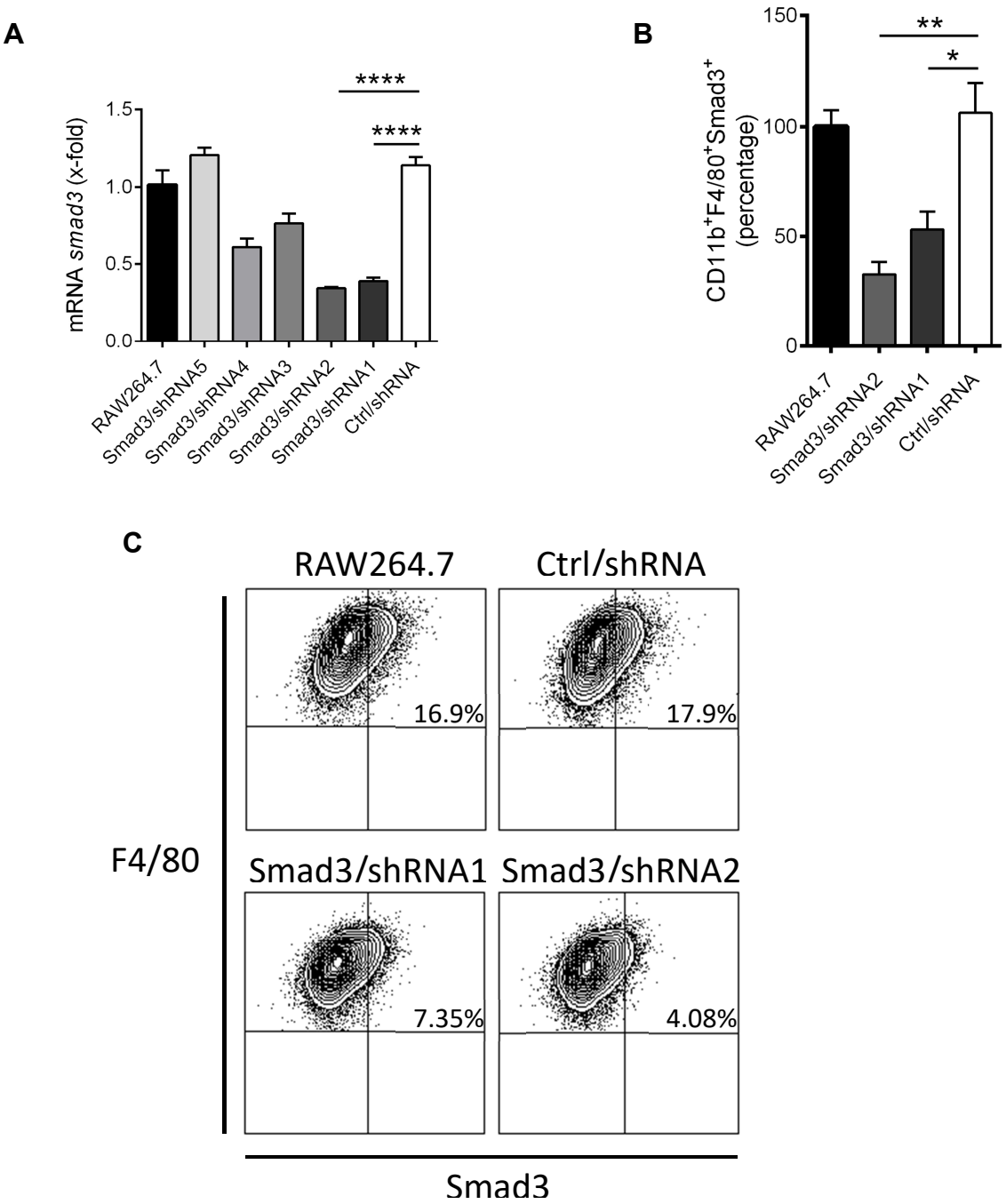

Fig. 16.2: Lentiviral knock down of Smad3 in RAW264.7 macrophages.
(A) Knock down efficiency of the gene *smad3* in several clones of RAW264.7 macrophages, qPCR. Expression was normalized to *gapdh* mRNA expression. All values are presented as the mean ± SEM. ****p<0.001 vs. Ctrl/shRNA, one-way ANOVA. (B) Knock down efficiency of the protein Smad3 in $CD11b^+F4/80^+$ RAW264.7 macrophages, flow cytometry analysis. The frequency of CD11b+F4/80+Smad3+ positive cells in untransduced RAW264.7 macrophages was set to 100% for calculating relative values. All values are presented as the mean ± SEM. *p<0.05 and **p<0.01 vs. Ctrl/shRNA, one-way ANOVA. (C) Flow cytometry analyses of Smad3 knock down efficiency in $CD11b^+F4/80^+$ RAW264.7 macrophages. Previously gated for $F4/80^+CD11b^+$ double positive macrophages. All samples (A-C) were untreated and incubated for 24h. RAW264.7 = untransduced cells, Smad3/shRNA1 = RAW264.7 macrophages transduced with clone1, Smad3/shRNA2 = RAW264.7 macrophages transduced with clone2, Ctrl/shRNA = RAW264.7 macrophages transduced with NonMammalian control shRNA.

In Fig. 16.2A, the knock down efficiency of *smad3* gene expression is shown. In addition, the knock down efficiency was also studied on the protein level. The different cell lines were seeded with $1x10^6$ per ml and could rest overnight. For flow cytometry analyses the different cell lines were gated for $CD11b^+F4/80^+Smad3^+$ positive cells by using isotype antibodies for F4/80 and CD11b. The Smad3 staining was done with a 1st antibody directed against Smad3 and a 2nd PE-labeled antibody against the Fc-region of the anti-Smad3 antibody. To identify the Smad3-negative cell population, one sample per cell line was stained with F4/80, CD11b and the 2nd PE-labeled antibody, only.

The RAW264.7-Ctrl/shRNA cells had the same frequencies of $CD11b^+F4/80^+Smad3^+$ positive cells as the untransduced RAW264.7 macrophages. Both cell lines, RAW264.7-Smad3/shRNA1 and RAW264.7-Smad3/shRNA2, showed a significant reduction of intracellular Smad3. The clone RAW264.7-Smad3/shRNA2 (approx. 32.8% $CD11b^+F4/80^+Smad3^+$ positive cells) displayed the strongest reduction of Smad3 (Fig. 16.2B), and this was in accordance with *smad3* mRNA levels (Fig. 16.2A). The shRNA sequences used for the lentiviral transductions are shown in Chap. II-1.8 (Tab. 13). To summarize, the reduced mRNA expression of *smad3* corresponded to less Smad3 protein levels.

9.2 Inhibition of IL-27 by TGFβ1 is Smad3 dependent

Smad2/Smad3 is a central signaling pathway of TGFβ signal transduction. As shown in Fig. 14.6, TGFβ1 inhibits the expression of *il-27p28* and *ebi3* in macrophages. To test the hypothesis if Smad3 is important for the TGFβ1-mediated IL-27 inhibition, the Smad3 knock down cell lines were used for experiments.

First, the TGFβ1-mediated phosphorylation of Smad2/3 was evaluated. BMDMs (C57BL/6J) were generated, seeded with $1x10^6$ cells per sample and could rest overnight. The BMDMs were stimulated with 100ng/ml LPS and LPS + 10ng/ml TGFβ1 for 30min. Flow cytometry staining of phosphorylated pSmad3 (pS423/pS425)/pSmad2 (pS465/pS467) was performed as described in Chap. II-2.4.3.

Figure 16.3A shows the histogram of the $CD11b^+F4/80^+pSmad3/2^+$ cells (previously gated for $F4/80^+CD11b^+$ macrophages). The median of the pSmad3/2 fluorescence

intensity (FI) is shown in Fig. 16.3B. In response to LPS treatment, the pSmad3/2 FI was significantly reduced in comparison to the pSmad3/2 FI in the unstimulated control BMDMs. With LPS + TGFβ1 a significant increase of the pSmad3/2 FI was observed. Smad3 was significantly phosphorylated after TGFβ1 stimulation in BMDMs.

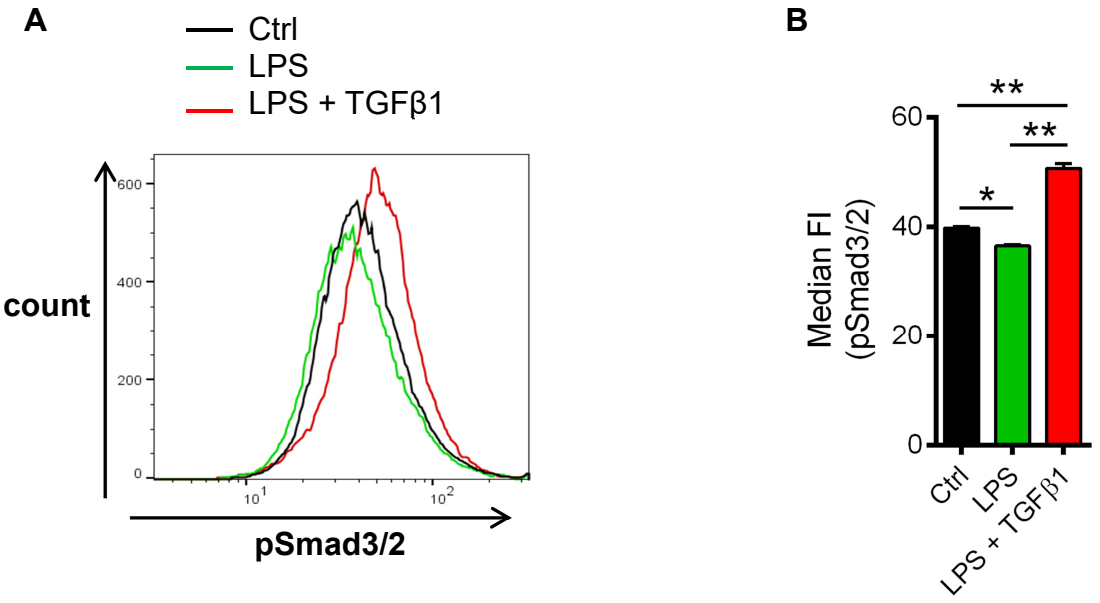

Fig. 16.3: Smad3 phosphorylation by TGFβ1 in macrophages.
(A) Histogram of F4/80$^+$CD11b$^+$pSmad3/2$^+$ macrophages, flow cytometry analysis. (B) Median Fluorescence Intensity (FI) of F4/80$^+$CD11b$^+$pSmad3/2$^+$ macrophages. 1x10^6 BMDMs were stimulated with 100ng/ml LPS (green) or LPS + 10ng/ml TGFβ1 (red) for 30min at 37°C, 5% CO_2. Ctrl = unstimulated cells (black). All values are presented as the mean ± SEM. **p<0.01 vs. Ctrl or LPS, one-way ANOVA. Phosphorylation of pSmad3 (pS423/pS425)/pSmad2 (pS465/pS467) is shown.

Smad3 was significantly phosphorylated after TGFβ1 treatment in BMDMs. To assess the specific role of Smad3 for the TGFβ1-mediated inhibition mechanism, the Smad3 knock down cell lines (Chap. II-1.9, Tab. 16) were used. 5x10^5 cells/sample/ml were seeded and could rest for 2h without further treatment. The cells were stimulated with 100ng/ml LPS or LPS + 50pg/ml TGFβ1 overnight. As expected, the RAW264.7-Ctrl/shRNA cell line showed the same inhibition of IL-27p28 mediated by TGFβ1 as the untransduced RAW264.7 macrophages (approx. 30% IL-27p28 release). The cell line RAW264.7-Smad3/shRNA2 (approx. 61.4% IL-27p28 release) had the strongest recovery of the IL-27p28 inhibition by TGFβ1. This effect was also observed with the cell clone RAW264.7-Smad3/shRNA1 (approx. 42.7% IL-27p28 release) (Fig. 16.4A).

These observations were further confirmed by qPCR analysis of *il-27p28* mRNA (Fig. 16.4B) and *ebi3* mRNA (Fig. 16.4C). For the Smad3 knock down cell lines, the RAW264.7-Smad3/shRNA2 displayed resistance to the TGFβ1-mediated inhibition of *il-27p28* mRNA. Similar effects were noted for the RAW264.7-Smad3/shRNA1 cell clone, although the efficacy of this shRNA1 appeared somewhat lower. The *ebi3* mRNA expression was only studied for the RAW264.7-Smad3/shRNA2 cell clone. The RAW264.7-Smad3/shRNA2 cells significantly recovered the TGFβ1-mediated inhibition of *ebi3* mRNA expression. But this effect on the *ebi3* mRNA expression was not quite as strong as for the *il-27p28* mRNA expression. In summary, the TGFβ1-mediated inhibition of IL-27p28 protein and the mRNA expressions of *il-27p28* and *ebi3* after LPS stimulation relied on Smad3.

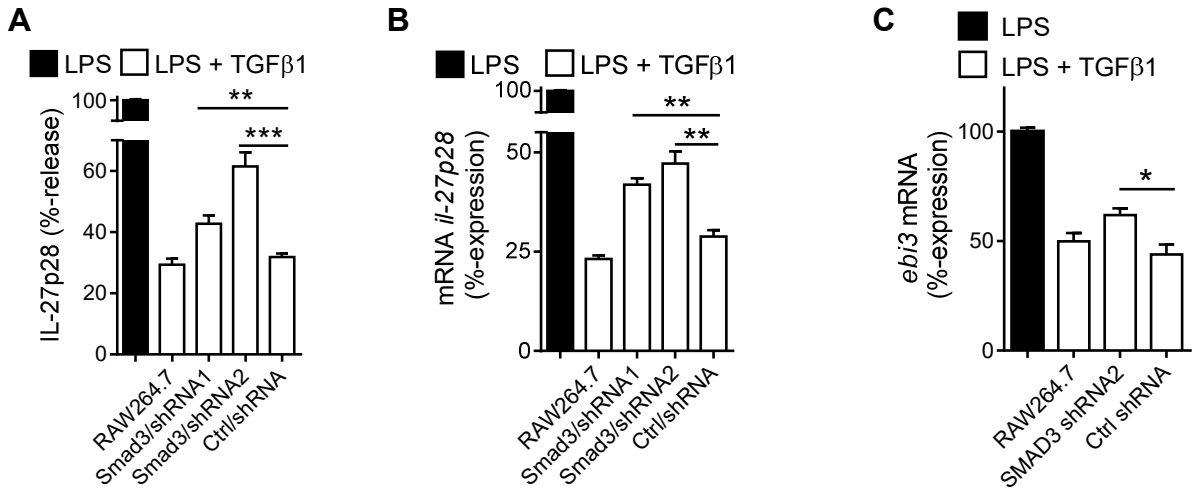

Fig. 16.4: Smad3 knock down nullified TGFβ1-mediated inhibition.
(A) Relative release of IL-27p28, ELISA. (B) Relative expression of *il-27p28* mRNA, qPCR. (C) Relative expression of *ebi3* mRNA, qPCR. $5x10^5$ cells were stimulated with 100ng/ml LPS or LPS + 50pg/ml TGFβ1 for 17.5h (A) or 6h (B and C) at 37°C, 5% CO_2. RAW264.7 = untransduced cells, Smad3/shRNA1 = RAW264.7 macrophages transduced with clone1, Smad3/shRNA2 = RAW264.7 macrophages transduced with clone2, Ctrl/shRNA = RAW264.7 macrophages transduced with NonMammalian control shRNA. The IL-27p28 release of LPS treated RAW264.7 macrophages was set to 100%. Expression was normalized to *gapdh* mRNA expression. All values are presented as the mean ± SEM. *p<0.05, **p<0.01 and ***p<0.005 vs. Ctrl/shRNA, one-way ANOVA (A + B) or Student's t test (C).

9.3 Binding of Smad3 to the *il-27p28* and *ebi3* promoter regions

As shown above, Smad3 was important for the TGFβ1-mediated inhibition of IL-27p28 release and of the *il-27p28* and *ebi3* mRNA expression in LPS treated RAW264.7 macrophages. TGFβ1 increased the DNA binding of Smad3. In the next step, the binding of Smad3 to the *il-27p28* and *ebi3* promoter was analyzed. $1x10^7$ BMDMs per sample were seeded and allowed to rest overnight. The cells were stimulated with 100ng/ml LPS or with LPS + 10ng/ml TGFβ1 for 3h to obtain samples for Chromatin Immunoprecipitation (ChIP), which was performed as described in Chap. II-2.5.9. Sonicated DNA without immunoprecipitation was used as input control.

Indeed, Smad3 bound to the *il-27p28* promoter. The binding of Smad3 to the *il-27p28* promoter after LPS stimulation was reduced in comparison to unstimulated cells. On the other hand, Smad3 binding to the *il-27p28* promoter was approx. 4-fold increase in response to LPS + TGFβ1 treatment as compared to LPS treatment alone (Fig. 16.5A). Smad3 also bound to the *ebi3* promoter (Fig. 16.5B). Similar to the findings for the *il-27p28* promoter, Smad3 bound less to the *ebi3* promoter after LPS stimulation in comparison to unstimulated cells. Again, the binding of Smad3 to the *ebi3* promoter was approx. 4-fold higher after LPS + TGFβ1 stimulation in comparison to LPS alone.

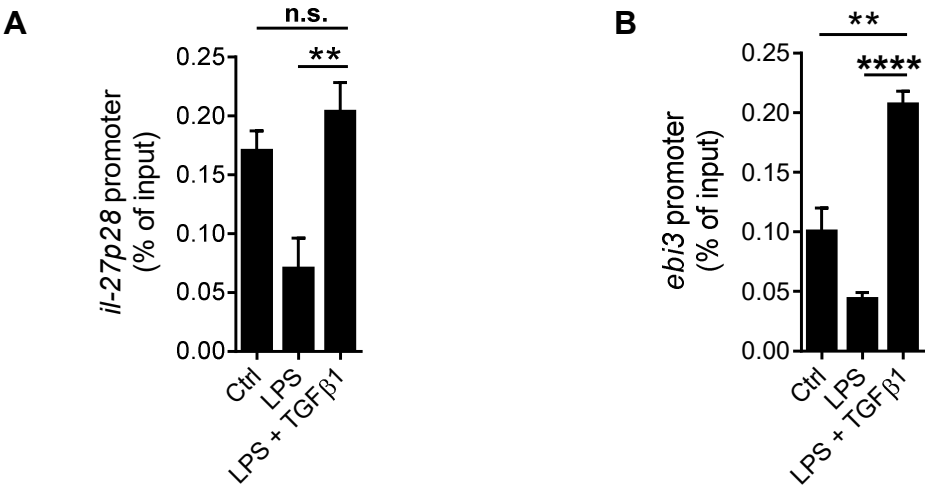

Fig. 16.5: Smad3 directly bound to the promoter regions of the IL-27 subunits.
(A) Smad3 directly bound to the *il-27p28* promoter region, ChIP. (B) Smad3 directly bound to the *ebi3* promoter region, ChIP. 10^7 C57BL/6J BMDMs were stimulated with 100ng/ml LPS or LPS + 10ng/ml TGFβ1 for 3h (37°C, 5% CO_2). Ctrl = unstimulated cells. Sonicated DNA without immunoprecipitation was used as input control. All values are presented as the mean ± SEM. **p<0.01 and ****p<0.001 vs. Ctrl or LPS, one-way ANOVA. n.s. = not significant.

In Fig. 16.6, the sequence of the *il-27p28* promoter is shown and the sequence of the *ebi3* promoter is shown in Fig. 16.7. The putative Smad3 binding sites (CAGA, (212)) are shown in bolt and underlined. The locations of the different primers used for the ChIP analysis are indicated.

Fig. 16.6: Sequence of a part of the mouse *il-27p28* promoter.
Putative Smad3 binding sites (CAGA) are shown in bolt and underlined. Primers used for ChIP analysis are indicated. IRF-E = interferon regulatory factor binding element. +1 = translational initiation codon.

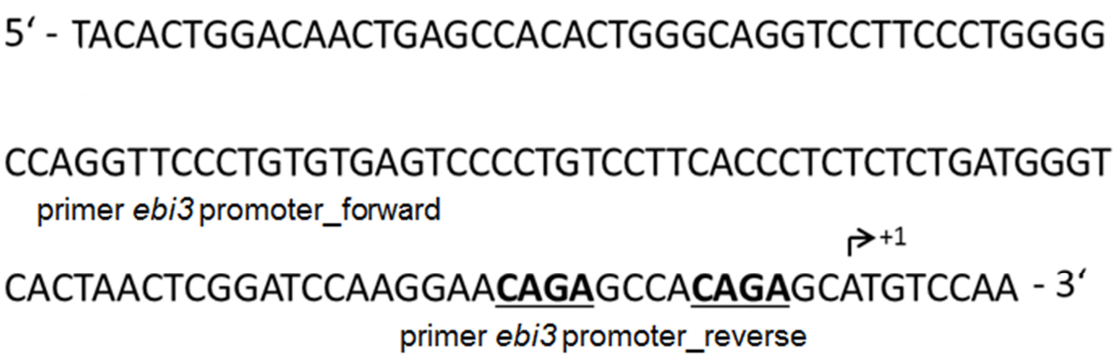

Fig. 16.7: Sequence of a part of the mouse *ebi3* promoter.
Putative Smad3 binding sites (CAGA) are shown in bolt and underlined. Primers used for ChIP analysis are indicated. +1 = translational initiation codon.

10 The p38 MAP Kinase participates in TGFβ1-mediated inhibition of IL-27 in Macrophages

The p38 MAP Kinase (MAPK) is rapidly phosphorylated in response to TLR4-activation by LPS. The phosphorylation of p38 MAPK was analyzed to investigate the impact of TGFβ1 regarding the phosphorylation status of p38 MAPK in macrophages. $2x10^6$ C57BL/6J BMDMs per sample were seeded and could rest overnight to reduce stress-induced phosphorylation. The cells were stimulated with 100ng/ml LPS or with LPS + 10ng/ml TGFβ1 for 1h. Next, a phospho-Bio-Plex was performed as described in Chap. II-2.3.3. Treatment of LPS + TGFβ1 induced a 2.5-fold increase of the p38 MAPK phosphorylation at the position Thr180/Tyr182 in comparison to LPS alone (Fig. 17.1).

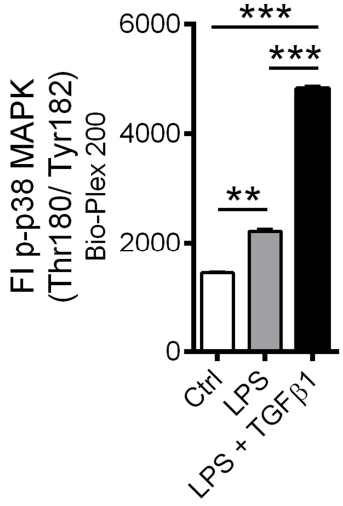

Fig. 17.1: p38 MAPK phosphorylation by TGFβ1 in BMDMs.
$2x10^6$ C57BL/6J BMDMs were stimulated with 100ng/ml LPS or LPS + 10ng/ml TGFβ1 for 1h (37°C, 5% CO_2), bead-based assay for phospho-p38; phospho-BioPlex. Ctrl = unstimulated cells. FI = Fluorescence intensity. All values are presented as the mean ± SEM. **p<0.01 and ***p<0.005 vs. Ctrl or LPS, one-way ANOVA.

In a next experiment, it was studied how the p38 MAPK phosphorylation was related to the IL-27p28 response in macrophages. BMDMs were stimulated with 100ng/ml LPS or with LPS + 10ng/ml TGFβ1 for 24h. In addition, severak p38 MAPK inhibitors were added to the LPS and LPS + TGFβ1 samples. Three different inhibitors were used for the inhibition of the p38 MAPK: SB203580 (10µM, binds the ATP binding pocket), PH-797804 (10nM, ATP-competitive) and BIRB796 (50nM, allosteric binding and conformational change of the ATP site, (274)). The optimal concentrations of the different p38 MAPK inhibitors were determined in pre-experiments (data not shown). The different inhibitors were reconstituted in DMSO. The DMSO had no effects to the cells (Fig. 14.13).

All three p38 MAPK inhibitors increased the IL-27p28 secretion after LPS treatment (Fig. 17.2, black bars). The inhibitor SB203580 had the strongest effects. Treatment

of BMDMs with LPS + TGFβ1 (Fig. 17.2, white bars) reduced the IL-27p28 release by approx. 80% in comparison to LPS treatment. The inhibition of the p38 MAPK by SB203580 recovered the inhibitory effect of TGFβ1. The inhibitors PH-797804 and BIRB796 also reduced the TGFβ1-mediated inhibition of IL-27p28, but this effect was less as compared to SB203580.

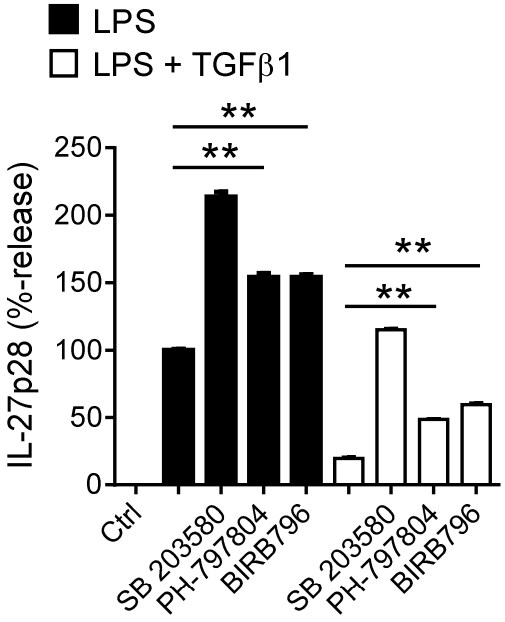

Fig. 17.2: IL-27p28 secretion after p38 MAPK inhibition.
$5x10^5$ C57BL/6J BMDMs were stimulated with 100ng/ml LPS (black bars) or with LPS + 10ng/ml TGFβ1 (white bars) for 24h (37°C, 5% CO_2) before quantified by ELISA. Concentrations used for the inhibitors: SB203580 (10µM), PH-797804 (10nM) and BIRB796 (50nM). IL-27p28 release after LPS stimulation was set to 100%. Ctrl = unstimulated cells. All values are presented as the mean ± SEM. **p<0.01 vs. LPS or LPS + TGFβ1, one-way ANOVA.

In summary, the p38 MAPK was strongly phosphorylated in BMDMs by TGFβ1 treatment and p38 MAPK was involved in the TGFβ1-mediated inhibition of IL-27p28 in LPS-activated BMDMs.

11 Inhibition of IL-27p28 by TGFβ1 in Macrophages was IL-10 mediated

Bosmann et al., 2014 (229) showed that IL-10 inhibited the IL-27p28 production after LPS in macrophages. Furthermore, the production of IL-10 in macrophages is p38 MAPK dependent (225) (226) and TGFβ1 treatment resulted in an increased phosphorylation of p38 MAPK (Fig. 17.1). Therefore, the TGFβ1-mediated IL-10 release was studied. BMDMs (C57BL/6J) were stimulated with 100ng/ml LPS or with LPS + 10ng/ml TGFβ1. The supernatants were collated at the time points 0h, 3h, 6h, 9h and 24h.

The samples stimulated with LPS + TGFβ1 contained significantly more IL-10 in the supernatants as the LPS-treated samples after 9h. The unstimulated control samples did not show any IL-10 release. Summarizing, TGFβ1 induced IL-10 secretion in LPS treated BMDMs (Fig. 18.1).

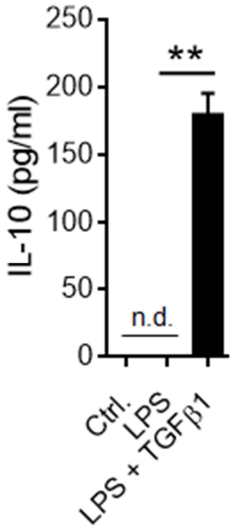

Fig. 18.1: IL-10 release induced by TGFβ1 in BMDMs.
$5x10^5$ C57BL/6J BMDMs were stimulated with 100ng/ml LPS or with LPS + 10ng/ml TGFβ1 at 37°C, 5% CO_2 for 9h. IL-10 quantification by ELISA. Ctrl = unstimulated cells. All values are presented as the mean ± SEM. **p<0.01 vs. LPS, Student's t test.

To study the effect of IL-10 induction by TGFβ1, the IL-10 receptor (IL-10R) was blocked by using an α-IL-10R antibody. PEMs of C57BL/6J mice were generated and $5x10^5$ cells/sample/ml were seeded. The α-IL-10R antibody and the isotype antibody (ratIgG1) were added with 10µg/ml to the cell culture medium at the same time point such as LPS (100ng/ml) and LPS + TGFβ1 (1ng/ml). The stimulation was done for 24h. In the α-IL-10R antibody treated samples, the inhibition of IL-27p28 was partly abolished in comparison to the isotype (ratIgG1) treated samples after LPS + TGFβ1 treatment (Fig. 18.2A). The non-antibody treated sample and the isotype (ratIgG1) treated sample had comparable IL-27p28 amounts after LPS + TGFβ1 treatment.

Less TGFβ1-mediated inhibition of IL-27p28 in LPS-activated BMDMs was also observed in IL-10-deficient BMDMs (B6.IL-$10^{-/-}$) in comparison to wild type C57BL/6J BMDMs (Fig. 18.2B). The cells were stimulated with 100ng/ml LPS or with LPS + 500pg/ml TGFβ1 for 24h. These data suggested that the inhibition of IL-27p28 by TGFβ1 in BMDMs was partly relied on the presence of IL-10.

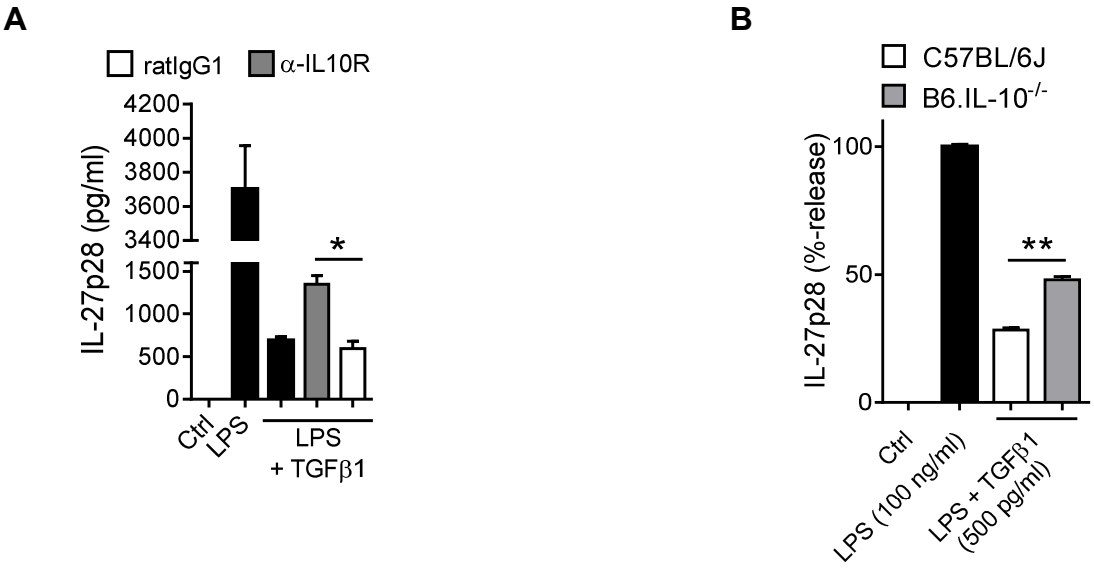

Fig. 18.2: The TGFβ1-mediated inhibition of IL-27p28 was IL-10 dependent.
(A) 5x10^5 C57BL/6J PEMs were stimulated with 100ng/ml LPS or with LPS + 1ng/ml TGFβ1 for 24h before IL-27p28 quantification by ELISA. The IL-10R blocking antibody (α-IL-10R) and the isotype control antibody (ratIgG1) were added with 10µg/ml. (B) 5x10^5 BMDMs were stimulated with 100ng/ml LPS or with LPS + 500pg/ml TGFβ1 for 24h before IL-27p28 quantification by ELISA. The IL-27p28 release in the LPS treated sample was set to 100%. Cells were incubated at 37°C, 5% CO_2. Ctrl = unstimulated cells. All values are presented as the mean ± SEM. *p<0.05 and **p<0.01 vs. ratIgG1 or C57BL/6J, Student's t test.

The presented data suggested IL-10 as a secondary mediator in TGFβ1-mediated inhibition of IL-27p28 in macrophages. As a matter of fact, Kitani et al., 2003 (275) have described Smad binding elements (SBE) in the *il-10* promoter. This may suggest that IL-10 gene expression is under the control of Smad3. The influence of Smad3 on the expression levels of IL-10 was studied by using Smad3 knock down RAW264.7 macrophages. The cells were stimulated with 100ng/ml LPS or with LPS + 100pg/ml TGFβ1. The clone RAW264.7-Smad3/shRNA2 was used for these experiments because of the high knock down efficiency of Smad3 (Fig. 16.2A and 16.2B). The Smad3 knock down RAW264.7 macrophages (Smad3/shRNA2) released significantly less IL-10 concentrations in comparison to the transduction-control macrophages (Ctrl/shRNA). The cultures of untransduced macrophages

(RAW264.7) and the Smad3 knock down RAW264.7 macrophages (Smad3/shRNA2) reached the same levels of IL-10. Figure 18.3 shows the relative release of IL-10 in RAW264.7 macrophages after lentiviral knock down of Smad3. As expected, the TGFβ1-induced IL-10 release was Smad3 dependent.

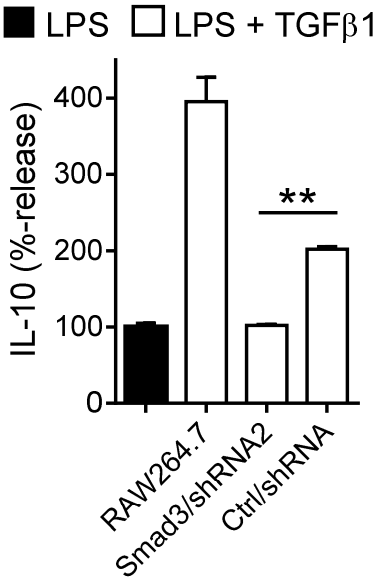

Fig. 18.3: TGFβ1-mediated IL-10 release in macrophages was Smad3-dependent.
$5x10^5$ cells were stimulated with 100ng/ml LPS or with LPS + 100pg/ml TGFβ1 for 17.5h (37°C, 5% CO_2) before IL-10 quantification by ELISA. The IL-10 release in the LPS treated sample was set to 100%. All values are presented as the mean ± SEM. **p<0.01 vs. Ctrl/shRNA, Student's t test.

12 Tristetraprolin is involved in TGFβ1-mediated inhibition of IL-27

12.1 Tristetraprolin as a mediator of TGFβ1

TGFβ1 activated the p38 MAPK signaling pathway (Fig. 17.1). A downstream molecule of p38 MAPK signaling is Tristetraprolin (TTP). Therefore, a potential role of TTP for TGFβ-mediated inhibition of IL-27p28 was evaluated. Littermate control ($TTP^{+/+}$) BMDMs and TTP KO BMDMs ($TTP^{-/-}$) were generated. The BMDMs were stimulated wit 100ng/ml LPS or with LPS + 500pg/ml TGFβ1 for 24h.

In TTP KO BMDMs, an increase in the IL-27p28 release after LPS + TGFβ1 treatment in comparison to littermate control BMDMs ($TTP^{+/+}$) was observed (Fig. 19.1). IL-27p28 was not detectable in unstimulated samples (Ctrl). These data indicate that TTP was required for a complete inhibition of IL-27p28 by TGFβ1 in BMDMs.

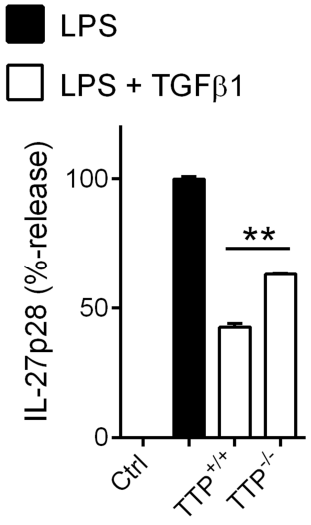

Fig. 19.1: The TGFβ1-mediated inhibition of IL-27p28 was Tristetraprolin-dependent.
$5x10^5$ BMDMs were stimulated with 100ng/ml LPS or with LPS + 500pg/ml TGFβ1 (white bars) for 24h (37°C, 5% CO_2) before quantified by ELISA. IL-27p28 release after LPS stimulation was set to 100% (black bar). $TTP^{+/+}$ = littermate control macrophages, $TTP^{-/-}$ = Tristetraprolin knock out macrophages. All values are presented as the mean ± SEM. **p<0.01 vs. $TTP^{+/+}$, Student's t test.

These data were confirmed by flow cytometry analyses (Fig. 19.2). BMDMs (C57BL/6J) were stimulated with 100ng/ml LPS or with LPS + 500pg/ml TGFβ1 for 20h. Two hours after the stimulation, monensin (golgi transport inhibitor) was added. The BMDMs were stained for CD11b, F4/80 and IL-27p28. The isotype antibodies were used to gate the negative populations.

Littermate control BMDMs ($TTP^{+/+}$) and TTP KO BMDMs ($TTP^{-/-}$) were gated for $F4/80^+CD11b^+$ double positive macrophages. Intracellular staining of IL-27p28 showed 16.7% $F4/80^+IL\text{-}27p28^+$ double positive macrophages in the LPS treated littermate control $TTP^{+/+}$ cells. This IL-27p28 positive population was reduced by TGFβ1 to 2.72%. The $F4/80^+IL\text{-}27p28^+$ double positive population in LPS treated

$TTP^{-/-}$ macrophages was 2.4-fold (39.2%) higher as compared to the comparable population in littermate control $TTP^{+/+}$ macrophages. With addition of TGFβ1, the $F4/80^{+}IL\text{-}27p28^{+}$ double positive population was reduced only to 25.8%.

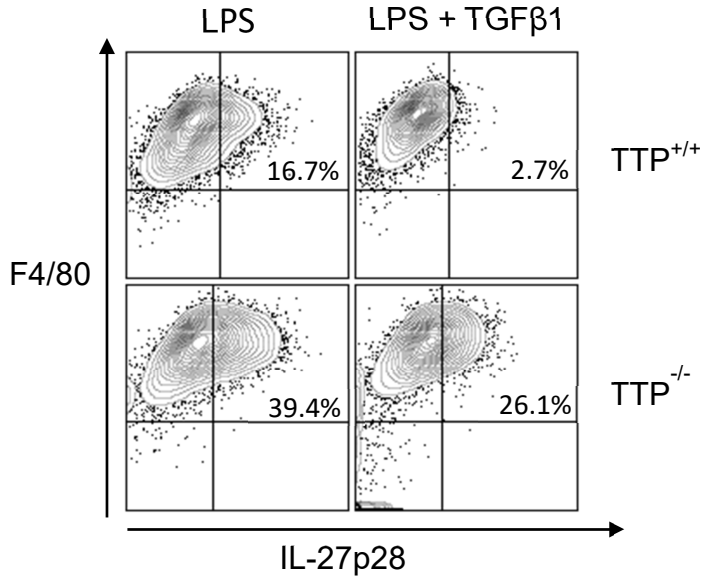

Fig. 19.2: TGFβ1-mediated inhibition of IL-27p28 was influenced by Tristetraprolin in $F4/80^{+}CD11b^{+}$ double positive macrophages.
$1x10^6$ BMDMs were stimulated with 100ng/ml LPS or with LPS + 500pg/ml TGFβ1 for 20h (37°C, 5% CO_2) before flow cytometry analyses. Monensin was added after 2h. IL-27p28 staining after LPS stimulation was set to 100%. $TTP^{+/+}$ = littermate control macrophages, $TTP^{-/-}$ = Tristetraprolin knock out macrophages.

To further investigate the role of TTP, the *ttp* mRNA expression values were studied in macrophages. BMDMs (C57BL/6J) were generated, $5x10^5$ cells/sample/ml were seeded and the cells could rest overnight without further treatment. The BMDMs were stimulated wit 100ng/ml LPS or with LPS + 10ng/ml TGFβ1. The samples were collected at the indicated time points. At the 3h time point, the expression level of *ttp* mRNA in LPS-stimulated BMDMs was similar to the expression level in LPS + TGFβ1 stimulated BMDMs. After 3h, the expression levels increased constantly in LPS-activated BMDMs until the 9h time point. In LPS + TGFβ1 stimulated BMDMs, the expression levels decreased constantly until the 9h time point. After 24h, the expression levels of all studied conditions were on a comparable level (Fig. 19.3). The unstimulated cells (Ctrl) did not show a relevant *ttp* mRNA expression over the whole kinetic.

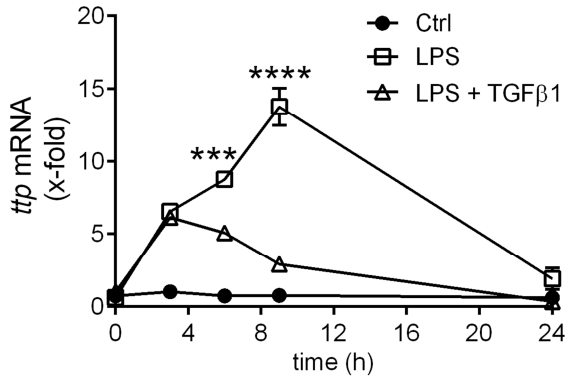

Fig. 19.3: Kinetic of *ttp* mRNA expression in BMDMs.
$5x10^5$ C57BL/6J BMDMs were stimulated with 100ng/ml LPS or LPS + 10ng/ml TGFβ1 at 37°C, 5% CO_2 for 3h, 6h, 9h and 24h. The 0h samples were collected at the time of stimulation. The *ttp* mRNA expressions were analyzed by qPCR. Expressions were normalized to *gapdh* mRNA expression.
All values are presented as the mean ± SEM. ***p<0.005 and ****p<0.001 vs. LPS, one-way ANOVA. Ctrl = unstimulated cells.

These results indicated that TTP was involved in the TGFβ1-mediated inhibition of IL-27p28 in LPS-stimulated BMDMs. Furthermore, TGFβ1 also inhibited the *ttp* mRNA expression in LPS-stimulated BMDMs.

12.2 Myeloid Tristetraprolin as a regulator of bleomycin-induced pulmonary fibrosis

In Fig. 19.1, the role of Tristetraprolin (TTP) in TGFβ1-mediated inhibition of IL-27p28 is shown. During pulmonary fibrosis, IL-27 is a key player (276). In the next step, the influence of TTP on IL-27 in bleomycin-induced pulmonary fibrosis was studied. Wild type C57BL/6J mice (WT) were bone marrow transplanted with littermate control $TTP^{+/+}$ (Wt) and $TTP^{-/-}$ bone marrow as described in Chap. II-2.1.9. After five weeks, 1U/kg BW bleomycin was instilled i.t. and lung samples were collected after three weeks. To confirm if the transplantation was successful, the bone marrow was isolated and mRNA for *ttp* was assessed. In $TTP^{-/-}$ transplanted mice, *tristetraprolin* mRNA expression was not detectable (n.d.) (Fig. 19.4).

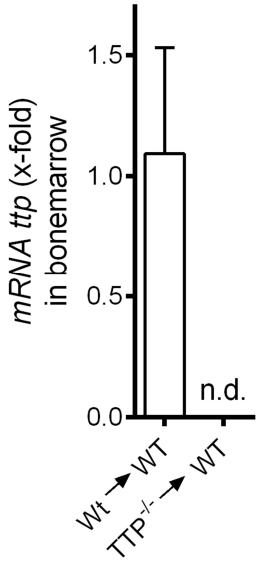

Fig. 19.4: Confirmation of $TTP^{-/-}$ bone marrow transplantation.
Successful bone marrow transplantation was confirmed by *ttp* mRNA expression, qPCR in the recipient mice bone marrow after reconstitution (5 weeks), n ≥ 3/group. 1U/kg BW bleomycin in 40µl 0.9% NaCl was instilled i.t.. $TTP^{-/-}$ = Tristetraprolin knock out, WT = wild type (C57BL/6J), Wt = $TTP^{+/+}$ (littermate control). Expression was normalized to *gapdh* mRNA expression. The values are presented as the mean ± SEM. n.d. = not detectable.

$TTP^{-/-}$ bone marrow chimeric mice ($TTP^{-/-}$ → WT) showed less symptoms of pulmonary fibrosis in comparison to the control group of $TTP^{+/+}$ transplanted mice (Wt → WT). In lungs of $TTP^{-/-}$ chimeric mice, significantly less *collagen I,V* mRNA was expressed as compared to the $TTP^{+/+}$ chimeric mice (Fig. 19.5A). The lungs of $TTP^{-/-}$ transplanted mice also contained less collagen I,V (Fig. 19.5B).

The TGFβ1 amount in the BALF was decreased in $TTP^{-/-}$ transplanted mice in comparison to the $TTP^{+/+}$ transplanted mice (Fig. 19.5C). On the other hand, approx. three times higher IL-27p28 levels were detected in $TTP^{-/-}$ transplanted mice in comparison to the $TTP^{+/+}$ transplanted mice (Fig. 19.5D). This data support the *in vitro* results of Fig. 19.1. Taken together, myeloid TTP influenced bleomycin-induced pulmonary fibrosis to more severe symptoms.

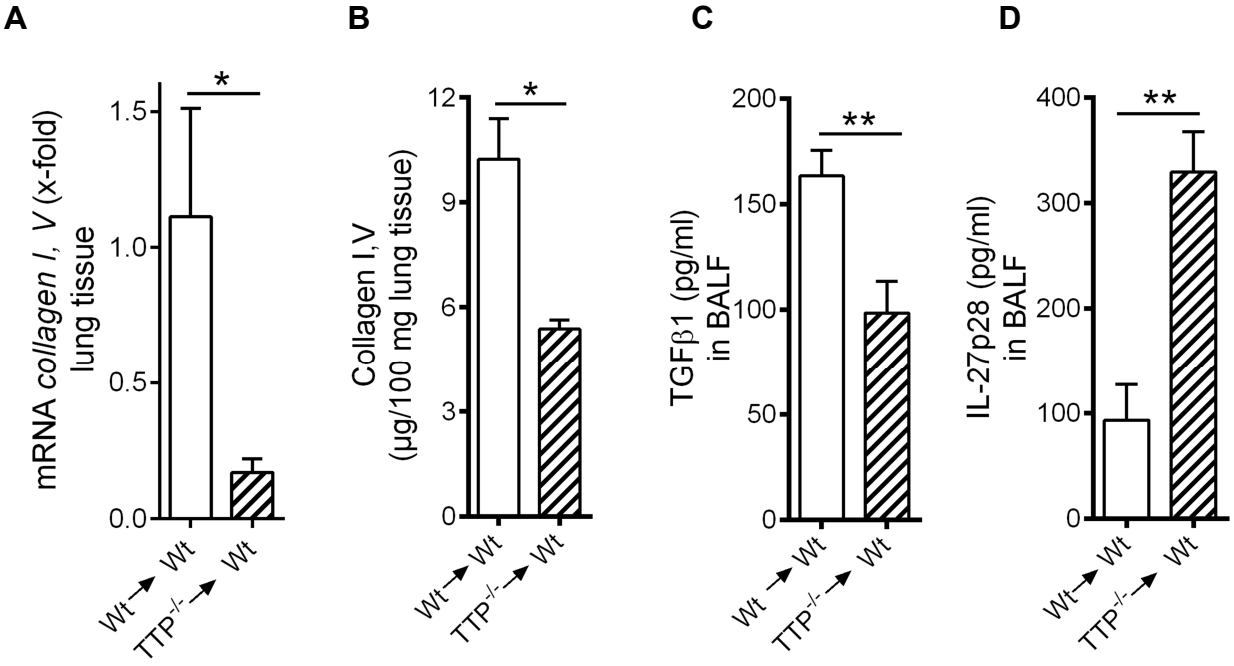

Fig. 19.5: Bleomycin-induced pulmonary fibrosis in dependency of Tristeraprolin.
(A) Expression of collagen I,V mRNA in whole lung tissue. Expression was normalized to *gapdh* mRNA expression, qPCR. (B) Total collagen I,V amount in whole lung tissue, collagen assay. (C) TGFβ1 amount in the BALF, ELISA. (D) IL-27p28 amount in the BALF of $TTP^{-/-}$ chimeric mice, ELISA.
Mice were housed for five weeks after bone marrow transplantation. 1U/kg BW bleomycin in 40µl 0.9% NaCl was instilled i.t.. $TTP^{-/-}$ = Tristetraprolin knock out, WT = wild type (C57BL/6J), Wt = $TTP^{+/+}$ (littermate controls). All values are presented or expressed as the mean ± SEM. *p<0.05 and **p<0.01 vs. Wt→WT, Student's t test. Wt → WT: eight male mice; $TTP^{-/-}$ → WT: five male mice.

IV Discussion

1 Time course of bleomycin-induced pulmonary fibrosis

Bleomycin is a pulmonary fibrosis inducing drug (277). The collagen I,V amount in the lung increased constantly after bleomycin application in the following four weeks (Fig. 8.1). After 0.9% NaCl instillation (sham-group) the collagen I,V amount also increased over time. This is contrary to the recent literature where instillation of 0.9% NaCl does not force any fibrotic effects (no histopathological changes, no elevated levels of hydoxyproline levels as a part of collagen) (278). The contrary results can be due to the fact that Izbicki and colleagues used 11-12 weeks old male C57BL/6J mice. In this report, 8 weeks old male C57BL/6J mice were used. The four-week kinetic was mainly performed to establish the best time points of sample collection for the used method of bleomycin application.

Macrophages infiltrated the lungs after bleomycin application (Fig. 8.2) and IL-27p28 (Fig. 8.3A) increased in the BALF. Macrophages were the source of IL-27p28, *in vivo* (Fig. 14.1). In parallel, the TGFβ1 amount was increasing in the BALF by time (Fig. 8.3B). At the highest concentration of TGFβ1 (week 2), the IL-27p28 amount was decreasing constantly. In addition, $CD4^+$ T cells started to infiltrate the lungs and the mediastinal lymph nodes (Fig. 8.4). This demonstrated an orchestrated immune response. The initiated immune response was confirmed by the migration of pro-fibrotic $CD4^+$IL-$17A^+$ (Th17) cells and anti-fibrotic $CD4^+IFN\gamma^+$ (Th1) cells into the lungs (Fig. 8.5). In the end, the cell types are orchestrated by different cell adhesion molecules during the response to lung injury (279). The BALF of sham mice did not contain relevant numbers of $CD4^+$ T cells, Th1 or Th17 cells. No immune response was initiated in the sham-group.

2 Neutrophils and extracellular histones in bleomycin-induced pulmonary fibrosis

In the literature, the effects of extracellular histones and NETs were mainly studied in models of acute diseases (72) (93) (94) (87). The novelty of the present work is the influence of extracellular histones on pulmonary fibrosis in a chronic disease model, four weeks after the application of bleomycin.

After bleomycin application, extracellular histones were detected in the BALF within two days (Fig. 10.1A). During this acute phase, bleomycin injures the alveolar epithelium and drives necrosis of capillary endothelium (272) with an enhanced release of histones. In other acute diseases such as acute kidney injury, histones are released in a similar fashion (92). Another source of extracellular histones in the BALF is the formation of neutrophil extracellular traps (NETs). This was shown by an increased amount of citrullinated H3 (H3-Cit) in the BALF after two days (Fig. 10.5A). H3-Cit is a marker for NET building by neutrophils (75). The uncitrullinated extracellular histones (Fig. 10.1A) appeared to decrease faster than the H3-Cit (Fig. 10.5A). After lung injury, influx of plasma into the alveolar space occurs and protein C can be activated during this process. Activated protein C has been described to cleave extracellular histones and reduce their cytotoxicity (93). This can explain the decreased extracellular histone amount in the BALF after three days. In the future, it has to be further analyzed if H3-Cit is protected from the protein C mediated cleavage. A bone marrow transplantation experiment supported the role of neutrophils as a source of extracellular histones (Fig. 10.3). If only the myeloid cells, such as neutrophils, contained the histone reporter genotype (C57BL/6J → $H2BeGFP^{+/-}$) the eGFP fluorescence intensity in the BALF was reduced by half in comparison to the group where all cells had the histone reporter genotype ($H2BeGFP^{+/-}$ → $H2BeGFP^{+/-}$). In both groups, the bleomycin-mediated lung damage was comparable (Fig. 10.4). So, the differences in the fluorescence intensity were due to the chimeric genotypes.

Neutrophils infiltrate the lungs very rapidly and reach their maximal numbers three days after bleomycin application (278). In the past, several groups failed to figure out a clear pro-fibrotic role using neutrophils depleting antibodies (280) (281). One possibility of the unclear studies could be cross-reactivity or FcγR binding. In the present work, the $Ly6G^{+}CD11b^{+}$ neutrophils were depleted by using diphtheria toxin (DTX) prior to the bleomycin application. After three days of DTX, the numbers of $Ly6G^{+}CD11b^{+}$ neutrophils in the blood was decreased (18.7% vs. 9.6%) (Fig. 9.1). For several reasons the depletion of neutrophils may have been not complete: Neutrophils are mobilized in very high numbers from the bone marrow during inflammatory diseases within several hours (282). The plasma half-time (t1/2) of DTX is approx. 9-12h (283) and the biological activity is expected to expire within 2-3 days (4-5 x t1/2 = end of biological activity). The ensuing emergency neutropoiesis may

recover the DTX-mediated neutrophil depletion. This may results in a rapid recovery of the neutrophil numbers in the blood. The very early depletion of $Ly6G^+CD11b^+$ neutrophils was sufficient to influence the pathophysiology of bleomycin-induced pulmonary fibrosis. After two weeks, the neutrophil numbers in the BALF were similar in both strains. In the end, depletion of neutrophils resulted in less severe signs of pulmonary fibrosis (Fig. 9.3 and Fig. 9.4). In addition, less mRNA expression was observed for the epithelial-mesenchymal transition (EMT)-specific transcription factors Slug, Snail and Zeb2 as well as for the endothelial-mesenchymal transition (EndMT) markers FSP-1, Vimentin and α-SMA, if neutrophils were depleted. In summary, $Ly6G^+CD11b^+$ neutrophils are critically important for the pathophysiology of bleomycin-induced pulmonary fibrosis.

The recent work describes neutrophils involved in the pathophysiology of bleomycin-induced pulmonary fibrosis by producing NETs (H3-Cit in BALF, Fig. 10.5B). So far, the pathophysiology of neutrophils during pulmonary fibrosis had been described by a production of reactive oxygen species (ROS) (284). Furthermore, NET formation based on ROS production had been described (71). This suggests that NET formation and ROS production can reinforce each other. Chrysanthopoulou et al., 2014 (285) identified an increased percentage of NET building neutrophils after incubation with bleomycin. NETs activate fibroblasts *in vitro* and result in an increased collagen production by lung fibroblasts after 48h (285). All results of Chrysanthopoulou and colleagues were generated with in vitro cultures of human cells. In the present work, the results were generated in murine cells and in vivo models to expand the results of Chrysanthopoulou and colleagues. In turn, BALF of bleomycin treated mice induced the release of H3-Cit by PENs, *in vitro*. This effect was inhibited by rmIL-27 (Fig. 10.7A). IL-27 was previously described as a negative regulator of human neutrophils (172) and murine neutrophils (286). Both receptor subunits WSX-1 (IL-27RA) and gp130 are expressed in murine neutrophils (286). The inhibitory effect of IL-27 on the H3-Cit release was confirmed by us *in vivo*. IL-$27RA^{-/-}$ mice released significantly more H3-Cit per 1,000 cells into BALF as compared to the C57BL/6J control group (Fig. 10.7B). The H3-Cit amount was normalized, because in the IL-$27RA^{-/-}$ mice significantly lower numbers of neutrophils were present in BALF. An additional mechanism for less pulmonary fibrosis in neutrophil depleted mice may be the missing neutrophil elastase. Mice lacking

neutrophil elastase are resistant to bleomycin-induced pulmonary fibrosis by a suggested defect in TGFβ activation (287).

The importance of histones for the pathophysiology of bleomycin-induced pulmonary fibrosis was confirmed by blockade of histones. The functionality of the anti-histone antibody was previously shown in sepsis experiments with a better outcome for histone blocked mice (91). Mice with blocked histones during bleomycin-induced pulmonary fibrosis had less severe symptoms of pulmonary fibrosis as compared to mice which received the control antibody (Fig. 10.9 and Fig. 10.10). The influence of histones on pulmonary fibrosis was observable by reduced mRNA expression of EMT-specific transcription factors and EndMT-markers (Fig. 10.12). In addition, the endothelial cell marker CD31 was more observable after histone blockade (Fig. 10.13). The elevated IL-27p28 levels after histone blockade resulted in antagonizing TGFβ1-mediated EMT. This supports the results of Dong et al., 2016 (288). There, *in vitro* studies of human alveolar epithelial cells showed that TGFβ1-induced EMT was attenuated by IL-27-increased expressions of epithelial phenotypic markers. In the recent literature the role of EMT or EndMT during pulmonary fibrosis is debated controversial (289) (47) (46) (49) (48). Rock and colleagues used lineage tracing studies to identify that there is no evidence for EMT during bleomycin-induced pulmonary fibrosis. Nevertheless, the recent work found elevated levels of EndMT and EMT markers in lung tissues (Fig. 10.12 and Fig. 10.13). In the future, this should be further analyzed to identify the source of these analyzed EndMT and EMT markers.

The blockade of histones reduced the total number of $CD4^+Foxp3^+$ Tregs in the mediastinal lymph nodes after 14 days (Fig. 10.14A). The expression levels of different stress-induced genes such as heat shock proteins (Hsp) were studied by Next Generation Sequencing (NGS, RNA-Sequencing), four weeks after bleomycin application. Purified $CD4^+CD25^+$ Tregs of the mediastinal lymph nodes were used for NGS (Fig. 11.2). In the histone blocked group, significantly less stress-induced genes such as *hspa1b* were expressed. This was confirmed by *in vitro* experiments with purified naïve $CD4^+CD25^+$ Tregs. Here, histones increased the mRNA expression of *hspa1b* and rmIL-27 was able to decrease the expression (Fig. 11.3). In conclusion, there were direct effects of histones and IL-27 on purified naïve $CD4^+CD25^+$ Tregs *in vitro*. This confirmed the results of Wojno et al., 2011 (290) where IL-27 limited Treg

populations. The IL-27RA (WSX-1) is expressed on nearly all $CD3^+CD4^+$ T cells (Fig. 11.4). These data is in accordance with Villarino et al., 2005 (291). Here, the IL-27RA (WSX-1) was monitored on Tregs from spleens. The studied heat shock proteins have been reported to complex with Foxp3 in Tregs to increase the survival rate and the inhibitory power of the Tregs (245) (246). A positive correlation was seen between the expression of *hspa1b* (Fig. 11.2) and the total number of $CD4^+Foxp3^+$ Tregs in the mediastinal lymph nodes (Fig. 10.14). The modified expression levels of the stress-induced genes in the $CD4^+CD25^+$ Tregs were not a transient effect. These $CD4^+CD25^+$ Tregs had manifested phenotypes which were kept in an adoptive transfer approach. Transplanted purified $CD4^+CD25^+$ Tregs of histone blocked mice reduced the *collagen I,V* mRNA expression in lung tissue and the collagen I,V amount in the lung (Fig. 11.5) in comparison to the $CD4^+CD25^+$ Tregs of the isotype antibody group. The released extracellular histones affected $CD4^+CD25^+$ Tregs which influence the severity of bleomycin-induced pulmonary fibrosis. Extracellular histones/NETs, as a part of the innate immune response, have been described to prime Tregs and are able to link innate and adaptive immune responses (292).

3 IL-27 as a regulator of Bleomycin-induced pulmonary fibrosis

So far, the recent literature reports a controversial role of IL-27 during pulmonary fibrosis (293) (276). Kim and colleagues reported a pro-fibrotic effect of IL-27. The blockade of IL-27 resulted in reduced hydroxyproline levels an increased IL-27 amounts (293). The other group injected IL-27 which in turn attenuated the severity of bleomycin-induced pulmonary fibrosis. This describes an anti-fibrotic effect of IL-27 during pulmonary fibrosis (276). Furthermore, IL-27 attenuates the pro-fibrotic effects of TGFβ1 in murine lung fibroblasts (294) and is able to reduce EMT in human alveolar epithelial cells (288). To identity the role of IL-27 during pulmonary fibrosis, the present work used $IL\text{-}27RA^{-/-}$ mice for bleomycin-induced pulmonary fibrosis as a first approach. Missing IL-27RA signaling ($IL\text{-}27RA^{-/-}$) resulted in more severe pulmonary fibrosis (Fig. 12.1 and Fig. 12.2). This describes IL-27 as an anti-fibrotic cytokine during bleomycin-induced pulmonary fibrosis under the used conditions. The anti-fibrotic role of IL-27 is strengthening by the report that IL-27 inhibits Th17 cells (295) (156). This correlates with Fig. 12.3, where Th17 cells were significantly increased in $IL\text{-}27RA^{-/-}$ mice in comparison to wild type mice. The $IL\text{-}27RA^{-/-}$ mice

showed approx. three times more *collagen I,V* mRNA expression as compared to the wild type mice (Fig. 12.2B). During bleomycin-induced pulmonary fibrosis, Th17 cells express two cytokines: IL-17A and IL-17F (296). The disease is IL-17A dependent whereas IL-17F was not further analyzed by IL-17F$^{-/-}$ mice (106). The cytokine IL-17A modulates epithelial cells by increasing the synthesis and secretion of collagen and reduces the degradation of collagen. Furthermore, IL-17A induces EMT in alveolar epithelial cells in a TGFβ1-dependent manner (107). This was confirmed in the present work with an *in vivo* experiment of bleomycin-induced pulmonary fibrosis in IL-17A/F double knock out (IL-17DKO) mice. The IL-17DKO mice had significantly less collagen I,V amount in the lung in comparison to the C57BL/6J control mice (Fig. 12.4). But the difference of the collagen I,V amount in the lungs was not as big as in dependence of IL-27 signaling, for example (Fig. 12.2A). Lo Re et al., 2010 (297) already showed that IL-17 alone is not the master regulator of fibrosis in different models.

IL-27 promotes IFNγ-producing Th1 cells (155). When the IL-27RA signaling was abolished (IL-27RA$^{-/-}$) the amount of Th1 cells was reduced in BALF (Fig. 12.3). These mice are able to produce physiological correct IL-27 but the target cells are not able to recognize the secreted IL-27. There is a pro-fibrotic and an anti-fibrotic role known for IFNγ. As a pro-fibrotic role, Chen and colleagues (2000) (175) observed significantly lower lung collagen in IFNγ$^{-/-}$ mice in comparison to wild type mice after bleomycin application. On the other hand, Jiang et al., 2004 (298) found enhanced fibrosis after pre-treatment of wild type mice with an IFNγ-neutralizing antibody and less fibrosis was observed after injection of exogenous IFN-γ. This indicates an anti-fibrotic role of IFNγ. The present work indicates an anti-fibrotic role for IFNγ. All results of the present work were in accordance with Dong et al., 2015 (276). They showed, that IL-27 alleviated bleomycin-induced pulmonary fibrosis combined with IL-27-induced production of IFN-γ producing Th1 cells. Taken together, two studies indicated an anti-fibrotic role of IFN-γ. In a preclinical study a time point dependent effect of IFN-γ was observed. Only patients with early-stage pulomonary fibrosis were responsible for IFN-γ treatment (299). This can explain the contrary results in the literature. Jiang et al., 2004 (298) and Dong et al., 2015 (276) injected IFN-γ or IL-27 in the beginning of the experiment. Chen and colleagues, 2000 (175), used IFN-γ$^{-/-}$ mice over the whole time of the study.

In addition, Tregs ($CD4^+Foxp3^+$) were significantly reduced in the BALF of IL-$27RA^{-/-}$ mice in comparison to wild type mice (Fig. 12.3). Because of the missing IL-27 signaling more Th17 cells were seen (Fig. 12.3). Th17 cells have been reported to secrete IL-21 (300). The cytokine IL-21 suppresses Foxp3 in Tregs (300). In summary, IL-27 is able to suppress Th17 cells and can in turn influence the Treg population. A second possibility is the IL-21 mediated inhibition of IL-2 secretion (301) and IL-2 is essential for Treg function (302). On the other hand, IL-27 can directly inhibit Tregs (168). This is contrary to Fig. 12.3, where less Tregs were found in the IL-$27RA^{-/-}$ mice. One possibility for this discrepancy is the elevated level of Th17 cells in IL-$27RA^{-/-}$ mice. The Th17-mediated effects on Tregs (IL-21 and indirect IL-2 inhibition) could be stronger than the direct inhibition of IL-27 on Tregs.

4 Platelet-derived TGFβ1 as a regulator during bleomycin-induced pulmonary fibrosis

The novelty of the bleomycin-induced pulmonary fibrosis model with PF4Cre/$TGFβ1^{fl/fl}$ mice is the role of platelet-derived TGFβ1. So far, mainly alveolar macrophages were thought to be the major source of TGFβ1 during bleomycin-induced pulmonary fibrosis (303). When TGFβ1 produced by platelets was missing, the mRNA expression of *collagen I,V* in lung tissue and the collagen I,V amount in the lung was reduced (Fig. 13.6). These results are fitting to the literature, because TGFβ1 has been observed to be the central pro-fibrotic factor (304). The platelet-derived TGFβ1 had effects on the IL-27p28 production in bleomycin-induced pulmonary fibrosis as well. When TGFβ1 produced by platelets was missing, significantly more IL-27p28 in the BALF was detected (Fig. 13.7).

The supernatants of thrombin-activated murine washed platelets from TGFβ1-deficient platelets (PF4Cre/$TGFβ1^{fl/fl}$) failed to inhibit the LPS-mediated IL-27p28 release in C57BL/6J BMDMs (Fig. 13.2A). These data indicate that TGFβ1 is the major mediator of platelets which inhibits the IL-27p28 secretion in macrophages. As shown in Figure 13.1, platelets contain huge amounts of TGFβ1 and release it after activation by thrombin (305). Activation of washed platelets with histones leads to aggregation (306). This histone-mediated aggregation resulted in an increased TGFβ1 release (Fig. 13.1). *In vivo*, histones i.t. resulted in a TGFβ1 release in the BALF (Fig. 13.4). Mice of the strain PF4Cre/$TGFβ1^{fl/fl}$ had decreased TGFβ1 levels in

the BALF. This supports that extracellular histones, released after bleomycin administration, can activate platelets in the lung and that platelets are the major source of TGFβ1 in the lung. These findings are in accordance with the recent literature. It has been described that NETs can induce platelet activation, coagulation and thrombosis (86) (307) (306). There was nearly no TGFβ1 release detectable after thrombin activation by the PF4Cre/TGFβ1$^{fl/fl}$ platelets (Fig. 13.2A). In Fig. 13.3 is shown, that the aggregation of the washed platelets was not affected, if TGFβ1 is missing (PF4Cre/TGFβ1$^{fl/fl}$). This was first shown by Meyer et al., 2012 (308). *In vivo*, the amount of TGFβ1 in the plasma of bleomycin treated mice was dramatically decreased in the mouse strain with TGFβ1-deficient platelets (PF4Cre/TGFβ1$^{fl/fl}$) (Fig. 13.2B). Still, a small amount of TGFβ1 was detectable. This can be due to the fact that the cre recombinase mediated genetic deletion is not 100% efficient (253). Of course, the detected TGFβ1 in the plasma could also be secreted by other cell types. This has to be further analyzed.

5 Role of regulatory T cells in bleomycin-induced pulmonary fibrosis

If Tregs promote or protect from pulmonary fibrosis depends on the time point which is analyzed (309). In the early stage (depletion of Tregs three days before bleomycin application), Tregs have a pro-fibrotic role during bleomycin-induced pulmonary fibrosis. In the late stage (depletion of Tregs nine and 16 days after bleomycin administration), Tregs have an anti-fibrotic role during bleomycin-induced pulmonary fibrosis (309). In humans, less Treg numbers are correlating with more severe clinical parameters of pulmonary fibrosis (310) (311). This observation fits to the fact that Tregs are anti-fibrotic in the late stage because the sample collection in humans is made in an advanced stage of the disease.

The present data are in accordance with this time-dependent Treg effects. After blockade of histones, Tregs seem to be pro-fibrotic after two weeks of bleomycin-induced pulmonary fibrosis. After four weeks of bleomycin-induced pulmonary fibrosis, Tregs seem to be anti-fibrotic in IL-27RA$^{-/-}$ mice where the Treg numbers are reduced and the collagen amount is increased. Garibaldi et al., 2014 (312) described an anti-fibrotic role of Tregs after 14 days of bleomycin application (Treg depletion on day 7). This intermediate time point is closer to the late stage and supports the known literature. Contrary, Lo Re et al., 2011 (297) showed a pro-fibrotic effect of

Tregs by depletion on day 10 and 11 after experiment start. Here, the Tregs were analyzed in silica (SiO_2) induced pulmonary fibrosis model induced by pharyngeal instillation of bleomycin. Furthermore, Lo Re and colleagues used C57BL/6 mice for their study. In the present work C57BL/6J mice were used. The data of the present work and Lo Re et al., 2011 (297) are not directly comparable because of the different application methods, the different used chemicals and the different mouse substrains. Taken together, a clear statement to the role of Tregs during pulmonary fibrosis is not possible at the moment.

6 Inhibition of IL-27p28 by TGFβ1

TGFβ1 suppresses different immune responses such as the IL-12 induction of LPS-treated murine macrophages (313). IL-27p28 as a member of the IL-12 family was also clearly inhibited by TGFβ1 after LPS stimulation in murine macrophages on the protein level (Fig. 14.7). The mRNA expression profiles of the two subunits *p28* and *ebi3* showed different TGFβ1-mediated inhibitions during kinetic observations (Fig. 14.6). From the beginning, the subunit *ebi3* was stronger inhibited by TGFβ1 than the subunit *p28*. It is described that the p28 subunit is able to be expressed without EBI3 and has biological functions such as limiting the production of IL-17 and IL-10 (314). This can be a possibility that the mRNA expression of *p28* and *ebi3* were inhibited differently by TGFβ1. The suppression of IL-27p28 was not a cell type specific effect, because it was seen in different cell types such as BMDMs, RAW264.7, PECs, MH-S and primary alveolar macrophages (AMs) (Fig. 14.2). The strongest inhibition of IL-27p28 in AMs could be due to the fact that AMs were only seeded wit $2x10^5$ cells/sample/ml. The other cell types were seeded with $5x10^5$ cells/sample/ml. This resulted in a higher TGFβ1 amount per cell.

TGFβ1 is able to interfere with both signaling pathways: MyD88- and TRIF-dependent (Fig. 14.11). This is contrary to Naiki et al., 2005 (315), where TGFβ1 inhibited the MyD88-dependent TLR4 signaling after LPS stimulation, whereby the TRIF-dependent signaling was not inhibited. The data of Naiki and colleagues were generated with the help of human dermal microvessel endothelial cells (HMEC) whereas the present work was working with murine BMDMs. This can explain the contrary results. Furthermore, the inhibition power of TGFβ1 was dependent on the IL-27p28 inducing stimulus (Fig. 14.10). The TLR2 stimuli Zymosan and LTA were

nearly totally inhibited by TGFβ1. The triggered TLR2 only signals with the help of MyD88 (316). This explains the strong TGFβ1-mediated inhibition of the TLR2 agonists. LPS is a stimulus which is able to stimulate MyD88- and TRIF-dependent pathways (158) (159). In consequence, there was less TGFβ1-mediated inhibition of LPS-induced IL-27p28 in comparison to TLR2-induced IL-27p28 (Zymosan, LTA) (Fig. 14.10). The $TRIF^{-/-}$ BMDMs showed a comparable TGFβ1-mediated IL-27p28 inhibition after LPS such as the TGFβ1-mediated IL-27p28 inhibition of the TLR2 stimuli. In both conditions, the TRIF pathway was not activated or could not be activated.

Classically activated macrophages (M1) released significantly more IL-27p28 after LPS stimulation than alternatively activated macrophages (M2) (Fig. 14.9). Furthermore, IFNγ alone stimulates BMDMs for IL-27p28 production (Fig. 14.10). These results are also important during bleomycin-induced pulmonary fibrosis. M1 macrophages are polarized by IFNγ and IFNγ has been described as an anti-fibrotic cytokine with direct effects on fibroblasts (Chap. I-1.1). The results show that IFNγ also has anti-fibrotic effects by stimulating macrophages producing more IL-27p28. In contrast, IL-4 polarized M2 macrophages produce less IL-27p28. This indicates that macrophages are a central target of fibrosis-mediating cytokines (IFNγ, IL-4) to orchestrate the level of anti-fibrotic IL-27p28 (276).

7 Role of TGFβ receptors I and II during bleomycin-induced pulmonary fibrosis and TGFβ1-mediated inhibition of IL-27p28

For the TGFβ1-mediated inhibition of IL-27p28 the TGFβ-receptor II (TbRII) on macrophages was needed (Fig. 14.12). In the present work, a direct correlation between the TbRII on macrophages, the IL-27p28 amount and the severity of pulmonary fibrosis was shown. Mice with a mainly macrophage-targeted TbRII (LysMCre/$TbRII^{fl/fl}$) knock out had significantly less collagen I,V amount in the lung as compared to the control mice ($TbRII^{fl/fl}$) (Fig. 15.2A). Because of the lost TGFβ1 signaling more IL-27p28 was found in the BALF (Fig. 15.2B). In the end, a mainly macrophage-targeted TbRII knock out attenuated the severity of bleomycin-induced pulmonary fibrosis indirectly by an increased production of IL-27p28. Macrophages were the source of IL-27p28 *in vivo* (Fig. 14.1) and *in vitro* studies figured out an

abolished TGFβ1-mediated inhibition of IL-27p28 in TbRII knock out macrophages (Fig. 14.12B). The elevated IL-27p28 level after LPS stimulation in TbRII knock out macrophages in comparison to LPS stimulated littermate control macrophages was due to the fact, that macrophages are able to produce TGFβ1 (Fig. 14.5) (317). This self-inhibitory effect was not possible, if the TbRII was knocked out. On the other hand, the TGFβ1-mediated inhibition of IL-27p28 was not totally abolished in the TbRII knock out macrophages. This is due to the fact that the cre recombinase is of incomplete efficacy (253). When the TGFβ Receptor I (TbRI) was inhibited with the specific inhibitor SB431542, the inhibition of LPS-mediated IL-27p28 production in macrophages was alleviated as well (Fig. 14.12A). This is in accordance with Inman et al., 2002 (318), where SB431542 was described as a potent and specific inhibitor of “Transforming Growth Factor-β Superfamily Type I Activin Receptor-Like Kinase (ALK) Receptors”. Taken together, the data indicate that both receptors are critically needed for the TGFβ1-mediated inhibition of IL-27p28 in LPS-stimulated macrophages.

8 Confirmation of Smad3 knock down

So far, all *in vitro* and *in vivo* experiments were done with mice on a C57BL/6J background. The Smad3 knock down was performed with RAW264.7 macrophages. This cell line is on a BALB/c background (ATCC® TIB-71™). Nevertheless, the TGFβ1-mediated inhibition of IL-27p28 in RAW264.7 macrophages was comparable to the inhibition in other macrophage types on a C57BL/6J background (Fig. 14.2).

The RAW264.7 macrophages were successfully transduced by the lentiviruses. This was confirmed by the resistance to puromycin (Fig. 16.1) because the lentiviral plasmid carries a puromycin resistance gene (Fig. 6). In addition, the knock down of the s*mad3* gene by the different clones was shown at the mRNA level (Fig. 16.2A) and at the protein level in $CD11b^{+}F4/80^{+}Smad3^{+}$ macrophages (Fig. 16.2B). Initially, five clones were used for the Smad3 knock down. The different clones show different knock down efficiencies. This is in accordance with Zhang et al., 2014 (319). Here, the efficiency of a shRNA mediated knock down in RAW264.7 cells also depends on the single clone.

9 Inhibition by TGFβ1 is Smad3 dependent

In the present work, the TGFβ1-mediated inhibition of IL-27p28 after LPS treatment in dependence of Smad3 in macrophages was studied. In previous studies it was shown that TGFβ1 inhibits the macrophage activation marker inducible nitric-oxide synthase (iNOS) (320) (321). But TGFβ1 failed to inhibit iNOS, if Smad3 was mutated (322). In the present work, Smad3 was knocked down and similar results were observed: Smad3 was needed for the TGFβ1-mediated inhibition of IL-27p28 secretion in RAW264.7 macrophages after LPS stimulation (Fig. 16.4A). The TGFβ1-mediated inhibition of the mRNA expression of *il-27p28* and *ebi3* was also Smad3-dependent (Fig. 16.4 and Fig. 16.4C). This indicates a direct transcriptional regulation by Smad3. Indeed, the activated pSmad3 directly bound to the *il-27p28* promoter and to the *ebi3* promoter (Fig. 16.5). For both promotors, the untreated samples observed higher pSmad3 binding as compared to the LPS treated sample. This can be explained by TGFβ1 release of BMDMs under untreated conditions (Fig. 14.5) which induced higher pSmad3 levels. Both promoters contain the Smad binding element (SBE) CAGA (Fig. 16.6 and Fig. 16.7). The direct binding of pSmad3 to the promoters could result in the inhibitory effect of Smad3 on the LPS-mediated IL-27p28 production in macrophages. Another possibility of higher IL-27p28 levels in Smad3 knock down RAW264.7 macrophages is a higher NF-κB activation. It has been demonstrated that TGFβ1$^{-/-}$ and Smad3$^{-/-}$ mice show higher pro-inflammatory cytokine levels and higher NF-κB activation (323).

In turn, LPS directly influences the Smad3 activity (324). Smad3 is phosphorylated at the positions Thr179 and Ser208 in the Smad3 linker region between the MH1 and MH2 domains by a TLR4–IRAK1–ERK1/2 pathway (324). The linker region between has been described to interact with nuclear coactivators (324). It is possible, that the LPS-mediated phosphorylation of Thr179 and Ser208 in the Smad3 linker region affects the binding of Smad3 to the *il-27p28* and *ebi3* promoters. Furthermore, the TLR4–IRAK1–ERK1/2 pathway activates c-Jun which functions as a co-repressor of Smad3 (325). Together, this can be reasons of decreased Smad3 binding to the *il-27p28* and *ebi3* promoters after LPS stimulation.

10 The p38 MAP Kinase and IL-10 as regulators of TGFβ1-mediated inhibition of IL-27p28

In the present work, the p38 MAPK was highly phosphorylated after TGFβ1 treatment in macrophages. An intermediate phosphorylation level was seen after LPS stimulation (Fig. 17.1). The p38 MAPK, as an important mediator of TGFβ1 signaling, was confirmed by different publications in different cell types (326) (327) (328). The p38 MAPK is also phosphorylated by LPS (329). Inhibition of the p38 MAPK signaling pathway by different inhibitors (SB203580, PH-797804 and BIRB796) abolished the TGFβ1-mediated inhibition of IL-27p28 secretion after LPS stimulation in macrophages (Fig. 17.2). The inhibitor SB203580 is also known to suppress the activation of Smad3 (330). This could be the reason for the strongest recovery of the TGFβ1-mediated inhibition of IL-27p28 by using SB203580. The other inhibitors (PH-797804 and BIRB796) show a partly recovery of the TGFβ1-mediated inhibition of IL-27p28. This is supported by Blink et al., 2001 (331) where the inhibition of p38 MAPK resulted in an increased cytokine release by macrophages. As a negative feedback loop the p38 MAPK signaling pathway inhibits the production of IL-27 in human monocytes (332).

IL-10 was part of the TGFβ1-mediated inhibition of IL-27p28 in LPS treated macrophages. This was shown by IL-10 receptor blocking experiments (Fig. 18.2A) and IL-10 KO experiments (Fig. 18.2B). In addition, IL-10 expression was Smad3-dependent (Fig. 18.3). This confirmed the results of Kitani et al., 2003 (275) where a SBE in the murine *il-10* promoter was identified at position -901. In Fig. 18.1, the release of IL-10 after LPS in comparison to LPS + TGFβ1 treatment of C57BL/6J BMDMs is shown. Ma et al., 2001 (226) showed in human macrophages, that the p38 MAPK also increased the IL-10 production in an additional negative feedback loop resulting in quiescence of immune responses. Because of the 2.5 times higher p38 MAPK phosphorylation in LPS + TGFβ1 treated BMDMs in comparison to LPS treated BMDMs (Fig. 17.1), the IL-10 release is stronger after TGFβ1 treatment. The inhibitory mechanism of IL-27p28 by IL-10 was recently discovered. Bosmann and colleagues, 2014 (229) showed that IL-10 requires STAT3 but not SOCS3 for suppression of IL-27p28.

11 The mechanism of Tristetraprolin-mediated inhibition of IL-27p28

To study the role of myeloid Tristetraprolin (TTP), wild type C57BL/6J mice were transplanted with bone marrow of $TTP^{-/-}$ mice. *In vivo*, the cytokine IL-27p28 was significantly more secreted in $TTP^{-/-}$ bone marrow chimeric mice after bleomycin application. During the natural course of fibrosis this resulted in a reduced amount of lung collagen I,V in such lungs because IL-27 was identified as an anti-fibrotic cytokines in the present work.

In preliminary *in vitro* studies, the effect of TTP in TGFβ1-mediated inhibition of IL-27p28 in LPS activated BMDMs was shown (Fig. 19.1). This confirmed the results of Gu et al., 2013 (333) where the *il-27p28* mRNA expression was increased in $TTP^{-/-}$ macrophages in comparison to wild type macrophages, stimulated by LPS or IFNγ. In Fig. 20, the 3' untranslated region (3'UTR) of the *il-27p28* gene is shown. Five putative TTP binding sites (AU-rich elements) are indicated. Du and Sriram (1998) (313) showed that IL-12p40 such as IL-27p28 a member of the IL-12 family, was influenced by TGFβ1 via transcriptional inhibition and via reduction of the mRNA stability. On the other hand, Gu et al., 2013 (333) observed no differences in *p35* and *p40* mRNA stability in macrophages when wild type and $TTP^{-/-}$ cells were compared. Nonetheless, this study has also shown an increased IL-12p40 release after LPS stimulation in $TTP^{-/-}$ macrophages. This leads to the conclusion that IL-12 (333) and IL-27p28 could be regulated by TTP at the transcriptional level. It has been observed that TTP can shuttle between the cytoplasm and the nucleus (334). A possible mechanism how TTP suppresses the production of IL-12 is by blocking NF-κB nuclear translocation (333). This should also be tested for IL-27p28 because the cytokines IL-12 and IL-27 are both NF-κB-dependent (335) and both are target genes of TTP. Schichl et al., 2009 (336) have already postulated an inhibitory effect of TTP on NF-κB activity. In addition, other groups have reported that TTP suppressed NF-κB signaling at the transcriptional corepressor level by recruiting histone deacetylases (HDACs) to the NF-κB targeted promoters (334).

The expression of TTP is increased after TGFβ1 treatment in the human T cell line HuT78 and Smad binding elements (SBE) are found in the human *ttp* promoter (337). In the present work, TGFβ1 inhibited the *ttp* mRNA expression in C57BL/6J BMDMs (Fig. 19.3). The murine *ttp* promoter does not contain Smad binding elements (338) in distinction from the human *ttp* promoter (337). The species differences and the cell

type differences may provide an explanation for the contrary results (as described above).

5‘ - **GACCTGCTGCTGCTGTCCCTGCCCAGGCGCCCAGGCTCAGCCTGGGATTCCTAA**

CACCTAGCTTCAAGCCCTATGGAGTGACCTTCCAGCTCCCTCCCTCGCCCGTTAAGACT

CTAAGGCTGGAGTCTGGCCAATCACAGGACAGGCTCTAGCTCGTTTGCCTTAGACCAG

GCAGGGCTTCACTAGCTCCCAGCCCTGACCCAATAATTTAAAAGCCCTCCAGTCCTTAC

CAGATATTTATTTCTTGGATATTTATTTATTTTTAAGAAATGGTTTATTTATTGTTTCACTCT

TGAGTTAGGCCACCATGCTGGGTGCCTAATAAAGCCATCCAGCCCGG - 3‘

#1 #2 #3 #4 #5

Fig. 20: 3‘ UTR of the murine *il-27p28* gene.

The *il-27p28* mRNA sequence is shown in bolt. Five possible AU rich elements (AREs) are underlined.

In summary, TTP affects mRNA stability while without a requirement for de novo protein synthesis (339). TGFβ1 activates the p38 MAPK signaling pathway (Fig. 17.1) (327). In turn, p38 MAPK regulates mRNA stability (340) by stabilizing via AREs (341). In addition, mitogens such as p38 MAPK mediate direct phosphorylation of TTP and can influence the subcellular localization of TTP (342). This supports that TTP has an inhibitory effect on the NF-κB activity (336) (333) besides the direct mRNA degradation.

12 Conclusions

The results of the present work identify extracellular histones derived by NETs and non-hematopoietic cells as key effector elements during bleomycin-induced pulmonary fibrosis. This is mediated by a multiple cellular interaction of neutrophils, platelets and macrophages. Extracellular histones modulate molecular cytokine networks by triggering the release of TGFβ1 from platelets. The release of TGFβ1 may supports a pro-fibrotic Th17 cell population and inhibit the macrophage-derived, anti-fibrotic IL-27 (Fig. 21). Furthermore, several mechanisms including signaling pathways of TGFβ1-mediated inhibition of IL-27p28 in macrophages were identified (Fig. 22). Taken together, platelets appear to modulate the adaptive immune system in an indirect fashion by influencing the production of IL-27 in macrophages. In future, extracellular histones as central key effector elements are a promising novel treatment option for pulmonary fibrosis. This may expand current treatments with approved drugs such as nintedanib and pirfenidone.

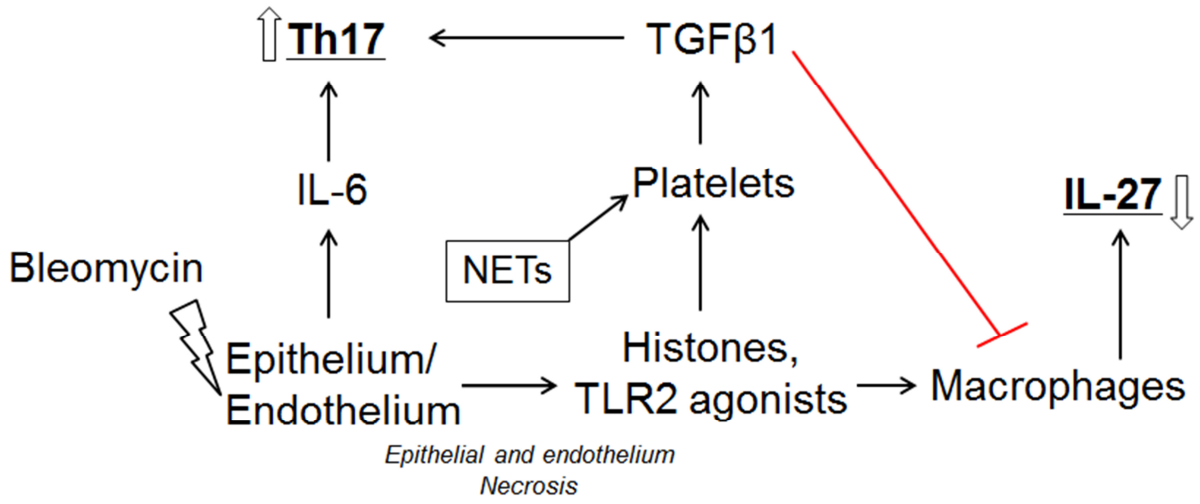

Fig. 21: A model of the cellular processes during bleomycin-induced pulmonary fibrosis.
Bleomycin injures the epithelium/endothelium in the lungs. Extracellular histones released by necrosis or derived from Neutrophil extracellular traps (NETs) can trigger platelets to secrete TGFβ1. The released TGFβ1, together with IL-6 increases the numbers of pro-fibrotic Th17 cells. Endogenous TLR2 agonists released by the necrotic epithelium/endothelium would trigger the release of anti-fibrotic IL-27 by macrophages. This is inhibited by elevated TGFβ1 levels because of histones-mediated platelet activation. Black arrows: triggers/induces; red line: inhibits.

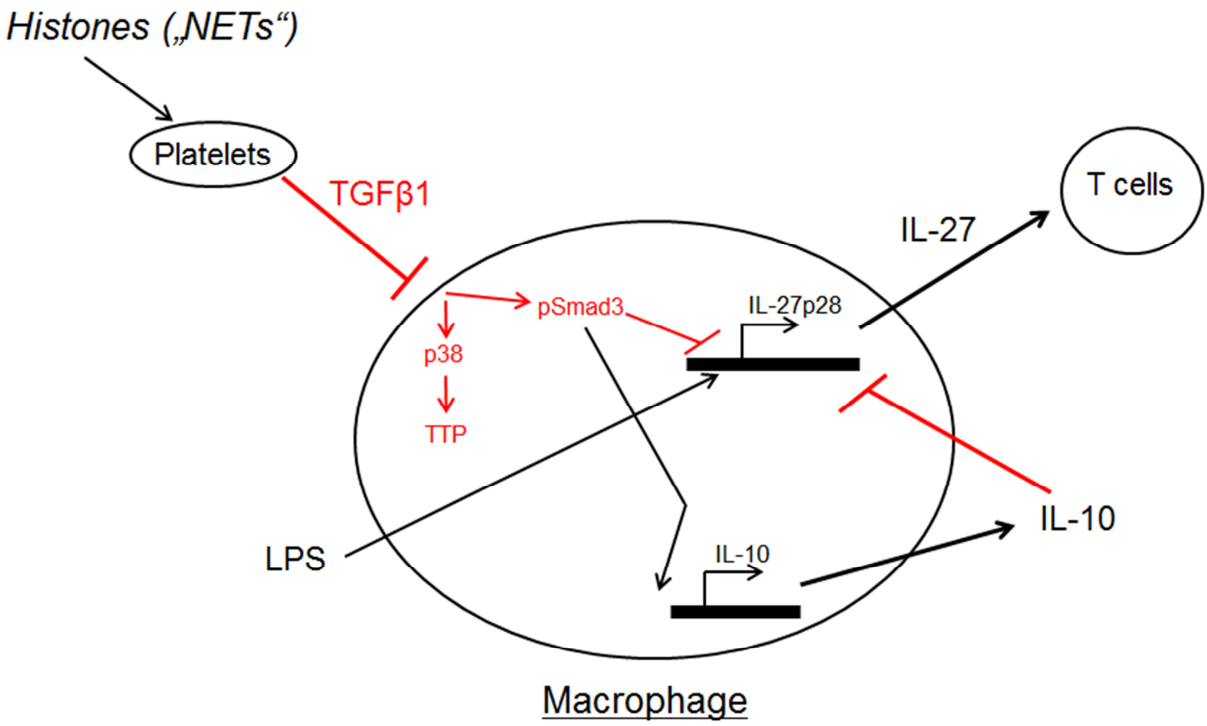

Fig. 22: Interaction model of several mediators of TGFβ1-induced inhibition of IL-27p28 in macrophages.
LPS stimulates the production of IL-27 in macrophages. This is inhibited by TGFβ1. The binding of TGFβ1 to the TGFbRI and TGFbRII receptors results in phosphorylated Smad3 (pSmad3). This appears to directly inhibit the transcription of the subunits *il-27p28* and *ebi3*. The TGFβ1-dependent inhibition is also mediated by p38 phosphorylation and Tristetraprolin (TTP) activation. On the other hand, pSmad3 induces the production of IL-10. Once secreted, IL-10 inhibits the IL-27 production in an autocrine or paracrine manner. Black: triggers/induces; red: inhibits.

V Outlook

The future work will be dedicated to accumulate further information about the role of extracellular histones during the chronic phase of bleomycin-induced pulmonary fibrosis. In the present work, mice with (tissue specific) genetic deficiency of PAD4 were not yet studied in the model of bleomycin-induced pulmonary fibrosis. Furthermore, it would be interesting to characterize if the degradation of H3-Cit is altered in comparison to uncitrullinated histones in BALF. A role of Tregs was studied by adoptive T cell transfer experiments. More studies are needed to investigate the specific roles of Tregs during pulmonary fibrosis. This may be achieved by using Treg-depleted mice in the model of bleomycin-induced pulmonary fibrosis. Treg suppression assays could be helpful to investigate the influence of purified Tregs on conventional T cells. The extracellular histones increased the expression of stress-induced proteins such as heat shock proteins in Tregs. Heat shock proteins are thought to stabilize the Treg specific transcription factor, Foxp3. Whether a direct stabilization of Foxp3 occurs in response to extracellular histones and how this is related to heat shock proteins in Tregs remains to be analysed. In a next step, the signaling mechanisms initiated by the extracellular histones have to be identified. Platelet-derived TGFβ1 driving bleomycin-induced pulmonary fibrosis was studied using a cre/lox mouse strain. Another part of the future work may focus on further details studies on TGFβ1 inhibitory mechanisms. In the present work, lentiviral knock down cell lines were used to identity Smad3 as a mediator of TGFβ1. Promoter binding studies were used to prove Smad3 binding at the promoters of *il-27p28* and *ebi3*. However, this provided no information about the locations of the Smad binding elements (SBEs). Promoter studies have to be done to identify the specific SBEs required for the inhibition of IL-27 by TGFβ1. Furthermore, it could be analysed how the phosphorylation of the Smad3 linker modulate the Smad3 translocation between the cytoplasm and the nucleus. Tristetraprolin is involved in the TGFβ1-mediated inhibition of IL-27p28 in macrophages. The present work did not analyse the mRNA stability of il-27p28 in dependence of TTP. In the future, efforts in this direction could provide more information about the molecular mechanism of TTP effects.

To translate the research findings to clinical relevancies it would be very interesting to study the H3-Cit amount in samples of patients with pulmonary fibrosis. In future, the anti-H4 therapy could be studied with the help of a clinical trial.

VI Abbreviations

Tab. 24: Abbreviations used in the present work.

Abbreviation	Description
%	Percent
°C	Degree Celsius
µg	microgram
µl	microliter
µM	micromolar
µm²	Square micrometer
5'ppp-dsRNA	5' triphosphate double stranded RNA
A	Adenine
A. Ham.	American Hamster
ADP	Adenosine diphosphate
AKI	Acute kidney injury
ALK	Activin receptor-like kinase
AM	Alveolar macrophages
AP-1	Activator protein-1
APC	Allophycocyanin
Approx.	Approximately
AREs	AU-rich elements
Arg	Arginine
Asp	Aspartic acid
ATP	Adenosine triphosphate
BALF	Broncho alveolar lung fluid
BD	Becton Dickinson
BMDMs	Bone marrow derived macrophages
BMP	Bone morphogenic protein
bp	basepair(s)
BPI	Bactericidal/permeability-increasing protein
BW	Bodyweight
C	Cytosin
C. albicans	*Candida albicans*
cAMP	cyclic adenosinemonophosphate
CD	Cluster of differentiation
cDNA	complementary desoxyribonucleic acid
Chap.	Chapter
Chip	Chromatin immuno precipitation
cm	centimeter
CO_2	Carbon dioxide
co-Smad	common mediator Smad
Cre	Cre recombinase (derived from the P1 Bacteriophage)
Ctrl.	Control
Cys	Cysteine
DAMP	damage-associated molecular pattern

DAPI	4',6-diamidino-2-phenylindole
DC	Dendritic cell
ddATP	Dideoxyadenosine triphosphate
ddCTP	Dideoxycytidine triphosphate
ddGTP	Dideoxyguanosine triphosphate
ddTTP	Dideoxythymidine triphosphate
DKO	double knock out
DMSO	dimethyl sulfoxide
ds	double-stranded
DTX	Diphtheria toxin
E. coli	*Escherichia coli*
EBI3/ ebi3	Epstein-Barr virus induced gene 3
ECM	Extracellular matrix
eGFP	enhanced green fluorescent protein
ELISA	Enzyme linked immunosorbent assay
EMT	Epithelial to mesenchymal transition
EndMT	Endothelial to mesenchymal transition
EPCR/ *epcr*	Endothelial protein C receptor
ERK	extracellular-signal-regulated kinases
FACS	Fluorescence activated cell sorting
Fe	Ferrum
FI	Fluorescenceintensity
Fig.	Figure
FITC	Fluorescein isothiocyanate
fl/fl	flox/flox
Foxp3	Forkhead box p3
FSP-1/ *fsp-1*	Fibroblast-specific protein 1
FX/ *fx*	Factor 10
g	gram
G	Guanine
GAPDH/ *gapdh*	Glyceraldehyde 3-phosphate dehydrogenase
GDF	Growth/differentiation factor
GFP	Green fluorescent protein
Glu	Glutamic acid
Gly	Glycine
GM-CSF	Granulocyte-macrophage colony-stimulating factor
gp130	glycoprotein 130
h	hour(s)/human
H1	Histone 1
H2A	Histone 2A
H2B	Histone 2B
H3(-Cit)	(citrullinated) Histone 3
H4	Histone 4
HDAC	Histone deacetylase
His	Histidine
HIV-1	Human immunodeficiency virus 1
Hsp	Heat shock protein

i.p.	intraperitoneal
i.t.	intratracheal
i.v.	intravenous
iDTR	inducible Diphtheria toxin receptor
IFN-γ	Interferon-γ
IL-	Interleukin-
IL-27RA	IL-27 receptor alpha
iNOS	inducible nitric oxide synthase
IRAK	Interleukin-1 receptor-associated kinase
IRF	Interferon regulatory transcription factor
IRF-E	interferon regulatory factor binding element
I-Smad	inhibitory Smad
Jak	Januskinase
kDa	kilo Dalton
kg	kilogram
KO	knock out
LAM	Lipoarabinomannan
LAP	Latency Associated Peptide
LLC	Large Latent Complex
LN	Lymph node
LPS	Lipopolysaccharide
LTA	Lipoteichoic acid
LTBP	latent *TGF beta* binding protein
Ly6G	Lymphocyte antigen 6G
LysM	Lysozyme M
m	murine
M1	Classically activated macrophages
M2	Alternatively activated macrophages
MACS	Magnetic activated cell sorting
MAD	Mothers against decapentaplegic
MAP(K)	Mitogen-activated protein (kinases)
mg	milligram
MH	MAD homology domains
MHC	Major histocompatibility complex
mIgG	murine immunglobuline
min	Minute(s)
minus/minus	Homozygous, knock out
ml	milliliter
MPO	Myeloperoxidase
mRNA	messenger ribonucleic acid
mU	milli units
MyD88	Myeloid Differentiation Primary Response 88
Mφ	Macrophage
N/D	not detectable
NaCl	Sodium chloride
NETs	Neutrophil extracellular traps

NFκB	nuclear factor k-light-chain-enhancer of activated B cells
ng	nanogram
NGS	Next Generation Sequencing
NLR	NOD-like receptors
nM	nanomolar
nm	nanometer
NOD	Nucleotide binding oligomerization domain
OD	optical density
p	phospho/ protein
PAD (4)	Protein Arginine Deiminase (4)
PAMPs	Pathogen-associated molecular patterns
PBS	Phosphate buffered saline
PDGF	Platelet derived growth factor
PE	Phycoerythrin
PECAM-1	Platelet endothelial cell adhesion molecule 1
PEMs	Peritoneal elicited macrophages
PENs	Peritoneal elicited neutrophils
PF4	Platelet factor 4
pg	picogram
PGN	Peptidoglycan
plus/minus	Heterozygous
plus/plus	Homozygous, wild type
PMN	Polymorphonuclear leukocytes
Poly(I:C)	Polyinosinic-polycytidylic acid
Pro	Proline
PRR	Pattern recognition receptor
R	receptor
RGD	Protein motif of Arg-Gly-Asp
RGE	mutated protein motif of Arg-Gly-Glu
Rig-I	Retinoic acid inducible gene I
rmIL-27	recombinant murine IL-27
RNA	Ribonucleic acid
RORγt	RAR-related orphan receptor *gamma t*
ROS	Reactive oxygen species
R-Smad	Receptor-regulated Smad
RT qPCR	Real time quantitative polymerase chain reaction
S. aureus	*Staphylococcus aureus*
S. Ham.	Syrian Hamster
SAPK	stress-activated protein kinase
SARA	Smad anchor for receptor activation
SBE	Smad binding element
SEM	Standard error of the mean
Ser	Serine
shRNA	short hairpin RNA
SiO_2	Silica
SLC	small latent *TGF beta* complex

SMA	Smooth muscle actin
Smad	Small mothers against decapentaplegic
ss	single-stranded
SS	Disulfide bond
SS-X-S	Protein motif of Ser-Ser-X-Ser
STAT	Signal Transducer And Activator Of Transcription
T	Thymin
Tab.	Table
TARC	Translational Animal Research Center
TbR	Transforming growth factor β receptor
TCCR	T cell cytokine receptor
td Tomato	tandem dimer Tomato
TGFb1	Transforming growth factor β1
TGFβ(1)	Transforming growth factor β(1)
Th	T helper
Thermo Sc.	Thermo Scientific
Thr	Threonine
TIR	Toll/IL-1R domain
TIRAP	Toll−interleukin 1 receptor (TIR) domain−containing adapter protein
TLR	Toll-like receptor
TRAF6	TNF Receptor-Associated Factor 6
TRAM	TRIF-related adaptor molecule
Treg	regulatory T cell
TRIF	TIR-domain-containing adapter-inducing interferon-β
TTP	Tristetraprolin
Tyk2	Tyrosine kinase 2
U	Uracil
UTR	Untranslated region
UV	ultraviolett light
wk	week(s)
WT	Wild type (C57BL/6J)
Wt	Littermate control
x	times
α	alpha; anti
γ	gamma
δ	Delta
κ	kappa

VII Figures

VIII Tables

IX Literature

1. *Interstitial lung disease: Is interstitial lung disease the same as scleroderma lung disease?* **Murray, Lynne A., Rubinowitz, Ami and Herzog, Erica L.** 2012, Current opinion in rheumatology, Vol. 24, pp. 656-662.

2. *Accelerated Variant of Idiopathic Pulmonary Fibrosis: Clinical Behavior and Gene Expression Pattern.* **Carrillo, Guillermo, et al., et al.** 2007, PLoS ONE.

3. *Bleomycin-induced pulmonary fibrosis in fibrinogen-null mice.* **Hattori, Noboru, et al., et al.** 2000, The Journal of Clinical Investigation, Vol. 106, pp. 1341-1350.

4. *An official ATS/ERS/JRS/ALAT statement: idiopathic pulmonary fibrosis: evidence-based guidelines for diagnosis and management.* **Raghu, Ganesh, et al., et al.** Mar 2011, Am J Respir Crit Care Med, Vol. 183, pp. 788-824.

5. *Pharmacological treatment of idiopathic pulmonary fibrosis : from the past to the future.* **Antoniou, Katerina M., Margaritopoulos, George A. and Siafakas, Nikos M.** 2013, European Respiratory Review issue, Vol. 129, pp. 281-291.

6. *Idiopathic pulmonary fibrosis.* **King, Jr, Talmadge E., Pardo, Annie and Selman, Moisés.** Dec 2011, Lancet, Vol. 378, pp. 1949-1961.

7. *American Thoracic Society/European Respiratory Society International Multidisciplinary Consensus Classification of the Idiopathic Interstitial Pneumonias.* **Society, American Thoracic and Society, European Respiratory.** 2002, Am J Respir Crit Care Med, Vol. 165, pp. 277-304.

8. *Detection of Herpes Simplex Virus Type-1 in Patients with Fibrotic Lung Diseases.* **Lasithiotaki, Ismini, et al., et al.** 2011, PLos ONE, Vol. 6.

9. *Abnormal lung aging in chronic obstructive pulmonary disease and idiopathic pulmonary fibrosis.* **Faner, Rosa, et al., et al.** Aug 2012, Am J Respir Crit Care Med, Vol. 186, pp. 306-313.

10. *Molecular and cellular mechanisms of pulmonary fibrosis.* **Todd, Nevins W., Luzina, Irina G. and Atamas, Sergei P.** s.l. : Fibrogenesis & Tissue Repair, 2012, Fibrogenesis & Tissue Repair, Vol. 5. ISSN: Fibrogenesis & Tissue Repair.

11. *Type 1/Type 2 Cytokine Paradigm and the Progression of Pulmonary Fibrosis.* **Lukacs, Nicholas W., et al., et al.** 2001, Chest, pp. 5-8.

12. *Mechanisms of Neutrophil Accumulation in the Lungs of Patients with Idiopathic Pulmonary Fibrosis.* **Hunninghake, Gary W., et al., et al.** 1981, The Journal of Clinical Investigation, Vol. 68, pp. 259-269.

13. *Baseline BAL Neutrophilia Predicts Early Mortality in Idiopathic Pulmonary Fibrosis.* **Kinder, Brent W., et al., et al.** 2008, Chest, Vol. 133, pp. 226-232.

14. *Role of interferon-gamma in the evolution of murine bleomycin lung fibrosis.* **Segel, Michael J., et al., et al.** Dec 2003, Am J Physiol Lung Cell Mol Physiol, Vol. 285, pp. L1255--L1262.

15. *Unique functions of the type II interleukin 4 receptor identified in mice lacking the interleukin 13 receptor alpha1 chain.* **Ramalingam, Thirumalai R., et al., et al.** Jan 2008, Nat Immunol, Vol. 9, pp. 25-33.

16. *Lung interleukin-4 gene expression in a murine model of bleomycin-induced pulmonary fibrosis.* **Gharaee-Kermani, M., et al., et al.** Aug 2001, Cytokine, Vol. 15, pp. 138-147.

17. *IL-4 and IL-13 specifically increase adhesion molecule and inflammatory cytokine expression in human lung fibroblasts.* **Doucet, Christelle, et al., et al.** 1998, International Immunology, Vol. 10, pp. 1421-1433.

18. *The interactions between inflammation and coagulation.* **Esmon, Charles T.** 2005, British Journal of Haematology, Vol. 131, pp. 417-430.

19. *Platelet-derived Growth Factor Is Chemotactic for Fibroblasts.* **Seppa, Heikki, et al., et al.** 1982, The Journal of Cell Biology, Vol. 92, pp. 584-588.

20. *Extracellular matrix deposition by primary human lung fibroblasts in response to TGF-beta1 and TGF-beta3.* **Eickelberg, O., et al., et al.** May 1999, Am J Physiol, Vol. 276, pp. L814--L824.

21. *Induction of epithelial-mesenchymal transition in alveolar epithelial cells by transforming growth factor-beta1: potential role in idiopathic pulmonary fibrosis.* **Willis, Brigham C., et al., et al.** May 2005, Am J Pathol, Vol. 166, pp. 1321-1332.

22. *Global analysis of gene expression in pulmonary fibrosis reveals distinct programs regulating lung inflammation and fibrosis.* **Kaminski, Naftali, et al., et al.** 2000, PNAS, Vol. 97, pp. 1778-1783.

23. *Reactive nitrogen species inhibit alveolar epithelial fluid transport after hemorrhagic shock in rats.* **Pittet, J. F., et al., et al.** 10, May 2001, Journal of immunology (Baltimore, Md. : 1950), Vol. 166, pp. 6301-6310. ISSN: 0022-1767.

24. *Rearrangement of adherens junctions by transforming growth factor-beta1: role of contraction.* **Hurst, V. and I., V., et al., et al.** Apr 1999, Am J Physiol, Vol. 276, pp. L582--L595.

25. *The integrin alpha v beta 6 binds and activates latent TGF beta 1: a mechanism for regulating pulmonary inflammation and fibrosis.* **Munger, J. S., et al., et al.** Feb 1999, Cell, Vol. 96, pp. 319-328.

26. *Epithelial-mesenchymal transitions in development and disease.* **Thiery, Jean Paul, et al., et al.** Nov 2009, Cell, Vol. 139, pp. 871-890.

27. *Epithelial-mesenchymal plasticity in carcinoma metastasis.* **Tsai, Jeff H. and Yang, Jing.** Oct 2013, Genes Dev, Vol. 27, pp. 2192-2206.

28. *A causal role for E-cadherin in the transition from adenoma to carcinoma.* **Perl, Anne-Karina, et al., et al.** 1998, Nature, Vol. 392, pp. 190-193.

29. *The epithelial-mesenchymal transition generates cells with properties of stem cells.* **Mani, Sendurai A., et al., et al.** 2008, Cell, Vol. 133, pp. 704-715.

30. *Epithelial-to-mesenchymal transition of peritoneal mesothelial cells is regulated by an ERK/NF-kappaB/Snail1 pathway.* **Strippoli, Raffaele, et al., et al.** 2008, Dis Model Mech, Vol. 1, pp. 264-274.

31. *The transcription factor snail controls epithelial-mesenchymal transitions by repressing E-cadherin expression.* **Cano, A., et al., et al.** Feb 2000, Nat Cell Biol, Vol. 2, pp. 76-83.

32. *The zinc-finger protein slug causes desmosome dissociation, an initial and necessary step for growth factor-induced epithelial-mesenchymal transition.* **Savagner, P., Yamada, K. M. and Thiery, J. P.** Jun 1997, J Cell Biol, Vol. 137, pp. 1403-1419.

33. *Bmi1 is essential in Twist1-induced epithelial-mesenchymal transition.* **Yang, Muh-Hwa, et al., et al.** Oct 2010, Nat Cell Biol, Vol. 12, pp. 982-992.

34. *The transcription factor Slug represses E-cadherin expression and induces epithelial to mesenchymal transitions: a comparison with Snail and E47 repressors.* **Bolós, Victoria, et al., et al.** Feb 2003, J Cell Sci, Vol. 116, pp. 499-511.

35. *Twist is a transcriptional repressor of E-cadherin gene expression in breast cancer.* **Vesuna, Farhad, et al., et al.** Mar 2008, Biochem Biophys Res Commun, Vol. 367, pp. 235-241.

36. *The basics of epithelial-mesenchymal transition.* **Kalluri, Raghu and Weinberg, Robert A.** 2009, The Journal of Clinical Investigation, Vol. 119, pp. 1420-1428.

37. *Idiopathic pulmonary fibrosis: an altered fibroblast proliferation linked to cancer biology.* **Vancheri, Carlo.** Jul 2012, Proc Am Thorac Soc, Vol. 9, pp. 153-157.

38. *Epithelial origin of myofibroblasts during fibrosis in the lung.* **Willis, Brigham C., duBois, Roland M. and Borok, Zea.** Jun 2006, Proc Am Thorac Soc, Vol. 3, pp. 377-382.

39. *Notch induces myofibroblast differentiation of alveolar epithelial cells via transforming growth factor-beta-Smad3 pathway.* **Aoyagi-Ikeda, Kana, et al., et al.** Jul 2011, Am J Respir Cell Mol Biol, Vol. 45, pp. 136-144.

40. *Evidence that fibroblasts derive from epithelium during tissue fibrosis.* **Iwano, Masayuki, et al., et al.** 2002, The Journal of Clinical Investigation, Vol. 110, pp. 341-350.

41. *Alveolar epithelial cell mesenchymal transition develops in vivo during pulmonary fibrosis and is regulated by the extracellular matrix.* **Kim, Kevin K., et al., et al.** 2006, PNAS, Vol. 103, pp. 13180-13185.

42. *Targeted disruption of TGF-beta1/Smad3 signaling protects against renal tubulointerstitial fibrosis induced by unilateral ureteral obstruction.* **Sato, Misako, et al., et al.** 10, Nov 2003, The Journal of clinical investigation, Vol. 112, pp. 1486-1494. ISSN: 0021-9738.

43. *The role of endothelial-to-mesenchymal transition in cancer progression.* **Potenta, S., Zeisberg, E. and Kalluri, R.** 2008, British Journal of Cancer, Vol. 99, pp. 1375-1379.

44. *Endothelial-to-mesenchymal transition contributes to cardiac fibrosis.* **Zeisberg, Elisabeth M., et al., et al.** 2007, Nature Medicine, Vol. 13, pp. 952-961.

45. *Epithelial-mesenchymal transition and its implications for fibrosis.* **Kalluri, Raghu and Neilson, Eric G.** 2003, The Journal of Clinical Investigation, Vol. 112, pp. 1776-1784.

46. *An essential role for resident fibroblasts in experimental lung fibrosis is defined by lineage-specific deletion of high-affinity type II transforming growth factor β receptor.* **Hoyles, Rachel K., et al., et al.** Jan 2011, Am J Respir Crit Care Med, Vol. 183, pp. 249-261.

47. *Multiple stromal populations contribute to pulmonary fibrosis without evidence for epithelial to mesenchymal transition.* **Rock, Jason R., et al., et al.** Dec 2011, Proc Natl Acad Sci U S A, Vol. 108, pp. E1475--E1483.

48. *Epithelial-mesenchymal transition in lung development and disease: does it exist and is it important?* **Bartis, Domokos, et al., et al.** Aug 2014, Thorax, Vol. 69, pp. 760-765.

49. *EMT and interstitial lung disease: a mysterious relationship.* **Kage, Hidenori and Borok, Zea.** Sep 2012, Curr Opin Pulm Med, Vol. 18, pp. 517-523.

50. *New antibiotics, bleomycin A and B.* **Umezawa, H., et al., et al.** Sep 1966, J Antibiot (Tokyo), Vol. 19, pp. 200-209.

51. **Dingermann, Theo and Hiller, Karl and Schneider, Georg and Zündorf, Ilse.** *Schneider Arzneidrogen.* s.l. : Elsevier, 2004. Vol. 5. Auflage.

52. *Internalisation of the bleomycin molecules responsible for bleomycin toxicity: a receptor-mediated endocytosis mechanism.* **Pron, G., et al., et al.** Jan 1999, Biochem Pharmacol, Vol. 57, pp. 45-56.

53. *Chronic Interstitial Pulmonary Fibrosis Produced in Hamsters by Endotracheal Bleomycin.* **Snider, Gordon L., et al., et al.** 1978, AMERICAN REVIEW OF RESPIRATORY DISEASE, Vol. 117, pp. 289-297.

54. *Bleomycin-induced Pulmonary Fibrosis.* **Phan, Sem H., Thrall, Roger S. and Williams, Catherine.** 1981, AMERICAN REVIEW OF RESPIRATORY DISEASE, Vol. 124, pp. 428-434.

55. *The bleomycin animal model: a useful tool to investigate treatment options for idiopathic pulmonary fibrosis?* **Moeller, Antje, et al., et al.** 2008, Int J Biochem Cell Biol, Vol. 40, pp. 362-382.

56. *An active intermediate formed in the reaction of bleomycin-Fe(II) complex with oxygen.* **Kuramochi, H., et al., et al.** May 1981, J Antibiot (Tokyo), Vol. 34, pp. 576-582.

57. *Sequence specific cleavage of DNA by the antitumor antibiotics neocarzinostatin and bleomycin.* **Andrea, Alan D. D. and Haseltine, William A.** 1978, Proc. Natl. Acad. Sci., Vol. 75, pp. 3608-3612.

58. *Very high cytotoxicity of bleomycin introduced into the cytosol of cells in culture.* **Poddevin, B., et al., et al.** Dec 1991, Biochem Pharmacol, Vol. 42 Suppl, pp. S67--S75.

59. **Murphy, Kenneth M.** *Janeway's Immunobiology.* 8 edition. s.l. : Garland Science, 2012.

60. *Innate immune responses to infection.* **Tosi, Michael F.** 2005, Journal of Allergy and Clinical Immunology, Vol. 116, pp. 241-249.

61. *C-TYPE LECTIN RECEPTORS ON DENDRITIC CELLS AND LANGERHANS CELLS.* **Figdor, Carl G., Kooyk, Yvette Van and Adema, Gosse J.** 2002, Nature Reviews | Immunology, Vol. 2, pp. 77-84.

62. *MECHANISMS OF PHAGOCYTOSIS IN MACROPHAGES.* **Aderem, Alan and Underhill, David M.** 1999, Annu. Rev. Immunol., pp. 593-623.

63. *Protective and pathogenic functions of macrophage subsets.* **Murray, Peter J. and Wynn, Thomas A.** Nov 2011, Nat Rev Immunol, Vol. 11, pp. 723-737.

64. *Modern concepts on the role of inflammation in pulmonary fibrosis.* **Homer, Robert J., et al., et al.** Jun 2011, Arch Pathol Lab Med, Vol. 135, pp. 780-788.

65. *Neutrophils and immunity: challenges and opportunities.* **Nathan, Carl.** Mar 2006, Nat Rev Immunol, Vol. 6, pp. 173-182.

66. *Chemokines and leukocyte traffic.* **Baggiolini, M.** Apr 1998, Nature, Vol. 392, pp. 565-568.

67. *The neutrophil as a cellular source of chemokines.* **Scapini, Patrizia, et al., et al.** 2000, Immunological Reviews, Vol. 177, pp. 195-203.

68. *Neutrophils and intracellular pathogens: beyond phagocytosis and killing.* **Appelberg, Rui.** Feb 2007, Trends Microbiol, Vol. 15, pp. 87-92.

69. *Neutrophil granules and secretory vesicles in inflammation.* **Faurschou, Mikkel and Borregaard, Niels.** Nov 2003, Microbes Infect, Vol. 5, pp. 1317-1327.

70. *Unconventional Roles of the NADPH Oxidase: Signaling, Ion Homeostasis, and Cell Death.* **Steinberg, Benjamin E. and Grinstein, Sergio.** 2007, Science STKE.

71. *Novel cell death program leads to neutrophil extracellular traps.* **Fuchs, Tobias A., et al., et al.** 2007, The Journal of Biological Chemistry, Vol. 176, pp. 231-241.

72. *Neutrophil Extracellular Traps Kill Bacteria.* **Brinkmann, Volker, et al., et al.** 2004, Science, Vol. 303, pp. 1532-1536.

73. *Dying for a cause: NETosis , mechanisms behind an antimicrobial cell death modality.* **Remijsen, Q., et al., et al.** s.l. : Nature Publishing Group, 2011, Cell Death and Differentiation, Vol. 18, pp. 581-588. ISSN: 1350-9047.

74. *Histone Deimination As a Response to Inflammatory Stimuli in Neutrophils.* **Neeli, Indira, Khan, Salar N. and Radic, Marko.** 2008, The Journal of Immunology, Vol. 180, pp. 1895-1902.

75. *Histone hypercitrullination mediates chromatin decondensation and neutrophil extracellular trap formation.* **Wang, Yanming, et al., et al.** 2009, Journal of Cell Biology, Vol. 184, pp. 205-213.

76. *PAD4 is essential for antibacterial innate immunity mediated by neutrophil extracellular traps.* **Li, Pingxin, et al., et al.** Aug 2010, J Exp Med, Vol. 207, pp. 1853-1862.

77. *Beneficial suicide: why neutrophils die to make NETs.* **Brinkmann, Volker and Zychlinsky, Arturo.** Aug 2007, Nat Rev Microbiol, Vol. 5, pp. 577-582.

78. *Neutrophils in the activation and regulation of innate and adaptive immunity.* **Mantovani, Alberto, et al., et al.** Aug 2011, Nat Rev Immunol, Vol. 11, pp. 519-531.

79. *NETosis.* **Mesa, Miguel Antonio and Vasquez, Gloria.** 2012, Autoimmune Diseases.

80. *Beta-hydroxybutyrate abrogates formation of bovine neutrophil extracellular traps and bactericidal activity against mammary pathogenic Escherichia coli.* **Grinberg, Navit, et al., et al.** Jun 2008, Infect Immun, Vol. 76, pp. 2802-2807.

81. *Neutrophil extracellular traps capture and kill Candida albicans yeast and hyphal forms.* **Urban, Constantin F., et al., et al.** 2006, Cellular Microbiology, Vol. 8, pp. 668-676.

82. *Neutrophil Extracellular Traps Mediate a Host Defense Response to Human Immunodeficiency Virus-1.* **Saitoh, Tatsuya, et al., et al.** s.l. : Elsevier Inc., 2012, Cell Host and Microbe, Vol. 12, pp. 109-116. ISSN: 1931-3128.

83. *An endonuclease allows Streptococcus pneumoniae to escape from neutrophil extracellular traps.* **Beiter, Katharina, et al., et al.** Feb 2006, Curr Biol, Vol. 16, pp. 401-407.

84. *Platelet TLR4 activates neutrophil extracellular traps to ensnare bacteria in septic blood.* **Clark, Stephen R., et al., et al.** 2007, Nature Medicine, Vol. 13, pp. 463-469.

85. *Eosinophil and neutrophil extracellular DNA traps in human allergic asthmatic airways.* **Dworski, Ryszard, et al., et al.** May 2011, J Allergy Clin Immunol, Vol. 127, pp. 1260-1266.

86. *Extracellular DNA traps promote thrombosis.* **Fuchs, Tobias A., et al., et al.** 2010, PNAS, Vol. 107, pp. 15880-15885.

87. *Platelets induce neutrophil extracellular traps in transfusion-related acute lung injury.* **Caudrillier, Axelle, et al., et al.** 2012, The Journal of Clinical Investigation, Vol. 122, pp. 2661-2671.

88. *Neutrophil extracellular traps directly induce epithelial and endothelial cell death: a predominant role of histones.* **Saffarzadeh, Mona, et al., et al.** 2012, PLoS One, Vol. 7, p. e32366.

89. **Youngson.** *Collins Dictionary of Human Biology.* 1. s.l. : Harper Collins Pb, 2006. ISBN 0-00-722134-7.

90. *Histone H2A variants H2AX and H2AZ.* **Redon, Christophe, et al., et al.** 2002, Current Opinion in Genetics & Development, Vol. 12, pp. 162-169.

91. *Extracellular histones are mediators of death through TLR2 and TLR4 in mouse fatal liver injury.* **Xu, Jun, et al., et al.** 2011, The Journal of Immunology, Vol. 187, pp. 2626-2631.

92. *Histones from dying renal cells aggravate kidney injury via TLR2 and TLR4.* **Allam, Ramanjaneyulu, et al., et al.** Aug 2012, J Am Soc Nephrol, Vol. 23, pp. 1375-1388.

93. *Extracellular histones are major mediators of death in sepsis.* **Xu, Jun, et al., et al.** 2009, Nature Medicine, Vol. 15, pp. 1318-1321.

94. *Extracellular histones are essential effectors of C5aR- and C5L2-mediated tissue damage and inflammation in acute lung injury.* **Bosmann, Markus, et al., et al.** Dec 2013, FASEB J, Vol. 27, pp. 5010-5021.

95. *A human B lymphocyte specific antigen.* **Greaves, M. F. and Brown, G.** Nov 1973, Nat New Biol, Vol. 246, pp. 116-119.

96. *Restriction of in vitro T cell-mediated cytotoxicity in lymphocytic chorio-meningitis within a syngeneic or semiallogeneic system.* **Zinkernagel, R. M. and Doherty, P. C.** 1974, Nature, Vol. 248, pp. 701-702.

97. *Functional role of type I and type II interferons in antiviral defense.* **Müller, U., et al., et al.** Jun 1994, Science, Vol. 264, pp. 1918-1921.

98. *MHC class II interaction with CD4 mediated by a region analogous to the MHC class I binding site for CD8.* **König, R., Huang, L. Y. and Germain, R. N.** Apr 1992, Nature, Vol. 356, pp. 796-798.

99. *Acquisition of lymphokine-producing phenotype by CD4+ T cells.* **Seder, R. A. and Paul, W. E.** 1994, Annu Rev Immunol, Vol. 12, pp. 635-673.

100. *Transforming growth factor-beta induces development of the T(H)17 lineage.* **Mangan, Paul R., et al., et al.** May 2006, Nature, Vol. 441, pp. 231-234.

101. *IL-6 programs Th-17 cell differentiation by promoting sequential engagement of the IL-21 and IL-23 pathways.* **Zhou, Liang, et al., et al.** 2007, Nature Immunology, Vol. 8, pp. 967-974.

102. *IL-21 initiates an alternative pathway to induce proinflammatory Th17 cells.* **Strom, Terry B., et al., et al.** 2007, Nature, Vol. 448, pp. 484-488.

103. *IL-23 promotes maintenance but not commitment to the Th17 lineage.* **Stritesky, Gretta L., Yeh, Norman and Kaplan, Mark H.** 2008, The Journal of Immunology, Vol. 181, pp. 5948-5955.

104. *The orphan nuclear receptor RORgammat directs the differentiation program of proinflammatory IL-17+ T helper cells.* **Ivanov, Ivaylo I., et al., et al.** Sep 2006, Cell, Vol. 126, pp. 1121-1133.

105. *Interleukin (IL) -22 and IL-17 are coexpressed by Th17 cells and cooperatively enhance expression of antimicrobial peptides.* **Liang, Spencer C., et al., et al.** 2006, The Journal of Experimental Medicine, Vol. 203, pp. 2271-2279.

106. *Bleomycin and IL-1beta-mediated pulmonary fibrosis is IL-17A dependent.* **Wilson, Mark S., et al., et al.** Mar 2010, J Exp Med, Vol. 207, pp. 535-552.

107. *Blocking IL-17A promotes the resolution of pulmonary inflammation and fibrosis via TGF-beta1-dependent and -independent mechanisms.* **Mi, Su, et al., et al.** Sep 2011, J Immunol, Vol. 187, pp. 3003-3014.

108. *Neutrophil recruitment by human IL-17 via C-X-C chemokine release in the airways.* **Laan, M., et al., et al.** Feb 1999, J Immunol, Vol. 162, pp. 2347-2352.

109. *IL-17 stimulates intraperitoneal neutrophil infiltration through the release of GRO alpha chemokine from mesothelial cells.* **Witowski, J., et al., et al.** Nov 2000, J Immunol, Vol. 165, pp. 5814-5821.

110. *Endogenous IL-17 as a mediator of neutrophil recruitment caused by endotoxin exposure in mouse airways.* **Miyamoto, Masahide, et al., et al.** May 2003, J Immunol, Vol. 170, pp. 4665-4672.

111. *Interleukin-17 Contributes to Generation of Th1 Immunity and Neutrophil Recruitment during Chlamydia muridarum Genital Tract Infection but Is Not Required for Macrophage Influx or Normal Resolution of Infection.* **Scurlock, Amy M., et al., et al.** 2011, Infection and Immunity, Vol. 79, pp. 1349-1362.

112. *IL-17 and TNF-α sustain neutrophil recruitment during inflammation through synergistic effects on endothelial activation.* **Griffin, Gabriel K., et al., et al.** Jun 2012, J Immunol, Vol. 188, pp. 6287-6299.

113. *Neutrophil elastase promotes myofibroblast differentiation in lung fibrosis.* **Gregory, Alyssa D., et al., et al.** Aug 2015, J Leukoc Biol, Vol. 98, pp. 143-152.

114. *Cutting edge: TGF-beta induces a regulatory phenotype in CD4+CD25- T cells through Foxp3 induction and down-regulation of Smad7.* **Fantini, Massimo C., et al., et al.** May 2004, J Immunol, Vol. 172, pp. 5149-5153.

115. *Inducing and expanding regulatory T cell populations by foreign antigen.* **Kretschmer, Karsten, et al., et al.** 2005, Nature Immunology, Vol. 6, pp. 1219-1227.

116. *Conversion of peripheral CD4+CD25- naive T cells to CD4+CD25+ regulatory T cells by TGF-beta induction of transcription factor Foxp3.* **Chen, WanJun, et al., et al.** Dec 2003, J Exp Med, Vol. 198, pp. 1875-1886.

117. *TGF-beta induces Foxp3 + T-regulatory cells from CD4 + CD25 - precursors.* **Fu, Shuang, et al., et al.** Oct 2004, Am J Transplant, Vol. 4, pp. 1614-1627.

118. *Human T cell activation.* **Hara, B. Y. Toshiro, Fu, Shuman and Hansen, John A.** 1985, The Journal of Experimental Medicine, Vol. 161, pp. 1513-1524.

119. *The murine homologue of the T lymphocyte antigen CD28. Molecular cloning and cell surface expression.* **Gross, J. A., St John, T. and Allison, J. P.** Apr 1990, J Immunol, Vol. 144, pp. 3201-3210.

120. *The B7-CD28 superfamily.* **Sharpe, Arlene H. and Freeman, Gordon J.** Feb 2002, Nat Rev Immunol, Vol. 2, pp. 116-126.

121. *Mechanisms of fibrosis: therapeutic translation for fibrotic disease.* **Wynn, Thomas A. and Ramalingam, Thirumalai R.** Jul 2012, Nat Med, Vol. 18, pp. 1028-1040.

122. *An Essential Role for Interleukin 10 in the Function of Regulatory T Cells That Inhibit Intestinal Inflammation.* **Asseman, By Chrystelle, et al., et al.** 1999, The Journal of Experimental Medicine, Vol. 190, pp. 995-1003.

123. *The inhibitory cytokine IL-35 contributes to regulatory T-cell function.* **Collison, Lauren W., et al., et al.** Nov 2007, Nature, Vol. 450, pp. 566-569.

124. *CD4+CD25+ Immune Regulatory Cells Are Required for Induction of Tolerance to Alloantigen via Costimulatory Blockade.* **Taylor, By Patricia A., Noelle, Randolph J. and Blazar, Bruce R.** 2001, The Journal of Experimental Medicine, Vol. 193, pp. 1311-1317.

125. *Use of Ly6G-specific monoclonal antibody to deplete neutrophils in mice.* **Daley, Jean M., et al., et al.** 2008, Journal of Leukocyte Biology, Vol. 83, pp. 64-70.

126. *Lung environment determines unique phenotype of alveolar macrophages.* **Guth, Amanda M., et al., et al.** 2009, American Journal of Physiology - Lung Cellular and Molecular Physiology, Vol. 296, pp. 936-946.

127. *TH1 AND TH2 CELLS: Different Patterns of Lymphokine Secretion Lead to Different Functional Properties.* **Mosmann, T. R. and Coffman, R. L.** 1989, The Annual Review of Immunology, Vol. 7, pp. 145-173.

128. *The lineage decisions of helper T cells.* **Murphy, Kenneth M. and Reiner, Steven L.** Dec 2002, Nat Rev Immunol, Vol. 2, pp. 933-944.

129. *Development, cytokine profile and function of human interleukin 17-producing helper T cells.* **Wilson, Nicholas J., et al., et al.** Sep 2007, Nat Immunol, Vol. 8, pp. 950-957.

130. *Immunologic self-tolerance maintained by activated T cells expressing IL-2 receptor alpha-chains (CD25). Breakdown of a single mechanism of self-tolerance causes various autoimmune diseases.* **Sakaguchi, S., et al., et al.** Aug 1995, J Immunol, Vol. 155, pp. 1151-1164.

131. *Control of Regulatory T Cell Development by the Transcription Factor Foxp3.* **Hori, Shohei, Nomura, Takashi and Sakaguchi, Shimon.** 2003, Science, Vol. 299, pp. 1057-1061.

132. *INNATE IMMUNE RESPONSES TO MICROBIAL POISONS: Discovery and Function of the Toll-Like Receptors.* **Beutler, Bruce.** 2003, Annu. Rev. Pharmacol. Toxicol., pp. 609-628.

133. *Pathogen recognition and innate immunity.* **Akira, Shizuo, Uematsu, Satoshi and Takeuchi, Osamu.** Feb 2006, Cell, Vol. 124, pp. 783-801.

134. *Toll-Like Receptors and Tissue Remodeling: The Pro/Cons Recent Findings.* **Micera, Alessandra, et al., et al.** 2015, Journal of Cellular Physiology, Vol. 231, pp. 531-544.

135. *Toll-Like Receptor 11 (TLR11) Interacts with Flagellin and Profilin through Disparate Mechanisms.* **Hatai, Hirotsugu, et al., et al.** 2016, PLoS One, Vol. 11, p. e0148987.

136. *Recognition of profilin by Toll-like receptor 12 is critical for host resistance to Toxoplasma gondii.* **Koblansky, A. Alicia, et al., et al.** Jan 2013, Immunity, Vol. 38, pp. 119-130.

137. *Role of Toll-like receptor 13 in innate immune recognition of group B streptococci.* **Signorino, Giacomo, et al., et al.** Dec 2014, Infect Immun, Vol. 82, pp. 5013-5022.

138. *Blood Platelets Are Assembled Principally at the Ends of Proplatelet Processes Produced by Differentiated Megakaryocytes.* **Italiano, Joseph E., et al., et al.** 1999, The Journal of Cell Biology, Vol. 147, pp. 1299-1312.

139. *Platelets in lung biology.* **Weyrich, Andrew S. and Zimmerman, Guy A.** 2013, Annu Rev Physiol, Vol. 75, pp. 569-591.

140. *A biphasic response of platelets to serotonin.* **White, J. G.** 3, 1970, Scandinavian journal of haematology, Vol. 7, pp. 145-151. ISSN: 0036-553X.

141. *Kinetic studies of the mechanism of thrombocytopenia in patients with human immunodeficiency virus infection.* **Ballem, P. J., et al., et al.** Dec 1992, N Engl J Med, Vol. 327, pp. 1779-1784.

142. *GPVI and integrin alphaIIb beta3 signaling in platelets.* **Watson, S. P., et al., et al.** Aug 2005, J Thromb Haemost, Vol. 3, pp. 1752-1762.

143. *Platelet Activation by Extracellular Matrix Proteins in Haemostasis and Thrombosis.* **Watson, Steve P.** 2009, Current Pharmaceutical Design, Vol. 15, pp. 1358-1372.

144. *New insights into the haemostatic function of platelets.* **Wei, Andrew H., et al., et al.** 2009, British Journal of Haematology, Vol. 147, pp. 415-430.

145. *Activation of platelet function through G protein-coupled receptors.* **Offermanns, Stefan.** Dec 2006, Circ Res, Vol. 99, pp. 1293-1304.

146. *Change in Protein Phenotype without a Nucleus: Translational Control in Platelets.* **Weyrich, Andrew S., et al., et al.** 2004, SEMINARS IN THROMBOSIS AND HEMOSTASIS, Vol. 30, pp. 491-498.

147. *Activated platelets mediate inflammatory signaling by regulated interleukin 1beta synthesis.* **Lindemann, S., et al., et al.** Aug 2001, J Cell Biol, Vol. 154, pp. 485-490.

148. *Mechanisms of Actin Rearrangements Mediating Platelet Activation.* **Hartwig, John H.** 1992, The Journal of Cell Biology, Vol. 118, pp. 1421-1442.

149. *Development of platelet secretory granules.* **King, Sarah M. and Reed, Guy L.** Aug 2002, Semin Cell Dev Biol, Vol. 13, pp. 293-302.

150. *Characterization of the proteins released from activated platelets leads to localization of novel platelet proteins in human atherosclerotic lesions.* **Coppinger, Judith A., et al., et al.** 2004, Blood, Vol. 103, pp. 2096-2104.

151. *Synthesis of transforming growth factor-beta 1 by megakaryocytes and its localization to megakaryocyte and platelet alpha-granules.* **Fava, R. A., et al., et al.** Nov 1990, Blood, Vol. 76, pp. 1946-1955.

152. *Lymphokines, interleukins, cytokines: function and action.* **Kaufmann, S. H.** Jul 1987, Immun Infekt, Vol. 15, pp. 127-134.

153. *Origin and physiological roles of inflammation.* **Medzhitov, Ruslan.** Jul 2008, Nature, Vol. 454, pp. 428-435.

154. *Acute inflammation. A review.* **Ryan, G. B. and Majno, G.** Jan 1977, Am J Pathol, Vol. 86, pp. 183-276.

155. *IL-27, a Heterodimeric Cytokine Composed of EBI3 and p28 Protein, Induces Proliferation of Naive CD4+ T Cells.* **Pflanz, Stefan, et al., et al.** 2002, Immunity, Vol. 16, pp. 779-790.

156. *Modulation of inflammation by interleukin-27.* **Bosmann, Markus and Ward, Peter A.** Dec 2013, J Leukoc Biol, Vol. 94, pp. 1159-1165.

157. *Defective LPS Signaling in C3H/HeJ and C57BL/10ScCr Mice: Mutations in Tlr4 Gene.* **Poltorak, Alexander, et al., et al.** 1998, Science, Vol. 282, pp. 2085-2088.

158. *Mal (MyD88-adapter-like) is required for Toll-like receptor-4 signal transduction.* **Fitzgerald, Katherine A., et al., et al.** 2001, Nature, Vol. 413, pp. 78-83.

159. *LPS-TLR4 signaling to IRF-3/7 and NF-kappaB involves the toll adapters TRAM and TRIF.* **Fitzgerald, Katherine A., et al., et al.** Oct 2003, J Exp Med, Vol. 198, pp. 1043-1055.

160. *Phosphoinositide-Mediated Adaptor Recruitment Controls Toll-like Receptor Signaling.* **Kagan, Jonathan C. and Medzhitov, Ruslan.** 2006, Cell, Vol. 125, pp. 943-955.

161. *Cloning and characterization of two Toll/Interleukin-1 receptor-like genes TIL3 and TIL4: evidence for a multi-gene receptor family in humans.* **Chaudhary, P. M., et al., et al.** Jun 1998, Blood, Vol. 91, pp. 4020-4027.

162. *A human homologue of the Drosophila Toll protein signals activation of adaptive immunity.* **Medzhitov, R., Preston-Hurlburt, P. and Janeway, C. A.** 6640, Jul 1997, Nature, Vol. 388, pp. 394-397. ISSN: 0028-0836.

163. *A MAP Kinase Targeted by Endotoxin and Hyperosmolarity in Mammalian Cells.* **Han, J., et al., et al.** 1994, Science, Vol. 265, pp. 808-811.

164. *TRAM couples endocytosis of Toll-like receptor 4 to the induction of interferon-beta.* **Kagan, Jonathan C., et al., et al.** Apr 2008, Nat Immunol, Vol. 9, pp. 361-368.

165. *Roles for LPS-dependent interaction and relocation of TLR4 and TRAM in TRIF-signaling.* **Tanimura, Natsuko, et al., et al.** 2008, Biochemical and Biophysical Research Communications, Vol. 368, pp. 94-99.

166. *Critical Role of the IFN-Stimulated Gene Factor 3 Complex in TLR-Mediated IL-27p28 Gene Expression Revealing a Two-Step Activation Process.* **Molle, Celine, Goldman, Michel and Goriely, Stanislas.** 2010, The Journal of Immunology, Vol. 184, pp. 1784-1792.

167. *LPS/TLR4 signal transduction pathway.* **Lu, Yong-chen, Yeh, Wen-chen and Ohashi, Pamela S.** 2008, Cytokine, Vol. 42, pp. 145-151.

168. *IL-27 inhibits the development of regulatory T cells via STAT3.* **Huber, Magdalena, et al., et al.** Feb 2008, Int Immunol, Vol. 20, pp. 223-234.

169. *Interleukins 27 and 6 induce STAT3-mediated T cell production of interleukin 10.* **Stumhofer, Jason S., et al., et al.** 2007, Nature Immunology, pp. 1363-1371.

170. *IL-27 Suppresses CD28-Medicated IL-2 Production through Suppressor of Cytokine Signaling 3.* **Owaki, Toshiyuki, et al., et al.** 2006, The Journal of Immunology, Vol. 176, pp. 2773-2780.

171. *Timed action of IL-27 protects from immunopathology while preserving defense in influenza.* **Liu, Francesca Diane M., et al., et al.** May 2014, PLoS Pathog, Vol. 10, p. e1004110.

172. *Interleukin-27 as a Negative Regulator of Human Neutrophil Function.* **Li, J. P., et al., et al.** 2010, Scandinavian Journal of Immunology, Vol. 72, pp. 284-292.

173. *WSX-1 and Glycoprotein 130 Constitute a Signal-Transducing Receptor for IL-27.* **Pflanz, Stefan, et al., et al.** 2004, The Journal of Immunology, Vol. 172, pp. 2225-2231.

174. *Cloning and Characterization of a Novel Class I Cytokine Receptor.* **Sprecher, Cindy A., et al., et al.** 1998, Biochemical and Biophysical Research Communications, Vol. 246, pp. 82-90.

175. *Development of Th1-type immune responses requires the type I cytokine receptor TCCR.* **Chen, Qi, et al., et al.** 2000, Nature, Vol. 407, pp. 916-920.

176. *IL-27 and IFN-alpha signal via Stat1 and Stat3 and induce T-Bet and IL-12Rbeta2 in naive T cells.* **Hibbert, Linda, et al., et al.** Sep 2003, J Interferon Cytokine Res, Vol. 23, pp. 513-522.

177. *The biology and therapeutic potential of interleukin 27.* **Batten, Marcel and Ghilardi, Nico.** Jul 2007, J Mol Med (Berl), Vol. 85, pp. 661-672.

178. *New class of transforming growth factors potentiated by epidermal growth factor: Isolation from non-neoplastic tissues.* **Roberts, Anita B., et al., et al.** 1981, PNAS, Vol. 78, pp. 5339-5343.

179. *Distinct transforming growth factor-beta (TGF-beta) receptor subsets as determinants of cellular responsiveness to three TGF-beta isoforms.* **Cheifetz, S. and Hernandez, H. and Laiho, M. and ten Dijke P and Iwata K, K. and Massagué, J.** 1990, The Journal of Biological Chemistry, Vol. 265, pp. 20533-20538.

180. *Diagnosis of primary cancer of the liver.* **Kew, M. C., Santos, Dos and H., A. and Sherlock, S.** Nov 1971, Br Med J, Vol. 4, pp. 408-411.

181. *Two forms of transforming growth factor-beta distinguished by multipotential haematopoietic progenitor cells.* **Ohta, M., et al., et al.** 1987, Nature, Vol. 329, pp. 539-541.

182. *TGF-beta signal transduction.* **Massagué, J.** 1998, Annu Rev Biochem, Vol. 67, pp. 753-791.

183. *TGF-beta latency: biological significance and mechanisms of activation.* **Gleizes, P. E., et al., et al.** 1997, Stem Cells, Vol. 15, pp. 190-197.

184. *Latent transforming growth factor-beta: structural features and mechanisms of activation.* **Munger, J. S., et al., et al.** May 1997, Kidney Int, Vol. 51, pp. 1376-1382.

185. *Evidence that furin is an authentic transforming growth factor-beta1-converting enzyme.* **Dubois, C. M., et al., et al.** Jan 2001, Am J Pathol, Vol. 158, pp. 305-316.

186. *A role of the latent TGF-beta 1-binding protein in the assembly and secretion of TGF-beta 1.* **Miyazono, K., et al., et al.** May 1991, EMBO J, Vol. 10, pp. 1091-1101.

187. *TGF-β activation and function in immunity.* **Travis, Mark A. and Sheppard, Dean.** 2014, Annu Rev Immunol, Vol. 32, pp. 51-82.

188. *Review of the activation of TGF-beta in immunity.* **Taylor, Andrew W.** Jan 2009, J Leukoc Biol, Vol. 85, pp. 29-33.

189. *Latent TGF-β structure and activation.* **Shi, Minlong, et al., et al.** Jun 2011, Nature, Vol. 474, pp. 343-349.

190. *Absence of integrin-mediated TGFbeta1 activation in vivo recapitulates the phenotype of TGFbeta1-null mice.* **Yang, Zhiwei, et al., et al.** Mar 2007, J Cell Biol, Vol. 176, pp. 787-793.

191. *Arginyl-glycyl-aspartic acid (RGD): a cell adhesion motif.* **D'Souza, E., Ginsberg, M. H. and Plow, Edward F.** 1991, Cell, pp. 246-250.

192. *Mice that lack activity of alphavbeta6- and alphavbeta8-integrins reproduce the abnormalities of Tgfb1- and Tgfb3-null mice.* **Aluwihare, Poshala, et al., et al.** Jan 2009, J Cell Sci, Vol. 122, pp. 227-232.

193. *Integrin alphaVbeta6-mediated activation of latent TGF-beta requires the latent TGF-beta binding protein-1.* **Annes, Justin P., et al., et al.** Jun 2004, J Cell Biol, Vol. 165, pp. 723-734.

194. *Perturbation of transforming growth factor (TGF)-beta1 association with latent TGF-beta binding protein yields inflammation and tumors.* **Yoshinaga, Keiji, et al., et al.** Dec 2008, Proc Natl Acad Sci USA, Vol. 105, pp. 18758-18763.

195. *Integrins and the activation of latent transforming growth factor beta1 - an intimate relationship.* **Wipff, Pierre-Jean and Hinz, Boris.** Sep 2008, Eur J Cell Biol, Vol. 87, pp. 601-615.

196. *Betaglycan presents ligand to the TGF beta signaling receptor.* **López-Casillas, F., Wrana, J. L. and Massagué, J.** Jul 1993, Cell, Vol. 73, pp. 1435-1444.

197. *Expression cloning of the TGF-beta type II receptor, a functional transmembrane serine/threonine kinase.* **Lin, H. Y., et al., et al.** Feb 1992, Cell, Vol. 68, pp. 775-785.

198. *Expression Cloning of an Activin Receptor, a Predicted Transmembrane Serine Kinase.* **Mathews, Lawrence S. and Vale, Wylie W.** 1991, Cell, Vol. 65, pp. 973-982.

199. *Signaling via hetero-oligomeric complexes of type I and type II serine/threonine kinase receptors.* **ten Dijke, P., Miyazono, K. and Heldin, C. H.** Apr 1996, Curr Opin Cell Biol, Vol. 8, pp. 139-145.

200. *TGF beta signals through a heteromeric protein kinase receptor complex.* **Wrana, J. L., et al., et al.** Dec 1992, Cell, Vol. 71, pp. 1003-1014.

201. *Responsiveness to transforming growth factor-beta (TGF-beta) restored by genetic complementation between cells defective in TGF-beta receptors I and II.* **Laiho, M., et al., et al.** May 1991, J Biol Chem, Vol. 266, pp. 9108-9112.

202. *Transcriptional control by the TGF-beta/Smad signaling system.* **Massagué, J. and Wotton, D.** Apr 2000, EMBO J, Vol. 19, pp. 1745-1754.

203. *Controlling TGF-beta signaling.* **Massagué, J. and Chen, Y. G.** Mar 2000, Genes Dev, Vol. 14, pp. 627-644.

204. *Partnership between DPC4 and SMAD proteins in TGF-beta signalling pathways.* **Lagna, G., et al., et al.** Oct 1996, Nature, Vol. 383, pp. 832-836.

205. *A human Mad protein acting as a BMP-regulated transcriptional activator.* **Liu, Fang, et al., et al.** 1996, Nature, Vol. 381, pp. 620-623.

206. *Receptor-associated Mad homologues synergize as effectors of the TGF-beta response.* **Zhang, Y., et al., et al.** Sep 1996, Nature, Vol. 383, pp. 168-172.

207. *A novel mesoderm inducer , Madr2 , functions in the activin signal transduction pathway.* **Baker, Julie C. and Harland, Richard M.** 1996, GENES & DEVELOPMENT, pp. 1880-1889.

208. *Drosophila Mad binds to DNA and directly mediates activation of vestigial by Decapentaplegic.* **Kim, J., et al., et al.** Jul 1997, Nature, Vol. 388, pp. 304-308.

209. *Smad4 and FAST-1 in the assembly of activin-responsive factor.* **Chen, X., et al., et al.** Sep 1997, Nature, Vol. 389, pp. 85-89.

210. *Mutations increasing autoinhibition inactivate tumour suppressors Smad2 and Smad4.* **Hata, A., et al., et al.** Jul 1997, Nature, Vol. 388, pp. 82-87.

211. *Dual role of the Smad4/DPC4 tumor suppressor in TGFbeta-inducible transcriptional complexes.* **Liu, F., Pouponnot, C. and Massagué, J.** Dec 1997, Genes Dev, Vol. 11, pp. 3157-3167.

212. *Crystal structure of a Smad MH1 domain bound to DNA: insights on DNA binding in TGF-beta signaling.* **Shi, Y., et al., et al.** Sep 1998, Cell, Vol. 94, pp. 585-594.

213. *A mechanism of repression of TGFβ/ Smad signaling by oncogenic Ras.* **Kretzschmar, Marcus, et al., et al.** 1999, GENES & DEVELOPMENT, Vol. 13, pp. 804-816.

214. *The TGF-beta family mediator Smad1 is phosphorylated directly and activated functionally by the BMP receptor kinase.* **Kretzschmar, M., et al., et al.** Apr 1997, Genes Dev, Vol. 11, pp. 984-995.

215. *MADR2 is a substrate of the TGFbeta receptor and its phosphorylation is required for nuclear accumulation and signaling.* **Macías-Silva, M., et al., et al.** Dec 1996, Cell, Vol. 87, pp. 1215-1224.

216. *Phosphorylation of Ser465 and Ser467 in the C terminus of Smad2 mediates interaction with Smad4 and is required for transforming growth factor-beta signaling.* **Souchelnytskyi, S., et al., et al.** Oct 1997, J Biol Chem, Vol. 272, pp. 28107-28115.

217. *SARA, a FYVE domain protein that recruits Smad2 to the TGFbeta receptor.* **Tsukazaki, T., et al., et al.** Dec 1998, Cell, Vol. 95, pp. 779-791.

218. *Mechanisms of TGF-beta signaling from cell membrane to the nucleus.* **Shi, Yigong and Massagué, Joan.** Jun 2003, Cell, Vol. 113, pp. 685-700.

219. *Nucleocytoplasmic shuttling of signal transducers.* **Xu, Lan and Massagué, Joan.** Mar 2004, Nat Rev Mol Cell Biol, Vol. 5, pp. 209-219.

220. *The MAD-related protein Smad7 associates with the TGFbeta receptor and functions as an antagonist of TGFbeta signaling.* **Hayashi, H., et al., et al.** Jun 1997, Cell, Vol. 89, pp. 1165-1173.

221. *Smad6 inhibits signalling by the TGF-beta superfamily.* **Imamura, T., et al., et al.** Oct 1997, Nature, Vol. 389, pp. 622-626.

222. *MAP Kinases.* **Chen, Zhu, et al., et al.** 2001, Chemical Reviews, Vol. 101, pp. 2449-2476.

223. *Regulation of Receptor-Dependent Activation of the Innate Immune Response.* **Ulevitch, Richard J.** 2003, The Journal of Infectious Diseases, Vol. 187, pp. 351-355.

224. *Differential regulation and properties of MAPKs.* **Raman, M., Chen, W. and Cobb, M. H.** 2007, Oncogene, Vol. 26, pp. 3100-3112.

225. *The p38 MAPK pathway inhibits tristetraprolin-directed decay of interleukin-10 and pro-inflammatory mediator mRNAs in murine macrophages.* **Tudor, Corina, et al., et al.** Jun 2009, FEBS Lett, Vol. 583, pp. 1933-1938.

226. *The p38 mitogen-activated kinase pathway regulates the human interleukin-10 promoter via the activation of Sp1 transcription factor in lipopolysaccharide-stimulated human macrophages.* **Ma, W., et al., et al.** Apr 2001, J Biol Chem, Vol. 276, pp. 13664-13674.

227. *The p38/MK2-driven exchange between tristetraprolin and HuR regulates AU-rich element-dependent translation.* **Tiedje, Christopher, et al., et al.** Sep 2012, PLoS Genet, Vol. 8, p. e1002977.

228. *New insights into the molecular mechanism of interleukin-10-mediated immunosuppression.* **Grütz, Gerald.** Jan 2005, J Leukoc Biol, Vol. 77, pp. 3-15.

229. *Interruption of macrophage-derived IL-27(p28) production by IL-10 during sepsis requires STAT3 but not SOCS3.* **Bosmann, Markus, et al., et al.** Dec 2014, J Immunol, Vol. 193, pp. 5668-5677.

230. *Understanding and exploiting the endogenous interleukin-10/STAT3-mediated anti-inflammatory response.* **Murray, Peter J.** 2006, Current Opinion in Pharmacology, Vol. 6, pp. 379-386.

231. *Science in medicine Macrophage plasticity and polarization: in vivo veritas.* **Sica, Antonio and Mantovani, Alberto.** 2012, The Journal of Clinical Investigation, Vol. 122, pp. 787-795.

232. *Macrophage plasticity and interaction with lymphocyte subsets: cancer as a paradigm.* **Biswas, Subhra K. and Mantovani, Alberto.** s.l. : Nature Publishing Group, 2010, Nature immunology, Vol. 11, pp. 889-896. ISSN: 1529-2908.

233. *IL-10-producing macrophages preferentially clear early apoptotic cells.* **Xu, Wei, et al., et al.** Jun 2006, Blood, Vol. 107, pp. 4930-4937.

234. *Production of cytokines by mouse B cells: B lymphomas and normal B cells produce interleukin 10.* **Garra, Anne O., et al., et al.** 1990, International Immunology, Vol. 2, pp. 821-832.

235. *Mast cell-derived interleukin 10 limits skin pathology in contact dermatitis and chronic irradiation with ultraviolet B.* **Grimbaldeston, Michele A., et al., et al.** Oct 2007, Nat Immunol, Vol. 8, pp. 1095-1104.

236. *Regulation of monocyte IL-10 synthesis by endogenous IL-1 and TNF-alpha: role of the p38 and p42/44 mitogen-activated protein kinases.* **Foey, A. D., et al., et al.** Jan 1998, J Immunol, Vol. 160, pp. 920-928.

237. *IL-10-producing regulatory B cells (B10 cells) in autoimmune disease.* **Kalampokis, Ioannis, Yoshizaki, Ayumi and Tedder, Thomas F.** 2013, Arthritis Res Ther, Vol. 15 Suppl 1, p. S1.

238. *Interleukin 10 acts on regulatory T cells to maintain expression of the transcription factor Foxp3 and suppressive function in mice with colitis.* **Murai, Masako, et al., et al.** 2009, Nature Immunology, Vol. 10, pp. 1178-1184.

239. **Ritossa.** *A new puffing pattern induced by heat shock and DNP in Drosophila.* s.l. : Experimentia, 1962.

240. *THE HEAT-SHOCK PROTEINS.* **Lindquist, S. and Craig, E. A.** 1988, Annual Review of Genetics, Vol. 22, pp. 631-677.

241. *Heat Shock Protein 70 kDa: Molecular Biology, Biochemistry and Physiology.* **Kiang, Juliann G. and Tsokos, George C.** 1998, Pharmacology & Therapeutics, Vol. 80, pp. 183-201.

242. *Heat shock proteins, cellular chaperones that modulate mitochondrial cell death pathways.* **Parcellier, Arnaud, et al., et al.** 2003, Biochemical and Biophysical Research Communications, Vol. 304, pp. 505-512.

243. *The MHC class I antigen presentation pathway: strategies for viral immune evasion.* **Hewitt, Eric W.** 2003, Immunology, Vol. 110, pp. 163-169.

244. *HEAT-SHOCK PROTEINS INDUCE T-CELL REGULATION OF CHRONIC INFLAMMATION.* **Eden, Willem Van, Zee, Ruurd Van Der and Prakken, Berent.** 2005, Nature, Vol. 5, pp. 318-330.

245. *Inhibition of HDAC9 increases T regulatory cell function and prevents colitis in mice.* **de Zoeten and Edwin, F., et al., et al.** Feb 2010, Gastroenterology, Vol. 138, pp. 583-594.

246. *Histone Deacetylase 6 and Heat Shock Protein 90 Control the Functions of Foxp3+ T-Regulatory Cells.* **Zoeten, Edwin F. De, et al., et al.** 2011, MOLECULAR AND CELLULAR BIOLOGY, Vol. 31, pp. 2066-2078.

247. *mRNA Degradation: an Important Process in Controlling Gene Expression.* **Blackshear, P. J.** 2002, Biochemical Society Transactions, Vol. 30, pp. 945-952.

248. *Evidence that Tristetraprolin Binds to AU-Rich Elements and Promotes the Deadenylation and Destabilization of Tumor Necrosis Factor Alpha mRNA.* **Lai, W. S., et al., et al.** 1999, MOLECULAR AND CELLULAR BIOLOGY, Vol. 19, pp. 4311-4323.

249. *Interactions of CCCH Zinc Finger Proteins with mRNA.* **Lai, W. S. and Blackshear, Perry J.** 2001, The Journal of Biological Chemistry, Vol. 276, pp. 23144-23154.

250. *Evidence that tristetraprolin is a physiological regulator of granulocyte-macrophage colony-stimulating factor messenger RNA deadenylation and stability.* **Carballo, Ester, Lai, Wi S. and Blackshear, Perry J.** 2000, Blood, Vol. 95, pp. 1891-1900.

251. *A pathogenetic role for TNF alpha in the syndrome of cachexia, arthritis, and autoimmunity resulting from tristetraprolin (TTP) deficiency.* **Taylor, G. A., et al., et al.** May 1996, Immunity, Vol. 4, pp. 445-454.

252. *WSX-1 is required for the initiation of Th1 responses and resistance to L. major infection.* **Yoshida, H., et al., et al.** Oct 2001, Immunity, Vol. 15, pp. 569-578.

253. *Pf4-Cre transgenic mice allow the generation of lineage-restricted gene knockouts for studying megakaryocyte and platelet function in vivo.* **Tiedt, Ralph, et al., et al.** 2007, Blood, Vol. 109, pp. 1503-1507.

254. *Generation of mice with a conditional allele for transforming growth factor beta 1 gene.* **Azhar, Mohamad, et al., et al.** 6, Jun 2009, Genesis (New York, N.Y. : 2000), Vol. 47, pp. 423-431. ISSN: 1526-968X.

255. *Conditional gene targeting in macrophages and granulocytes using LysMcre mice.* **Clausen, B. E., et al., et al.** 4, Aug 1999, Transgenic research, Vol. 8, pp. 265-277. ISSN: 0962-8819.

256. *Interleukin-10-deficient mice develop chronic enterocolitis.* **Kühn, R., et al., et al.** 2, Oct 1993, Cell, Vol. 75, pp. 263-274. ISSN: 0092-8674.

257. *IL-17A and IL-17F do not contribute vitally to autoimmune neuro-inflammation in mice.* **Haak, Stefan, et al., et al.** 1, Jan 2009, The Journal of clinical investigation, Vol. 119, pp. 61-69. ISSN: 0021-9738.

258. *Dynamic in vivo imaging and cell tracking using a histone fluorescent protein fusion in mice.* **Hadjantonakis, Anna-Katerina and Papaioannou, Virginia E.** Dec 2004, BMC biotechnology, Vol. 4, p. 33. ISSN: 1472-6750.

259. *Catchup: a mouse model for imaging-based tracking and modulation of neutrophil granulocytes.* **Hasenberg, Anja, et al., et al.** 5, May 2015, Nature methods, Vol. 12, pp. 445-452. ISSN: 1548-7105.

260. *A Cre-inducible diphtheria toxin receptor mediates cell lineage ablation after toxin administration.* **Buch, Thorsten, et al., et al.** 6, Jun 2005, Nature methods, Vol. 2, pp. 419-426. ISSN: 1548-7091.

261. *PAD4-mediated neutrophil extracellular trap formation is not required for immunity against influenza infection.* **Hemmers, Saskia, et al., et al.** 2011, PLoS One, Vol. 6, p. e22043.

262. *Activation of murine macrophages.* **Mosser, David M. and Zhang, Xia.** Nov 2008, Curr Protoc Immunol, Vol. Chapter 14, p. Unit 14.2.

263. *Complement activation product C5a is a selective suppressor of TLR4-induced, but not TLR3-induced, production of IL-27(p28) from macrophages.* **Bosmann, Markus, et al., et al.** May 2012, J Immunol, Vol. 188, pp. 5086-5093.

264. *CD11c+ alveolar macrophages are a source of IL-23 during lipopolysaccharide-induced acute lung injury.* **Bosmann, Markus, et al., et al.** May 2013, Shock, Vol. 39, pp. 447-452.

265. *Comparison of conditioning regimens for alveolar macrophage reconstitution and innate immune function post bone marrow transplant.* **Hubbard, L. L. and Ballinger, M. N. and Wilke, C. A. and Moore, B. B.** 2008, Exp Lung Res, Vol. 34, pp. 263-75.

266. *The outcome of polymicrobial sepsis is independent of T and B cells.* **Bosmann, Markus, et al., et al.** Oct 2011, Shock, Vol. 36, pp. 396-401.

267. *Accurate whole human genome sequencing using reversible terminator chemistry.* **Bentley, David R., et al., et al.** Nov 2008, Nature, Vol. 456, pp. 53-59.

268. *Sequencing technologies - the next generation.* **Metzker, Michael L.** Jan 2010, Nat Rev Genet, Vol. 11, pp. 31-46.

269. *Mouse models of bleomycin-induced pulmonary fibrosis.* **Walters, Dianne M. and Kleeberger, Steven R.** Mar 2008, Curr Protoc Pharmacol, Vol. Chapter 5, p. Unit 5.46.

270. *Macrophages: master regulators of inflammation and fibrosis.* **Wynn, Thomas A. and Barron, Luke.** Aug 2010, Semin Liver Dis, Vol. 30, pp. 245-257.

271. *Body condition scoring: a rapid and accurate method for assessing health status in mice.* **Ullman-Culleré, M. H. and Foltz, C. J.** Jun 1999, Lab Anim Sci, Vol. 49, pp. 319-323.

272. *Mechanisms of bleomycin-induced lung damage.* **Hay, John, Shahzeidi, Shahriar and Laurent, Geoffrey.** 1991, Archives of Toxicology, Vol. 65, pp. 81-94. ISBN: 0340576191000.

273. *The significance of macrophage polarization subtypes for animal models of tissue fibrosis and human fibrotic diseases.* **Wermuth, Peter J. and Jimenez, Sergio A.** 2015, Clin Transl Med., Vol. 4.

274. *Inhibition of p38 MAP kinase by utilizing a novel allosteric binding site.* **Pargellis, Christopher, et al., et al.** 4, Apr 2002, Nature structural biology, Vol. 9, pp. 268-272. ISSN: 1072-8368.

275. *Transforming growth factor (TGF)-beta1-producing regulatory T cells induce Smad-mediated interleukin 10 secretion that facilitates coordinated immunoregulatory activity and*

amelioration of TGF-beta1-mediated fibrosis. **Kitani, Atsushi, et al., et al.** Oct 2003, J Exp Med, Vol. 198, pp. 1179-1188.

276. *IL-27 alleviates the bleomycin-induced pulmonary fibrosis by regulating the Th17 cell differentiation.* **Dong, Zhaoxing, et al., et al.** 2015, BMC Pulmonary Medicine, p. 15:13.

277. *Progress toward improving animal models for idiopathic pulmonary fibrosis.* **Degryse, Amber L. and Lawson, William E.** Jun 2011, Am J Med Sci, Vol. 341, pp. 444-449.

278. *Time course of bleomycin-induced lung fibrosis.* **Izbicki, G., et al., et al.** 2002, International Journal of Experimental Pathology, Vol. 83, pp. 111-129.

279. *Cell adhesion molecules regulate fibrotic process via Th1/Th2/Th17 cell balance in a bleomycin-induced scleroderma model.* **Yoshizaki, Ayumi, et al., et al.** Aug 2010, J Immunol, Vol. 185, pp. 2502-2515.

280. *Bleomycin-induced pulmonary fibrosis in hamsters: effect of neutrophil depletion on lung collagen synthesis.* **Clark, J. G. and Kuhn, 3rd, C.** Oct 1982, Am Rev Respir Dis, Vol. 126, pp. 737-739.

281. *Influence of early neutrophil depletion on MMPs/TIMP-1 balance in bleomycin-induced lung fibrosis.* **Manoury, Boris, et al., et al.** Jul 2007, Int Immunopharmacol, Vol. 7, pp. 900-911.

282. *Neutrophil mobilization and clearance in the bone marrow.* **Furze, Rebecca C. and Rankin, Sara M.** Nov 2008, Immunology, Vol. 125, pp. 281-288.

283. *Diphtheria toxin effects on brain-tumor xenografts. Implications for protein-based brain-tumor chemotherapy.* **Wrobel, C. J., et al., et al.** Jun 1990, J Neurosurg, Vol. 72, pp. 946-950.

284. *Integrating mechanisms of pulmonary fibrosis.* **Wynn, Thomas A.** Jul 2011, J Exp Med, Vol. 208, pp. 1339-1350.

285. *Neutrophil extracellular traps promote differentiation and function of fibroblasts.* **Chrysanthopoulou, Akrivi, et al., et al.** 2014, Journal of Pathology, Vol. 233, pp. 294-307.

286. *Protection from lethal septic peritonitis by neutralizing the biological function of interleukin 27.* **Wirtz, Stefan, et al., et al.** Aug 2006, J Exp Med, Vol. 203, pp. 1875-1881.

287. *Mice lacking neutrophil elastase are resistant to bleomycin-induced pulmonary fibrosis.* **Chua, Felix, et al., et al.** Jan 2007, Am J Pathol, Vol. 170, pp. 65-74.

288. *IL-27 inhibits the TGF-β1-induced epithelial-mesenchymal transition in alveolar epithelial cells.* **Dong, Zhaoxing, et al., et al.** 2016, BMC Cell Biol, Vol. 17, p. 7.

289. *Cellular and molecular mechanisms of chronic inflammation-associated organ fibrosis.* **Ueha, Satoshi, Shand, Francis H. W. and Matsushima, Kouji.** 2012, Front Immunol, Vol. 3, p. 71.

290. *A Role for IL-27 in Limiting T Regulatory Cell Populations.* **Wojno, Elia D. Tait, et al., et al.** 2011, The Journal of Immunology, Vol. 187, pp. 266-273.

291. *Positive and negative regulation of the IL-27 receptor during lymphoid cell activation.* **Villarino, Alejandro V., et al., et al.** Jun 2005, J Immunol, Vol. 174, pp. 7684-7691.

292. *T lymphocyte priming by neutrophil extracellular traps links innate and adaptive immune responses.* **Tillack, Kati, et al., et al.** Apr 2012, J Immunol, Vol. 188, pp. 3150-3159.

293. *TLR2-mediated production of IL-27 and chemokines by respiratory epithelial cells promotes bleomycin-induced pulmonary fibrosis in mice.* **Kim, Hye Sung, et al., et al.** Oct 2011, J Immunol, Vol. 187, pp. 4007-4017.

294. *IL-27 attenuates the TGF-β1-induced proliferation, differentiation and collagen synthesis in lung fibroblasts.* **Dong, Zhaoxing, et al., et al.** Feb 2016, Life Sci, Vol. 146, pp. 24-33.

295. *IL-27 blocks RORc expression to inhibit lineage commitment of Th17 cells.* **Diveu, Caroline, et al., et al.** May 2009, J Immunol, Vol. 182, pp. 5748-5756.

296. *IL-1 and IL-23 Mediate Early IL-17A Production in Pulmonary Inflammation Leading to Late Fibrosis.* **Gasse, Pamela, et al., et al.** 2011, PLos ONE, Vol. 6.

297. *IL-17A-producing gammadelta T and Th17 lymphocytes mediate lung inflammation but not fibrosis in experimental silicosis.* **Lo Re, Sandra, et al., et al.** Jun 2010, J Immunol, Vol. 184, pp. 6367-6377.

298. *Regulation of pulmonary fibrosis by chemokine receptor CXCR3.* **Jiang, Dianhua, et al., et al.** 2004, The Journal of Clinical Investigation, Vol. 114, pp. 291-299.

299. *Interferon gamma-1b in the treatment of idiopathic pulmonary fibrosis.* **Pacanowski, Michael A. and Amsden, Guy W.** Oct 2005, Ann Pharmacother, Vol. 39, pp. 1678-1686.

300. *Essential autocrine regulation by IL-21 in the generation of inflammatory T cells.* **Nurieva, Roza, et al., et al.** 2007, Nature, Vol. 448, pp. 480-484.

301. *IL-21 inhibits T cell IL-2 production and impairs Treg homeostasis.* **Attridge, Kesley, et al., et al.** 2012, Blood, Vol. 119, pp. 4656-4665.

302. *Interleukin-2 is essential for CD4+CD25+ regulatory T cell function.* **Rosa, Maurus De, et al., et al.** 2004, The European Journal of Immunology, Vol. 34, pp. 2480-2488.

303. *Plasmin regulates the activation of cell-associated latent TGF-beta 1 secreted by rat alveolar macrophages after in vivo bleomycin injury.* **Khalil, N., et al., et al.** Aug 1996, Am J Respir Cell Mol Biol, Vol. 15, pp. 252-259.

304. *Original articles Effect of antibody to transforming growth factor β on bleomycin induced accumulation of lung collagen in mice.* **Giri, Shri N., Hyde, Dallas M. and Hollinger, Mannfred A.** 1993, Thorax, Vol. 48, pp. 959-966.

305. *Transforming Growth Factor-beta in Human Platelets.* **Assoians, Richard K., et al., et al.** 1983, The Journal of Biological Chemistry, Vol. 258, pp. 7155-7160.

306. *Histone induced platelet aggregation is inhibited by normal albumin.* **Lam, Fong W., et al., et al.** s.l. : Elsevier Ltd, 2013, Thrombosis Research, Vol. 132, pp. 69-76. ISSN: 0049-3848.

307. *Extracellular histones promote thrombin generation through platelet-dependent mechanisms: involvement of platelet TLR2 and TLR4.* **Semeraro, Fabrizio, et al., et al.** Aug 2011, Blood, Vol. 118, pp. 1952-1961.

308. *Platelet TGF-β1 contributions to plasma TGF-β1, cardiac fibrosis, and systolic dysfunction in a mouse model of pressure overload.* **Meyer, Alexander, et al., et al.** Jan 2012, Blood, Vol. 119, pp. 1064-1074.

309. *Differential role of regulatory T cells in early and late stages of pulmonary fibrosis.* **Boveda-Ruiz, Daniel, et al., et al.** Feb 2013, Immunobiology, Vol. 218, pp. 245-254.

310. *Global impairment of CD4+CD25+FOXP3+ regulatory T cells in idiopathic pulmonary fibrosis.* **Kotsianidis, Ioannis, et al., et al.** Jun 2009, Am J Respir Crit Care Med, Vol. 179, pp. 1121-1130.

311. *Regulatory T cells with reduced repressor capacities are extensively amplified in pulmonary sarcoid lesions and sustain granuloma formation.* **Rappl, Gunter, et al., et al.** Jul 2011, Clin Immunol, Vol. 140, pp. 71-83.

312. *Treg Depletion Leads To Increased Fibrocyte Recruitment After Bleomycin-Induced Lung Injury.* **Garibaldi, B. T., et al., et al.** 2014, The American Journal of Respiratory and Critical Care Medicine, Vol. 189, p. A1257.

313. *Mechanism of inhibition of LPS-induced IL-12p40 production by IL-10 and TGF-beta in ANA-1 cells.* **Du, C. and Sriram, S.** Jul 1998, J Leukoc Biol, Vol. 64, pp. 92-97.

314. *A role for IL-27p28 as an antagonist of gp130-mediated signaling.* **Stumhofer, Jason S., et al., et al.** Dec 2010, Nat Immunol, Vol. 11, pp. 1119-1126.

315. *Transforming growth factor-beta differentially inhibits MyD88-dependent, but not TRAM- and TRIF-dependent, lipopolysaccharide-induced TLR4 signaling.* **Naiki, Yoshikazu, et al., et al.** Feb 2005, J Biol Chem, Vol. 280, pp. 5491-5495.

316. *TLR signaling.* **Kawai, Taro and Akira, Shizuo.** 1, Feb 2007, Seminars in immunology, Vol. 19, pp. 24-32. ISSN: 1044-5323.

317. *Cytokine production by M-CSF- and GM-CSF-induced mouse bone marrow-derived macrophages upon coculturing with late apoptotic cells.* **Yamazaki, Takahiro, Nagata, Kisaburo and Kobayashi, Yoshiro.** 2, Feb 2008, Cellular immunology, Vol. 251, pp. 124-130. ISSN: 1090-2163.

318. *SB-431542 is a potent and specific inhibitor of transforming growth factor-beta superfamily type I activin receptor-like kinase (ALK) receptors ALK4, ALK5, and ALK7.* **Inman, Gareth J., et al., et al.** Jul 2002, Mol Pharmacol, Vol. 62, pp. 65-74.

319. *SAMHD1 Restricts HIV-1 Replication and Regulates Interferon Production in Mouse Myeloid Cells.* **Zhang, Ruonan, et al., et al.** 2014, PLos ONE, Vol. 9.

320. *Nitric Oxide Synthase Isozymes.* **Förstermann, Ulrich, et al., et al.** 1994, Hypertension, Vol. 23, pp. 1121-1131.

321. *Deactivation of macrophages by transforming growth factor-beta.* **Tsunawaki, S., et al., et al.** Jul 1988, Nature, Vol. 334, pp. 260-262.

322. *Transforming growth factor-beta 1 inhibition of macrophage activation is mediated via Smad3.* **Werner, F., et al., et al.** Nov 2000, J Biol Chem, Vol. 275, pp. 36653-36658.

323. *Aberrant Toll receptor expression and endotoxin hypersensitivity in mice lacking a functional TGF-beta 1 signaling pathway.* **McCartney-Francis, Nancy, Jin, Wenwen and Wahl, Sharon M.** Mar 2004, J Immunol, Vol. 172, pp. 3814-3821.

324. *Lipopolysaccharide inhibits transforming growth factor-beta1-stimulated Smad6 expression by inducing phosphorylation of the linker region of Smad3 through a TLR4-IRAK1-ERK1/2 pathway.* **Kim, Eun-Ye and Kim, Byung-Chul.** Mar 2011, FEBS Lett, Vol. 585, pp. 779-785.

325. *c-Jun inhibits transforming growth factor beta-mediated transcription by repressing Smad3 transcriptional activity.* **Dennler, S., et al., et al.** Sep 2000, J Biol Chem, Vol. 275, pp. 28858-28865.

326. *Identification of a member of the MAPKKK family as a potential mediator of TGF-beta signal transduction.* **Yamaguchi, K., et al., et al.** Dec 1995, Science, Vol. 270, pp. 2008-2011.

327. *Activation of the mitogen-activated protein kinase pathway by transforming growth factor-beta.* **Yue, J. and Mulder, K. M.** 2000, Methods Mol Biol, Vol. 142, pp. 125-131.

328. *Transforming growth factor-beta-induced apoptosis is mediated by Smad-dependent expression of GADD45b through p38 activation.* **Yoo, Jiyun, et al., et al.** Oct 2003, J Biol Chem, Vol. 278, pp. 43001-43007.

329. *Enhanced TLR4 reactivity following injury is mediated by increased p38 activation.* **Maung, Adrian A., et al., et al.** 2005, Journal of Leukocyte Biology, Vol. 78, pp. 565-573.

330. *Crosstalk between p38 and Smad3 through TGF-β1 in JEG-3 choriocarcinoma cells.* **Xu, Qian, et al., et al.** Oct 2013, Int J Oncol, Vol. 43, pp. 1187-1193.

331. *p38 Mitogen-Activated Protein Kinase Inhibition Increases Cytokine Release by Macrophages In Vitro and During Infection In Vivo.* **Blink, Bernt Van Den, et al., et al.** 2001, The Journal of Immunology, Vol. 166, pp. 582-587.

332. *IL-27 activates human monocytes via STAT1 and suppresses IL-10 production but the inflammatory functions of IL-27 are abrogated by TLRs and p38.* **Kalliolias, George D. and Ivashkiv, Lionel B.** May 2008, J Immunol, Vol. 180, pp. 6325-6333.

333. *Suppression of IL-12 production by tristetraprolin through blocking NF-kcyB nuclear translocation.* **Gu, Ling, et al., et al.** Oct 2013, J Immunol, Vol. 191, pp. 3922-3930.

334. *RNA-destabilizing factor tristetraprolin negatively regulates NF-kappaB signaling.* **Liang, Jian, et al., et al.** Oct 2009, J Biol Chem, Vol. 284, pp. 29383-29390.

335. *Regulation of IL-27 p28 gene expression in macrophages through MyD88- and interferon-gamma-mediated pathways.* **Liu, Jianguo, Guan, Xiuqin and Ma, Xiaojing.** Jan 2007, J Exp Med, Vol. 204, pp. 141-152.

336. *Tristetraprolin impairs NF-kappaB/p65 nuclear translocation.* **Schichl, Yvonne M., et al., et al.** Oct 2009, J Biol Chem, Vol. 284, pp. 29571-29581.

337. *Transcriptional regulation of tristetraprolin by transforming growth factor-beta in human T cells.* **Ogawa, Kenji, et al., et al.** Aug 2003, J Biol Chem, Vol. 278, pp. 30373-30381.

338. *Regulation and inflammatory effects of Tristetraprolin in Macrophages.* **Jalonen, Ulla.** 2008.

339. *The role of transforming growth factor beta signaling in messenger RNA stability.* **Dibrov, Alexander, Kashour, Tarek and Amara, Francis M.** 2006, Growth Factors, Vol. 24, pp. 1-11. ISBN: 0897719050.

340. *Transforming growth factor-beta1 activates interleukin-6 expression in prostate cancer cells through the synergistic collaboration of the Smad2, p38-NF-kappaB, JNK, and Ras signaling pathways.* **Park, Jae-Il, et al., et al.** Jul 2003, Oncogene, Vol. 22, pp. 4314-4332.

341. *p38 Mitogen-Activated Protein Kinase-Dependent and -Independent Signaling of mRNA Stability of AU-Rich Element-Containing Transcripts.* **Frevel, Mathias A. E., et al., et al.** 2003, MOLECULAR AND CELLULAR BIOLOGY, Vol. 23, pp. 425-436.

342. *Mitogens stimulate the rapid nuclear to cytosolic translocation of tristetraprolin, a potential zinc-finger transcription factor.* **Taylor, G. A., et al., et al.** Feb 1996, Mol Endocrinol, Vol. 10, pp. 140-146.

X Acknowledgments

Firstly, I would like to express my sincere gratitude to my external supervisor. He offerd me the possibility to work with the very interesting topic and I had a lot of freedom to fulfil my own scientific ideas. It was a very intensive and interesting time for me. He supported me during the whole time of my PhD thesis and was always helpful if needed.

Besides my external supervisor, I would like to thank the Scientific Director of the CTH for the insightful comments, but also for the hard questions which incented me to widen my perspectives.

A special thank goes to the General Manager of the CTH. He always had an open ear for problems and was very helpful. He was a big support for me.

I would like to thank the internal supervisor of my PhD thesis for the possibility to write my PhD thesis at the CTH.

Of course, I want to thank all members of the CTH – especially the PhD students of the building 708. We were a great team and I will miss you all! It was always possible to get distracted from work if you wanted to. Special thanks go to my first colleague. We worked together very well and had a very intensive exchange of ideas belonging to the projects. Furthermore, I would like to thank our Post-Doc for his help in my writing process.

I cannot thank my parents enough. They gave me the opportunity to study biology and supported me my whole life. My wife was always there for me and helped me through frustrating moments. My grandmother also supported me and made a major contribution to a wonderful childhood and youth. Together with my parents-in-law and my brother-in-law my family helped me a lot to have a clear mind besides work. Thank you all! My best friends had a lot of comprehension for less time during the PhD thesis. Thanks!

Last but not least, our wonderful cat was a possibility to have a lot of fun after work, every day.